2019

Development of nanostructured material based electrochemical sensors for food safety and quality control

Manikandan, Venkatesh S.

Development of Nanostructured Material Based Electrochemical Sensors for Food Safety and Quality Control

By

Venkatesh S. Manikandan

A dissertation submitted in partial fulfillment of the requirements of the degree of

Doctor of Philosophy Biotechnology

Lakehead University, Thunder Bay, Ontario, Canada

Abstract

The issue of foodborne related illnesses due to additives and contaminants poses a significant challenge to food processing industries. Electrochemical-based strategies offer simple and robust analytical tools, which are ideal for food safety and the quality assessment process, in contrast to conventional instrumentation methods. The development of nanomaterials based electrochemical sensors has garnered significant attention due to their capacity for accurate analytical quantification, which has strong potential toward the replacement of conventional techniques by offering advantages such as high sensitivity and selectivity, real-time monitoring, and ease of use.

During my Ph.D. study, four distinct types of nanostructured materials were used to develop electrochemical sensors for the detection of food preservatives in food and beverage products. The consumption of excessive amounts of nitrite (NO_2^-) can be detrimental to the human body. In light of this, we developed an electrochemical sensor based on cobalt oxide nanosheets and gold nanoparticles (Co_3O_4/Au) for NO_2^- sensing. The nanomaterial was synthesized through the electrodeposition of gold (Au) on Co_3O_4 nanosheets. The Co_3O_4/Au/GCE was capable of electrooxidizing nitrite with a higher anodic peak current, and the sensor exhibited excellent linearity with a limit of detection (LOD) value of 0.11 μM.

A nanoporous gold microelectrode was synthesized for the determination of contaminants (hydrazine, N_2H_4) and preservatives (sulfite (SO_3^{2-}), nitrite (NO_2^-)). The fabricated microelectrode was characterized via scanning electron microscope (SEM) and energy dispersive X-ray spectroscopy (EDX). The nanoporous gold microelectrode exhibited excellent electrochemical performance for the simultaneous electrochemical oxidation of N_2H_4, SO_3^{2-}, and NO_2^-. In addition, the nanoporous gold microelectrode possessed high selectivity and stability. The performance of

the electrochemical sensor was further validated using actual samples such as water, wine, apple cider beer, and beef with good recovery rates, thereby confirming its potential for food safety and quality control applications.

A novel electrochemical sensor was developed using fluorine-doped graphene oxide (F-GO) for the detection of caffeic acid (CA). The fabricated nanomaterial was systematically characterized using SEM and X-ray photoelectron spectroscopy (XPS). The electrochemical investigation of F-GO/GCE for CA oxidation revealed that it demonstrated high electrocatalytic activity compared with other electrodes (e.g., bare GCE and GO/GCE). The analytical quantitation of CA recorded with the F-GO/GCE produced a stable oxidation signal over the selected CA concentration range (0.5 μM to 100.0 μM, R^2 = 0.9960) with a LOD value of 0.018 μM. The fabricated sensor successfully exhibited the capacity to directly detect CA in assorted wine samples without pretreatment.

To further explore the applications of the F-GO, a nanocomposite material synthesized with Au and F-GO was employed for the development of an Au/F-rGO/GCE sensor for the detection of vanillin. The electrochemical performance and the analytical capabilities of this novel electrochemical sensor were investigated using electrochemical techniques such as CV and DPV. The excellent sensitivity, selectivity, augmented electrocatalytic activity, and reproducibility of these developed electrochemical sensors can be attributed to the high conductivity of the nanostructured materials. The dimensions and morphologies of the developed nanomaterials played a critical role in enhancing the electrochemical performance of these sensors.

Acknowledgements

Foremost, I would like to express my sincere thanks to my supervisor Dr. Aicheng Chen for all his hope, efforts and valuable time he has put on me. His guidance and immense knowledge in electrochemistry and materials science helped me during my research and writing of this thesis. Besides my advisor, I would like to thank the my advisory committee: Dr. Gautam Das and Dr. Wensheng Qin and for their support, encouragement and insightful comments.

I would like to thank all the current and former members of Dr. Chen's research group for providing me with an ideal working place. Thanks to Jesse Donadapati, Emmanuel Boatang, Dylan Siltamaki, Joshua van der Zalm, Joseph Cirone, Sharon Chen, Jiali Wen, Sharon Abner, Sharmila Durairaj, Antony Raj Thirupathi, Motasser Hossain, Frank Boehm, Dr. Nur Hosain, Dr. Zhonggang Liu, Dr. Boopathi Sidhureddy, Dr. Syed Rahin Ahmad, Dr. Balram Adhikari, Frank, Dr. Maduraiveeran Govindhan, Dr. Mona Amiri, Dr. Wu, Dr. Sapandbir Thind for their friendship and collaboration. I thank both the faculty and the staff members of the Department of Chemistry and biotechnology for their support, encouragement and friendship.

I also thank the University of Guelph for giving me the opportunity to carry out my research activities as visiting research scholar and allowing me to utilize their instrument facilities.

My biggest thanks to ever loving parents, sister, fiancée and my friends. There are no words that can truly express the level of gratitude and appreciation I have for you. I will always value the support that you have given me and the sacrifices you have made to give me the life that I have.

List of Figures

2.1. Schematic illustration of diverse types of nanomaterials for the electrochemical monitoring of different analytes in food and beverages…….....16

2.2. SEM image of K-doped graphene (A); AFM image of graphene sheets (B); and TEM image of nitrogen-doped graphene sheets (C)……...17

2.3. FE-SEM images of the polypyrrole nanowires (A) and the Au/polypyrrole (B); and SEM image of the nanoporous gold microelectrode (C)…….19

2.4. TEM (a, b) and HR-TEM (c, d) images of worm-like Au–Pd/RGO (A), XRD pattern of Au-Pd/RGO (B), SEM image of GNPs/MWCPE (C), (D) TEM images of (a) graphene, (b) Pt nanoparticles and (c and d) graphene/Pt nanocomposite under different magnifications, SEM image of Pt/SWCNT/GCE (E) and EDX pattern for Pt/SWCNT/GCE (F)……...24

2.5. (A) DPVs of 0.5 M H_2SO_4 containing various concentrations of N_2H_4 at the Pd/MWNT–Nafion modified electrode; (B) CVs of 5.0×10^{-4} M N_2H_4 in 0.1 M PBS (pH 7.0, scan rate 50 mV s−1) at bare GCE (a), PPy/GCE (b), Au/GCE (c) and Au/PPy/GCE (d); (D) DPV responses for the increasing concentration of hydrazine……....27

2.6. SEM image of the graphene-QDs/Au-NPs (A), CVs of MG oxidation at different electrode, bare GCE (a), graphene-QDs/GCE (b), Au-NPs/GCE (c), and graphene-QDs/Au-NPs /GCE; curve (d) and curves (a, b, c and e) shows the response in the absence and in presence of 4.0×10^{-5} mol L−1 MG, respectively in a 0.05 M H_2SO_4 buffer solution.....29

2.7. SEM image of Fe_3O_4-Si4Pic$^+$Cl$^-$/Au-NPs-Si4Pic$^+$Cl$^-$ (A), CVs for the oxidation of 10 µmol L^{-1} BPA at (a) bare GCE, (b) Si4Pic$^+$Cl$^-$/GCE, (c) Au NPs-Si4Pic$^+$Cl$^-$/GCE (d) Fe_3O_4 NPs-Si4Pic$^+$Cl$^-$/GCE, and (e) Fe_3O_4-Si4Pic$^+$Cl$^-$/Au-NPs-Si4Pic$^+$Cl$^-$/GCE, scan rate of 100 mV s^{-1} in BR buffer pH 9.0 (B), DPVs of BPA oxidation in increasing concentration (0.05 µM - 10.0 µM) at Au-Pd NPs/GNs-GCE in 0.1 M PBS, pH 7.5; the calibration plot is shown in the inset (C), The amperometric responses of BPA oxidation at the Cu_2O/rGO/GCE modified electrode in presence of interference compounds (D)…….....32

2.8. CV responses of bare GCE, GO/GCE, and NDC/GCE for the oxidation of 5 mM $[Fe(CN)_6]^{3-/4-}$ in 0.1 M KCl (A), DPV responses of NDC/GCE toward CA oxidation in presence of interference molecules 0.05 M PB solution (B), CV responses of Pd–Au/PEDOT/rGO/GCE at different scan rates of 10.0 - 500.0 mV s−1 in a BR buffer, at pH 3.0 (C), DPV responses of Pd–Au/PEDOT/rGO/GCE to subsequent additions of CA (0.001 - 55.0 µm) in a BR buffer, at pH 3.0 (D)…….....36

2.9. DPVs at PEDOT/MWCNT/Nafion/GCE for increasing concentrations of caffeine in the range of 0.1 - 2.0 mM in 0.1 M Na-PBS (A), SWV responses of poly(AHNSA) with increasing concentrations of caffeine from 0.06 - 40.0 µm (B)…….....38

2.10. Amperometric responses of the graphene/Pt-modified GC electrode for different ascorbic acid concentrations (0.15 - 34.40 µM) ……...40

2.11. DPVs recorded for increasing sulphite concentrations, from 5.0 - 4000.0 µm in 0.1 M PBS buffer, pH 6.5 (A) and the respective calibration curve (inset), Amperometric response of the AuNPs/Gr/Ch/GCE sensor for successive additions of SO_3^{2-} in 0.1 M PBS, at pH 7.0, with the inset showing the respective calibration curve (B)…….....43

2.12. DPV (A) and amperometric (B) responses of increasing nitrite concentrations (5.0 - 8000.0 μmol L^{-1}) at a B-doped cubic SiC NWs electrode in 0.1 M PBS; DPV response for the electrochemical oxidation of 250.0 μM nitrite at a gold nanoporous microelectrode (C), DPV responses for the increasing concentration of NO_2^- (5.0 - 4000.0 μM), in 0.1 M PBS (pH 6.5) (D)……..45

4.1. The SEM image of the Co_3O_4 nanosheets (A) and the SEM image of the Au deposited on the surface of the Co_3O_4 nanosheets (B); EDX spectrum for the Co_3O_4 nanosheets and Au deposited Co_3O_4 nanosheets (C).....88

4.2. CV curves recorded for the oxidation of 1.0 mM nitrite with Au deposited at different times (1.0, 2.0, 3.0, 5.0, 7.5, 10.0 and 12.5 minutes) on the Co_3O_4 nanosheets (A); Plot illustrating the improvement in the anodic peak current with respect to increasing Au deposition time in 0.1 M PBS pH 4.5…….....90

4.3. LSV curves show the comparison of the performance of Co_3O_4/Au/GCE (blue line), bare GCE (red line), Au/GCE (green line), Co_3O_4/GCE (light green line), at the scan rate of 50 mV s^{-1} in 0.1 M PBS pH 4.5……91

4.4. CV (A) and DPV (B) curves of the Co_3O_4/AuNPs/GCE recorded in the absence (dotted lines) and in the presence (solid lines) of 1.0 mM of NO_2^-; (C) shows the comparison of the performance of different modified electrodes (scan rate of 50 mV s^{-1}), where the supporting electrolyte was 0.1 M PBS (pH 4.5)…….....92

4.5. CV curves of the Co_3O_4/AuNPs/GCE measured in (A) 1.0 mM NO_2^- at various scan rates (10, 20, 40, 50, 60, 70, 80, 90, 100 mV s^{-1}); (B) represents the corresponding linear relationship between

the oxidation peak current I_p and the square root of the scan rate $\upsilon^{1/2}$ (inset shows the relation between log of scan rate vs. peak potential, electrolyte medium : 0.1 M PBS (pH 4.5).....95

4.6. CV response recorded with the Co_3O_4/AuNPs/GCE toward the oxidation of NO_2^- at different concentrations ranging from 250.0 to 3000.0 μM (A); and the corresponding plot of anodic peak current vs. increasing concentration of NO_2^- (B), Electrolyte medium: 0.1 M PBS (pH 4.5), at the scan rate of 50 mV s^{-1}.....96

4.7. CV response of the Co_3O_4/AuNPs/GCE toward the oxidation of 1.0 mM NO_2^- at different pHs (3.5 - 8.5) in 0.1 M PBS, at the scan rate of 50 mV s^{-1}…….....97

4.8. SWV responses obtained with Co_3O_4/AuNPs/GCE toward the oxidation of NO_2^- in a concentration range from 1.0 μM to 4000.0 μM (A); the corresponding calibration plot for anodic peak current vs concentration (B) in 0.1 M PBS electrolyte solution (pH 4.5) …….....99

4.9. Stability measurement of the Co_3O_4/AuNPs/GCE toward 1.0 mM NO_2^- oxidation over consecutive 30 DPV measurements (A); DPV response recorded in presence of 1.0 mM NO_2^- with 4 different Co_3O_4/AuNPs/GCEs representing the reproducibility of the sensor (B) in 0.1 M PBS buffer solution (pH 4.5) ……...101

4.10. Interference response of the Co_3O_4/AuNPs/GCE for the oxidation of 1.0 mM NO_2^- in the presence of 5-fold (5.0 mM) concentration of interfering molecules (glucose, CH_3COONa, $CuSO_4$, $MgCl_2$, KCl and NH_4NO_3), in 0.1 M PBS electrolyte medium (pH 4.5) ……....102

4.11. SWV of the Co_3O_4/Au/GCE recorded in 0.1 M PBS (pH 4.5) showing the presence of nitrite in the Canadian minced beef sample…….103

5.1. The SEM image of the gold microwire before alloying/dealloying treatment (A); SEM image of the gold microelectrode after the alloying/dealloying process…….122

5.2. Cyclic voltammograms of the unmodified gold microelectrode (red line) and the fabricated nanoporous gold microelectrode (blue curve) recorded in 0.1 M H_2SO_4 electrolyte medium at the scan rate of 20 mV s^{-1}…….....123

5.3. The CV curves of the nanoporous gold microelectrode recorded in the absence (dotted lines) and in the presence (solid lines) of 250 µM of: (A) N_2H_4, (C) SO_3^{2-} and (E) NO_2^- at the scan rate of 20 mV s^{-1}, where the supporting electrolyte was 0.1 M PBS (pH 6.5). (B), (D) and (E) represents the corresponding DPV curves obtained for the oxidation of N_2H_4, SO_3^{2-} and NO_2^-…….125

5.4. (A) The CV and (B) DPV responses of the unmodified gold microelectrode (red line) and the nanoporous gold microelectrode (blue line) towards N_2H_4, SO_3^{2-} and NO_2^- in 0.1 M PBS (pH 6.5). The concentration of each is 500.0 µM. The black dash line was baseline derived from the nanoporous gold microelectrode……..127

5.5. Peak current response for the oxidation of 500 µM N_2H_4, SO_3^{2-} and 250 µM NO_2^- in 0.1 M PBS solution at different pH values: 5.0, 5.5, 6.0, 6.5 and 7.0……128

5.6. CV curves of the nanoporous gold microelectrode measured in (A) 250.0 µM H_2H_4, (B) 250.0 µM SO_3^{2-}, (C) 250.0 µM NO_2^- at various scan rates (20, 50, 75, 100, 125, 150, 175 mV s^{-1}); (D), (E) and (F) represents the corresponding linear relationship between the oxidation peak current I_p and the square root of the scan rate $v^{1/2}$ of the respective analytes in the electrolyte medium of 0.1 M PBS (pH 6.5)……....130

5.7. (A) CVs of the nanoporous gold microelectrode recorded in in 0.1 M PBS (pH 6.5) containing 250 µM N_2H_4, 250 µM SO_3^{2-} and 250 µM NO_2^- at different scan rates (20, 50, 75, 100, 125, 150 mV s^{-1}); (B), (C) and (D) The linear relationship between the oxidation peak current I_p and the square root of the scan rate $v^{1/2}$, respectively……...131

5.8. DPV responses of gold microelectrode towards the oxidation of (A) N_2H_4, (C) SO_3^{2-}, (E) NO_2^- in a concentration range from 5 μM to 4 mM in 0.1 M PBS electrolyte medium (pH 6.5). (B), (D) and (F) The corresponding calibration plots. Each point was expressed as the mean ± standard deviation (n= 3).....133

5.9. DPV responses of gold microelectrode for simultaneous oxidation of (A) N_2H_4, SO_3^{2-} and NO_2^- in a concentration range from 5.0 μM to 4.0 mM in 0.1 M PBS (pH 6.5). (B), (C) and (D) represent their corresponding calibration plots. Each point was expressed as the mean ± standard deviation (n= 3) 134

5.10. Interference response of the nanoporous gold microelectrode for the oxidation of 500.0 μM of N_2H_4, SO_3^{2-} and NO_2^- in the presence of 10-fold concentrations of $H_2PO_4^-$, HPO_4^{2-}, CO_3^{2-}, F^-, Cl^-, NO_3^-, SO_4^{2-}, Na^+, K^+, Ca^{2+}, Mg^{2+} and Zn^{2+}.....135

5.11. (A) Stability measurement of the nanoporous gold microelectrode on the simultaneous oxidation of N_2H_4, SO_3^{2-} and NO_2^- for 30 consecutive scans. The concentration of each was 500.0 μM; (B) Long-term stability of the nanoporous gold microelectrode over a period of ten days....136

5.12. DPVs of the nanoporous gold microelectrode recorded in 0.1 M PBS (pH 6.5) showing the (A) presence of sulfite in the Chile wine and (B) presence of nitrite in the Canadian minced beef sample. The black dashed line in the DPVs represent the baseline derived (in the absence of the analyte) from the nanoporous gold microelectrode.....139

6.1. SEM images of the synthesized (A) graphene oxide (GO) and (B) fluorinated graphene oxide (F-GO).....155

6.2. (A) XPS spectra (survey scan) of GO and FGO; (B) high-resolution XPS spectrum of C1s of GO and the fitting curves; (C) high-resolution XPS spectrum of C1s of F-GO and the fitting curves; and (D) high-resolution XPS spectrum of F1s of F-GO.....156

6.3. (A) CV curves of the bare GCE (black dashed line), GO/GCE (blue line), and F-GO/GCE (red line) in the presence of 0.1 M KCl containing 5.0 mM $[Fe(CN)_6]^{3-/4-}$ at the scan rate of 50 mV s^{-1}; (B) CV curves of the F-GO/GCE recorded in the presence of 5 mM $[Fe(CN)_6]^{3-/4-}$ in 0.1 M KCl at various scan rates, ranging from 10 - 100 mV s^{-1}; (C) the corresponding plots of vs the anodic/cathodic peak current vs the square root of the scan rates.....158

6.4. CV curves of bare GCE (dashed black line), GO/GCE (blue line), and F-GO/GCE (red line) recorded in the absence of CA (A); F-GO/GCE response in the presence of 50.0 μM CA (B); comparison of the modified GCEs in the presence of 50.0 μM CA (C) in a 0.1 M B-R buffer solution pH 2.65, at a scan rate of 50 mV s^{-1}.....160

6.5. CV response of F-GO/GCE recorded in the presence of 50.0 μM CA at different scan rates varying between 10 to 200 mV s-1 (A) and the subsequent plot of anodic/cathodic peak current vs. the scan rate (mV s^{-1}) (B), in 0.1 M B-R buffer medium.....162

6.6. CV curves for the oxidation of 30.0 μM CA at different pHs (2.6 - 7.3) (A); the resulting plot of anodic peak current vs pH (B) and the corresponding plot of the anodic peak potential vs pH (insert of D). Electrolyte medium: 0.1 M B-R buffer solution (pH 2.65); Scan rate : 50 mV s^{-1}....164

6.7. CV responses of F-GO/GCE for the oxidation/reduction of CA at different concentrations, ranging from 10.0 to 70.0 μM (A); and the corresponding plots of anodic/cathodic peak current vs. the concentration of CA (B) in a 0.1 M B-R buffer solution pH 2.65; Scan rate: 50 mV s^{-1}.....165

6.8. DPV responses of F-GO/GCE for the detection of CA in the concentration ranging from 0.5 to 100.0 μM (A); the corresponding calibration plot for the anodic peak current vs concentration (B) in a 0.1 M B-R buffer solution (pH 2.65)……167

6.9. DPV curves of the F-GO/GCE recorded in 50.0 μM CA over 30 consecutive measurements (A); DPV response of F-GO/GCE measured in 50.0 μM CA for 10 days (B). Electrolyte: a 0.1 M B-R buffer solution (pH 2.65).....170

6.10. DPV response recorded in the presence of 50.0 μM CA with four different F-GO/GCEs (C); and interference response of the F-GO/GCE for the detection of 100.0 μM CA in the presence of 1.0 mM *p*-coumaric acid, hydroquinone, trans-ferulic acid, gallic acid, glucose and ascorbic acid (D). Electrolyte: a 0.1 M B-R buffer solution (pH 2.65).....171

6.11. DPV response of F-GO/GCE for the detection of CA in different brands (wine samples I - IV) of red wine. Electrolyte: 0.1 M B-R buffer solution (pH 2.65).....173

6.12. DPV response of F-GO sensor obtained for the detection of CA directly in wine sample....174

7.1. CV curves of the bare GCE (green line), GO/GCE (red line) and Au/rF-GO/GCE (red line) in the presence of 0.1 M KCl containing 5.0 mM $[Fe(CN)_6]^{3-/4-}$ at the scan rate of 50 mV s^{-1}.....191

7.2. CV curves at various scan rates (10 - 200 mV s^{-1}) (A); the corresponding plot of scan rate vs anodic/cathodic peak current values 192

7.3. LSV (A) and DPV (B) displaying the curves recorded with Au modified Au/F-rGO/GCE towards the oxidation of 500.0 μM vanillin (with Au deposition at different times: 125s, 250s, 500s and 750s, at the scan rate of 50 mV s^{-1}, in 0.1M PBS pH 7.0 193

7.4. Plot displaying the trend in increasing Au deposition time and changing anodic peak current (values calculated from the LSV data) 194

7.5. CV displaying the curves obtained with Au/F-rGO/GCE towards the oxidation of 500.0 μM vanillin, at the scan rate of 50 mVs^{-1} (A); DPV response recorded with Au/F-rGO/GCE toward the oxidation of 500.0 μM, in 0.1 M PBS electrolyte medium, pH 7.0 196

7.6. CV curves recorded with bare GCE (black line), Au/GCE (red line) and Au/ F-rGO/GCE (blue line) toward the oxidation of 500.0 μM, at the scan rate of 50 mVs^{-1}, in 0.1 M PBS electrolyte medium, pH 7.0 197

7.7. LSV responses of Au/F-rGO/GCE toward the oxidation/reduction of vanillin at different concentrations ranging from 300.0 to 1500.0 μM (A); and the corresponding plot of anodic peak current vs. concentration of vanillin (B), in 0.1 M PBS buffer solution pH 7.0, at the scan rate of 50 mV s^{-1} 199

7.8. CV response of F-rGO/GCE recorded in the presence of 50.0 μM CA at numerous scan rates varying between 10 to 200 mV/s (A); and the subsequent plot of anodic peak current vs. scan rate (mV s^{-1}) (B), in 0.1 M PBS pH 7.0 200

7.9. DPV responses of F-rGO/GCE the oxidation of CA in a concentration range from 0.5 μM to 100.0 μM (A); the corresponding calibration plot for anodic peak current vs concentration (B) in 0.1 M B-R buffer solution (pH 2.65) 202

7.10. LSV response recorded in presence of 500.0 μM vanillin with 4 different Au/F-rGO/GCEs (A); and plot representing the anodic peak current value estimated from the individual electrodes (B), in 0.1 M PBS electrolyte solution, pH 7.0 203

7.11. Stability measurement of the Au/F-rGO/GCE toward 500.0 μM vanillin oxidation over 25 consecutive LSV scans, in 0.1 M PBS electrolyte solution, pH 7.0.....204

List of Tables

Table 2.1. List of various electrochemical sensors associated with electrochemical techniques for the detection of different target analytes.....49

Table 4.1. Comparison of the electrochemical performance of Co_3O_4/AuNPs/GCE sensor other reported sensors toward CA detection.....100

Table 4.2. Performance of the Co_3O_4/Au/GCE electrode for the determination of NO_2^- in bottled water.....104

Table 5.1. The performance of the nanoporous gold microelectrode for the simultaneous detection of the three analytes (N_2H_4, SO_3^{2-} and NO_2^-) for 30 consecutive scans.....137

Table 5.2. The long-term stability of the nanoporous gold microelectrode for the simultaneous determination of N_2H_4, SO_3^{2-} and NO_2^- over a period of ten days.....137

Table 5.3. Performance of the nanoporous gold microelectrode for the determination of N_2H_4, $SO_3^{2-}$and NO_2^- in wine, beer, beef, and water.....140

Table 6.1. Comparison of the electrochemical performance of F-GO/GCE sensor with reported sensors toward CA detection.....168

Table 6.2. Performance of the F-GO/GCE electrode for the determination of CA in different brands of wine.....172

List of Abbreviations and Symbols

AA	Ascorbic Acid
BuChE	Butylcholinesterase
B-R	Briton Robinson
CA	Chronoamperometry/ Caffeic Acid
CILE	Carbon Ionic Liquid Electrode
CNT	Carbon Nanotubes
CV	Cyclic Voltammetry
CPE	Carbon Paste Electrode
CRGO	Chemically Reduced Graphene Oxide
DA	Dopamine
DHP	Dihexadecyl Hydrogen Phosphate
DPV	Differential Pulse Voltammetry
EASA	Electrochemical Active Surface Area
ERGO	Electrochemically reduced graphene oxide
FGO	Fluorine doped graphene oxide
FDA	Food and Drug Administration
FeHCF	Iron hexacyanoferrate
GCE	Glassy carbon electrode
Au	Gold
GN	Graphene Nanosheet
GO	Graphene oxide
N_2H_4	Hydrazine

LOD	Limit of Detection
μM	Micromolar
mM	Millimolar
MIP	Molecularly Imprinted Polymer
MWCNT	Multi walled Carbon Nanotube
ND	Nanodendrite
nM	nanomolar
NO_2^-	Nitrite
Pd	Palladium
PBS	Phosphate Buffer Solution
Pt	Platinum
PEDOP	Poly(3,4-ethylenedioxypyrrole)
PEDOT	Poly(3,4-ethylenedioxythiophene)
QD	Quantum Dot
rGO	Reduced Graphene Oxide
SEM	Scanning Electron Microscopy
Ag	Silver
SWCNT	Single Walled Carbon Nanotube
SO_3^{2-}	Sulfite
SWAdSV	Square Wave Anodic Stripping Voltammetry
SWV	Square Wave Voltammetry
TEM	Transmission Electron Microscopy
WHO	World Health Organization

XRD	X-ray Diffraction Spectroscopy
XPS	X-ray Photoelectron Spectroscopy

Table of Contents

Abstract ..... **i**

Acknowledgements ..... **iii**

List of Figures ..... **iv**

List of Tables ..... **xiii**

List of Abbreviations and Symbols ..... **xiv**

Chapter 1: Introduction and Thesis Scope **1**

1.1 Role of nanomaterials and their significance **2**

1.2 Role of electrochemical sensors for the detection of food additives and contaminants **3**

1.3. Thesis scope **4**

References: **7**

Chapter 2: Literature Review* **10**

2.1 Introduction **10**

2.2 Electrochemical techniques **12**

2.3. Nanomaterials **15**

2.3.1 Carbon-based nanomaterials 17

2.3.2 Gold based nanomaterials 19

2.3.3 Metal Nanocomposites 22

2.4. Electrochemical sensors for the detection of food additives and contaminants **25**

2.4.1 Hydrazine 26

2.4.2 Malachite green 28

2.4.3 Bisphenol A 31

2.4.4 Caffeic acid 35

2.4.5 Caffeine 37

2.4.6 Ascorbic Acid 39

2.4.7 Sulfite 41
2.4.8 Nitrite 43
2.5. Electrochemical based immunosensors 46
2.6. Summary and Outlook 47
References 51
Chapter 3: Materials and Methods 78
3.1 Introduction 78
3.2 Experimental 78
3.2.1 Materials 78
3.2.2 Instruments and Electrochemical Experiments 79
3.2.3 Fabrication of Electrodes 79
3.3 Summary 82
Chapter 4: Electrochemical Detection of Nitrite Based on Co_3O_4-Au Nanocomposites for Food Quality Control 83
4.1. Introduction 83
4.2. Experimental Section 86
4.2.1. Reagents 86
4.2.2 Characterization and electrochemical measurements 86
4.2.3 Electrode preparation and modification 87
4.2.4. Sample preparation 87
4.3. Results and Discussion 87
4.3.1. Surface morphology and optimization of the Au deposition time 88
4.3.2 Comparison of performances of the modified electrodes 89
4.3.3 Electrochemical behaviour of NO_2^- using CV and DPV 93
4.3.4 Effect of scan rate, concentration and electrolyte pH 93

4.3.5 Analytical determination of NO_2^- 98

4.3.6. Stability, reproducibility and interference measurements 102

4.3.7. Real sample analysis 104

4.4. Conclusions 105

References 105

Chapter 5: Simultaneous Detection of Hydrazine, Sulfite, and Nitrite Based on a Nanoporous Gold Microelectrode* 115

5.1. Introduction 115

5.2. Experimental Section 118

5.2.1. Reagents 119

5.2.2. Electrode preparation and modification 119

5.2.3. Sample preparation 120

5.2.4. Characterization techniques 120

5.3. Results and Discussion 121

5.3.1. Surface morphology and electrochemical characterization 121

5.3.2. Electrochemical oxidation of individual N_2H_4, SO_3^{2-} and NO_2^- analytes 124

5.3.3. Effects of the pH of the electrolyte and the scan rate 128

5.3.4. Detection limit and calibration plots 132

5.3.5. Interference and stability measurements 135

5.3.6. Real sample analysis 138

5.4. Conclusions 141

References 141

Chapter 6: Sensitive Electrochemical Detection of Caffeic Acid in Wine Based on Fluorine-doped Graphene Oxide* 150

6.1. Introduction 150

6.2. Experimental section 153

6.2.1. Reagents 153
6.2.2. Electrode preparation and modification 153
6.2.3. Characterization techniques 154
6.3. Results and Discussion 155
6.3.1 Morphology and electrochemical characterization 155
6.3.2 Electrooxidation behaviour of CA 159
6.3.3 Effect of scan rate, electrolyte pH, and concentration 161
6.3.4 Analytical determination of CA 166
6.3.5. Stability, reproducibility, and interference measurements 169
6.3.6 Real sample analysis 172
6.4. Conclusion 174
References 175
Chapter 7: Electrochemical Sensor Based on Gold and Fluorine-doped Graphene Oxide for the Detection of Vanillin 186
7.1 Introduction 186
7.2.1. Reagents 188
7.3. Results and discussion 190
7.3.1 Electrochemical characteristic of Au/F-rGO/GCE 190
7.3.3 Optimization of the Au deposition time 195
7.3.2 Electrochemical behaviour of vanillin using CV and DPV 195
7.3.4 Effect of concentration and scan rate 198
7.3.5 Analytical determination of vanillin 201
7.3.6 Stability, reproducibility and interference measurements 204
7.4. Conclusion 205
References 206

Chapter 8: Conclusion and Future Work..... 212

Chapter 1: Introduction and Thesis Scope

Food safety and quality are of primary global concern due to the existence of vast quantities of chemical preservatives/additives and biological contamination that are encountered during the production of processed foods and beverages. Despite the rapid upsurge in domestic and international standards for food quality and safety, there continues to be a growing demand for these products. This translates to the food industry having to ensure the utmost quality and safety of their products for consumers. An article published by WHO indicated that due to the lack of rigorous food safety and quality control processes, foodborne ailments severely impact the financial systems of underdeveloped nations. Additionally, an estimate released by the Center for Disease Control and Prevention (United States) disclosed that over 9 million cases of food contamination (chemical/biological in nature) are reported every year in North America. On a global scale, there are an estimated 1.5 billion reported incidents of diarrhea yearly, of which three-quarters are attributed to biological infections from food sources. As a result, it has become imperative for food and beverage industries to uphold high quality and safety standards for their products. Presently, established analytical techniques such as hydrodynamic chromatography (HDC), high-performance liquid chromatography (HPLC), gas chromatography (GC), inductive coupled plasma atomic emission spectroscopy (ICP-OES), size exclusion chromatography (SEC), and matrix-assisted laser desorption/ionization (MALDI-TOF) are used for food and beverage testing. However, on the downside, these techniques are expensive, time-consuming and arduous. Therefore, it is of enormous importance to developing analytical methods for the rapid and accurate detection and quantification of food preservatives/additives and contaminants. Typically, most chemical analyses are performed in centralized laboratories, where only a limited number of samples can be tested. In order to address the setbacks that are linked to food-related diseases,

electrochemically based analytical methods are an excellent choice to effectively ease the investigation of additives and contaminants for large batches of product in the food industry. Though progress has been made with conventional analytical testing procedures, these methods involve complex multistep sample pretreatment stages, which are labour intensive and expensive to perform. Thus, food processing industries are inclining toward new and innovative methods that are economical, convenient, and accurate, combined with speed and efficiency to further improve the safety testing and quality control of foods and beverages.

1.1 Role of nanomaterials and their significance

Nanotechnology involves the alteration of structures at the atomic scale, and the characterization and fabrication of nanomaterials with at least one dimension in the range of from 1 to 100 nanometers (nm) or below.[1] By reducing the dimensions of a given material to the nanoscale, its physical and chemical attributes can be notably transformed in contrast to the properties of the identical material observed at the macroscale. It has been projected that the nanotechnology industry will contribute ~$3 trillion to the world economy in five years.[2] At present, there are many companies and research labs around the world that are focused on the fabrication of new classes of nanomaterials with an extensive range of applications, including medical therapeutics and diagnostics, energy generation and conservation, DNA, computing, and building materials. Remarkable advancements have also been made in the synthesis of different nanomaterials for biomedicine, biofuel cells, and energy storage applications.[3-5] Nanomaterials based electrochemical sensors offer the benefits of a reliable point of care diagnostics with improved safety, reliability, and rapid-testing capabilities. Over the last decade, advances in nanotechnology have risen steeply, which continues to create an ever-growing demand by permeating the market.[6] The technological advancement and potential uses of nanomaterials

toward the development of sensitive electrochemical sensors are inevitable in the food industry to facilitate safety and quality control monitoring.[7,8]

Recent progress in nanotechnology, coupled with advancements in nanomaterials synthesis have enabled prospects for the development of enhanced sensing systems and portable instrumentation. Electrochemical detection systems are readily available via inexpensive platforms such as patterned paper, which facilitates on-site analysis.[9] These portable, low cost and user-friendly sensors function as an alternative to conventional analytical methods for point-of-care analysis and food quality control.[10, 11] There is extensive literature that describes the application of screen-printed carbon electrodes (SPCE) as a portable electrochemical sensor platform for environmental monitoring as well as pharmaceutical and food quality control.[12-14] Miniaturized graphene oxide-ionic liquid based electrochemical devices have been demonstrated for the very sensitive electrochemical detection of a wide variety of electroactive targets of importance, encompassing food analyses, environmental monitoring, and clinical diagnoses.[15]

1.2 Role of electrochemical sensors for the detection of food additives and contaminants

The development of nanomaterials based electrochemical sensors is an active area of research that is predicted to deliver state-of-the-art technologies for maintaining food integrity, which will supplant traditional techniques.[16] Electrochemistry based analytical methods and electrochemical sensors have positively impacted multiple fields, including medical diagnostics, environmental analyses, food sciences, enzymatic kinetics, and pharmacology.[17-19] Various signal amplification strategies coupled with functional nanomaterials have recently garnered considerable interest in the emergence of high-performance analytical tools for the trace level determination of analytes. Products derived from nanotechnology include an extensive range of

materials that have strong potential to enhance the stability, selectivity, sensitivity, and measuring capabilities of sensors. Nanotechnology is most widely employed in electronics, sensing, biomaterials, and catalysis, and has more recently made its way into the food industry.[20,21]

The perpetual demand for processed foods and beverages directly forces the implementation of stringent safety and quality standards. Innovative approaches must be put into practice to meet the requirements for maintaining the safety of food and beverages. Electrochemical sensors may serve as alternatives to conventional methods; thus, improving portability and rapid response, while negating the requirements of highly skilled operators and high-cost operation. The development of these sensors for the determination of different preservatives/contaminants in numerous food matrices will have high value. Electroanalytical techniques coupled with distinct nanomaterials offer direct and efficient methods for the detection of hydrazine, sulfite, nitrite, caffeic acid, and vanillin. High-performance nanomaterials based electrochemical sensors have, and will continue to unlock, myriad prospects in the research and development of advanced analytical devices for the safety and quality control of foods and beverages.

1.3. Thesis scope

The aim of this Ph.D. thesis is to elucidate the synthesis and integration of novel nanomaterials toward the development of high-performance electrochemical sensors, for the detection and determination of preservatives and contaminants in foods. The specific objectives of this Ph.D. project are to investigate the electrochemical performance of different carbon and metal-based nanomaterials/nanocomposites for the detection and determination of various preservatives and contaminants in different food matrices. Carbon-based materials such as graphene, graphene oxide (GO), carbon nanotubes (CNTs) possess advantageous attributes such as high conductivity, rapid

heterogeneous electron transfer, and large surface areas, making them ideal materials for the electrochemical detection of a wide range of targeted molecules.[22-24] Gold (Au) is one of the most popular metal for sensor development exhibiting excellent catalytic and electrochemical properties, and gold nanoparticles have been employed for the fabrication of a wide array of sensors. From an electroanalytical standpoint, Au nanoparticles gained a research appreciation due to their excellent conductivity, biological compatibility, and high surface to volume ratio. Furthermore, the combination of metal nanoparticles with carbon-based materials increases the overall electrochemical performance of nanostructured materials. The use of metallic nanocomposites and bimetallic nanostructures might vastly improve electrochemical activity, sensitivity, and selectivity for the detection of compounds in food and beverage matrices.

Chapter 2 of this thesis assesses the various state-of-the-art nanomaterials based electrochemical sensors that have been developed and reported for their applicability in the detection of food additives and contaminants. Various electrochemical techniques and an array of nanomaterials for sensing applications are discussed in detail. Distinct types of food preservatives/additives and contaminants are comprehensively compared, as well as the nanomaterials and electrochemical techniques currently used to detect them, including their appropriate figures of merit. Further, the applications and advantages of electrochemical sensors for the detection of various analytes in foods and beverages are highlighted.

Chapter 3 introduces basic materials, methods, characterization techniques, and synthetic methods employed for the fabrication of various carbon and metal-based nanomaterials or nanocomposites.

Chapter 4 introduces the development of an electrochemical sensor based on cobalt oxide (Co_3O_4) nanosheets and gold (Au) for nitrite (NO_2^-) sensing. This nanomaterial was fabricated by electrodepositing gold (Au) on Co_3O_4 nanosheets. The experimental results revealed that the Co_3O_4/Au was capable of electrooxidizing nitrite with a higher anodic peak current value, coupled with high selectivity and good stability. The performance of the developed sensor was scrutinized further using commercial bottle water with good recovery rates.

In Chapter 5, the development of a high-performance electrochemical sensor is described that used a gold microelectrode with a nanoporous surface structure which was further employed for the simultaneous detection and determination of hydrazine (N_2H_4), sulfite (SO_3^{2-}), and nitrite (NO_2^-) in water, beer, and beef samples. The nanoporous structure attained on the gold microelectrode was achieved by employing an alloying/dealloying method. The nanostructured material exhibited a high surface area and increased roughness. The 3D nanoporous structure played a significant role in enhancing electrochemical sensing capabilities, and improved selectivity for the simultaneous oxidation of N_2H_4, SO_3^{2-}, and NO_2^-.

In Chapter 6, Fluorine (F) was doped with graphene oxide (F-GO) and was used for the development of a novel electrochemical sensor for the detection of caffeic acid (CA) in red wine. Doping F with GO multiplied the electrochemically active surface area (EASA) of the F-GO by ~10 times, in contrast, to GO. Moreover, the F-GO sensor possessed good sensitivity, long-term stability, and reproducibility. The practical application of the F-GO electrochemical sensor was tested using commercially available wine. This study also showed that the developed sensor was capable of detecting CA in red wine without pretreatment.

Chapter 7 presents the fabrication of a novel electrochemical sensor for the detection of vanillin. The sensor was developed using F-GO as the carbon support material, and Au was

deposited on the carbon surface. The presence of F and Au significantly improved the overall electrochemical performance of the nanostructured material. This improved electrochemical activity was associated with the increased surface area, and the synergistic effect of metal-metal and metal-graphene, thereby increased the availability of active sites.

Chapter 8 presents concluding remarks from the above chapters and presents an overall summary of the thesis.

References:

1. K. D. Sattler, Handbook of nanophysics: principles and methods, ed., CRC press, 2010.
2. M. C. Roco, C. A. Mirkin and M. C. Hersam, Nanotechnology research directions for societal needs in 2020: retrospective and outlook, ed., Springer Sci. Bus. Media, 2011.
3. A. Chen and S. Chatterjee, Nanomaterials based electrochemical sensors for biomedical applications, *Chem. Soc. Rev.* 42 (2013) 5425-5438.
4. Y. Umasankar, B.-R. Adhikari and A. Chen, Effective immobilization of alcohol dehydrogenase on carbon nanoscaffolds for ethanol biofuel cell, *Bioelectrochem.* 118 (2017) 83-90.
5. E. Martínez-Periñán, W. C. Foster, P. M. Down, Y. Zhang, X. Ji, E. Lorenzo, D. Kononovs, I. A. Saprykin, N. V. Yakovlev, A. G. Pozdnyakov and E. C. Banks, Graphene encapsulated silicon carbide nanocomposites for high and low power energy storage applications, *Carbon* 3 (2017) 20.
6. S. Logothetidis, in *Nanostructured Materials and Their Applications*, Springer Berlin, Heidelberg, 2012, pp. 1-22.

7. N. Duran and P. D. Marcato, Nanobiotechnology perspectives. Role of nanotechnology in the food industry: a review, *Int. J. Food Sci. Tech.* 48 (2013) 1127-1134.

8. B. Srilatha, Nanotechnology in agriculture, *J. Nanomedic. Nanotechnol.* 2 (2011) 5.

9. J. G. Osteryoung and R. A. Osteryoung, Square wave voltammetry, *Anal. Chem.* 57 (1985) 101-110.

10. A. Chen and B. Shah, Electrochemical sensing and biosensing based on square wave voltammetry, *Anal. Methods* 5 (2013) 2158-2173.

11. B. Uslu and S. A. Ozkan, Electroanalytical Methods for the Determination of Pharmaceuticals: A Review of Recent Trends and Developments, *Anal. Let.* 44 (2011) 2644-2702.

12. M. Khairy, B. G. Mahmoud and C. E. Banks, Simultaneous determination of codeine and its co-formulated drugs acetaminophen and caffeine by utilising cerium oxide nanoparticles modified screen-printed electrodes, *Sens. Actuat. B Chem.* 259 (2018) 142-154.

13. C. H. Hamann, A. Hamnett and W. Vielstich, Electrochemistry, 2nd ed., Wiley-VCH, Weinheim, 2007.

14. P. Shivappa Adarakatti, C. W. Foster, C. E. Banks, A. K. N. S and P. Malingappa, Calixarene bulk modified screen-printed electrodes (SPCCEs) as a one-shot disposable sensor for the simultaneous detection of lead(II), copper(II) and mercury(II) ions: Application to environmental samples, *Sens. Actuat. A Phys.* 267 (2017) 517-525.

15. D. A. Brownson and C. E. Banks, Graphene electrochemistry: an overview of potential applications, *Analyst* 135 (2010) 2768-2778.

16. M. Govindhan, B.-R. Adhikari and A. Chen, Nanomaterials-based electrochemical detection of chemical contaminants, *RSC Adv.* 4 (2014) 63741-63760.

17. H. S. Toh, K. Tschulik, C. Batchelor-McAuley and R. G. Compton, Electrochemical quantification of iodide ions in synthetic urine using silver nanoparticles: a proof-of-concept, *Analyst* 139(16) (2014) 3986-3990.

18. P. Guan, Y. Li, J. Zhang and W. Li, Non-Enzymatic Glucose Biosensor Based on CuO-Decorated CeO2 Nanoparticles, *Nanomaterials* 6 (2016) 159.

19. G. Favero, G. Fusco, F. Mazzei, F. Tasca and R. Antiochia, Electrochemical characterization of graphene and mwcnt screen-printed electrodes modified with aunps for laccase biosensor development, *Nanomaterials* 5 (2015) 1995-2006.

20. N. Sozer and J. L. Kokini, Nanotechnology and its applications in the food sector, *Trends biotechnol.* 27 (2009) 82-89.

21. C. Chellaram, G. Murugaboopathi, A. John, R. Sivakumar, S. Ganesan, S. Krithika and G. Priya, Significance of nanotechnology in food industry, *APCBEE Procedia* 8 (2014) 109-113.

22. M. Pumera, Graphene-based nanomaterials and their electrochemistry, *Chem. Soc. Rev.* 39 (2010) 4146-4157.

23. M. Pumera, A. Ambrosi, A. Bonanni, E. L. K. Chng and H. L. Poh, Graphene for electrochemical sensing and biosensing, *TrAC* 29 (2010) 954-965.

24. C. S. Lim, C. K. Chua and M. Pumera, Detection of biomarkers with graphene nanoplatelets and nanoribbons, *Analyst* 139 (2014) 1072-1080.

Chapter 2: Literature Review*

2.1 Introduction

Food safety is a major global concern due to the existence of vast quantities of chemical additives that are currently used in the production of foods and beverages. Food safety has been placed among the top 11 primacies by the World Health Organization (WHO). A report from WHO has suggested that due to the lack of proper food safety, foodborne ailments severely impacts the financial systems of underdeveloped nations. Moreover, an estimation by the U.S. Centers for Disease Control and Prevention revealed that over 9 million Americans become ill due to food contamination each year.[1] It has been estimated that 1,500 million cases of diarrhea are reported annually on a global scale, of which three-fourths are attributed to biological infection from food sources.[2] Conventional analytical techniques such as hydrodynamic chromatography (HDC), high-performance liquid chromatography (HPLC), size exclusion chromatography (SEC), and matrix-assisted laser desorption/ionization (MALDI-TOF) are expensive and laborious. A promising replacement is required to simplify the process of food safety testing.

Therefore, it is of monumental importance to developing analytical methods to swiftly and accurately detect and quantify food preservatives/additives and contaminants. Typically, most chemical analysis is performed in centralized laboratories, and only a limited number of samples can be tested. In order to address the setbacks that are linked to food-related diseases, electrochemical-based analytical methods are an excellent choice to effectively ease the investigation of additives and contaminants for large batches of product in the food industry.

---

*Most of this chapter has been published in the journal *Analyst*, **2018**, 143, 4537-4554.

Though progress has been made with conventional analytical testing procedures, these methods involve complex multistep sample pretreatment stages, which are labour intensive and expensive to perform. Thus, food processing industries prefer convenient, accurate, and efficient analytical models to more seamlessly improve the levels of safety and quality of foods and beverages. Nanomaterials based electrochemical sensors offer the benefits of a reliable point of care diagnostics with improved safety, reliability, and rapid-testing capabilities. Over the last decade, advances in nanotechnology have improved drastically, which continue to create an ever-growing demand by permeating the market.[3] It has been projected that the nanotechnology industry will contribute about $3 trillion to the world economy by 2020 while engaging at least 6 million workers by the end of the decade, which will contribute towards a dynamic change in the area of nanomaterials research.[4]

At present, there are many companies that are focused on the fabrication of new classes of nanomaterials, with a more extensive range of applications, including therapeutics and medical diagnostics, energy generation and conservation, DNA, computing, and building materials. Nanotechnology involves the alteration of structures at the atomic scale and the characterization and fabrication of nanomaterials with at least one dimension in the range of 1 to 100 nanometers (nm) or below.[5] By reducing the dimensions of a given material at the nanoscale, its physical and chemical attributes are significantly transformed in contrast to the properties of the identical material at the macroscale. Noteworthy progress has been made in synthesizing different nanomaterials for biomedical, biofuel cells and energy storage applications as well.[6-8] The technological advancement and potential uses of nanomaterials toward the development of sensitive electrochemical sensors are inevitable in the food industry for safety and quality control monitoring.[9,10]

Electroanalytical techniques have positively impacted multiple fields, including medical diagnostics, environmental analysis, food sciences, enzymatic kinetics, and pharmacology.[11-13] The development of nanomaterials based electrochemical sensors is an active research area that is predicted to deliver state-of-the-art technologies for maintaining food integrity that will supplant traditional techniques.[14] Various signal amplification strategies coupled with functional nanomaterials have recently garnered considerable interest in the emergence of high-performance analytical tools for the trace level determination of analytes. Products derived from nanotechnology include an extensive range of materials that have strong potential to enhance the stability, selectivity, sensitivity, and measuring capabilities of sensors. Nanotechnology is most widely employed in electronics, sensing, biomaterials, and catalysis, and has more recently made its way into the food industry.[15,16]

This review assesses various state-of-the-art nanomaterials based electrochemical sensors that have been developed and reported for their applicability in the detection of food additives and contaminants. Various electrochemical techniques and an array of nanomaterials for sensing applications are discussed in detail. Distinct types of food preservatives/additives and contaminants, the nanomaterials and electrochemical techniques used for the detection of these food additives, including the calibration range and the limits of detection, are comprehensively compared. Further, the applications and advantages of electrochemical sensors for the detection of different analytes in foods and beverages are highlighted.

2.2 Electrochemical techniques

To a significant degree, electrochemical techniques and their associated methods may be applied in the area of food chemistry, where either two-electrode or three-electrode systems can

be utilized for electrochemical sensing. A typical three-electrode electrochemical cell consists of a working electrode that is comprised of chemically stable and conductive materials, such as platinum, gold, or carbon (e.g., graphene oxide, graphene nanoplatelets, carbon nanotubes), a reference electrode (e.g., Ag/AgCl), and a counter electrode (e.g., graphite, platinum, gold).[17,18] Sensors are devices that detect changes in physical, chemical, or biological properties and convert these changes into measurable signals. Electrochemical sensors offer a diverse range of advantages such as instrumental robustness, low cost, and point of care application.

Durst and co-workers defined an electrochemical sensor as an independent integrated device that is efficient for providing accurate analytical information by means of a chemically modified element and an electrochemical signal transducer component that is linked to a data acquisition and processing system.[19] The sensitivity, selectivity, and stability of the designed sensors are dependent on the nanomaterials used and the sensing analytes.[20] The critical parameters of electrochemical sensors are sensitivity, detection limit, dynamic range, selectivity, linearity, response time, and stability.[21] A variety of electrochemical methods have been explored for the detection of food additives, biological contaminants, and heavy metals.[22-25] In electrochemistry, reactions under investigation typically generate a measurable (*amperometric*) current, a measurable (*potentiometric*) potential or charge accumulation, or measurably alter the (*conductometric*) conductive properties of a medium between electrodes.[26] Other types of electrochemical detection techniques, such as *impedimetric*, measures impedance (both resistance and reactance) through an electrochemical impedence spectroscopy method.[27,28]

Voltammetry belongs to a category of electroanalytical methods, through which analyte data can be obtained by varying the potential and subsequently measuring the resulting current. It is, therefore, considered as an amperometric technique. As there are many ways to vary a potential,

there are also many forms of voltammetry, linear sweep, differential staircase, normal pulse, reverse pulse, differential pulse, and more.[29,30]

Typically, voltammetric techniques such as cyclic voltammetry (CV), linear sweep voltammetry (LSV), differential pulse voltammetry (DPV), square wave voltammetry (SWV) are extremely useful in translating the processes involved at the electrode material surface toward the sensitive detection and determination of various target analytes.[31-37] The CV is one of the most widely employed voltammetric techniques for the acquisition of data regarding redox potential and electrochemical reaction rates (e.g., the chemical rate constant) of analyte solutions. The scan rate, $(V_2 - V_1)/(t_2 - t_1)$, is a critical factor, as the duration of a scan is important in order to provide sufficient time for a meaningful chemical reaction to occur. Varying the scan rate, therefore, yields correspondingly varied results.[38] DPV is a suitable technique for the detection of trace amounts of analytes that require high sensitivity.[39] The current is measured twice during each pulse period (prior to the pulse and following the pulse), and the difference between these two current values is calculated and displayed.

SWV is an effective electrochemical technique that is appropriate for analytical applications, understanding electrode mechanisms, and the measurement of electrokinetics.[40,41] SWV may be employed to investigate catalytic reactions, reversible and irreversible reactions, as well as reactions with sluggish electron transfer. Pulse techniques are based on the principle of variation in the decay rates of the charging and faradic currents. The charging current, as an exponential function, degenerates at a much more rapid rate than the faradic current, while the decay of the faradic current is inversely proportional to the square root of time.[42,43] Consequently, the capacitive current is almost negligible as compared to the faradaic current at the end of each pulse, thereby increasing the ratio of faradaic to non-faradaic current.[44] CA is one of the simplest

waveform potentiostats, where the current is monitored as a function of time.[43,41] These techniques play a key role in the development of electrochemical sensors and for the analytical quantification of the targeted molecules.

2.3. Nanomaterials

Recent developments in nanotechnology and nanomaterials synthesis have enabled opportunities for the development of advanced sensing systems and portable instrumentation. Electrochemical detection systems are readily available via inexpensive platforms such as patterned paper, which facilitates on-site analysis.[40] These portable, low cost and user-friendly sensors function as an alternative to conventional analytical methods for point-of-care analysis and food quality control.[41, 43]

There is extensive literature that describes the application of screen-printed carbon electrodes (SPCE) as a portable electrochemical sensor platform for environmental monitoring as well as pharmaceutical and food quality control.[44-46] Miniaturized graphene oxide-ionic liquid based electrochemical devices have been demonstrated for the very sensitive electrochemical detection of a wide variety of electroactive targets of importance, spanning food analyses, environmental monitoring, and clinical diagnosis.[47]

Nanomaterials play a crucial role in the development of the electrochemical sensors for molecule sensing. These nanostructured materials possess the desirable properties necessary to improve the overall electrochemical oxidation/reduction, aid in increasing the sensitivity and also help mitigate the drawbacks associated with selective detection and issues related with interference molecules and co-existing molecules/ions in different food and beverage matrices. Figure 2.1

represents a schematic diagram of different types of nanomaterials that are broadly used for the analysis of preservatives and contaminants in food and beverages.

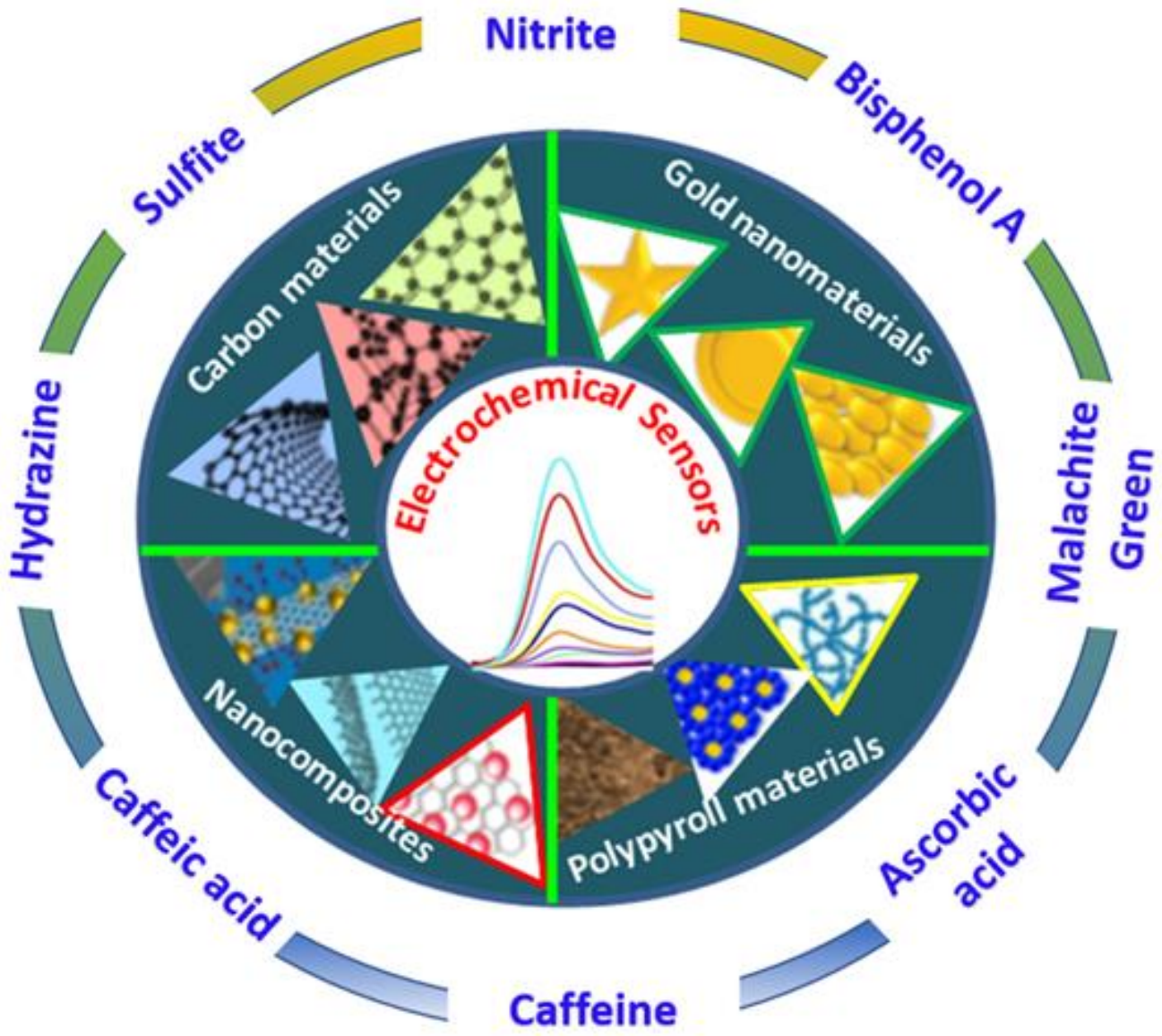

Figure 2.1 Schematic illustration of diverse types of nanomaterials for the electrochemical monitoring of different analytes in food and beverages.

2.3.1 Carbon-based nanomaterials

Since graphene was first characterized in 2004, a variety of graphene-based materials have been produced (e.g., electrochemically and chemically modified graphene) using various procedures.[48, 49] Graphene possesses attributes such as high conductivity, rapid heterogeneous electron transfer, and a large surface area, making it an ideal material for the electrochemical detection of a wide range of targeted molecules.[50-52] Chemically modified graphene and graphene-based materials have been employed for diverse applications owing to their superior analytical performance.[53-60] Graphene oxide (GO) is hydrophilic by nature and possesses the ability to disperse well in water as it holds hydrophilic functional groups (OH, COOH and epoxides) on the edge of the sheet and on the basal plane. Although, GO has lower conductivity in comparison to graphene, it is used as support material in biosensing applications.[61]

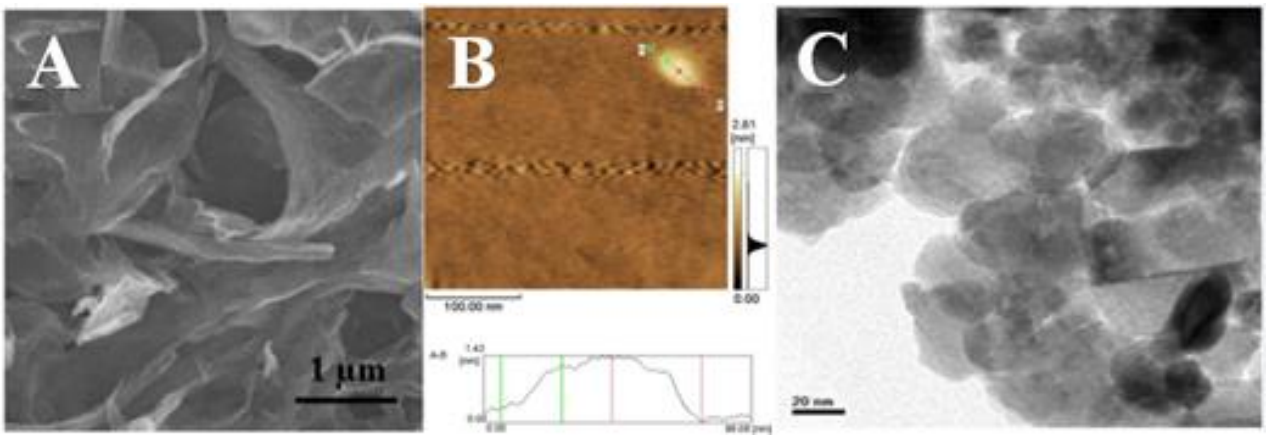

Figure 2.2. SEM image of K-doped graphene (A); AFM image of graphene sheets (B); and TEM image of nitrogen-doped graphene sheets (C). Adapted and reproduced with permission from ref. 64, ref. 127 and ref. 171, respectively.

Recently, an electrochemical sensor was reported based on fluorine doped graphene oxide for the detection of heavy metal ions Cd^{2+}, Pb^{2+}, Cu^{2+} and Hg^{2+}. Square wave anodic stripping

voltammetry was employed for the detection of the above-mentioned heavy metal ions. The contact between metal ions and the GCE surface should not be too strong or too weak for the stripping voltammetry technique. In comparison to GO, the F doped GO enables the formation of semi ionic C-F bond making the FGO/GCE a favorable platform for the accumulation of metal ions and for the stripping process. In addition, the presence of fluorine aided in enhancing the electrocatalytic activity. Li et al. developed a nafion-graphene composite film based electrochemical sensor for the detection of metal ions, Pb^{2+} and Cd^{2+}. The synergistic effect from graphene nanosheets and nafion promoted better sensitivity for the metal ion detections and also enhanced the anti-interference ability of the electrochemical sensor.[62, 63] Potassium was doped with graphene and was further used to modify a glassy carbon electrode (GCE), by Xiao-Rong et al., for the simultaneous determination of sulfite (SO_3^{2-}) in water under neutral conditions. It exhibited a linear response over the concentration range of from 2.5 μM to 10.3 mM, with a detection limit of 1.0 μM (S/N = 3) for SO_3^{2-}. The doping of graphene with K played a critical role in altering its electronic properties.[64]

A novel electrochemical sensor was developed based on hexadecyl trimethyl ammonium bromide (CTAB) functionalized graphene oxide (GO)/multiwalled carbon nanotubes (MWCNTs) (CTAB/GO/MWCNTs/GCE) for the simultaneous detection of ascorbic acid (AA) and nitrite. The amalgamation of GO and MWCNTs endowed the electrochemical sensor with high electrocatalytic activity, increased surface area, good stability and sensitivity. Moreover, the synergistic effect of the interaction between the functionalized CTAB, graphene oxide and MWCNTs provided the sensor with the capability to oxidize the molecules at less positive potentials with enhanced current response. The various beneficial properties of carbon based

materials may facilitate the selective oxidation and enhance the electrochemical activity toward oxidation of AA and nitrite in a simultaneous system.[65]

2.3.2 Gold based nanomaterials

Gold (Au) is one of the most popular materials that exhibit excellent catalytic and electrochemical properties. Since the emergence of gold nanoparticles, they have been employed for the fabrication of a wide array of sensors. From an electroanalytical standpoint, Au nanoparticles gained significant reputation due to its excellent conductivity, biological compatibility and high surface to volume ratio.

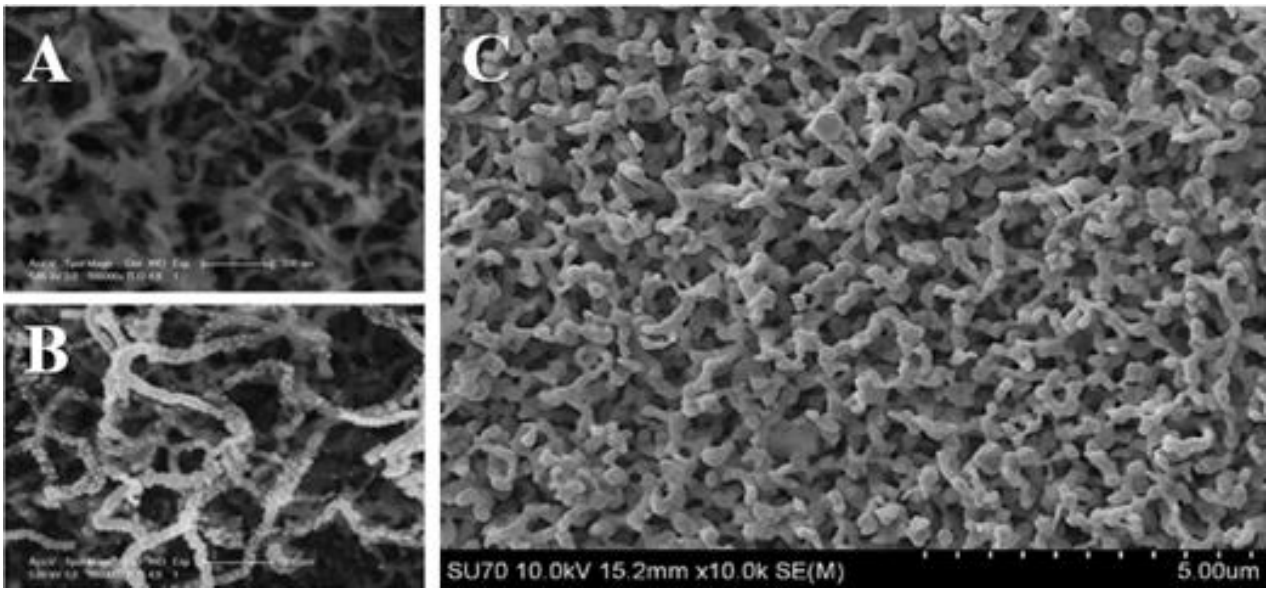

Figure 2.3. FE-SEM images of the polypyrrole nanowires (A) and the Au/polypyrrole (B), SEM image of the nanoporous gold microelectrode (C), Adapted and modified with permission from ref. 76 and ref. 77.

Methods such as surface-enhanced Raman spectroscopy, exploit gold nanoparticles as substrates to enable the measurement of the vibrational energies of chemical bonds. Further, in contrast to other materials, gold nanoparticles are dense, which renders them suitable as probes for

transmission electron microscopy.[66] Gold nanoparticles may be used for selective oxidation, or in certain cases, reduction. Gold nanoparticles have also been developed and tested for fuel cell applications.[67] This strategy could also be utilized for the label-free detection of proteins, pollutants, and other molecules. The inclusion of Au nanoparticles in nanomaterial synthesizing certainly revitalized the area of electrochemical sensors. Vast improvements have been made to the synthesis of Au nanoparticles for electrochemical sensing, however, researchers are faced with challenges, such as size control, morphology and monodisperse. The recent progress achieved in developing novel nanoporous Au material will play a key role in overcoming the aforementioned challenges. Hierarchical gold nanoporous material has been recently reported for biomedical applications.[68] Gold nanoparticles combined with 3D macroporous carbon structure for the sensitive detection of chlorogenic acid in therapeutic products.[69] Ali and co-workers fabricated a sensor for the qualitative detection of pork adulteration in meatballs.[70] Pascal et al. developed an electrochemical sensor using a gold microwire electrode for the simultaneous sensitive electrochemical detection of copper and mercury in seawater and dilute acid through the use of anodic stripping voltammetry.[71] Similarly, using a vibrating gold microwire electrode combined with stripping voltammetry, a rapid, reliable and low-cost sensor was developed by Soares and co-workers for the simultaneous electrochemical determination of arsenic, copper, mercury, and lead ions in freshwater.[72] Nanoporous gold prepared by alloying/dealloying method enhances the electrochemical sensing capability and increase the electrochemically active surface area of the gold nanostructure.[73]

Ding and co-workers prepared a nanoporous gold leaf by dealloying Au/Ag alloy in concentrated nitric acid medium. The resulting 3D nanostructured material consisted of ~3 layers of permeable pores and Au ligaments that facilitated the movement of small molecules within the

structural framework. The performance of the nanoporous gold leaf electrode exhibited excellent electrocatalytic behaviour toward nitrite oxidation. Also, the peak current obtained with nanoporous gold leaf electrode for the electrooxidation of nitrite was significantly higher in comparison to the glassy carbon electrode (GCE) and a planar gold electrode. The higher activity towards nitrite oxidation attributes to the increased surface area, high electron conductivity and high specific activity of the 3D nanoporous material. In addition, the presence of the several exposed Au sites on the radial curvature of the nanostructured material promoted to the higher specific activity of the nanoporous gold leaf.[74] Jia et al. developed a nanoporous gold electrode surface through a multicyclic electrochemical alloying/de-alloying processes in a "green" electrolyte that was composed of $ZnCl_2$ and benzyl alcohol. The resulting nanoporous gold film electrodes possessed an ultrahigh surface area and electrochemical activity coupled with excellent selectivity. This study provided a simplistic green route for the preparation of nanoporous metal film electrodes.[75]

Lin et al. reported on a novel electrochemical sensor that was fabricated via the electrodeposition of Au nanoparticles on polypyrrole (PPy) nanowires, which were coated onto a glassy carbon electrode (GCE) substrate. The Au nanoparticles were amalgamated with the pre-synthesized PPy nanowires and subsequently transformed into an Au nanoparticle-PPy matrix on the GCE. Figure 2.3B depicts FE-SEM images of the Au/PPy nanowire. The Au nanoparticles had a diameter of 15 nm and were aligned along the PPy nanowires. Further investigation of nanomaterial with XPS revealed an Au nanoparticle with face-centred cubic structure. The addition of PPy to the Au nanoparticle improved the electronic conductivity and enhanced the electron transfer rate.[76] Recently, nanoporous Au microelectrode was fabricated with good selectivity and high electrochemical active surface area. The nanoporous Au was prepared by

electrochemical alloying/dealloying method. The SEM image illustrates the nanoporous structure of the Au microelectrode (Figure 2.3C) and shows a definite 3D structure with pore sizes that vary between ~200.0 - 400.0 nm. The nanostructured material exhibited a high surface area and increased roughness. The 3D nanoporous structure played a significant role in enhancing the electrochemical sensing capabilities and improved selectivity toward the oxidation of hydrazine, sulfite and nitrite under simultaneous condition.[77]

2.3.3 Metal Nanocomposites

In order to enhance the electrochemical properties and sensitivity, as well as the selectivity of electrochemical sensors, metal oxides and their nanocomposites, are often synthesized by combining graphene-based materials, polymers such as polypyrrole, chitosan, PEDOT, and polystyrene. Infusing conductive polymer with metal-based nanomaterials significantly enhances the electrochemical catalytic activity, increases the specific surface area and mitigates the issue of selectivity toward the oxidation of desired molecules.[78-80]

An electrochemical sensor comprised of polypyrrole–chitosan–titanium dioxide (Ppy-CS-TiO_2) nanocomposite was developed for the detection of glucose. Interactions between the TiO_2 nanoparticles (NPs) and the conducting polymer resulted in enhanced current responses and improved the sensitivity toward the electro-oxidation of glucose.[81] Electrochemical sensors based on bimetallic Au-Pt/rGO nanocomposites, Au/Pt alloy and Au/rGO have also been reported. The combination of two metal nanoparticles and/or metal nanoparticles with carbon-based materials increases the overall electrochemical performance of the nanostructured material. The use of metallic nanocomposites and bimetallic nanostructures may vastly improve the electrochemical activity, sensitivity and selectivity towards the detection of compounds in food and beverage matrices. The improved electrochemical activity is associated with the increase in

surface area, synergistic effect of metal-metal and metal-graphene, increased availability of active sites.[82-84] Feng et al. fabricated worm-like Au–Pd nanostructures supported on rGO, which was based on a simple wet-chemical approach using polyethylene glycolmonooleyl ether (Brij-35) as a stabilizing agent.[85] The nanocrystals of this worm-like Au–Pd had an average width of 2.0 nm and length of 10.0 nm, and the nanocrystals were uniformly distributed and deposited on the surface of rGO. Peaks from the XRD pattern showed the efficient reduction of GO to rGO and revealed the development of single-phase Au-Pd alloy. Similarly, another bimetallic Au-Pd based composite nanomaterial was reported for the determination of caffeic acid (CA) by Thangavelu et al. The Au-Pd nanomaterial was electrochemically deposited on the graphene nanoflakes and was used for the sensitive determination of CA. The nanomaterial exhibited good electrocatalytic activity towards the oxidation of CA and possessed good sensitivity and a low detection limit of 6.0 nM. [86] Ghaedi and co-workers developed a modified material by combining gold nanoparticles with MWCNT using a carbon paste electrode as a substrate. The images generated by SEM revealed that the nanoparticles followed a randomly distributed pattern with a larger surface area. Further, the material combination displayed excellent electrocatalytic behaviour for the electrochemical oxidation of nitrite.[87] Using size-selected Pt nanoparticles, Wu et al. developed a metal nanocomposite by assembling these nanoparticles on a graphene surface. The TEM images in Figure 2.4 D reveal well distributed Pt nanoparticles on the surface of the graphene. The dimensions of the Pt nanoparticles were between 1.0 and 3.0 nm, whereas the size of the graphene was 750.0 nm. The composite electrode was employed for the electrochemical oxidation of ascorbic acid (AA), uric acid (UA), and dopamine (DA). This nanomaterial exhibited excellent distinguishing abilities through the provision of enhanced peak separation and large potential differences of 185 mV (AA-DA), 144 mV (DA-UA), and 329 mV (AA-UA) for the

electrochemical oxidation of the aforementioned analytes.[88] A novel electrochemical sensor, based on a Pt nanocomposite, was reported by Chen and co-workers for the electrochemical detection of α-Methylglyoxal.

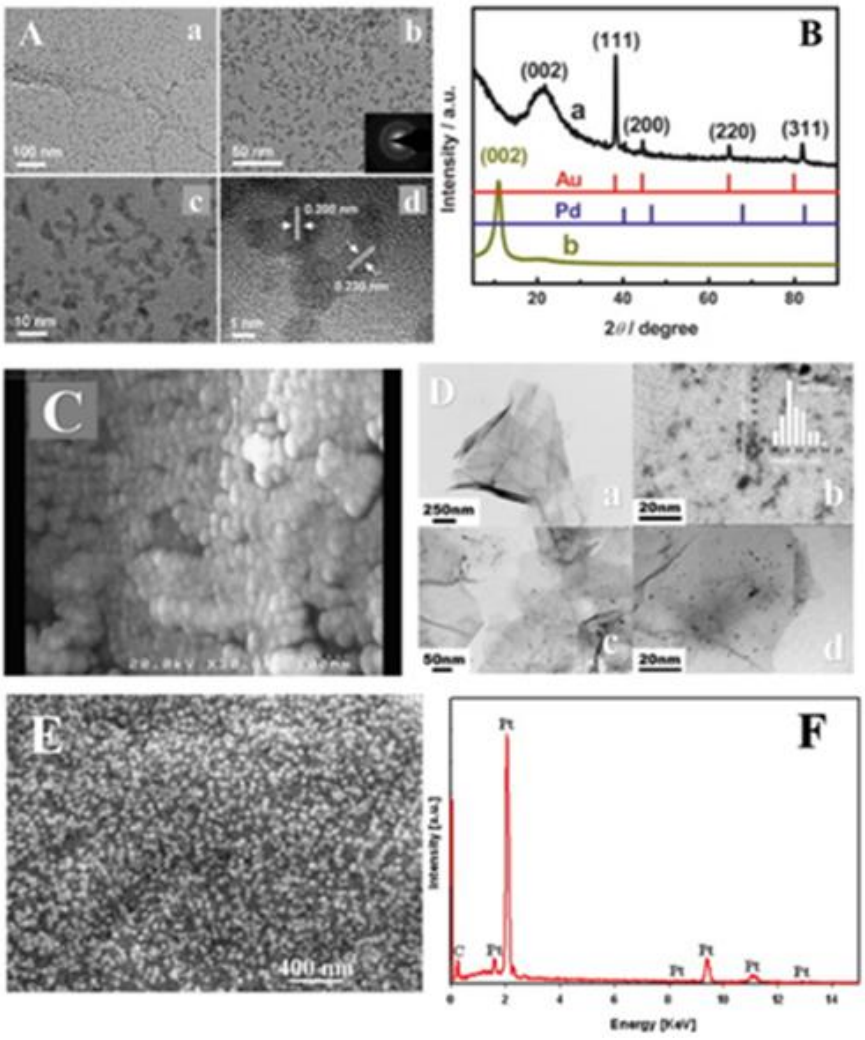

Figure 2.4. TEM (a, b) and HR-TEM (c, d) images of worm-like Au–Pd/RGO (A), XRD pattern of Au-Pd/RGO (B), SEM image of GNPs/MWCPE (C), (D) TEM images of (a) graphene, (b) Pt nanoparticles and (c and d) graphene/Pt nanocomposite under different magnifications, SEM image of Pt/SWCNT/GCE (E) and EDX pattern for Pt/SWCNT/GCE (F), Adapted and modified with permission from ref. 36, ref. 85, ref. 87 and ref. 88.

The platinum nanoparticles were deposited onto a GCE surface, which was coated with single-walled carbon nanotubes (SWCNTs). The FE-SEM image of the material revealed a uniformly distributed pattern of Pt nanoparticles on the SWCNT/GCE surface (Figure 2.4E).Further, the presence of Pt nanoparticles on SWCNT/GCE was confirmed by an EDS spectrum (Figure 2.4F). The sensor demonstrated good linearity in the increasing concentration range of from 0.1 - 100 μM, and a low detection limit of 2.8 nM. The sensor exhibited excellent sensitivity and selectivity and showed its ability to quantify α-Methylglyoxal in wine and beer samples.[36] Yegnaraman and co-workers reported an Au based nanocomposite material for the detection of AA, UA and DA. In this work, the authors addressed the challenges faced in detecting electroactive compounds in a mixture with improved selectivity. The nanocomposite film was synthesized by incorporating Au nanoparticles into the PEDOT polymer matrix and a thin film of the material was electrodeposited on the GCE. The modified electrode was able to detect AA, UA and DA simultaneously with superior selectivity and sensitivity. The PEDOT polymer matrix facilitated the catalytic oxidation of the three molecules with high selectivity and the formation of the Au nanoparticles within the nanofibrillar matrix allowed for high sensitivity and selectivity.[89]

2.4. Electrochemical sensors for the detection of food additives and contaminants

In view of the perpetual demand for processed foods and beverages, there are direct implications in regard to stringent demands for sustaining higher safety and quality standards. Along with the present quality control guidelines, novel approaches must be implemented to meet the requirements for maintaining and improving the safety and quality standards of food and beverages. Electrochemical sensors may serve as alternatives to conventional methods; thus, bettering portability and rapid response, also negate the requirement of highly skilled operators. The development of these sensors for the determination of different molecules in numerous food

matrices would be very beneficial. Electroanalytical techniques coupled with various nanomaterials based electrochemical sensors offer direct and efficient methods for the detection of food contaminants such as hydrazine, malachite green, bisphenol A, and some of the commonly used preservatives such as caffeic acid, caffeine, ascorbic acid, sulphite, and nitrite.

2.4.1 Hydrazine

Hydrazine (N_2H_4) and its products are commonly used in the manufacture of pesticides, chemical blowing agents, intermediates in pharmaceutical drugs, and for corrosion control in hot water heating systems in boiler water treatment systems.[90] The entry of N_2H_4 and its derivatives into the ambient environment is due to its usage and applications in aerospace fuels, explosives, and industrial chemicals.[91] N_2H_4 may readily be absorbed into the human body via oral ingestion, transdermal, or inhalation routes. Further, as N_2H_4 is lethal and volatile in nature, it may have detrimental effects on organs such as the kidneys, liver, and brain.[92] The Environmental Protection Agency (EPA) has designated N_2H_4 as a cancer-causing compound; hence, it is a major consideration for the International Agency for Research on Cancer (IARC).[93] The risk level of minimal N_2H_4 inhalation has been established to be 0.004 μg/ml.[64]

The National Institute for Occupational Safety and Health has a strict level for N_2H_4 that is permitted in the workplace atmosphere, which must not exceed 0.03 μg/mL when it is continuously measured over a two-hour period.[94] Due to the toxicological nature of hydrazine compounds, sensitive and reliable analytical techniques are required for the determination of N_2H_4. Nahid et al. have reported on a sensitive and selective electrochemical sensor for the determination of hydrazine through the use of a modified carbon nanotube paste electrode.[95] The fabricated electrode showed good electrocatalytic capability for the electrochemical oxidization of N_2H_4. This electrochemical sensor possessed a wide linear range of from 0.6 - 900.0 μM, and a low

detection limit of 0.13 μM. This selective sensor also demonstrated the precise determination of N_2H_4 in water samples. In other work, Lin and co-workers prepared an electrochemical sensor (Au/PPy) for the sensitive and selective

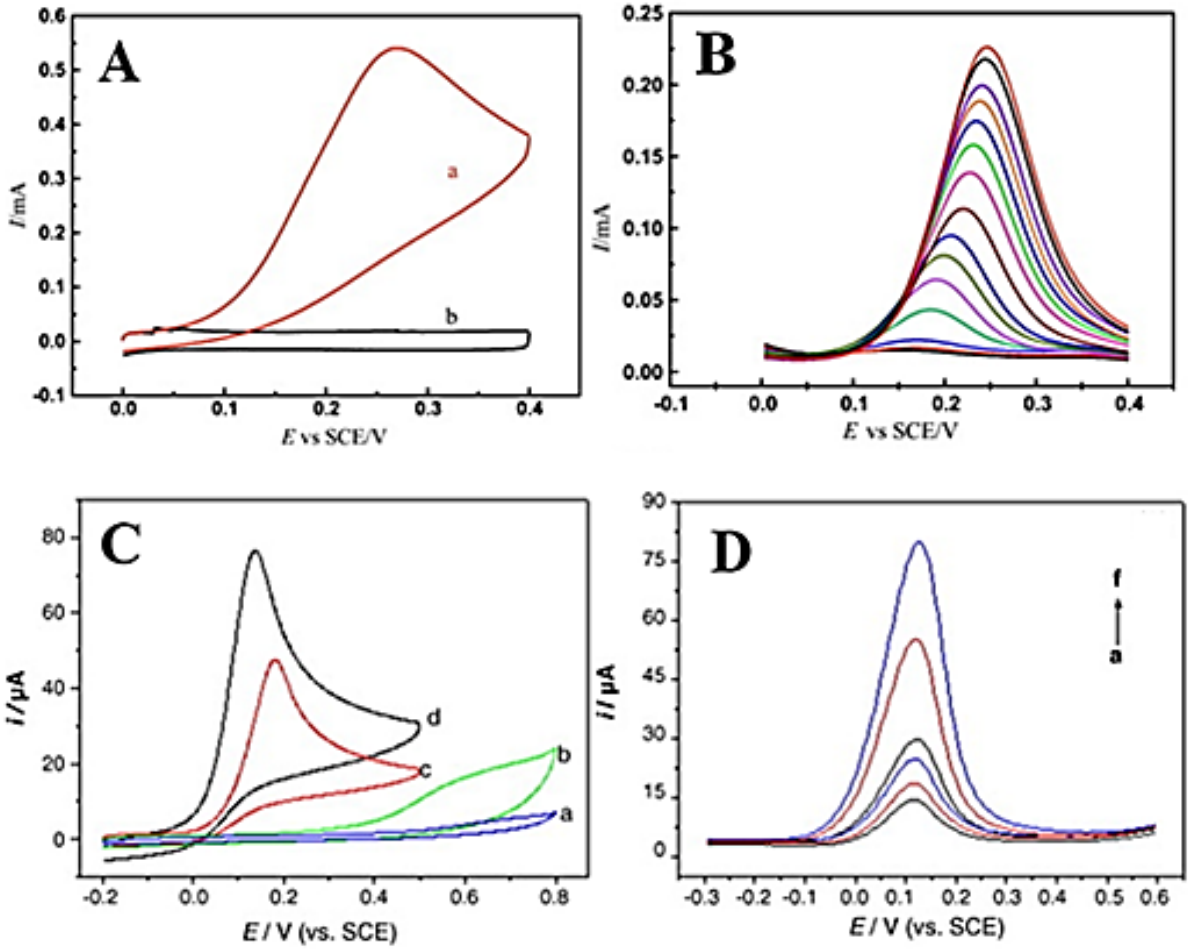

Figure 2.5. (A) DPVs of 0.5 M H_2SO_4 containing various concentrations of N_2H_4 at the Pd/MWNT–Nafion modified electrode; (B) CVs of 5.0×10^{-4} M N_2H_4 in 0.1 M PBS (pH 7.0, scan rate 50 mV s−1) at bare GCE (a), PPy/GCE (b), Au/GCE (c) and Au/PPy/GCE (d); (D) DPV responses for the increasing concentration of hydrazine, Adapted and modified with permission from ref. 76 and ref. 97.

detection of hydrazine. The CV revealed a well-defined and sharp peak for the oxidation of N_2H_4 (Figure. 2.5A). The oxidation peak potential for N_2H_4 occurred at 135 mV, which is useful for practical applicability, as there is less chance of interference from other compounds.

$$N_2H_5^+ \rightarrow N_2\,(g) + 5H^+ + 4e^-$$

The reaction mechanism for the electro-oxidation of hydrazine at the Au/PPy/GCE is a $4e^-$ process. Figure 2.5B shows the DPV responses to different concentrations of N_2H_4 with a linear calibration range of from 0.0010 - 0.50 mM. The developed hydrazine sensor had excellent sensitivity, good analytical reproducibility, and a detection limit of 0.20 μM. The improved electrochemical activity is attributed to high surface area of the nanomaterial, higher electron transfer rate due to the PPy nanowires and the electrocatalytic ability of Au nanoparticles.[76] Lu et al. used the complexing-reduction method, whereby a complex is formed by combining Pd nanoparticles and ethylenediamine-tetramethylenephosphonic (EDTMP) acid to produce an EDTMP-Pd complex. This catalyst was further modified by adding multiwall carbon nanotubes to form Pd/MWNTs, which was used as the sensor material. The CV depicted in Figure 2.5C exhibited higher activity for the oxidation of hydrazine in an acidic electrolyte solution. Furthermore, the responses from DPV showed a steady increase in the oxidation peak current with the subsequent addition of N_2H_4 (Figure 2.5D). The Pd/MWNT sensor exhibited good linearity across a broad calibration range of from 2.5 – 700.0 μM and had a low detection limit of 1.0 μM.[96]

2.4.2 Malachite green

Malachite green (MG), a byproduct of triphenylmethane, is used in the dyeing industry. It is notably used in the food industry and aquaculture due to its antifungal, antimicrobial and antiparasitic properties. By law, the use of MG is forbidden in the United States, China, Canada

and several other countries. Yet, the illegal use of MG in the aquafarming industry is still in practice owing to its low price and high effectiveness against fungus and bacteria.[97] However, toxicological tests and scientific investigations uncovered the presence of MG in the tissues of edible fish for a longer duration.[98] Due to the carcinogenic and mutagenic nature of MG, consuming such contaminated fish possess a health risk to human beings.[99] Presence of MG is

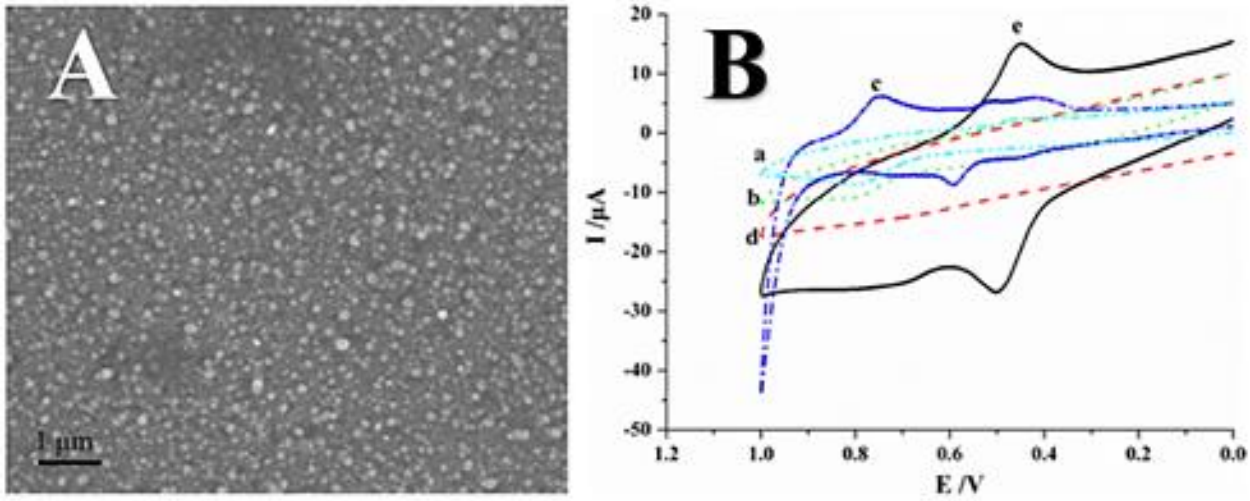

Figure 2.6. SEM image of the graphene-QDs/Au-NPs (A), CVs of MG oxidation at different electrode, bare GCE (a), graphene-QDs/GCE (b), Au-NPs/GCE (c), and graphene-QDs/Au-NPs /GCE; curve (d) and curves (a, b, c and e) shows the response in the absence and in presence of 4.0×10^{-5} mol L−1 MG, respectively in a 0.05 M H_2SO_4 buffer solution. Adapted and modified with permission from ref. 106

analyzed using conventional instruments such as HPLC-MS, surface enhanced Raman spectroscopy (SERS) and spectrophotometry due to their sensitivity and efficiency.[100-102] However, they might not particularly be applicable for on-site testing. Therefore, it is imperative to develop low-cost electrochemical sensors for the sensitive and selective determination of MG. Muresan et al. reported an electrochemical sensor for the detection of MG using CeO_2 and nafion.

The sensor exhibited good sensitivity and selectivity toward MG oxidation and exhibited good stability for 50 successive CV cycles and had a low detection limit of 3.20 μM. Also, the developed CeO_2-nafion sensor demonstrated its capability to detect MG in commercial biocide products.[103] Huang and co-workers developed a highly selective electrochemical sensor for the detection of MG utilizing MWCNT and dihexadecyl hydrogen phosphate (DHP), a special surfactant. The MWCNT-DHP modified electrode facilitated the electron transfer by decreasing the overpotential and enhanced the peak current obtained for the oxidation of MG. The electrode retained 90% of its initial peak current response for the oxidation of MG in the presence of a 200-fold concentration of ascorbic acid, caffeine, vitamin E and dopamine. Thus, proving the modified film electrode is very selective toward the determination of MG. In addition, the electrode exhibited excellent long-term stability for a period of 21 days, with a decrease of only 6.2 % from the initial value. The practical applicability of the electrochemical sensor to detect MG in fish samples yielded effective results, which was in consensus with the results from HPLC method.[97] In another work, hidayah and co-workers reported an electrochemical biosensor for the detection of MG using carbon paste electrode by immobilizing butyrylcholinesterase enzyme (BuChE) onto polypyrrole. The amperometric technique was utilized to determine the total MG content. The enzyme-modified electrochemical biosensor offered higher sensitivity, selectivity and successfully detected the presence of MG in tilapia fish. The sensor displayed good linearity over the wide concentration range from 0.00068 to 0.027 μM with a LOD limit at 0.00068 μM.[104] Wang and co-workers designed an electrochemical sensor based on graphene quantum dots/Au nanoparticles/GCE to quantify MG in salmon. Figure 6A shows the SEM image of graphene-QDs/Au-NPs multilayers. The surface morphological study revealed the uniformly dispersed quantum dots (10 - 15 nm in diameter) over the primarily distributed Au nanoparticles (150 - 300 nm in diameter). The

modification with graphene quantum dots and Au nanoparticle increased the electrochemical active surface area (EASA) of the GCE 4 times higher. The synergistic effect of quantum dots/Au nanoparticles decreased the peak potential to a less positive side (at 0.502 V) for the oxidation of MG and amplified the peak current obtained (Figure 2.6B, curve e). More notably, the absence of redox peak at the quantum dots/Au nanoparticle/GCE alludes the modified electrode's electrochemical inoperativeness within the particular potential window.[105]

2.4.3 Bisphenol A

Bisphenol A (2,2-bis-(4-hydroxyphenyl)-propane, BPA) is an important industrial compound used in the manufacturing of epoxy resins, plastic water bottles, and polycarbonate materials.[106,107] BPA is a xenobiotic and an endocrine disruptor that has the ability to mirror the function of androgen hormones and poses severe health risk to humans, such as brain damage, fertility issues and prostate cancer.[108] Also, it is catalogued as a non-biodegradable compound with high chemical resistance.[109] Analytical techniques such as high-performance liquid chromatography (HPLC), liquid chromatography-mass spectrometry (LC-MS), and gas chromatography-mass spectrometry (GC-MS) are used for the determination and quantification of BPA.[110-112] However, these expensive instruments demand long hours of analytical procedures, skilled personnel and strenuous sample preparation protocols. In this milieu, developing sensors for the electrochemical detection of BPA presents an inexpensive alternate route with the benefits of quick response time, simple operating procedure and real-time sensing. BPA is an electrochemically active molecule; however conventional unmodified electrodes yield sluggish response toward its oxidation. Therefore, it is of monumental importance to developing novel nanostructured materials with high surface area, excellent catalytic activity and stability for the electrochemical sensing of BPA. Several research articles are published based on several

nanostructured materials for the electrochemical detection of BPA. Spinelli et al. prepared a novel nanomaterial using ferro-ferric oxide nanoparticles (Fe_3O_4-NPs) and Au nanoparticles (Au-NPs). They fabricated the nanomaterial by stabilizing the Fe_3O_4-NPs and Au-NPs in a 3-n-propyl-4-picolinium silsesquioxane chloride polymer ($Si4Pic^+Cl^-$). The GCE was modified with the as-prepared nanomaterial (Fe_3O_4- $Si4Pic^+Cl^-$/Au-NPs-$Si4Pic^+Cl^-$/GCE).

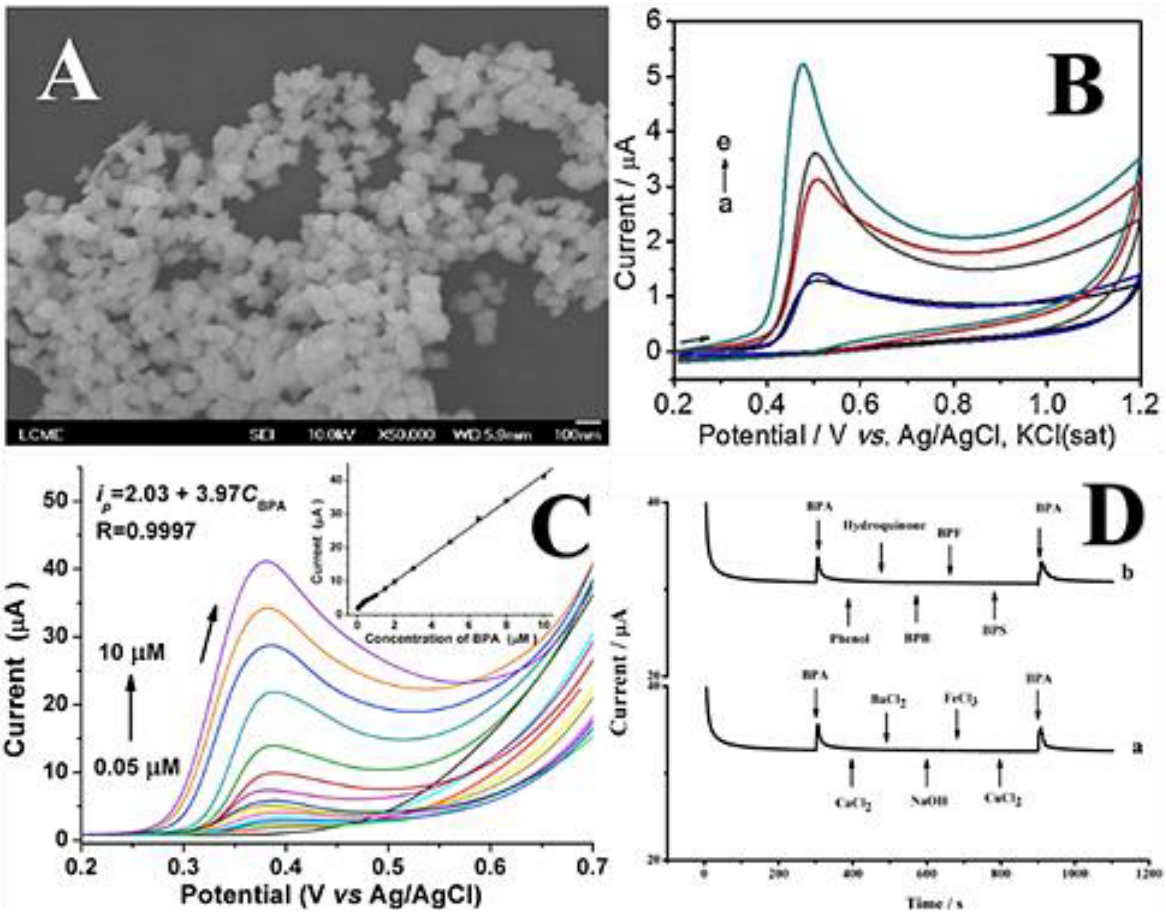

Figure 2.7. SEM image of Fe_3O_4-$Si4Pic^+Cl^-$/Au-NPs-$Si4Pic^+Cl^-$ (A), CVs for the oxidation of 10 μmol L^{-1} BPA at (a) bare GCE, (b) $Si4Pic^+Cl^-$/GCE, (c) Au NPs-$Si4Pic^+Cl^-$/GCE (d) Fe_3O_4 NPs-$Si4Pic^+Cl^-$/GCE, and (e) Fe_3O_4-$Si4Pic^+Cl^-$/Au-NPs-$Si4Pic^+Cl^-$/GCE, scan rate of 100 mV s^{-1} in BR buffer pH 9.0 (B), DPVs of BPA oxidation in increasing concentration (0.05 μM - 10 μM) at Au-Pd NPs/GNs-GCE in 0.1 M PBS, pH 7.5; the calibration plot is shown in the inset (C),

The amperometric responses of BPA oxidation at the Cu_2O/rGO/GCE modified electrode in presence of interference compounds (D), Adapted and modified with permission from ref. [113], ref. [114] and ref. [115]

The SEM investigation revealed that the nanoparticle was consistently distributed in the polymer structure (Figure. 2.7A). The developed electrochemical sensor was utilized for the analytical detection of BPA. The CV studies revealed a well-defined peak for the oxidation of BPA. The electrochemical reaction for the oxidation of BPA at the Fe3O4-Si4Pic$^+$Cl$^-$/Au-NPs-Si4Pic$^+$Cl$^-$/GCE is an irreversible process. The peak current for the oxidation of BPA is 4 times higher in comparison with the bare GCE (Figure 2.7B). The increased anodic current response for the oxidation of BPA arises from the high active surface area and the high conductivity imparted by Fe_3O_4-NPs and Au-NPs. The analytical performance of the electrochemical sensor tested using DPV revealed a detection limit of 7.0 nmol L^{-1} in the increasing linear range of 20.0 to 1400.0 nmol L^{-1} and yielded good recovery rates with real sample testing (90 - 120 %). Furthermore, the electrochemical sensor exhibited high precision, excellent sensitivity, selectivity and long-term stability. The synergistic effect of Fe_3O_4-NPs/Au-NPs played a significant role in enhancing the catalytic activity and electrochemical sensing ability toward the detection of BPA.[113]

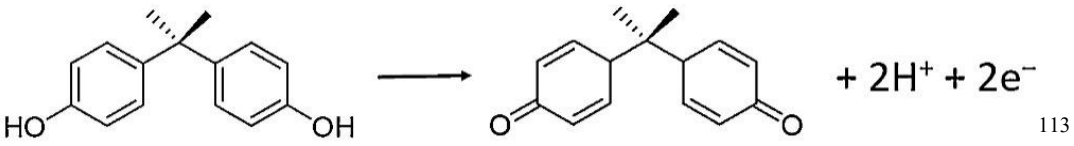

[113]

Chen and co-workers developed an electrochemical sensor using bimetallic nanoparticles and a carbon material for the electrochemical sensing of BPA. They loaded the graphene nanosheets with gold-palladium nanoparticles (Au-Pd NPs/GNs/GCE). The electrochemical characterization performed by CV elucidated that the electro-oxidation of BPA at the Au-Pd

NPs/GNs/GCE sensor occurred in two stages; (i) BPA is adsorbed onto the surface of nanostructured material because of the GNs excellent capacity for adsorption; (ii) the superior electrochemical activity of Au-Pd NPs elector-oxidizes the BPA adsorbed onto the surface. The GCE modified with Au-Pd NPs/GNs showed enhanced peak current response for BPA oxidation. The increased oxidation response is associated with the large electroactive surface area and high conductivity. The modification of the GCE improved the direct electron transfer for BPA oxidation at the electrode and lowered the oxidation peak potential. The analytical performance was tested using DPV by constructing a linear concentration curve for the BPA oxidation in the range of 0.05 μM to 10.0 μM (Figure 7C). The calibration curve showed a linear trend in each addition of BPA (R^2 = 0.997) and a LOD value of 8.0 nm. In addition, the electrochemical sensor unveiled high accuracy with real sample testing and had good stability. The combined advantages such as the high specific surface area of the nanomaterial, exceptional electron conductivity of GNs and the synergistic effect of Au and Pd played a significant role in enhancing the sensing capabilities of Au-Pd NPs/GNs/GCE sensor.[114]

In another work, Zhao et al. reported on a Cuprous oxide-reduced graphene oxide (Cu_2O/rGO) based electrochemical sensor for the determination of BPA. The synthesized Cu_2O/GO nanocomposite was coated on the GCE surface and electrochemically reduced to from Cu_2O/rGO/GCE. The electrochemical measurements performed using CV showed that the nanocomposite material oxidized BPA with higher peak current. The prepared nanocomposite material had a high surface area, improved conductivity and enhanced electron transfer rate between the modified electrode and BPA. Moreover, the linear relationship between peak current and increasing concentration yielded a linear trend for the selected concentration range (0.1 μmol L^{-1} to 80.0 μmol L^{-1}, R^2 = 0.998, LOD = 0.085 μmol L^{-1}). The amperometric measurement proved

the Cu_2O/rGO/GCE sensor's superior selectivity toward the oxidation of BPA in presence of interference molecules (Figure 2.7D). The excellent electrochemical activity of the fabricated sensor could be attributed to the synergistic effect Cu_2O-rGO, high conductivity of graphene and electrocatalytic properties of Cu_2O.[115]

2.4.4 Caffeic acid

Caffeic acid (CA, 3, 4-dihydroxycinnamic acid) is one of the most important compounds in the classification of phenolic acids. CA is commonly found in red wines, cloves, coffee, star anise, olive oil, as well as some vegetables and fruits. It has several pharmacological functions as it exhibits antioxidant, anti-inflammatory, antibacterial, and immune-modulatory properties.[116] Interestingly, some studies have reported that CA acts as an anti-tumour agent, while other reports showed that CA has carcinogenic effects.[117-119] Numerous methods for the determination of phenolic compounds and acids are available; however, the fabrication of electrochemical sensors for the quantitative detection of CA is necessary.[120,121] Santos and co-workers fabricated an electrochemical sensor by modifying a GCE with a poly(glutamic acid) (PG) film for the electrochemical detection and quantification of CA in red wine.[122] The chemically reduced graphene oxide sensor reported for the determination of CA oxidation showed good sensitivity and selectivity with minimal interference and high reproducibility.[123] Further, an electrochemical biosensor was prepared by Fernandes et al. for the detection and quantification of CA in white wine. This complex biosensor constructed by immobilizing green beans in the chitin matrix was incorporated into a carbon paste electrode. The caffeic acid content of white wine was investigated using square-wave voltammetry, where the biosensor showed high selectivity and long-term stability.[124] Glassy polymeric carbon electrodes modified with an electroactive poly(caffeic acid) film was used for the detection of CA in red wine.[125]

Chen H-A et al. recently developed a sensor based on the modification of GCE with nitrogen-doped carbon (NDC). From the cyclic voltammetric investigation, the redox peak current obtained with NDC/GCE was significantly higher than that of GO/GCE and bare GCE (Figure

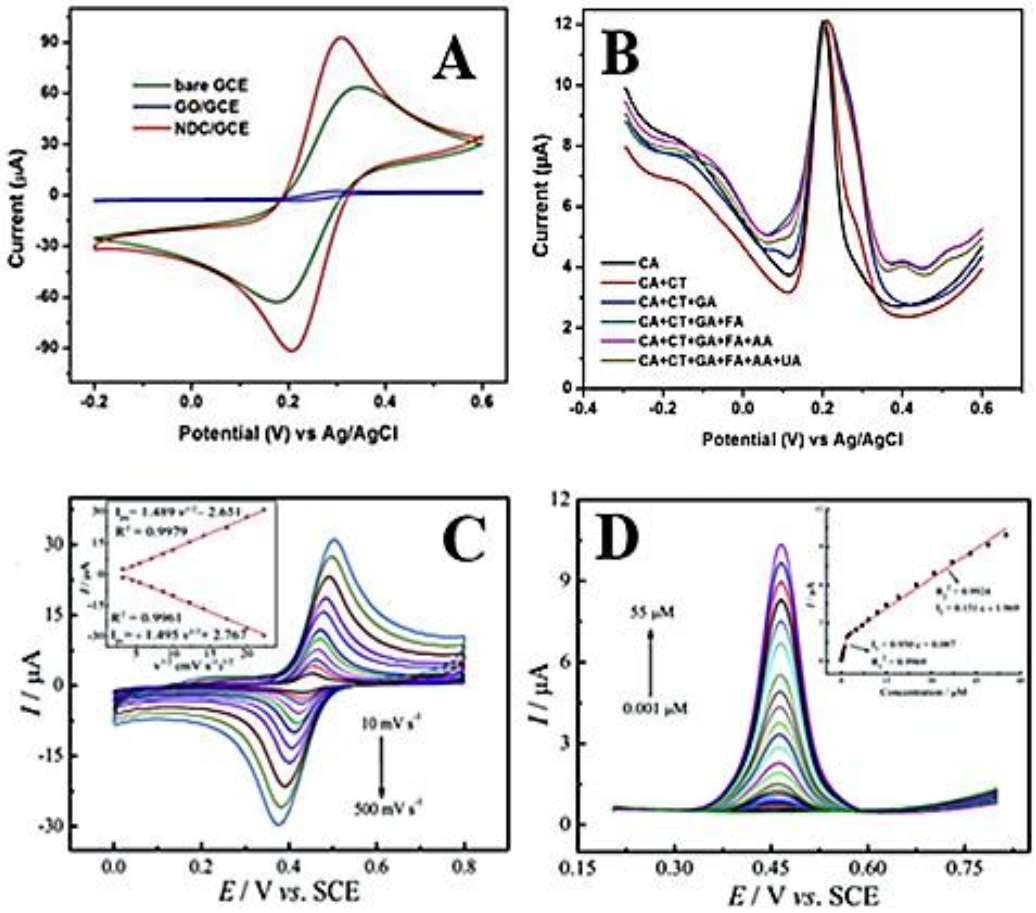

Figure 2.8. CV responses of bare GCE, GO/GCE, and NDC/GCE for the oxidation of 5 mM $[Fe(CN)_6]^{3-/4-}$ in 0.1 M KCl (A), DPV responses of NDC/GCE toward CA oxidation in presence of interference molecules 0.05 M PB solution (B), CV responses of Pd–Au/PEDOT/rGO/GCE at different scan rates of 10.0 - 500.0 mV s−1 in a BR buffer, at pH 3.0 (C), DPV responses of Pd–Au/PEDOT/rGO/GCE to subsequent additions of CA (0.001 - 55.0 μm) in a BR buffer, at pH 3.0 (D), Adapted and modified with permission from references. Adapted and modified with permission from ref. 127 and ref. 128.

2.8A). The NDC enhanced the electrocatalytic activity of the sensor for the oxidation of CA, which indicated the presence of electroactive functional groups. The oxidation of CA to O-quinone followed a 2-electron process.

$$C_9H_8O_4\ (CA) \rightarrow C_6H_4O_2\ (O\text{-quinone}) + 2H^+ + 2e^-$$

The electrochemical NDC/GCE sensor demonstrated good linearity over the wider calibration range of from 0.01 - 350 μM and a very low detection limit of 0.0024 μM for CA detection.[126] Yue and co-workers fabricated an electrochemical sensor for the determination of CA using Pd-Au/PEDOT/graphene nanoparticles. The presence of Pd/Au nanostructures enhanced the electrocatalytic activity and increased the surface area of the material for the electrochemical oxidation of caffeic acid. This sensor exhibited excellent sensing capabilities for the detection of CA. Figure. 2.8D illustrates the relationship between the concentration of, and the current from, CA oxidation, which was studied by employing DPV with a wider linear range of from 0.001 - 55 μM, and a lower detection limit of 0.37 nm. The excellent electrochemical sensing ability is attributed to the synergistic effect of Pd-Au interaction, high conductivity of graphene nanoparticles which promoted towards the sensitive determination of CA at the Pd-Au/PEDOT/graphene sensor.[127]

2.4.5 Caffeine

Caffeine (3,7-dihydro-1,3,7-trimethyl-1H-purine-2,6-dione, or 1,3,7-trimethylxanthine) is an active alkaloid component, which is present with other trace purines that are primarily found in cola nuts, cocoa beans, tea leaves, yerbamate, and guarana berries.[128] Caffeine is one of the most prevalent molecules that is present in a variety of teas, coffee-based beverages, and as an additive

in many energy and soft drinks. Studies also suggested that excessive caffeine consumption could be detrimental to the human body and can lead to headache, anxiety, stress, and an increased heart

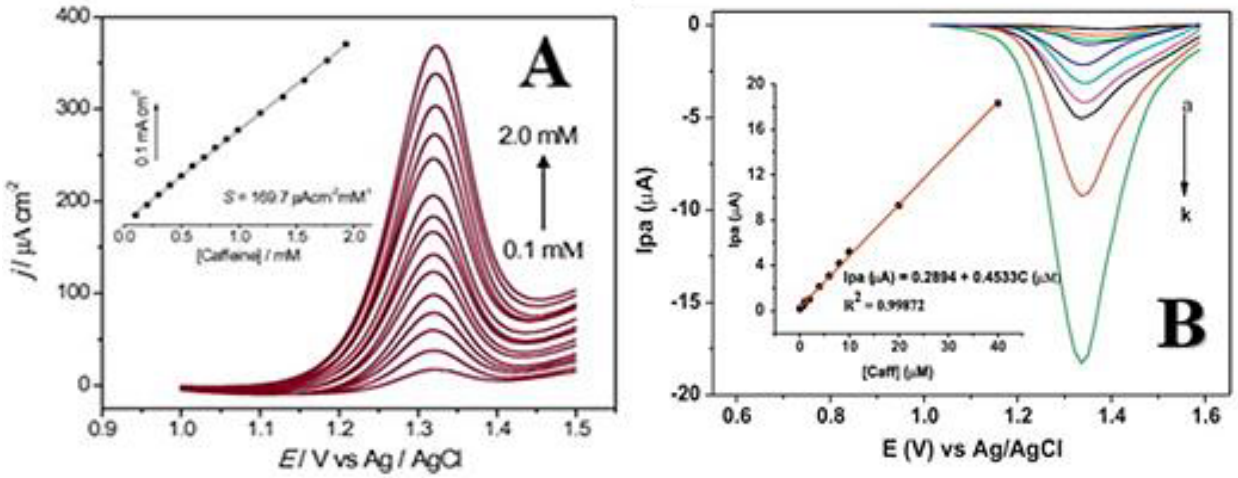

Figure 2.9. DPVs at PEDOT/MWCNT/Nafion/GCE for increasing concentrations of caffeine in the range of 0.1 - 2.0 mM in 0.1 M NaPBS (A), SWV responses of poly(AHNSA) with increasing concentrations of caffeine from 0.06 - 40.0 µm (B), Adapted and modified with permission from ref. 134 and ref. 135.

rate.[129] Although some drugs contain caffeine, due to the lack of substantiation of caffeine's negative effects, it is still used in the pharmacological preparation of painkillers.[130] Among the available conventional methods for the quantitative analysis of caffeine, chromatography-based techniques are beneficial. Nevertheless, chromatographic techniques are labour intensive and require multiple steps for sample preparation.[131,132] Recently, Curulli et al. proposed a facile electrochemical sensor for the detection of caffeine using gold nanoparticles (AuNPs). This hybrid nanocomposite film was synthesized using chitosan, which was reduced in the presence of oxalic acid to form chitosan-stabilized AuNPs. The reported sensor had a wider detection range of 5.0 µM to 50.0 mM, with a detection limit of 1.0 µM. The analytical evaluation performance revealed the sensor's ability to detect caffeine in tea, as well as carbonated and energy drink samples. The

results of testing with commercial samples showed that the obtained values were in close agreement with the results of HPLC-PDA. The 3D network of AuNPs formed within the chitosan matrix facilitated an efficient electron transfer ability, enhanced electrical conductivity, and increased selectivity.[33] An additional electrochemical sensor has been fabricated for the detection of caffeine through the electropolymerization of 4-Amino-3-hydroxynaphthalene sulfonic acid (AHNSA) on a GCE. Figure 2.9C shows the SWV curve, which reveals an enhanced current response for the polymer-modified electrode in contrast to the unmodified GCE for the oxidation of CA. The relationship between the increasing concentration of CA and its corresponding current response was investigated by subsequent addition, where the linear range for CA was 0.06 - 40.0 μM and the LOD was 0.067 μM. This sensor showed excellent responses to the spiked caffeine samples.[133] Brett et al. developed an electrochemical sensor that was based on multi-walled carbon nanotubes (MWCNTs) for the determination of caffeine in commercial beverages. The reported sensor had excellent sensitivity, with a very low detection limit of 38.0 nm, and a wide linear range. The results from testing with actual off-the-shelf samples also exhibited the sensor's amenability for commercial use.[134]

2.4.6 Ascorbic Acid

Ascorbic acid (AA) is known for its reductive properties, which is readily oxidable to dehydroascorbic acid. It acts as a powerful antioxidant, which fights against free-radical induced diseases, and plays a crucial role in the development and repair of collagen.[135] Despite such advantageous properties, high levels of AA in the human body may lead to gastric irritation and the formation of kidney stones.[136] AA can easily be altered when exposed to excessive heat, light, and atmospheric oxygen.[137] Thus, AA may be employed as a quality indicator that requires careful monitoring. There are sophisticated mainstream techniques for the determination of AA; however,

they require long hours for sample quantification, specific expertise, and in-depth knowledge of the operation of instrumentation. These factors have spurred the development of electrochemical

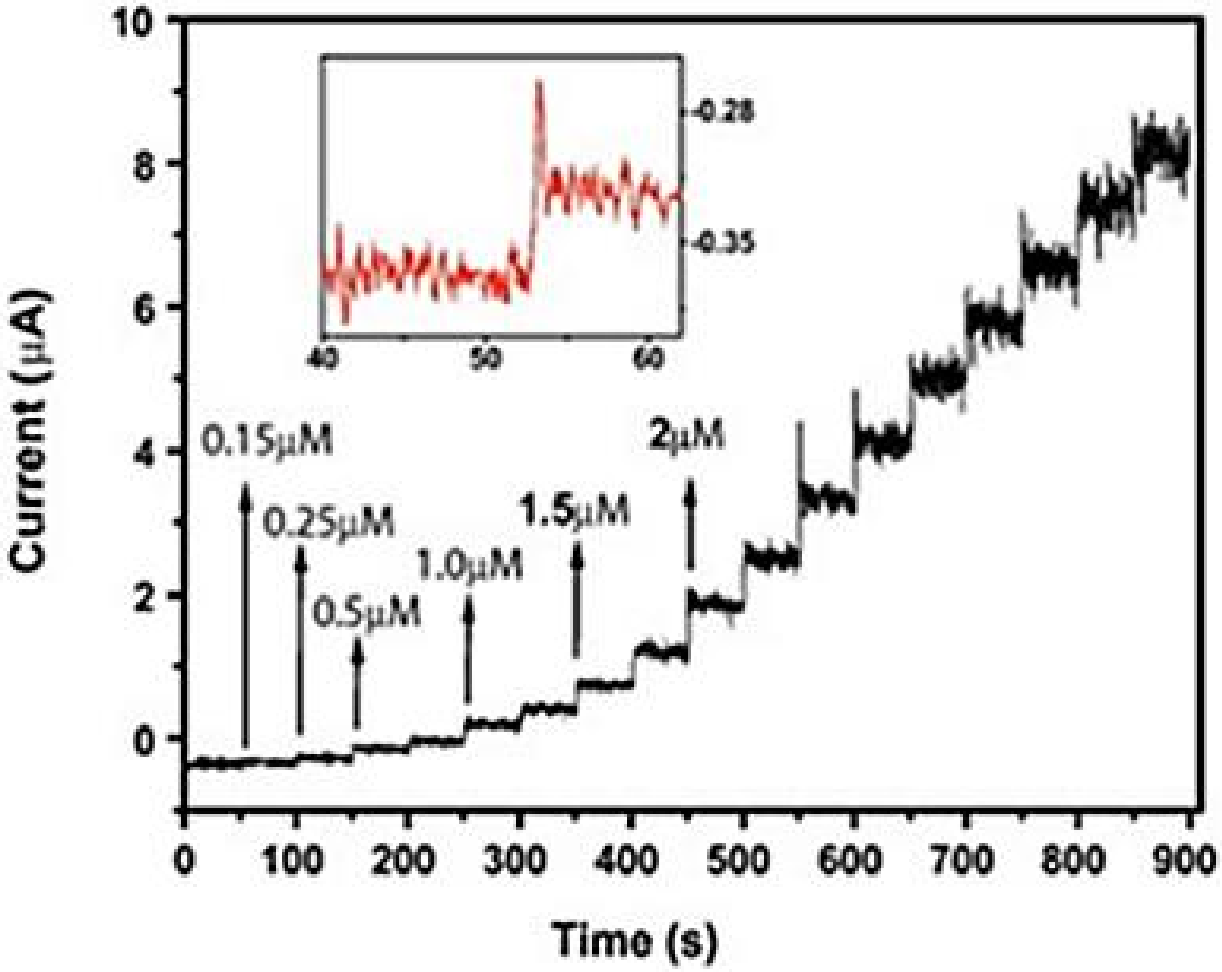

Figure 2.10. Amperometric responses of the graphene/Pt-modified GC electrode for different ascorbic acid concentrations (0.15 - 34.40 μM), Adapted and modified with permission from ref. 88.

sensors for the detection AA. Li et al. developed an electrode that was based on hexadecyl trimethyl ammonium bromide (CTAB) functionalized graphene oxide (GO)/MWNTs. The GCE was modified with the as-prepared material (CTAB-GO/MWNT), which was incorporated as a novel system for the determination of AA. The sensor exhibited good linearity over the increasing

concentration range from 5.0 - 300.0 μM with a detection limit of 1.0 μM.[65] A novel electrochemical sensor was reported using graphene/Pt nanoparticle nanocomposite for the electrochemical determination of AA. The CV responses for the graphene/Pt electrochemical sensor revealed a higher peak current for the oxidation of AA with the lowest onset potential (Figure 2.10). This sensor showed excellent performance in terms of peak potential with a low detection limit of 0.15 μM, and a calibration range between 0.15 - 34.40 μM. The presence of graphene aided in the uniform distribution of Pt nanoparticles and enhancing their electro-catalytic properties.[88] Moreover, stable and sensitive amperometric sensors have been reported for the detection of AA in commercial juice samples.[138,139]

2.4.7 Sulfite

Sulfite (SO_3^{2-}) is known for its excellent reducing properties and has played a pivotal role as a food additive for several decades.[140] It is primarily employed by the food industry for the prevention of oxidative deterioration and bacterial growth in foods and beverages during their production and plays a significant role in increasing the shelf life of these products.[141] Some of the common SO_3^{2-} containing foods are wine, alcoholic and non-alcoholic beer and cider, as well as bottled juices and concentrates.[142] Unfortunately, many people have an allergic reaction to SO_3^{2-}, which ranges from mild to severe, due to probable toxic and harmful effects that are associated with it. According to the FDA, it is compulsory for manufacturers to display caution labels on any food or beverage packaging that contains SO_3^{2-} of 10 ppm and above.[143,144] The excessive intake of SO_3^{2-} may cause headaches, nausea, and asthma.[145] Therefore, it is necessary to incorporate electrochemical sensors for the robust and precise quantification of sulfites in food and beverages. Recently, Chen et al. fabricated an electrochemical sensor based on the nanoporous gold microelectrode for the detection of SO_3^{2-}. The DPV measurements revealed the peak potential at

~0.30 V for the SO_3^{2-} oxidation. The SO_3^{2-} molecule was oxidized to SO_4^{2-} at the nanoporous gold sensor. The anodic reaction for the SO_3^{2-} oxidation is as follows:

$$SO_3^{2-} + H_2O \rightarrow SO_4^{2-} + 2H^+ + 2e^-$$

The electroanalytical performance of the sensor was tested by constructing a linear calibration curve, in the range of 5.0 μM to 4000.0 μM. Figure. 2.11A shows that peak current for SO_3^{2-} oxidation increased with subsequent increase in SO_3^{2-} concentration with an R^2 value of 0.995 and an LOD value of 0.3 μM. The electrochemical sensor exhibited good sensitivity, selectivity and stability. The sensor demonstrated good anti-interference ability and detected the presence of SO_3^{2-} in alcoholic beverages. The nanoporous structure on the surface allowed the movement of molecules through the pores and promoted toward the enhance peak current for the electro-oxidation of SO_3^{2-}.[77] Santos and co-workers fabricated a sensor using carbon-paste electrode that was modified with MWCNTs to quantify sulfite levels in various beverage samples using DPV and amperometry.

The electrochemical sensor exhibited an increasing current response to the subsequent addition of SO_3^{2-} in the linear range of from 25.0 - 500.0 μM, and a lower detection limit of 16.0 μM. The sensor was also tested for its performance with actual samples for SO_3^{2-} detection and produced good responses from the spiked samples.[146] Fang and co-workers developed a sensor for the sensitive electrochemical determination of sulphite by modifying a GCE with graphene, chitosan, and AuNPs.[147] Figure 2.11B reveals the analysis investigated with amperometry technique for increasing SO_3^{2-} concentration, and the respective current that was obtained from its oxidation. The electrochemical sensor exhibited superior electrochemical performance throughout the linear range of from 5.0 μM to 0.41 mM. The developed sensor did not show any interference when

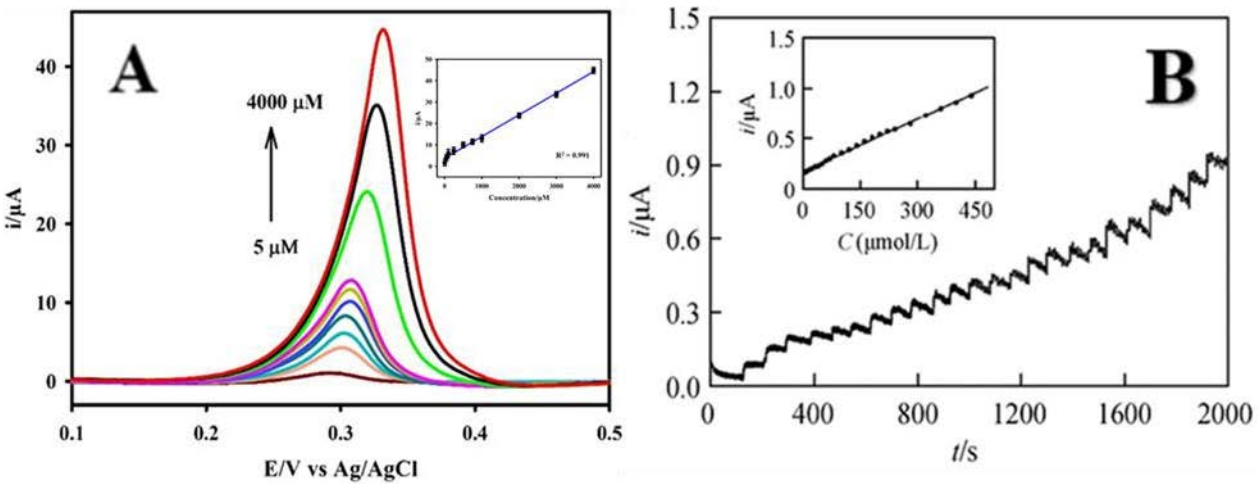

Figure 2.11. DPVs recorded for increasing sulphite concentrations, from 5.0 - 4000.0 µm in 0.1 M PBS buffer, pH 6.5 (A) and the respective calibration curve (inset), Amperometric response of the AuNPs/Gr/Ch/GCE sensor for successive additions of SO_3^{2-} in 0.1 M PBS, at pH 7.0, with the inset showing the respective calibration curve (B), Adapted and modified with permission from ref.147, 148 Copyright: Elsevier, 2015; Elsevier, 2013.

tested in the presence of ascorbic acid and dopamine and was also effective with actual off-the-shelf sample testing. In another work, Fatibello-Filho and Sartori developed an electrochemical sensor using MWCNTs, which was functionalized within a poly(allylamine hydrochloride) (PAH) film for the detection of SO_3^{2-}. LSV was employed to investigate the analytical quantification of SO_3^{2-} and a calibration plot was constructed to show the linear relationship between the changing concentration and increasing current. The linear range for the increasing SO_3^{2-} was 5.0 - 200.0 µM, and the sensor had a detection limit of 3.0 µM.[148]

2.4.8 Nitrite

From the food technology standpoint, nitrite is an important compound that has attracted the attention of analytical chemists and electrochemists in recent years. The primary function of NO_2^- as an additive is to enhance the shelf-life of perishable food items such as ham, salami, and

other processed meats. Also, it facilitates the preservation of the pink colour in meat products by forming nitroso-myoglobin.[149] On the other hand, NO_2^- has a noxious impact on the human body if it is added to food products at levels that are higher than prescribed safety standards.[150] Molecular NO_2^- possesses the ability to readily bind with hemoglobin to form methemoglobin, thus restricting the ability of red blood cells to transport oxygen.[151] The World Health Organization (WHO) has fixed a maximum limit of 3.0 mg L^{-1} (65.22 μM) for nitrite in drinking water.[152] Therefore, the quantification of NO_2^- is one of the critical aspects of food analysis. Among the different available methods for the determination of nitrite, electrochemical methods offer rapid, inexpensive, and safer means for its quantitative determination. John S.A and co-worker developed an electrochemical sensor for the quantitative determination of NO_2^- in milk samples. The sensor material was constructed using functionalized multi-walled carbon nanotubes (FMWCNTs) and 5-amino-1,3,4-thiadiazole-2-thiol (ATT). The nanostructured composite material showed good linearity with increasing NO_2^- from 10.0 nm - 1000.0 nm and a detection limit of 0.2 nm. The fabricated sensor demonstrated excellent anti-interference ability and its practical capability was scrutinized by quantifying the presence of nitrite in commercial milk samples.[153]

An electrochemical sensor was developed by Feng and co-workers for the oxidation of nitrite based on the interconnected platinum nanowire. Owing to the material's unique architecture, the electrochemical sensor exhibited high electrocatalytic activity and enhanced electroanalytical performance toward nitrite determination. The developed sensor showed good linearity throughout the very wide linear range of 1.0 μM - 132.0 mM and a low detection limit of 0.14 μM combined with excellent selectivity and good anti-interference ability.[155] Chou and co-workers reported on the fabrication of an electrochemical sensor for nitrite quantification based on boron-doped cubic SiC NWs (silicon carbide nanowires).

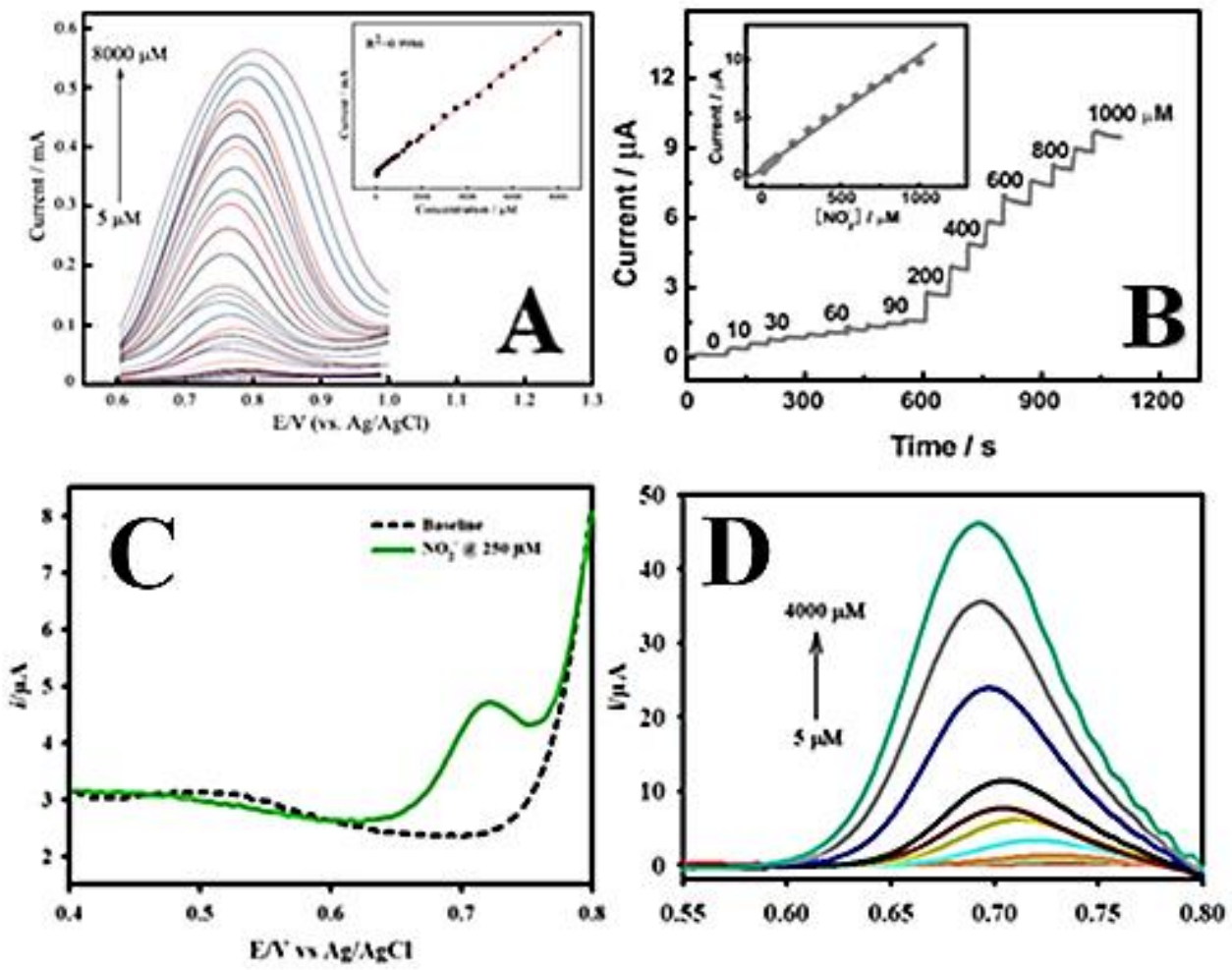

Figure 2.12. DPV (A) and amperometric (B) responses of increasing nitrite concentrations (5.0 - 8000.0 µm) at a B-doped cubic SiC NWs electrode in 0.1 M PBS; DPV response for the electrochemical oxidation of 250.0 µM nitrite at a gold nanoporous microelectrode (C), DPV responses for the increasing concentration of NO_2^- (5.0 - 4000.0 µm), in 0.1 M PBS (pH 6.5) (D), Adapted and modified with permission from ref. 85,155 and 77

This nanomaterial exhibited good sensitivity and selectivity, and a wide linear range of from 5.0 - 8000.0 µmol L^{-1} for NO_2^- (Figure. 2.12A and 2.12B).[154] In another reported work, Feng et al. synthesized a metal nanocomposite by utilizing Au-Pd and rGO for the amperometric detection of nitrite. This fabricated electrochemical sensor had high sensitivity and rapid response, a wider

linear range from 0.05 to 1000.0 µM, with a detection limit of 0.02 µM.[85] An electrochemical sensor based on a nanoporous gold microelectrode was used for the detection and determination of NO_2^-. Figure 2.12C shows the response obtained from DPV for the oxidation of 250.0 µM in 0.1 M PBS at pH 6.5. The anodic reaction mechanism at the nanoporous electrode is as follow:

$$NO_2^- + H_2O \rightarrow NO_3^- + 2H^+ + 2e^-$$

The fabricated sensor exhibited excellent sensitivity, high stability and wide linear range for increasing NO_2^-, from 5.0 - 4000.0 µmol L^{-1} (Figure. 2.12D).[77] Ding and co-workers developed an ultrathin gold electrode for the determination of nitrite. The amperometric study conducted with this electrode showed good linearity across a wide calibration range of increasing NO_2^- concentrations, from 1.0 µM to 1.0 mM. The electrode demonstrated good selectivity, high stability, and repeatability for the detection of NO_2^-.[150]

2.5. Electrochemical based immunosensors

Electrochemical-based immunosensors is deemed as a subclass of biosensors. The biological recognition element in an electrochemical immunosensor is either a fragment of an antibody or an antigen. The principle of immunosensors is based on the ability of the antibody to interact with the desired antigen.[155] Immunoglobulin (IgG) is the commonly used antibody in immunosensors with a molecular weight of 150 kDa.[156] Electrochemical immunosensors have the ability to detect and quantify contaminants because of the beneficial attributes such as enhanced sensitivity, lower limits of detection and swift analysis of the targeted molecule.[157, 158] Bisphenol A (BPA) is an extensively researched compound because of its associated toxicity and health risks to humans. Rahman and co-workers reported on the development of an immunosensor for the detection of BPA. The sensor was fabricated by binding antibody to polythiophene (functionalized

with COOH) covalently. The analytical performance was tested in the linear range from 1.0 to 100.0 ng mL^{-1} with a LOD value of 0.3 ng mL^{-1}.[159] Recently, Zhang et al. prepared a label-free electrochemical immunosensor for the quantitation of BPA using acetylene black, chitosan, gold composite (AB–CS–Au) and gold nanoparticles (Au NPs). The quantification of BPA was conducted in the increasing range of 0.0075 - 1.0 μmol L^{-1} with a LOD of 0.0065 μmol L^{-1}. The developed immunosensor demonstrated excellent sensitivity, selectivity toward the determination of BPA and long-term stability.[160] Another important molecule is malachite green (MG) that is used as a biocide in fish farming. This may cause possible cross-contamination and enter into the water sources and pose a severe threat to the human immune system.[161] Zhu and co-workers modified a GCE with bovine serum albumin and decorated it Au nanoclusters (BSA/Au-NCs) for the determination of MG. The analytical performance of the sensor was improved by modifying the GCE with 1, 4-phenylenediamine and covalently bonded to the prepared BSA/Au-NCs. Furthermore, a polyclonal antibody was immobilized onto the surface of the nanostructured material. The calibration curve constructed for MG determination was in the concentration range of 0.1 to 10.0 ng mL^{-1} and LOD value of 0.03 ng mL^{-1}. The electrochemical immunosensor exhibited excellent testing capabilities in real samples with good recovery rates (89.7 - 99.2%).[162]

2.6. Summary and Outlook

Electrochemical techniques and nanomaterials have demonstrated the capacity to enhance detection and confirmed their competency over conventional analytical methods. A variety of electrochemical sensors based on these reported nanomaterials and their fabrication methods have shown superior performance, high selectivity and sensitivity, followed by their ability to detect the target analytes at low concentrations. In terms of selectivity and electrode modification, a plethora of nanostructured materials are developed to overcome the challenges of selective oxidation of

targeted molecules. The excellent sensitive, selective and enhanced electrocatalytic toward the quantitation of the targeted molecules sensors can be attributed to the high conductivity of the carbon nanostructured materials, the synergistic effect of the noble bimetallic and monometallic nanoparticles and other metal nanocomposites. The size and shape of the nanomaterial also played a substantial role in the enhancement of the electrochemical catalytic performance of the reported sensors. The infusion of conductive polymer materials with metal and carbon nanostructured materials increased the specific surface area and improved the distribution of nanoparticles along the surface of the nanomaterial. In addition to that, electrochemical immunosensors is a growing area that is extensively looked at and improved upon by the researchers with novel nanomaterials in terms of the type of detection, improving selectivity and increasing the sensitivity. The future of nanomaterials is very promising for sensing applications and have greater potential for research. A comparative study of the applications of reported nanomaterial based electrochemical sensors for different food contaminants/additives is listed in Table 2.1.

Although most of the reported sensors exhibited possible usefulness as portable instruments, most of them have been verified only in the laboratory. Precise and thorough validation studies using established methods are imperative to transition these electrochemical sensors to real applications in the industrial model for food and beverage safety testing. The impacts of environmental constraints, storage, and operational stability in the field ought to be ascertained. Also, there are concerns relating to the probable toxicity of these nanomaterials. This aspect should be further taken into consideration and addressed prior to progressing with their introduction to the consumer market. There is an overabundance of reported electrochemical sensors for the detection of additives and contaminants; however, the number of commercially available sensors for the detection of additives and toxic contaminants remains negligible.

Table 2.1. List of various electrochemical sensors associated with electrochemical techniques for the detection of different target analytes

Nanomaterial	Target analyte	Electrochemical technique	Linear range	LOD	Ref
ZnO/CNTs/ILCPE	Ascorbic acid	DPV	0.1 – 450 µM	0.07 µM	[163]
Graphene/Pt nanocomposite	Ascorbic acid	CA	0.15 – 34.4 µM	0.15 µM	[88]
Pd/CNFs/CPE	Ascorbic acid	DPV	0.05 – 4 mM	15.0 µM	[164]
Nitrogen doped graphene	Ascorbic acid	DPV	5 - 1300 µM	2.20 µM	[165]
Pt disc electrode	Ascorbic acid	SWV	0.1 - 10 mM	90.0 µM	[166]
MWCNT/GCE	Ascorbic acid and caffeine	SWV	10 - 500 µM	0.01 and 0.004 µM	[167]
MWCNT/PEDOT/Nafion/GCE	Caffeine	DPV	0.085 - 7 mM	0.04 µM	[134]
Functionalized MWCNT/GCE	Caffeine	DPV	10 - 100 µM	3.54 µM	[168]
Nafion/Gr/GCE	Caffeine	DPV	0.4 - 40 µM	0.12 µM	[169]
poly(AHNSA)	Caffeine	SWV	0.06 - 50 µM	0.067 µM	[133]
PST/Nafion/GCE	Caffeine	LSV	0.3 - 100 µM	0.10 µM	[170]
Nafion/GCE	Caffeine	DPV	0.99 - 10 µM	0.80 µM	[171]
Nafion/MWCNT/GCE	Caffeine	DPV	0.6 - 0.04 µM	0.23 µM	[132]
SWCNT/Carbon ceramic electrode	Caffeine	DPV	0.25 - 0.01 µM	0.12 µM	[172]
SWCNT/Carbon ceramic electrode	Caffeine	DPV	0.4 - 300 µM	0.25 µM	[173]
Large mesoporous carbon/Nafion/GCE	Caffeine	DPV	1.3 - 230 µM	0.47 µM	[174]
MIP/Carbon Paste	Caffeine	DPV	0.06 - 25 µM	0.02 µM	[175]
Nafion/Boron doped diamond	Caffeine	DPV	0.2 - 0.012 µM	0.10 µM	[176]
Boron doped diamond	Caffeine	SWV & DPV	0.5 - 0.83 µM	0.04 µM	[131]
AuNP/Gr nanosheets/GCE	Caffeic acid	DPV	0.5 - 50 µM	0.05 µM	[177]
PEDOT/Pt electrode	Caffeic acid	DPV	0.01 - 6500 µM	0.03 µM	[178]
CRGO/GCE	Caffeic acid	DPV & CA	0.01 - 800 µM	0.002 µM	[123]
Nafion/ERGO/GCE	Caffeic acid	SW-AdSV	0.1 - 10 µM	0.091 µM	[179]
Molecularly imprinted Siloxanes	Caffeic acid	DPV	0.5 - 60 µM	0.15 µM	[180]
Au-PEDOT/rGO/GCE	Caffeic acid	DPV	0.01 - 46 µM	0.004 µM	[181]
Pb/GCE	Caffeic acid	DPV	0.01 - 0.5 µM	0.004 µM	[182]
Activated GCE	Caffeic acid	DPV	0.1 - 1 µM	0.068 µM	[183]
Glassy Polymeric carbon	Caffeic acid	DPV	0.97 - 11 µM	0.29 µM	[125]

Green bean/Chitin/CPE	Caffeic acid	DPV	0.97 - 11 µM	0.29 µM	124
Sulfite oxidase/GCE	Sulfite	CV	200 - 2800 µM	20 µM	184
BF/IL/Graphene-nanosheets paste	Sulfite	SWV	0.05 - 50 µM	0.02 µM	185
MWCNT/Carbon paste electrode	Sulfite	SWV	25 - 500 µM	16 µM	146
FeHCF/GCE	Sulfite	CV	100 - 2380 µM	80 µM	186
nanostructured copper/Pt	Sulfite	CA	4.0 - 69.0 µM	1.2 µM	187
Chitosan-ferrocene/MWCNT/GCE	Sulfite	CA	5 - 1500 µM	2.8 µM	188
SO_X/Fe3O4@GNPs/Au	Sulfite	CV	0.50 - 1000 µM	0.15 µM	141
SOx/PBNPs/PPY/ITO	Sulfite	CV	0.50 - 1000 µM	0.12 µM	189
CILE	Sulfite	SWV	6–1000 µM	4 µM	145
K-doped Gr/GCE	Sulfite & Nitrite	DPV	0.5 to 3900 µM	0.2 µM	64
Au-Ag NPs/SPCE	Sulfite	CA	9.80 to 83.33 µM	5 µM	190
nano-Au/P3MT/GCE	Nitrite	CA	10 - 1000 µM	2.3 µM	191
Hb/Gr-AuNP/GCE	Nitrite	CA	0.05 to 1000 µM	0.01 µM	192
GNPs/MWCNT/CPE	Nitrite	SWV & CA	0.05–250.0 µM	0.01 µM	87
Au-Pd/rGO/GCE	Nitrite	CA	0.05 - 1000.0 µM	0.02 µM	85
Pd/SWCNT/GCE	Nitrite	DPV	2 - 1230.0 µM	0.25 µM	193
Au/ZnO/MWCNTs/GC	Nitrite	CA	7.8 - 4000.0 µM	4 µM	194
Cu-NDs/RGO/GCE	Nitrite	CA	1.25 - 13.0 mM	0.4 µM	195
PEDOT/MWCNTs-modified SPCEs	Nitrite	CA	0.05 - 1 mM	0.96 µM	196
Graphene nanoribbons/GCE	Nitrite	CA	0.5 to 105.0 µM	0.22 µM	197
Cu/MWCNT/RGO	Nitrite	SWV	0.1 - 75.0 µM	30 nM	198
Pd/CILE	Hydrazine	SWV	5.0 - 800.0 µM	0.82 µM	199
ZnO/CNTs	Hydrazine	SWV	0.7 - 550 µM	9.0 nM	200
PSS-graphene	Hydrazine	CA	3.0 - 300.0 µM	1 µM	201
PEDOP/MWCNTs–Pd/GCE	Hydrazine	CA	0.1 - 5000.0 µM	0.08 µM	202
Au/ SW nanohorns	Hydrazine	CA	0.005–3.345 mM	1.1 µM	203
Pd/MWCNTs	Hydrazine	DPV	2.5–700.0 µM	1 µM	96
AuNPs/CNTs-ErGO/GCE	Hydrazine	CA	0.3 - 319.0 µM	0.065 µM	204
Graphene QDs/Au-NPs/GCE	Malachite green	DPV	0.4 - 10.0 µM	0.1 µM	105
BuChE/PPy/CPE	Malachite green	DPV	0.00068 - 0.027 µM	0.00068 µM	104
MWCNT/DHP/GCE	Malachite green	DPV	0.05 - 8.0 µM	0.006 µM	97

Fe_3O_4-Si4Pic$^+$Cl$^-$/Au-NPs-Si4Pic$^+$Cl$^-$/GCE	Bisphenol A	DPV	20.0 - 1400.0 nM	7.0 nm	[113]
Au-Pd NPs/GNs/GCE	Bisphenol A	DPV	0.05 to 10.0 µM	8.0 nm	[114]
Cu_2O/rGO/GCE	Bisphenol A	DPV	0.1 to 80.0 µM	0.085 µM	[115]

* µM - micromolar, mM - millimolar, nM - nanomolar, PSS - poly (sodium styrenesulfonate), PST - Poly(safranine T), CILE - Carbon Ionic liquid electrode, Gr - Graphene, MWCNTs - Multiwalled Carbon nanotubes, CNT - Carbon nanotubes, CPE - Carbon paste electrode, ILCPE - Ionic liquid carbon paste electrode, GCE - Glassy carbon electrode, CRGO - Chemically reduced graphene oxide, ERGO - Electrochemically reduced graphene oxide, MIP - Molecularly imprinted polymer, ZnO - Zinc Oxide, Hb - Hemoglobin, FeHCF - Iron hexacyanoferrate, SO_X - Sulfite oxidase, AuNP - Gold nanoparticles, PEDOT - Poly(3,4-ethylenedioxythiophene), PEDOP - Poly(3,4-ethylenedioxypyrrole), Poly (AHNSA) - Poly (4-Amino-3-Hydroxynaphthalene Sulfonic Acid), P3MT - poly(3-methylthiophene), CV - cyclic voltammetry, DPV - Differential Pulse Voltammetry, SWV - Square wave voltammetry, CA - Chronoamperometry, SW-AdSV - Square wave Anodic Stripping Voltammetry, BuChE - butyrylcholinesterase, DHP - dihexadecyl hydrogen phosphate, Si4Pic$^+$Cl$^-$ - 3-n-propyl-4-picolinium silsesquioxane chloride, Cu_2O - Cuprous oxide, GNs- Graphene nanosheets

The validation and testing of statistically-relevant numbers of samples, comparability, and interlaboratory studies to validate the robustness of such platforms are the next critical steps for the achievement of industry level acceptance and regulatory approvals. It would be of high value if these sensors were to be incorporated by food manufacturing companies to monitor the safety and measure the quality of processed foods and beverages.

References

1. J. A. Painter, R. M. Hoekstra, T. Ayers, R. V. Tauxe, C. R. Braden, F. J. Angulo and P. M. Griffin, Attribution of Foodborne Illnesses, Hospitalizations, and Deaths to Food Commodities by using Outbreak Data, United States, 1998–2008, *Emerg. Infect. Dis.* 19 (2013) 407-415.

2. L. Yáñ ez, D. Ortiz, J. Calderón, L. Batres, L. Carrizales, J. Mejía, L. Martínez, E. García-Nieto and F. Díaz-Barriga, Overview of human health and chemical mixtures: problems facing developing countries, *Env. Health Persp.* 110 (2002) 901-909.

3. S. Logothetidis, in *Nanostructured Materials and Their Applications*, Springer Berlin, Heidelberg, 2012, pp. 1-22.

4. M. C. Roco, C. A. Mirkin and M. C. Hersam, Nanotechnology research directions for societal needs in 2020: retrospective and outlook, ed., Springer Sci. Bus. Media, 2011.

5. K. D. Sattler, Handbook of nanophysics: principles and methods, ed., CRC press, 2010.

6. A. Chen and S. Chatterjee, Nanomaterials based electrochemical sensors for biomedical applications, *Chem. Soc. Rev.* 42 (2013) 5425-5438.

7. Y. Umasankar, B.-R. Adhikari and A. Chen, Effective immobilization of alcohol dehydrogenase on carbon nanoscaffolds for ethanol biofuel cell, *Bioelectrochem.* 118 (2017) 83-90.

8. E. Martínez-Periñán, W. C. Foster, P. M. Down, Y. Zhang, X. Ji, E. Lorenzo, D. Kononovs, I. A. Saprykin, N. V. Yakovlev, A. G. Pozdnyakov and E. C. Banks, Graphene encapsulated silicon carbide nanocomposites for high and low power energy storage applications, *Carbon* 3 (2017) 20.

9. N. Duran and P. D. Marcato, Nanobiotechnology perspectives. Role of nanotechnology in the food industry: a review, *Int. J. Food Sci. Tech.* 48 (2013) 1127-1134.

10. B. Srilatha, Nanotechnology in agriculture, *J. Nanomedic. Nanotechnol.* 2 (2011) 5.

11. H. S. Toh, K. Tschulik, C. Batchelor-McAuley and R. G. Compton, Electrochemical quantification of iodide ions in synthetic urine using silver nanoparticles: a proof-of-concept, *Analyst* 139(16) (2014) 3986-3990.

12. P. Guan, Y. Li, J. Zhang and W. Li, Non-Enzymatic Glucose Biosensor Based on CuO-Decorated CeO2 Nanoparticles, *Nanomaterials* 6 (2016) 159.

13. G. Favero, G. Fusco, F. Mazzei, F. Tasca and R. Antiochia, Electrochemical characterization of graphene and mwcnt screen-printed electrodes modified with aunps for laccase biosensor development, *Nanomaterials* 5 (2015) 1995-2006.

14. M. Govindhan, B.-R. Adhikari and A. Chen, Nanomaterials-based electrochemical detection of chemical contaminants, *RSC Adv.* 4 (2014) 63741-63760.

15. N. Sozer and J. L. Kokini, Nanotechnology and its applications in the food sector, *Trends biotechnol.* 27 (2009) 82-89.

16. C. Chellaram, G. Murugaboopathi, A. John, R. Sivakumar, S. Ganesan, S. Krithika and G. Priya, Significance of nanotechnology in food industry, *APCBEE Procedia* 8 (2014) 109-113.

17. D. Grieshaber, R. MacKenzie, J. Voeroes and E. Reimhult, Electrochemical biosensors-sensor principles and architectures, *Sensors* 8 (2008) 1400-1458.

18. P. N. Bartlett, Bioelectrochemistry: fundamentals, experimental techniques and applications, ed., John Wiley & Sons, 2008.

19. R. A. Durst, Chemically modified electrodes: recommended terminology and definitions (IUPAC Recommendations 1997), *Pure Appl. Chem.* 69 (1997) 1317-1324.

20. A. Hierlemann and R. Gutierrez-Osuna, Higher-order chemical sensing, *Chem. rev.* 108 (2008) 563-613.

21. M. Bonizzoni and E. V. Anslyn, Combinatorial Methods for Chemical and Biological Sensors, *Journal of the American Chemical Society* 131 (2009) 14597-14598.

22. M. B. Gumpu, S. Sethuraman, U. M. Krishnan and J. B. B. Rayappan, A review on detection of heavy metal ions in water – An electrochemical approach, *Sens. Actuat. B Chem.* 213 (2015) 515-533.

23. G. Aragay and A. Merkoçi, Nanomaterials application in electrochemical detection of heavy metals, *Electrochim. Acta* 84 (2012) 49-61.

24. D. Tang, J. Tang, B. Su and G. Chen, Ultrasensitive Electrochemical Immunoassay of Staphylococcal Enterotoxin B in Food Using Enzyme-Nanosilica-Doped Carbon Nanotubes for Signal Amplification, *J. Agri. Food Chem.* 58 (2010) 10824-10830.

25. M. J. Moorcroft, J. Davis and R. G. Compton, Detection and determination of nitrate and nitrite: a review, *Talanta* 54 (2001) 785-803.

26. A. Chaubey and B. D. Malhotra, Mediated biosensors, *Biosens. Bioelectron.* 17 (2002) 441-456.

27. V. M. Mirsky, M. Riepl and O. S. Wolfbeis, Capacitive monitoring of protein immobilization and antigen–antibody reactions on monomolecular alkylthiol films on gold electrodes, *Biosens. Bioelectron.* 12 (1997) 977-989.

28. A. Guiseppi-Elie and L. Lingerfelt, in *Immobilisation of DNA on Chips I*, ed. C. Wittmann, Springer, Berlin, Heidelberg, 2005, pp. 161-186.

29. F.-G. Banica, Chemical sensors and biosensors: fundamentals and applications, ed., John Wiley & Sons, 2012.

30. E. Katz and I. Willner, Probing biomolecular interactions at conductive and semiconductive surfaces by impedance spectroscopy: routes to impedimetric immunosensors, DNA-sensors, and enzyme biosensors, *Electroanal.* 15 (2003) 913-947.

31. A. Pardakhty, S. Ahmadzadeh, S. Avazpour and V. K. Gupta, Highly sensitive and efficient voltammetric determination of ascorbic acid in food and pharmaceutical samples from aqueous solutions based on nanostructure carbon paste electrode as a sensor, *J. Mol. Liq.* 216 (2016) 387-391.

32. S. Gheibi, H. Karimi-Maleh, M. A. Khalilzadeh and H. Bagheri, A new voltammetric sensor for electrocatalytic determination of vitamin C in fruit juices and fresh vegetable juice using modified multi-wall carbon nanotubes paste electrode, *J. Food Sci. Tech.* 52 (2015) 276-284.

33. A. Trani, R. Petrucci, G. Marrosu, D. Zane and A. Curulli, Selective electrochemical determination of caffeine at a gold-chitosan nanocomposite sensor: May little change on nanocomposites synthesis affect selectivity?, *J. Electroanal. Chem.* 788 (2017) 99-106.

34. E. Molaakbari, A. Mostafavi and H. Beitollahi, Simultaneous electrochemical determination of dopamine, melatonin, methionine and caffeine, *Sens. Actuat. B Chem.* 208 (2015) 195-203.

35. K. Thangavelu, S. Palanisamy, S.-M. Chen, V. Velusamy, T.-W. Chen and S. K. Ramaraj, Electrochemical determination of caffeic acid in wine samples using reduced graphene oxide/polydopamine composite, *J. Electrochem. Soc.* 163 (2016) B726-B731.

36. S. Chatterjee and A. Chen, Voltammetric detection of the α-dicarbonyl compound: Methylglyoxal as a flavoring agent in wine and beer, *Anal. Chim. Acta* 751 (2012) 66-70.

37. B. Shah and A. Chen, Novel electrochemical approach for the monitoring of biodegradation of phenolic pollutants and determination of enzyme activity, *Electrochem. Commun.* 25 (2012) 79-82.

38. R. Pei, Z. Cheng, E. Wang and X. Yang, Amplification of antigen–antibody interactions based on biotin labeled protein–streptavidin network complex using impedance spectroscopy, *Biosens. Bioelectron.* 16 (2001) 355-361.

39. S. Lupu, F. Parenti, L. Pigani, R. Seeber and C. Zanardi, Differential Pulse Techniques on Modified Conventional-Size and Microelectrodes. Electroactivity of Poly [4, 4′-bis (butylsulfanyl)-2, 2′-bithiophene] Coating Towards Dopamine and Ascorbic Acid Oxidation, *Electroanal.* 15 (2003) 715-725.

40. J. G. Osteryoung and R. A. Osteryoung, Square wave voltammetry, *Anal. Chem.* 57 (1985) 101-110.

41. A. Chen and B. Shah, Electrochemical sensing and biosensing based on square wave voltammetry, *Anal. Methods* 5 (2013) 2158-2173.

42. V. K. Gupta, R. Jain, K. Radhapyari, N. Jadon and S. Agarwal, Voltammetric techniques for the assay of pharmaceuticals—a review, *Anal. biochem.* 408 (2011) 179-196.

43. B. Uslu and S. A. Ozkan, Electroanalytical Methods for the Determination of Pharmaceuticals: A Review of Recent Trends and Developments, *Anal. Let.* 44 (2011) 2644-2702.

44. C. H. Hamann, A. Hamnett and W. Vielstich, Electrochemistry, 2nd ed., Wiley-VCH, Weinheim, 2007.

45. M. Khairy, B. G. Mahmoud and C. E. Banks, Simultaneous determination of codeine and its co-formulated drugs acetaminophen and caffeine by utilising cerium oxide nanoparticles modified screen-printed electrodes, *Sens. Actuat. B Chem.* 259 (2018) 142-154.

46. P. Shivappa Adarakatti, C. W. Foster, C. E. Banks, A. K. N. S and P. Malingappa, Calixarene bulk modified screen-printed electrodes (SPCCEs) as a one-shot disposable sensor for the simultaneous detection of lead(II), copper(II) and mercury(II) ions: Application to environmental samples, *Sens. Actuat. A Phys.* 267 (2017) 517-525.

47. D. A. Brownson and C. E. Banks, Graphene electrochemistry: an overview of potential applications, *Analyst* 135 (2010) 2768-2778.

48. J. R. Potts, D. R. Dreyer, C. W. Bielawski and R. S. Ruoff, Graphene-based polymer nanocomposites, *Polymer* 52 (2011) 5-25.

49. F. Schedin, A. Geim, S. Morozov, E. Hill, P. Blake, M. Katsnelson and K. Novoselov, Detection of individual gas molecules adsorbed on graphene, *Nat. mater.* (9) (2007) 652-655.

50. M. Pumera, Graphene-based nanomaterials and their electrochemistry, *Chem. Soc. Rev.* 39 (2010) 4146-4157.

51. M. Pumera, A. Ambrosi, A. Bonanni, E. L. K. Chng and H. L. Poh, Graphene for electrochemical sensing and biosensing, *TrAC* 29 (2010) 954-965.

52. C. S. Lim, C. K. Chua and M. Pumera, Detection of biomarkers with graphene nanoplatelets and nanoribbons, *Analyst* 139 (2014) 1072-1080.

53. S. Y. Chee and M. Pumera, Comparison of the electroanalytical performance of chemically modified graphenes (CMGs) using uric acid, *Electrochem. Commun.* 20 (2012) 141-144.

54. M. S. Goh, A. Bonanni, A. Ambrosi, Z. Sofer and M. Pumera, Chemically-modified graphenes for oxidation of DNA bases: analytical parameters, *Analyst* 136 (2011) 4738-4744.

55. B. Sidhureddy, A. R. Thiruppathi and A. Chen, From graphite to interconnected reduced graphene oxide: one-pot synthesis and supercapacitor application, *Chem. Comm.* 53 (2017) 7828-7831.

56. B.-R. Adhikari, M. Govindhan, H. Schraft and A. Chen, Simultaneous and sensitive detection of acetaminophen and valacyclovir based on two dimensional graphene nanosheets, *J. Electroanal. Chem.* 780 (2016) 241-248.

57. S. J. Rowley-Neale, E. P. Randviir, A. S. Abo Dena and C. E. Banks, An overview of recent applications of reduced graphene oxide as a basis of electroanalytical sensing platforms, *Appl. Mater. Today*, DOI: 10.1016/j.apmt.2017.11.010 (2017).

58. B. Sinduja and S. A. John, Sensitive determination of tannic acid using blue luminescent graphene quantum dots as fluorophore, *RSC Adv.* 6 (2016) 59900-59906.

59. P. K. Sonkar, V. Ganesan, S. A. John, D. K. Yadav and R. Gupta, Non-enzymatic electrochemical sensing platform based on metal complex immobilized carbon nanotubes for glucose determination, *RSC Adv.* 6 (2016) 107094-107103.

60. L. Xiao, J. Yin, Y. Li, Q. Yuan, H. Shen, G. Hu and W. Gan, Facile one-pot synthesis and application of nitrogen and sulfur-doped activated graphene in simultaneous electrochemical determination of hydroquinone and catechol, *Analyst* 141 (2016) 5555-5562.

61. S. Alwarappan, S. Boyapalle, A. Kumar, C.-Z. Li and S. Mohapatra, Comparative Study of Single-, Few-, and Multilayered Graphene toward Enzyme Conjugation and Electrochemical Response, *J. Phys. Chem. C* 116 (2012) 6556-6559.

62. J. Li, S. Guo, Y. Zhai and E. Wang, High-sensitivity determination of lead and cadmium based on the Nafion-graphene composite film, *Anal. Chim. Acta* 649 (2009) 196-201.

63. J. Li, S. Guo, Y. Zhai and E. Wang, Nafion–graphene nanocomposite film as enhanced sensing platform for ultrasensitive determination of cadmium, *Electrochem. Commun.* 11(5) (2009) 1085-1088.

64. Y.-Y. Tang, C.-L. Kao and P.-Y. Chen, Electrochemical detection of hydrazine using a highly sensitive nanoporous gold electrode, *Anal. chim. acta* 711 (2012) 32-39.

65. Y. J. Yang and W. Li, CTAB functionalized graphene oxide/multiwalled carbon nanotube composite modified electrode for the simultaneous determination of ascorbic acid, dopamine, uric acid and nitrite, *Biosens. Bioelectron.* 56 (2014) 300-306.

66. S. D. Perrault and W. C. Chan, In vivo assembly of nanoparticle components to improve targeted cancer imaging, *Proc. Natl. Acad. Sci.* 107 (2010) 11194-11199.

67. D. T. Thompson, Using gold nanoparticles for catalysis, *Nano Today* 2 (2007) 40-43.

68. Z. Liu, A. Nemec-Bakk, N. Khaper and A. Chen, Sensitive electrochemical detection of nitric oxide release from cardiac and cancer cells via a hierarchical nanoporous gold microelectrode, *Anal. Chem.* 89 (2017) 8036-8043.

69. T. Zhang, M. Liu, Q. Zhang, Y. Wang, X. Kong, L. Wang, H. Wang and Y. Zhang, Sensitive determination of chlorogenic acid in pharmaceutical products based on the decoration of

3D macroporous carbon with Au nanoparticles via polyoxometalates, *Analyst* 142 (2017) 2603-2609.

70. M. Ali, U. Hashim, S. Mustafa, Y. Man and K. N. Islam, Gold nanoparticle sensor for the visual detection of pork adulteration in meatball formulation, *J. Nanomater.* 2012 (2012) 1.

71. P. Salaün and C. M. van den Berg, Voltammetric detection of mercury and copper in seawater using a gold microwire electrode, *Anal. chem.* 78 (2006) 5052-5060.

72. G. M. Alves, J. M. Magalhães, P. Salaün, C. M. Van den Berg and H. M. Soares, Simultaneous electrochemical determination of arsenic, copper, lead and mercury in unpolluted fresh waters using a vibrating gold microwire electrode, *Anal. chim. acta* 703 (2011) 1-7.

73. C. Xu, R. Wang, M. Chen, Y. Zhang and Y. Ding, Dealloying to nanoporous Au/Pt alloys and their structure sensitive electrocatalytic properties, *Phys. Chem. Chem. Phys.* 12(1) (2010) 239-246.

74. G. Xingbo, W. Liqin, L. Zhaona and D. Yi, Nanoporous gold leaf for amperometric determination of nitrite, *Electroanal.* 23 (2011) 381-386.

75. F. Jia, C. Yu, Z. Ai and L. Zhang, Fabrication of nanoporous gold film electrodes with ultrahigh surface area and electrochemical activity, *Chem. Mater.* 19 (2007) 3648-3653.

76. J. Li and X. Lin, Electrocatalytic oxidation of hydrazine and hydroxylamine at gold nanoparticle—polypyrrole nanowire modified glassy carbon electrode, *Sens. Actuat. B Chem.* 126 (2007) 527-535.

77. V. S. Manikandan, Z. Liu and A. Chen, Simultaneous detection of hydrazine, sulfite, and nitrite based on a nanoporous gold microelectrode, *J. Electroanal. Chem.* 819 (2018) 524-532.

78. H. Yoon, Current trends in sensors based on conducting polymer nanomaterials, *Nanomaterials* 3 (2013) 524-549.

79. Y. Gao, X. Wu, H. Wang, W. Lu and M. Guo, Highly sensitive detection of hesperidin using AuNPs/rGO modified glassy carbon electrode, *Analyst* 143 (2018) 297-303.

80. S. Guo, L. Xu, B. Xu, Z. Sun and L. Wang, A ternary nanocomposite electrode of polyoxometalate/carbon nanotubes/gold nanoparticles for electrochemical detection of hydrogen peroxide, *Analyst* 140 (2015) 820-826.

81. A. AL-Mokaram, M. A. Amir, R. Yahya, M. M. Abdi and H. N. M. E. Mahmud, The development of non-enzymatic glucose biosensors based on electrochemically prepared polypyrrole–chitosan–titanium dioxide nanocomposite films, *Nanomaterials* 7 (2017) 129.

82. Z. Liu, H. Forsyth, N. Khaper and A. Chen, Sensitive electrochemical detection of nitric oxide based on AuPt and reduced graphene oxide nanocomposites, *Analyst* 141 (2016) 4074-4083.

83. M. Govindhan, M. Amiri and A. Chen, Au nanoparticle/graphene nanocomposite as a platform for the sensitive detection of NADH in human urine, *Biosens. Bioelectron.* 66 (2015) 474-480.

84. Y.-C. Shi, J.-J. Feng, S.-S. Chen, G.-M. Tu, J.-R. Chen and A.-J. Wang, Simple synthesis of hierarchical AuPt alloy nanochains for construction of highly sensitive hydrazine and nitrite sensors, *Mater. Sci. Eng. C* 75 (2017) 1317-1325.

85. S.-S. Li, Y.-Y. Hu, A.-J. Wang, X. Weng, J.-R. Chen and J.-J. Feng, Simple synthesis of worm-like Au–Pd nanostructures supported on reduced graphene oxide for highly sensitive detection of nitrite, *Sens. Actuat. B Chem.* 208 (2015) 468-474.

86. K. Thangavelu, N. Raja, S.-M. Chen and W.-C. Liao, Nanomolar electrochemical detection of caffeic acid in fortified wine samples based on gold/palladium nanoparticles decorated graphene flakes, *J. Colloid Interface Sci.* 501 (2017) 77-85.

87. A. Afkhami, F. Soltani-Felehgari, T. Madrakian and H. Ghaedi, Surface decoration of multi-walled carbon nanotubes modified carbon paste electrode with gold nanoparticles for electro-oxidation and sensitive determination of nitrite, *Biosens. Bioelectron.* 51 (2014) 379-385.

88. C.-L. Sun, H.-H. Lee, J.-M. Yang and C.-C. Wu, The simultaneous electrochemical detection of ascorbic acid, dopamine, and uric acid using graphene/size-selected Pt nanocomposites, *Biosens. Bioelectron.* 26(8) (2011) 3450-3455.

89. J. Mathiyarasu, S. Senthilkumar, K. L. N. Phani and V. Yegnaraman, PEDOT-Au nanocomposite film for electrochemical sensing, *Materials Letters* 62 (2008) 571-573.

90. H.W. Schessl, Encyclopedia of Chemical Technology, ed., VCH, New York, 1995.

91. US Environmental Protection Agency, *Integrated Risk Information System (IRIS) on Hydrazine/Hydrazine Sulfate*, National Center for Environmental Assessment, Office of Research and Development Washington, DC, 1999.

92. G. Choudhary and H. Hansen, Human health perspective of environmental exposure to hydrazines: A review, *Chemosphere* 37 (1998) 801-843.

93. World Health Organization, *Environmental health criteria 68: hydrazine*, 1987.

94. National Institute for Occupational Safety, NIOSH pocket guide to chemical hazards, ed., DIANE Publishing, Cincinnati, OH, 2000.

95. N. Rastakhiz, A. Kariminik, V. Soltani-Nejad and S. Roodsaz, Simultaneous determination of phenylhydrazine, hydrazine and sulfite using a modified carbon nanotube paste electrode, *Int. J. Electrochem. Sci* 5 (2010) 1203-1212.

96. J. Zhao, M. Zhu, M. Zheng, Y. Tang, Y. Chen and T. Lu, Electrocatalytic oxidation and detection of hydrazine at carbon nanotube-supported palladium nanoparticles in strong acidic solution conditions, *Electrochim. Acta* 56 (2011) 4930-4936.

97. H. Yi, W. Qu and W. Huang, Electrochemical determination of malachite green using a multi-wall carbon nanotube modified glassy carbon electrode, *Microchim. Acta* 160 (2008) 291-296.

98. S. J. Culp and F. A. Beland, Malachite Green: A Toxicological Review, *J. Am. Coll. Toxicol.* 15 (1996) 219-238.

99. J. C. Hashimoto, J. A. R. Paschoal, J. F. de Queiroz and F. G. R. Reyes, Considerations on the Use of Malachite Green in Aquaculture and Analytical Aspects of Determining the Residues in Fish: A Review, *J. Aquat. Food Prod. T.* 20 (2011) 273-294.

100. C. Nebot, A. Iglesias, R. Barreiro, J. M. Miranda, B. Vázquez, C. M. Franco and A. Cepeda, A simple and rapid method for the identification and quantification of malachite green and its metabolite in hake by HPLC–MS/MS, *Food Control* 31 (2013) 102-107.

101. E. Ghasemi and M. Kaykhaii, Application of Micro-cloud point extraction for spectrophotometric determination of Malachite green, Crystal violet and Rhodamine B in aqueous samples, *Spectrochim. Acta A Mol. Biomol. Spectrosc.* 164 (2016) 93-97.

102. N.-N. Xu, Q. Zhang, W. Guo, Q.-T. Li and J. Xu, Au@PVP core-shell nanoparticles used as surface-enhanced raman spectroscopic substrate to detect malachite green, *Chinese J. Anal. Chem.* 44 (2016) 1378-1384.

103. A. M. Sacara, C. Cristea and L. M. Muresan, Electrochemical detection of malachite green using glassy carbon electrodes modified with CeO2 nanoparticles and nafion, *J. Electroanal. Chem.* 792 (2017) 23-30.

104. A. P. N. Hidayah, S. Faridah, M. S. N. Azura, A. R. Gayah, M. Othman and A. B. Fatimah, Malachite Green and Leuco-Malachite Green Detection in Fish Using Modified Enzyme Biosensor, *Procedia Chem.* 20 (2016) 85-89.

105. J. Hou, F. Bei, M. Wang and S. Ai, Electrochemical determination of malachite green at graphene quantum dots–gold nanoparticles multilayers–modified glassy carbon electrode, *J. Appl. Electrochem.* 43 (2013) 689-696.

106. D. A. Crain, M. Eriksen, T. Iguchi, S. Jobling, H. Laufer, G. A. LeBlanc and L. J. Guillette, An ecological assessment of bisphenol-A: Evidence from comparative biology, *Reprod. Toxicol.* 24 (2007) 225-239.

107. K. V. Ragavan, N. K. Rastogi and M. S. Thakur, Sensors and biosensors for analysis of bisphenol-A, *TrAC Trends Anal. Chem.* 52 (2013) 248-260.

108. M. V. Maffini, B. S. Rubin, C. Sonnenschein and A. M. Soto, Endocrine disruptors and reproductive health: The case of bisphenol-A, *Mol. Cell. Endocrinol.* 254-255 (2006) 179-186.

109. R. A. Torres, F. Abdelmalek, E. Combet, C. Pétrier and C. Pulgarin, A comparative study of ultrasonic cavitation and Fenton's reagent for bisphenol A degradation in deionised and natural waters, *J Hazard Mater* 146 (2007) 546-551.

110. Y. Wen, B.-S. Zhou, Y. Xu, S.-W. Jin and Y.-Q. Feng, Analysis of estrogens in environmental waters using polymer monolith in-polyether ether ketone tube solid-phase microextraction combined with high-performance liquid chromatography, *J. Chromatogr. A* 1133 (2006) 21-28.

111. J. Yonekubo, K. Hayakawa and J. Sajiki, Concentrations of bisphenol A, bisphenol A diglycidyl ether, and their derivatives in canned foods in Japanese markets, *J. Agric. Food Chem.* 56 (2008) 2041-2047.

112. J. Zhang, G. M. Cooke, I. H. Curran, C. G. Goodyer and X.-L. Cao, GC–MS analysis of bisphenol A in human placental and fetal liver samples, *J. Chromatogr. B* 879(2) (2011) 209-214.

113. E. R. Santana, C. A. de Lima, J. V. Piovesan and A. Spinelli, An original ferroferric oxide and gold nanoparticles-modified glassy carbon electrode for the determination of bisphenol A, *Sens. Actuat. B: Chem.* 240 (2017) 487-496.

114. B. Su, H. Shao, N. Li, X. Chen, Z. Cai and X. Chen, A sensitive bisphenol A voltammetric sensor relying on AuPd nanoparticles/graphene composites modified glassy carbon electrode, *Talanta* 166 (2017) 126-132.

115. R. Shi, J. Liang, Z. Zhao, A. Liu and Y. Tian, An electrochemical bisphenol A sensor based on one step electrochemical reduction of cuprous oxide wrapped graphene oxide nanoparticles modified electrode, *Talanta* 169 (2017) 37-43.

116. J. Li, J. Jiang, M. Liu, Z. Xu, P. Deng, D. Qian, C. Tong, H. Xie and C. Yang, Facile synthesis of MnO_2-embedded flower-like hierarchical porous carbon microspheres as an enhanced electrocatalyst for sensitive detection of caffeic acid, *Anal. Chim. Acta* 985 (2017) 155-165.

117. N. J. Kang, K. W. Lee, B. J. Shin, S. K. Jung, M. K. Hwang, A. M. Bode, Y.-S. Heo, H. J. Lee and Z. Dong, Caffeic acid, a phenolic phytochemical in coffee, directly inhibits Fyn kinase activity and UVB-induced COX-2 expression, *Carcinogenesis* 30 (2008) 321-330.

118. M. Nardini, C. Scaccini, L. Packer and F. Virgili, In vitro inhibition of the activity of phosphorylase kinase, protein kinase C and protein kinase A by caffeic acid and a procyanidin-rich pine bark (Pinus marittima) extract, *Biochim. Biophys. Acta* 1474 (2000) 219-225.

119. K. Robards and M. Antolovich, Analytical chemistry of fruit bioflavonoids: A review, *Analyst* 122 (1997) 11R-34R.

120. T. Zhang, M. Zhu, X. Chen and K. Bi, Simultaneous analysis of seven bioactive compounds in Sambucus Chinensis Lindl by HPLC, *Anal. Lett.* 43 (2010) 2525-2533.

121. Y. Peng, F. Liu and J. Ye, Determination of phenolic acids and flavones in Lonicera japonica Thumb. by capillary electrophoresis with electrochemical detection, *Electroanal.* 17 (2005) 356-362.

122. D. P. Santos, M. F. Bergamini, A. G. Fogg and M. V. B. Zanoni, Application of a Glassy Carbon Electrode Modified with Poly(Glutamic Acid) in Caffeic Acid Determination, *Microchim. Acta* 151 (2005) 127-134.

123. A. T. Ezhil Vilian, S.-M. Chen, Y.-H. Chen, M. Ajmal Ali and F. M. A. Al-Hemaid, An electrocatalytic oxidation and voltammetric method using a chemically reduced graphene oxide film for the determination of caffeic acid, *J. Colloid Interface Sci.* 423 (2014) 33-40.

124. S. C. Fernandes, I. R. W. Z. de Oliveira and I. C. Vieira, A green bean homogenate immobilized on chemically crosslinked chitin for determination of caffeic acid in white wine, *Enzyme Microb. Technol.* 40 (2007) 661-668.

125. L. F. da Silva, N. Ramos Stradiotto and H. P. Oliveira, Determination of Caffeic Acid in Red Wine by Voltammetric Method, *Electroanalysis* 20 (2008) 1252-1258.

126. N. Karikalan, R. Karthik, S.-M. Chen and H.-A. Chen, A voltammetric determination of caffeic acid in red wines based on the nitrogen doped carbon modified glassy carbon electrode, *Sci. Rep.* 7 (2017) 45924.

127. Z. Liu, B. Lu, Y. Gao, T. Yang, R. Yue, J. Xu and L. Gao, Facile one-pot preparation of Pd-Au/PEDOT/graphene nanocomposites and their high electrochemical sensing performance for caffeic acid detection, *RSC Adv.* 6 (2016) 89157-89166.

128. R. J. Clarke and R. Macrae, Coffee: physiology, ed., Springer Science & Business Media, 1988.

129. A. Smith, Effects of caffeine on human behavior, *Food Chem. Toxicol.* 40 (2002) 1243-1255.

130. C. J. Derry, S. Derry and R. A. Moore, Caffeine as an analgesic adjuvant for acute pain in adults, *The Cochrane Library* (2012).

131. B. C. Lourenção, R. A. Medeiros, R. C. Rocha-Filho, L. H. Mazo and O. Fatibello-Filho, Simultaneous voltammetric determination of paracetamol and caffeine in pharmaceutical formulations using a boron-doped diamond electrode, *Talanta* 78 (2009) 748-752.

132. S. Yang, R. Yang, G. Li, L. Qu, J. Li and L. Yu, Nafion/multi-wall carbon nanotubes composite film coated glassy carbon electrode for sensitive determination of caffeine, *J. Electroanal. Chem.* 639 (2010) 77-82.

133. M. Amare and S. Admassie, Polymer modified glassy carbon electrode for the electrochemical determination of caffeine in coffee, *Talanta* 93 (2012) 122-128.

134. A. Carolina Torres, M. M. Barsan and C. M. A. Brett, Simple electrochemical sensor for caffeine based on carbon and Nafion-modified carbon electrodes, *Food Chem.* 149 (2014) 215-220.

135. S. J. Padayatty, A. Katz, Y. Wang, P. Eck, O. Kwon, J.-H. Lee, S. Chen, C. Corpe, A. Dutta and S. K. Dutta, Vitamin C as an antioxidant: evaluation of its role in disease prevention, *J. Am. coll. Nutr.* 22 (2003) 18-35.

136. A. Hodgkinson, Oxalate content of foods and nutrition, ed., Academic Press London, UK 1977.

137. N. V. Bhagavan, in *Medical Biochemistry (Fourth Edition)*, Academic Press, San Diego, 2002, DOI: 10.1016/B978-012095440-7/50040-8, pp. 901-928.

138. P. J. O'Connell, C. Gormally, M. Pravda and G. G. Guilbault, Development of an amperometric l-ascorbic acid (Vitamin C) sensor based on electropolymerised aniline for pharmaceutical and food analysis, *Anal. Chim. Acta* 431 (2001) 239-247.

139. S. S. Kumar and S. S. Narayanan, Amperometric sensor for the determination of ascorbic acid based on cobalt hexacyanoferrate modified electrode fabricated through a new route, *Chem. Pharm. Bull.* 54 (2006) 963-967.

140. R. Rawal and C. S. Pundir, Development of electrochemical sulfite biosensor based on SOX/PBNPs/PPY modified Au electrode, *Biochem. Eng. J.* 71 (2013) 30-37.

141. R. Rawal, S. Chawla and C. S. Pundir, An electrochemical sulfite biosensor based on gold coated magnetic nanoparticles modified gold electrode, *Biosens. Bioelectron.* 31 (2012) 144-150.

142. S. L. Taylor, N. A. Higley and R. K. Bush, Sulfites in foods: uses, analytical methods, residues, fate, exposure assessment, metabolism, toxicity, and hypersensitivity, *Adv. Food Res.* 30 (1986) 1-76.

143. Food and Drug Administration, Food labeling: declaration of sulfiting agents, *Fed. Regist* 51 (1986) 25012-25026.

144. Food and Drug Administration, Sulfiting agents; revocation of GRAS status for use on fruits and vegetables intended to be served or sold raw to consumers, *Fed. Regist* 51 (1986) 1-25026.

145. A. Safavi, N. Maleki, S. Momeni and F. Tajabadi, Highly improved electrocatalytic behavior of sulfite at carbon ionic liquid electrode: Application to the analysis of some real samples, *Anal. Chim. Acta* 625 (2008) 8-12.

146. E. M. Silva, R. M. Takeuchi and A. L. Santos, Carbon nanotubes for voltammetric determination of sulphite in some beverages, *Food Chem.* 173 (2015) 763-769.

147. X. Wang, H. Li, M. Wu, S.-L. Ge, Y. Zhu, Q.-J. Wang, P.-G. He and Y.-Z. Fang, Simultaneous Electrochemical Determination of Sulphite and Nitrite by a Gold Nanoparticle/Graphene-Chitosan Modified Electrode, *Chinese J. Anal. Chem.* 41 (2013) 1232-1237.

148. E. R. Sartori and O. Fatibello-Filho, Simultaneous voltammetric determination of ascorbic acid and sulfite in beverages employing a glassy carbon electrode modified with carbon nanotubes within a poly (allylamine hydrochloride) film, *Electroanal.* 24 (2012) 627-634.

149. S. S. Mirvish, Role of N-nitroso compounds (NOC) and N-nitrosation in etiology of gastric, esophageal, nasopharyngeal and bladder cancer and contribution to cancer of known exposures to NOC, *Cancer Lett.* 93 (1995) 17-48.

150. X. Ge, L. Wang, Z. Liu and Y. Ding, Nanoporous gold leaf for amperometric determination of nitrite, *Electroanal.* 23 (2011) 381-386.

151. P. Miao, M. Shen, L. Ning, G. Chen and Y. Yin, Functionalization of platinum nanoparticles for electrochemical detection of nitrite, *Anal. bioanal. chem.* 399 (2011) 2407-2411.

152. WHO, Guidelines for drinking-water quality, in: W. H. Organization (Ed.)^(Eds.) 2004, p.^pp.

153. K. Rajalakshmi and S. A. John, Highly sensitive determination of nitrite using FMWCNTs-conducting polymer composite modified electrode, *Sens. Actuat. B Chem.* 215 (2015) 119-124.

154. T. Yang, L. Zhang, X. Hou, J. Chen and K.-C. Chou, Bare and boron-doped cubic silicon carbide nanowires for electrochemical detection of nitrite sensitively, *Sci. Rep.* 6 (2016) 24872.

155. R. M. Lequin, Enzyme immunoassay (EIA)/enzyme-linked immunosorbent assay (ELISA), *Clin. Chem.* 51 (2005) 2415-2418.

156. B. Piro, S. Shi, S. Reisberg, V. Noël and G. Anquetin, Comparison of Electrochemical Immunosensors and Aptasensors for Detection of Small Organic Molecules in Environment, Food Safety, Clinical and Public Security, *Biosensors* 6 (2016) 7.

157. A. Vasudev, A. Kaushik and S. Bhansali, Electrochemical immunosensor for label free epidermal growth factor receptor (EGFR) detection, *Biosens. Bioelectron.* 39(1) (2013) 300-305.

158. C. Zhu, G. Yang, H. Li, D. Du and Y. Lin, Electrochemical sensors and biosensors based on nanomaterials and nanostructures, *Anal. Chem.* 87 (2014) 230-249.

159. M. A. Rahman, M. J. Shiddiky, J.-S. Park and Y.-B. Shim, An impedimetric immunosensor for the label-free detection of bisphenol A, *Biosens. Bioelectron.* 22 (2007) 2464-2470.

160. X. Li, Y. Huang, M. Chen, Y. Tong and C. Zhang, A label-free electrochemical bisphenol A immunosensor based on chlorogenic acid as a redox probe, *Anal. Methods* 9(14) (2017) 2183-2188.

161. M.-C. Yang, J.-M. Fang, T.-F. Kuo, D.-M. Wang, Y.-L. Huang, L.-Y. Liu, P.-H. Chen and T.-H. Chang, Production of antibodies for selective detection of malachite green and the related triphenylmethane dyes in fish and fishpond water, *J. Agric. Food Chem.* 55 (2007) 8851-8856.

162. D. Zhu, Q. Li, X. Pang, Y. Liu, X. Wang and G. Chen, A sensitive electrochemical impedance immunosensor for determination of malachite green and leucomalachite green in the aqueous environment, *Anal. Bioanal. Chem.* 408 (2016) 5593-5600.

163. M. Bijad, H. Karimi-Maleh and M. A. Khalilzadeh, Application of ZnO/CNTs nanocomposite Ionic Liquid Paste Electrode as a sensitive voltammetric sensor for determination of ascorbic acid in food samples, *Food Anal. Methods* 6(6) (2013) 1639-1647.

164. J. Huang, Y. Liu, H. Hou and T. You, Simultaneous electrochemical determination of dopamine, uric acid and ascorbic acid using palladium nanoparticle-loaded carbon nanofibers modified electrode, *Biosens. Bioelectron.* 24(4) (2008) 632-637.

165. Z.-H. Sheng, X.-Q. Zheng, J.-Y. Xu, W.-J. Bao, F.-B. Wang and X.-H. Xia, Electrochemical sensor based on nitrogen doped graphene: Simultaneous determination of ascorbic acid, dopamine and uric acid, *Biosens. Bioelectron.* 34(1) (2012) 125-131.

166. A. M. Pisoschi, A. F. Danet and S. Kalinowski, Ascorbic Acid Determination in Commercial Fruit Juice Samples by Cyclic Voltammetry, *J. Autom. Methods Manag. Chem.* 2008 (2008) 937651.

167. V. K. Gupta, A. K. Jain and S. K. Shoora, Multiwall carbon nanotube modified glassy carbon electrode as voltammetric sensor for the simultaneous determination of ascorbic acid and caffeine, *Electrochim. Acta* 93 (2013) 248-253.

168. M. Amiri-Aref, J. B. Raoof and R. Ojani, A highly sensitive electrochemical sensor for simultaneous voltammetric determination of noradrenaline, acetaminophen, xanthine and caffeine based on a flavonoid nanostructured modified glassy carbon electrode, *Sens. Actuat. B Chem.* 192 (2014) 634-641.

169. J.-Y. Sun, K.-J. Huang, S.-Y. Wei, Z.-W. Wu and F.-P. Ren, A graphene-based electrochemical sensor for sensitive determination of caffeine, *Colloids Surf B Biointerfaces* 84 (2011) 421-426.

170. S. Guo, Q. Zhu, B. Yang, J. Wang and B. Ye, Determination of caffeine content in tea based on poly(safranine T) electroactive film modified electrode, *Food Chem.* 129 (2011) 1311-1314.

171. B. Brunetti, E. Desimoni and P. Casati, Determination of Caffeine at a Nafion-Covered Glassy Carbon Electrode, *Electroanal.* 19 (2007) 385-388.

172. B. Habibi, M. Abazari and M. H. Pournaghi-Azar, A Carbon Nanotube Modified Electrode for Determination of Caffeine by Differential Pulse Voltammetry, *Chinese J. Catal.* 33 (2012) 1783-1790.

173. B. Habibi, M. Abazari and M. H. Pournaghi-Azar, Simultaneous determination of codeine and caffeine using single-walled carbon nanotubes modified carbon-ceramic electrode, *Colloids Surf B Biointerfaces* 114 (2014) 89-95.

174. Y. Gao, H. Wang and L. Guo, Simultaneous determination of theophylline and caffeine by large mesoporous carbon/Nafion modified electrode, *J. Electroanal. Chem.* 706 (2013) 7-12.

175. T. Alizadeh, M. R. Ganjali, M. Zare and P. Norouzi, Development of a voltammetric sensor based on a molecularly imprinted polymer (MIP) for caffeine measurement, *Electrochim. Acta* 55 (2010) 1568-1574.

176. C. A. Martínez-Huitle, N. Suely Fernandes, S. Ferro, A. De Battisti and M. A. Quiroz, Fabrication and application of Nafion®-modified boron-doped diamond electrode as sensor for detecting caffeine, *Diam. Relat. Mater.* 19 (2010) 1188-1193.

177. Y. Zhang, Y. Liu, J. He, P. Pang, Y. Gao and Q. Hu, Electrochemical behavior of caffeic acid assayed with gold nanoparticles/graphene nanosheets modified glassy carbon electrode, *Electroanal.* 25 (2013) 1230-1236.

178. C. Bianchini, A. Curulli, M. Pasquali and D. Zane, Determination of caffeic acid in wine using PEDOT film modified electrode, *Food Chem.* 156 (2014) 81-86.

179. H. Filik, G. Çetintaş, A. A. Avan, S. Aydar, S. N. Koç and İ. Boz, Square-wave stripping voltammetric determination of caffeic acid on electrochemically reduced graphene oxide–Nafion composite film, *Talanta* 116 (2013) 245-250.

180. F. R. F. Leite, W. d. J. R. Santos and L. T. Kubota, Selective determination of caffeic acid in wines with electrochemical sensor based on molecularly imprinted siloxanes, *Sens. Actuat B Chem.* 193 (2014) 238-246.

181. Z. Liu, J. Xu, R. Yue, T. Yang and L. Gao, Facile one-pot synthesis of Au–PEDOT/rGO nanocomposite for highly sensitive detection of caffeic acid in red wine sample, *Electrochim. Acta* 196 (2016) 1-12.

182. K. Tyszczuk, A. Skalska-Kamińska and A. Woźniak, Voltammetric method using a lead film electrode for the determination of caffeic acid in a plant material, *Food Chem.* 125 (2011) 1498-1503.

183. G. Magarelli, J. G. da Silva, I. A. d. Sousa Filho, I. S. D. Lopes, J. R. SouzaDe, L. V. Hoffmann and C. S. P. de Castro, Development and validation of a voltammetric method for determination of total phenolic acids in cotton cultivars, *Microchem. J.* 109 (2013) 23-28.

184. E. Dinçkaya, M. K. Sezgintürk, E. Akyılmaz and F. N. Ertaş, Sulfite determination using sulfite oxidase biosensor based glassy carbon electrode coated with thin mercury film, *Food Chem.* 101 (2007) 1540-1544.

185. H. Beitollahi, S. Tajik and P. Biparva, Electrochemical determination of sulfite and phenol using a carbon paste electrode modified with ionic liquids and graphene nanosheets: Application to determination of sulfite and phenol in real samples, *Measurement* 56 (2014) 170-177.

186. T. García, E. Casero, E. Lorenzo and F. Pariente, Electrochemical sensor for sulfite determination based on iron hexacyanoferrate film modified electrodes, *Sens. Actuat. B Chem.* 106 (2005) 803-809.

187. T. R. L. Dadamos and M. F. S. Teixeira, Electrochemical sensor for sulfite determination based on a nanostructured copper-salen film modified electrode, *Electrochim. Acta* 54 (2009) 4552-4558.

188. H. Zhou, W. Yang and C. Sun, Amperometric sulfite sensor based on multiwalled carbon nanotubes/ferrocene-branched chitosan composites, *Talanta* 77 (2008) 366-371.

189. R. Rawal and C. S. Pundir, Development of an amperometric sulfite biosensor based on SOx/PBNPs/PPY modified ITO electrode, *Int. J. Biol. Macromol.* 51 (2012) 449-455.

190. B. Molinero-Abad, M. Alonso-Lomillo, O. Domínguez-Renedo and M. Arcos-Martínez, Amperometric determination of sulfite using screen-printed electrodes modified with metallic nanoparticles, *Microchim. Acta* 180 (2013) 1351-1355.

191. X. Huang, Y. Li, Y. Chen and L. Wang, Electrochemical determination of nitrite and iodate by use of gold nanoparticles/poly(3-methylthiophene) composites coated glassy carbon electrode, *Sens. Actuat. B Chem.* 134 (2008) 780-786.

192. J. Jiang, W. Fan and X. Du, Nitrite electrochemical biosensing based on coupled graphene and gold nanoparticles, *Biosens. Bioelectron.* 51 (2014) 343-348.

193. X.-H. Pham, C. A. Li, K. N. Han, B.-C. Huynh-Nguyen, T.-H. Le, E. Ko, J. H. Kim and G. H. Seong, Electrochemical detection of nitrite using urchin-like palladium nanostructures on carbon nanotube thin film electrodes, *Sens. Actuat. B Chem.* 193 (2014) 815-822.

194. A.-J. Lin, Y. Wen, L.-J. Zhang, B. Lu, Y. Li, Y.-Z. Jiao and H.-F. Yang, Layer-by-layer construction of multi-walled carbon nanotubes, zinc oxide, and gold nanoparticles integrated composite electrode for nitrite detection, *Electrochim. Acta* 56 (2011) 1030-1036.

195. D. Zhang, Y. Fang, Z. Miao, M. Ma, X. Du, S. Takahashi, J.-i. Anzai and Q. Chen, Direct electrodeposion of reduced graphene oxide and dendritic copper nanoclusters on glassy carbon electrode for electrochemical detection of nitrite, *Electrochim. Acta* 107 (2013) 656-663.

196. C.-Y. Lin, V. S. Vasantha and K.-C. Ho, Detection of nitrite using poly(3,4-ethylenedioxythiophene) modified SPCEs, *Sens. Actuat. B Chem.* 140 (2009) 51-57.

197. E. Mehmeti, D. M. Stanković, A. Hajrizi and K. Kalcher, The use of graphene nanoribbons as efficient electrochemical sensing material for nitrite determination, *Talanta* 159 (2016) 34-39.

198. H. Bagheri, A. Hajian, M. Rezaei and A. Shirzadmehr, Composite of Cu metal nanoparticles-multiwall carbon nanotubes-reduced graphene oxide as a novel and high

performance platform of the electrochemical sensor for simultaneous determination of nitrite and nitrate, *J. Hazard. Mater.* 324 (2017) 762-772.

199. N. Maleki, A. Safavi, E. Farjami and F. Tajabadi, Palladium nanoparticle decorated carbon ionic liquid electrode for highly efficient electrocatalytic oxidation and determination of hydrazine, *Anal. Chim. Acta* 611 (2008) 151-155.

200. H. Karimi-Maleh, M. Moazampour, A. A. Ensafi, S. Mallakpour and M. Hatami, An electrochemical nanocomposite modified carbon paste electrode as a sensor for simultaneous determination of hydrazine and phenol in water and wastewater samples, *Environ. Sci. Pollut. Res.* 21 (2014) 5879-5888.

201. C. Wang, L. Zhang, Z. Guo, J. Xu, H. Wang, K. Zhai and X. Zhuo, A novel hydrazine electrochemical sensor based on the high specific surface area graphene, *Microchim. Acta* 169 (2010) 1-6.

202. S. K. Kim, Y. N. Jeong, M. S. Ahmed, J.-M. You, H. C. Choi and S. Jeon, Electrocatalytic determination of hydrazine by a glassy carbon electrode modified with PEDOP/MWCNTs–Pd nanoparticles, *Sens. Actuat. B Chem.* 153 (2011) 246-251.

203. S. Zhao, L. Wang, T. Wang, Q. Han and S. Xu, A high-performance hydrazine electrochemical sensor based on gold nanoparticles/single-walled carbon nanohorns composite film, *Appl. Surf. Sci.* 369 (2016) 36-42.

204. Z. Zhao, Y. Sun, P. Li, W. Zhang, K. Lian, J. Hu and Y. Chen, Preparation and characterization of AuNPs/CNTs-ErGO electrochemical sensors for highly sensitive detection of hydrazine, *Talanta* 158 (2016) 283-291.

Chapter 3: Materials and Methods

3.1 Introduction

An overview of various types of nanomaterials employed in the detection and determination of common preservatives and contaminants in food and beverages was presented in previous chapters. Also, the shortcomings and the underlying challenges for commercial applications were discussed. In this chapter, the main experimental methodologies and techniques employed to synthesize and characterize materials will be described briefly. Details of the experimental procedures and equipment pertaining to each specific study are presented in Chapters 4-7.

3.2 Experimental

3.2.1 Materials

Hydrazine hydrate; sodium sulfite; sodium nitrite; orthophosphoric acid; sodium hydroxide; sodium dihydrogen phosphate monobasic; disodium hydrogen phosphate dibasic; sodium chloride; chloroauric acid; caffeic acid; potassium ferrocyanide and potassium chloride, were all obtained from Sigma-Aldrich. Glacial acetic acid and boric acid were purchased from Alfa Aesar.

A gold microwire (99.9%, diameter of Ø127 μm) was received from Sigma-Aldrich and was cut into 10 mm in length. Pt wire (99.9%, 0.5 mm diameter) were used as received from Alfa-Aesar. Glassy carbon electrodes (GCEs, dia. 3.0 mm) with a surface area of 0.05 cm^2 were purchased from Pine Research Instrumentation. The water was purified with the NANOpure® DiamondTM UV ultrapure water purification system was used for cleaning purposes and the

preparation of all samples and solutions. Gases utilized in all the experiments in this thesis are ultrapure argon (99.99%) and ultrapure nitrogen (99.9%).

3.2.2 Instruments and Electrochemical Experiments

The surface morphology and composition of the prepared nanomaterial were characterized using a Hitachi SU-70 Schottky Field Emission Scanning electron microscope (SEM) and an FEI Quanta FEG 250 SEM. The EDX pattern and elemental mapping of the samples were recorded via the EDX technique using a Hitachi Su-70 Schotty. X-ray photoelectron spectroscopy studies were done using a Thermo Scientific K-α XPS spectrometer. All samples were run at a takeoff angle (relative to the surface) of 90°. A monochromatic Al Kα X-ray source was utilized, with a spot area of 400 μm. Charge compensation was provided, and the position of the energy scale was adjusted to place the main C 1s feature (C−C) at 284.6 eV. All data analysis was performed using XPS peak software.

The catalytic activity and electrochemical performance of all the catalyst were investigated using a CHI-D660 potentiostat (CHI-660, CHI, USA). A three-electrode cell system was employed in all the electrochemical studies. A coiled platinum wire served as the counter electrode, which was flame treated and rinsed with double distilled water and a standard silver-silver chloride (Ag/AgCl) electrode was employed as the reference electrode. All measurements were conducted at room temperature (22 ± 2°C).

3.2.3 Fabrication of Electrodes

3.2.3.1 Fabrication of Co_3O_4/AuNPs sensor

The Co_3O_4 sheets were synthesized by chemical reduction followed by calcination in order to form the nanosheets. Initially, 4.0 mM of $Co(NO_3)_2$ was subjected to reduction under a constant state

of stirring using aqueous $NaBH_4$ solution (at a concentration of 0.1 g/10 mL). Then by centrifugation, the product obtained after the reduction process was gathered by centrifugation. The collected product was rinsed carefully with a solution mixture (water/ethanol) and was dried at 70 ˚C. Furthermore, the final washed product was annealed at 450 ˚C for 4 h.[1]

The Co_3O_4 nanosheets/Au modified glassy carbon electrode (GCE) was fabricated by dissolving the Co_3O_4 nanosheets in double distilled water (2.0 mg mL^{-1}). The prepared ink was drop-casted (3.0 µL) onto a GC electrode (d = 3.0 mm) surface and allowed to dry at room temperature (20.0 °C) for 4 h. The Co_3O_4/GCE was further modified by electrodepositing Au on the electrode (1.0 mM of $HAuCl_4.3H_2O$ in 0.1 M KNO_3) to form Co_3O_4/AuNPs/GCE.

3.2.3.2 Fabrication of the nanoporous gold microelectrode

A nanoporous gold microelectrode was fabricated by sealing a Ø127 µm Au wire within a pipette tip. And a 10-cm length copper wire was inserted into a 10-cm glass tube and its end was plunged into a conductive gold paste, which acted as a conductive adhesive. Subsequently, a 10-mm long gold microwire (Ø127 µm, 99.9%, Sigma-Aldrich) was fed halfway through the pipet tip until the microwire gently contacted with the copper wire. An epoxy resin was used to wrap the top and bottom ends of the pipette tips to seal them firmly. The microelectrode was kept in the oven at 60ºC for 90 min, followed by cooling in ambient air; and finally, the microwire was cut to 1.0 mm. The nanoporous structure of the gold microelectrode was attained through the application of an electrochemical alloying/dealloying method.[2]

3.2.3.3 Synthesis of FGO and fabrication of the F-GO sensor

FGO was synthesized by the improved Hummers' method with some modifications. Initially, a mixture was prepared by blending 1 g graphite, 90 mL of sulfuric acid (H_2SO_4), 10

ml of orthophosphoric acid (H_3PO_4), and 20 ml of hydrogen fluoride (HF). Secondly, the prepared mixture was stirred for 2 h vigorously; the temperature was kept at 50 °C. About 4.5 g of $KMnO_4$ was slowly added to this blend and stirred constantly for 15 h. Thirdly, the reaction mixture was supplemented with 100 ml of ice, also 5 ml of 30% H_2O_2 was added after a short while. Furthermore, the obtained final product (F-GO) was separated and thoroughly washed with 30% hydrochloric acid (HCl), pure water, ethanol, and diethyl ether. Lastly, the subsequent F-GO solid was kept in the oven at 50°C for drying.[3]

The prepared F-GO was mixed with water (4 mg/ml) and ultrasonicated for 1 h to ensure thorough mixing. Glassy carbon electrode (GCE) was polished with 1.0 and 0.3 μm alumina slurry, then washed with ethanol and water ultrasonically for 10 mins. The F-GO ink was drop cast on the surface of GCE and air dried for 24 h to obtain F-GO/GCE. The as-prepared F-GO/GCE was subjected to partial electrochemical reduction in 0.1 M Phosphate buffer solution at pH 7.4. Similarly, another GCE was prepared by drop casting graphene oxide (GO) on its surface using the same procedure. For comparison, a bare GCE and the GO/GCE was tested alongside F-GO/GCE for CA oxidation.

3.2.3.4 Synthesis of Au/F-rGO Nanocomposite

The F-GO ink prepared by mixing 2.0 mg/ml with water was ultrasonicated for 1 h. Glassy carbon electrode (GCE) was polished with 1.0 and 0.05 μm alumina slurry, then the polished electrodes were ultrasonicated in water for 5 mins. The prepared F-GO ink was drop cast on the surface of the GCE and left to air-dry for 4 h (F-GO/GCE). The as-prepared F-GO/GCE was subjected to electrochemical reduction in 0.1 M Phosphate buffer solution (PBS) at pH 7.4 (r-FGO/GCE). Additionally, gold was electrochemically deposited on the electrode (Au/F-

rGO/GCE) by immersing the F-rGO/GCE in a 0.1 M KNO_3 solution containing 2.0 mM $HAuCl_4$. Similarly, another GCE was prepared by electrodepositing gold on its surface using the same procedure (Au/GCE). For comparison of the electrochemical, the Au/GCE and unmodified bare GCE was tested together with Au/F-rGO/GCE toward the oxidation of vanillin.

3.3 Summary

This chapter has presented the materials used in this Ph.D. thesis. The experimental procedures and techniques used for the fabrication and characterization of gold, carbon and cobalt-based nanomaterials were discussed in detail. The following chapter will present the development and study of Co_3O_4 nanosheets/Au nanoparticle for the electrochemical detection of nitrite.

References

1. B. Sidhureddy, J. S. Dondapati and A. Chen, Shape-controlled synthesis of Co_3O_4 for enhanced electrocatalysis of the oxygen evolution reaction, *Chem. Commun.*, DOI: 10.1039/c8cc10194a (2019).
2. V. S. Manikandan, Z. Liu and A. Chen, Simultaneous detection of hydrazine, sulfite, and nitrite based on a nanoporous gold microelectrode, *J. Electroanal. Chem.* 819 (2018) 524-532.
3. A. R. Thiruppathi, B. Sidhureddy, W. Keeler and A. Chen, Facile one-pot synthesis of fluorinated graphene oxide for electrochemical sensing of heavy metal ions, *Electrochem. Commun.* 76 (2017) 42-46.

Chapter 4: Electrochemical Detection of Nitrite Based on Co_3O_4-Au Nanocomposites for Food Quality Control

4.1. Introduction

NO_2^- functions as an antimicrobial agent to preserve perishable food items such as ham, salami, and other processed meats.[1,2] It is also accountable for maintaining the pink colour in meat products by forming nitroso-myoglobin.[3] Despite these positive effects, NO_2^- has a downside associated with it, as it can be detrimental to the human body if supplemented in a surplus of the set safety limit (200 ppm).[4] Another drawback of having excess NO_2^- in the bloodstream is that it can swiftly attach with hemoglobin to form methemoglobin complex, thus tumbling the red blood cells oxygen carrying capacity.[5-7] Moreover, NO_2^- is transformed into an intoxicating compound (e.g. *N*-nitrosamines) in the stomach, which is a probable carcinogen.[8-10] There are numerous traditional methods for the determination of NO_2^-, such as titration, spectrofluorometry, chemiluminescence, phosphorimetry, spectrophotometry, and flow injection analysis (FIA).[11] However, these methods require large sample volumes, arduous pretreatment steps, and the preparation of reagents. Despite the practice of several instrumentation methods for NO_2^- determination, electrochemical techniques and -based sensors present an effective approach toward the direct detection and quantification because of their simplicity, high selectivity, long-term stability and good sensitivity.[12-18]

Electrochemical sensors and their methods of quantitation have various benefits, they are as follows: (i) The analytes can be detected and measured swiftly as strenuous sample preparation is eliminated; (ii) high selectivity is achievable because of the analytes specific oxidation/reduction potentials, which enable the determination of multiple analytes without the need for separation;

and (iii) the analytical capability of the sensor to analyze diverse food and beverage matrices.[19] Owing to the restrictions with multiple assays, time-consuming steps, irreversible loss in activity of the enzymatic electrochemical sensors, earlier attempts have been made to develop electrochemical sensors without incorporating a redox mediator.[20, 21] In recent years, several nanomaterial based electrochemical sensor has been reported for the detection of nitrite.[22-28] John S.A and co-worker developed an electrochemical sensor based on functionalized multi-walled carbon nanotubes (FMWCNTs) and 5-amino-1,3,4-thiadiazole-2-thiol (ATT) for the quantitative determination of NO_2^- in milk.[29] S-M. Chen et. al developed an electrochemical sensor by decorating graphene-multiwalled carbon nanotubes (GR-MWCNTs) with iron nanoparticles for quantitation of NO_2^-.[30]

Limitations associated with electrochemical sensors mandate the requirement for considerable electroactivity toward the analyte of detection. The electrochemical oxidation of NO_2^- occurs at a higher positive potential at the surface of bare glassy carbon electrodes (GCE), and there is a possibility that numerous species could adsorb on to the electrode surface and subdue its sensitivity and selectivity.[31] Moreover, the problems posed by the interfering species at higher concentrations than the analyte of interest could cause fluctuations in the electrochemical response and could eventually lead to electrode fouling. Therefore, the selectivity and sensitivity toward the detection of nitrite could be enhanced by employing the right electrocatalysts.

Gold (Au), a noble metal, is one of the most well studied and employed materials amongst researchers for the fabrication of sensors.[32] Compared to other Nobel metal based electrocatalyst, Au nanomaterials have advantageous attributes such as high stability, chemical robustness, faster electron transfer rate, mass transport, unique catalytic activity.[33] Au nanoparticles are extremely redox active with the remarkable possibility for uses in chemical and biological sensing.[34-36] Feng

et al. developed a metal nanocomposite using Au-Palladium (Pd) and reduced graphene oxide (rGO) for the determination of NO_2^-.[37] Maduraiveeran et. al. developed a silicate sol-gel embedded with Au nanoparticles to form a three-dimensional network and demonstrated the possible detection of NO_2^-.[38] Recently, a sensor based on a nanoporous gold microelectrode was reported for the electrochemical detection and determination of NO_2^-.[39] In another work, Ding and co-workers reported on the development of ultrathin gold electrode for the electrochemical sensing of NO_2^-.[40] Taking the exceptional individual properties of Au and Co_3O_4 into account, a combination of these two materials might yield greater electrochemical performance towards NO_2^- sensing. Also from an economic perspective, combining Au with metal oxides can make the nanomaterial significantly cheaper.

Cobalt oxide (Co_3O_4) nanosheets/nanoparticles have recently gained significant attention as they are economical, biocompatible, possess excellent electrocatalytic properties and good conductivity.[41, 42] Co_3O_4 with their promising capacitive characteristics makes it an apt material for a variety of applications such as supercapacitors, electrocatalysts and magnetic materials.[43-48] The increase of the available surface area enhances the ability of the composites to interact with other materials, are one of the main advantages of this type of material.[49] Due to its valuable properties, Co_3O_4 nanoparticles, by itself have been reported for an array of applications.[50-56] Until now, no literature work has been reported on the use of Co_3O_4/Au for the electrochemical detection of NO_2^-.

Herein, we report on the structural morphology and electrochemical performance of a nitrite sensor based on the Co_3O_4/Au nanocomposite modified GCE by a facile method. The Co_3O_4/Au prepared by drop casting Co_3O_4 ink followed by the electrodeposition of Au was employed for the detection of nitrite for the first time. The electrochemical performance and the

analytical capabilities of this nitrite sensor were investigated using linear sweep voltammetry (LSV), cyclic voltammetry (CV), Differential pulse voltammetry (DPV) and square-wave voltammetry (SWV). The fabricated sensor demonstrated good sensitivity, stability and satisfactory reproducibility.

4.2. Experimental Section

4.2.1. Reagents

Sodium dihydrogen phosphate monobasic, Disodium hydrogen phosphate dibasic, sodium nitrite, sodium hydroxide, orthophosphoric acid were purchased from Sigma-Aldrich. All reagents used for the experiments were of analytical grade. All the experiments were performed using deionized water (18.2 MΩ cm), and all glassware was carefully cleaned before each analysis. Phosphate buffer solution (PBS), pH 4.5 was chosen as the electrolyte medium to conduct all the electrochemical analysis. All the electrochemical experimentations were performed at room temperature, 20±2 °C.

4.2.2 Characterization and electrochemical measurements

Surface morphology and composition of the Co_3O_4/Au nanocomposite was characterized using a field-emission scanning electron microscopy (FE-SEM) (FEI QUANTA FEG 250) and energy-dispersive X-ray spectroscopy (EDX) (Hitachi SU-70). All the electrochemical studies were carried out in a nitrogen purged atmosphere, using a CHI - 660D electrochemical workstation with a typical three-electrode cell system. A glassy carbon electrode (GCE) was utilized as the working electrode substrate, platinum (Pt) wire as the counter electrode and 3M KCl Ag/AgCl as the reference electrode, respectively. Phosphate buffer (PB) (pH 4.5) was used as the supporting electrolyte.

4.2.3 Electrode preparation and modification

The Co_3O_4 sheets were synthesized by chemical reduction followed by calcination in order to form the nanosheets. Initially, 4.0 mM of $Co(NO_3)_2$ was subjected to reduction under a constant state of stirring using aqueous $NaBH_4$ solution (at a concentration of 0.1 g/10 mL). Then by centrifugation, the product obtained after the reduction process was gathered by centrifugation. The collected product was rinsed carefully with a solution mixture (water/ethanol) and was dried at 70 ˚C. Furthermore, the final washed product was annealed at 450 ˚C for 4 h.[57]

The Co_3O_4 nanosheets/Au modified GCE was fabricated by dissolving the Co_3O_4 nanosheets in double distilled water (2.0 mg mL^{-1}). The prepared ink was drop-casted (3.0 µL) onto a GCE (d = 3.0 mm) surface and allowed to dry at room temperature (20.0 °C) for 4 h. The Co_3O_4/GCE was further modified by electrodepositing Au on the electrode (1.0 mM of $HAuCl_4.3H_2O$ in 0.1 M KNO_3) to form Co_3O_4/Au/GCE. The as-fabricated GCE was used as the working electrode. Preceding the modification step, all the GC electrodes were polished with a 0.05 µM alumina slurry and ultrasonicated in ethanol and water for 10 min.

4.2.4. Sample preparation

The beef sample purchased from a local grocery store was used for (Canadian Minced Beef) nitrite analysis. About 5.0 g of the beef sample was treated with 50 ml of boiling water for 10 min. Then, using Whatman filter paper the treated mixture was filtered, and the final solution was adjusted to a pH of 4.5.

4.3. Results and Discussion

4.3.1. Surface morphology and optimization of the Au deposition time

The morphology of the Co_3O_4/Au was characterized using SEM. Figure 4.1 shows the SEM images of Co_3O_4/GCE and Co_3O_4/Au/GCE.

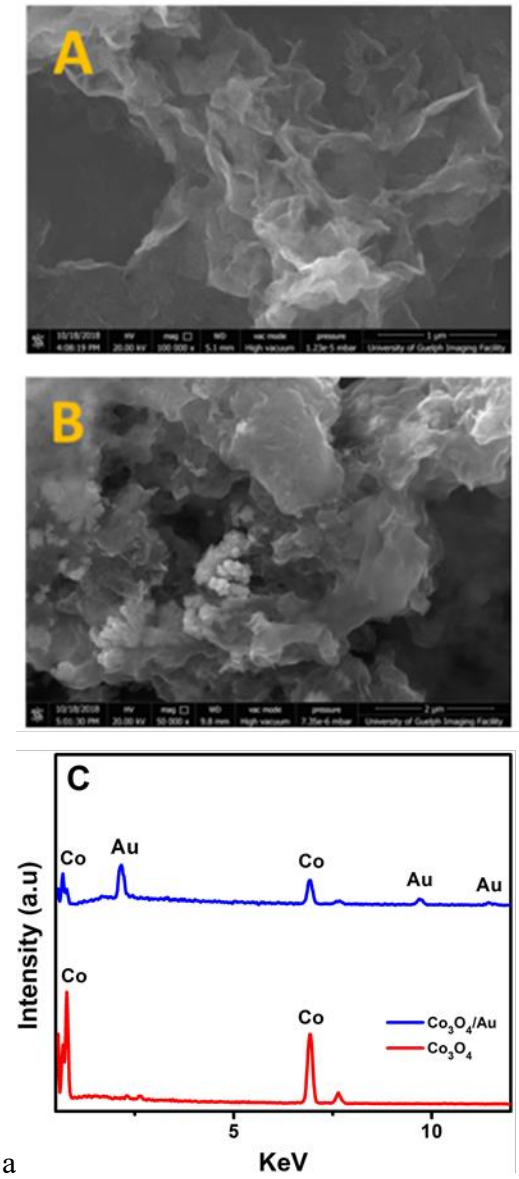

a

Figure. 4.1. The SEM image of the Co_3O_4 nanosheets (A) and the SEM image of the Au deposited on the surface of the Co_3O_4 nanosheets (B); EDX spectrum for the Co_3O_4 nanosheets and Au deposited Co_3O_4 nanosheets (C).

Figure 4.1A illustrates a typical SEM image of the Co_3O_4 nanosheet with 100000 magnification. It can be observed from the image that the structure of Co_3O_4 nanosheet was crumpled and had a transparent layer. From Figure 4.1B, it can be spotted that the Au is dispersed on the Co_3O_4 nanosheets. Also, this showed that Au is deposited on the sheets of Co_3O_4. Furthermore, EDX analysis was performed to confirm the presence of Au on Co_3O_4 sheets. Figure 4.1C shows the EDX spectrum of Co_3O_4 with peaks dedicated to only cobalt and Co_3O_4/Au with the presence of Au and cobalt.

The effect of the Au deposition on the Co_3O_4/GCE was studied using the amperometric i-t curve in 0.1 M KNO_3. Au/Co_3O_4 on the GCE was achieved by applying a potential of −0.4 V (vs Ag/AgCl) for 1.0, 2.0, 3.0, 5.0, 7.5, 10.0 and 12.5 min (Figure 4.2A). The current response increased with increasing Au deposition time and a peak current value for the anodic oxidation of NO_2^- was achieved at the deposition time of 7.5 min. Further, when the duration of Au deposition was increased from 7.5 to 10.0 and 12.5 min, the peak current value displayed a downward trend for the NO_2^- oxidation (Figure 4.2B). Therefore, 7.5 min was assigned as the optimal Au deposition time and was used in later experiments.

4.3.2 Comparison of performances of the modified electrodes

The electrochemical performance of Co_3O_4/Au/GCE (blue curve) towards the oxidation 1.0 mM NO_2^- in 0.1 M PB pH 4.5 was investigated by LSV and the resultant voltammogram is displayed in Figure 4.3. As an evaluation of the electrochemical performance, other modified electrodes such as bare GCE (red), Au/GCE (green) and Co_3O_4/GCE (light green) were tested and compared under similar conditions. A small anodic peak was observed for the bare GCE toward the oxidation of NO_2^- at 1.10 V, while a sharp oxidation peak was observed at 0.90 V for Au/GCE and broad oxidation peak appeared at ~1.07 V for Co_3O_4/GCE. On the contrary, a sharper oxidation

peak appeared at 0.86 V for the Co_3O_4/Au/GCE, with an increase of the anodic peak current by ~2.0 times and a slightly negative shift in the peak potential in comparison with the Co_3O_4/GCE and Au/GCE.

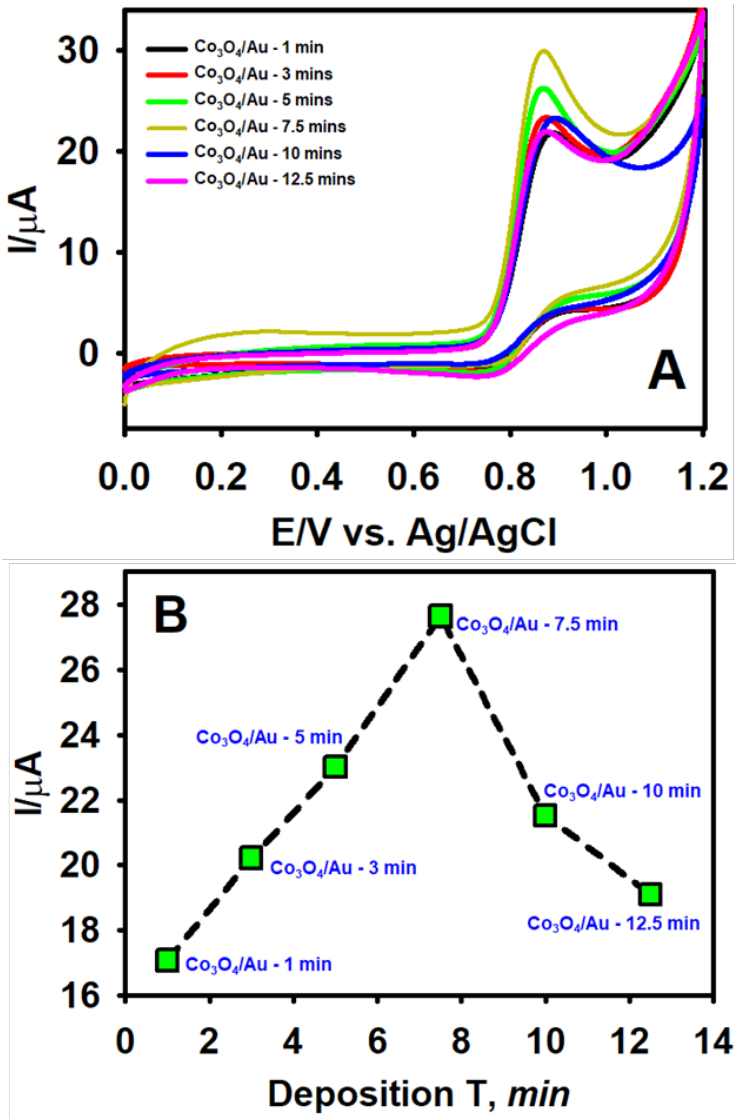

Figure 4.2. CV curves recorded for the oxidation of 1.0 mM nitrite with Au deposited at different times (1.0, 2.0, 3.0, 5.0, 7.5, 10.0 and 12.5 minutes) on the Co_3O_4 nanosheets (A); Plot illustrating the improvement in the anodic peak current with respect to increasing Au deposition time (T, min) (B) in 0.1 M PB pH 4.5.

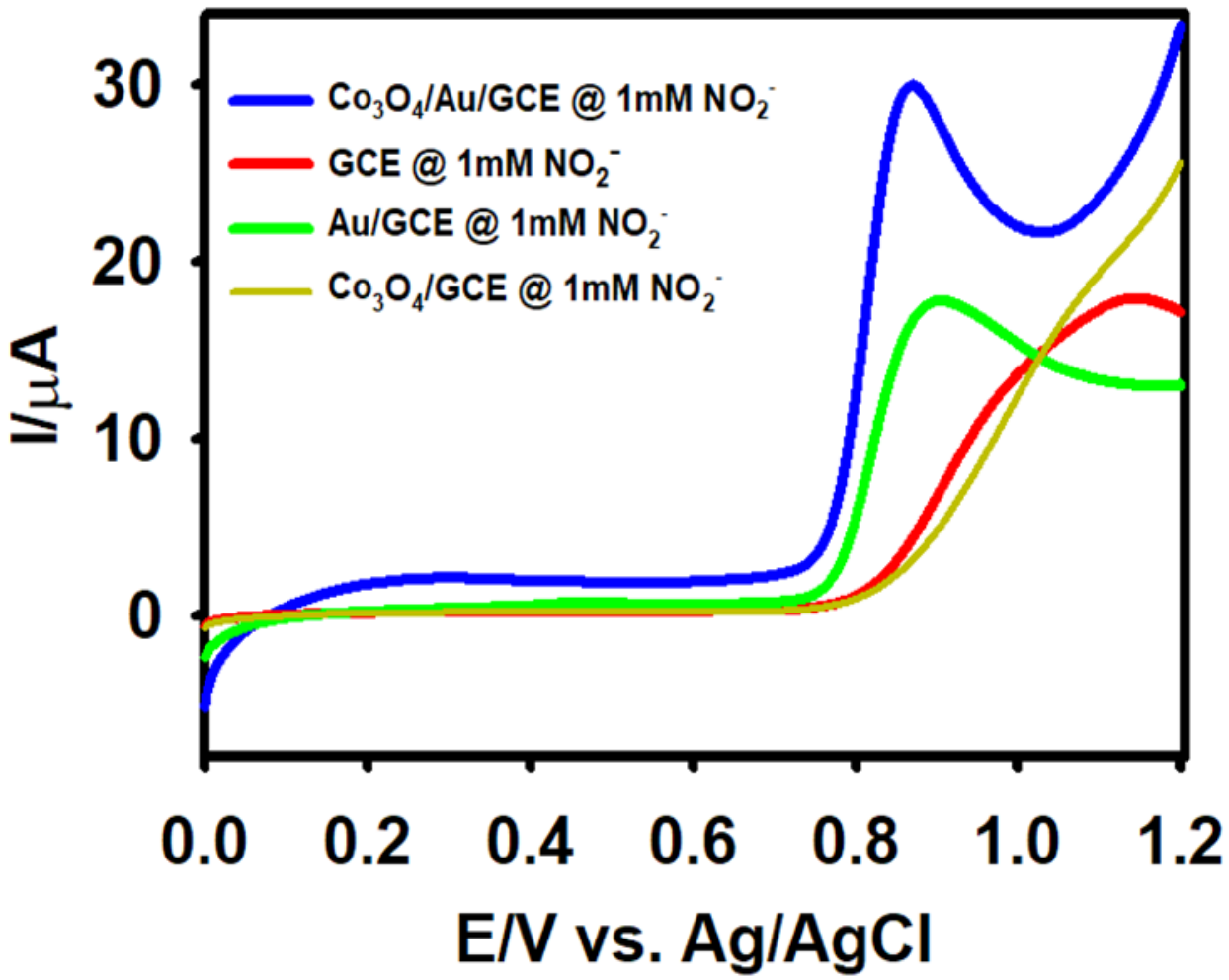

Figure. 4.3. LSV curves show the comparison of the performance of Co_3O_4/Au/GCE (blue line), bare GCE (red line), Au/GCE (green line), Co_3O_4/GCE (light green line), at the scan rate of 50 mV s^{-1} in 0.1 M PB pH 4.5.

The increase in peak current value coupled with a negative potential shift in the NO_2^- oxidation might be attributed to a faster electron transfer process at the Co_3O_4/Au/GCE. Thereby, displaying the synergistic ability of the Au and Co_3O_4 nanosheets to proficiently catalyze the electrooxidation of NO_2^-. Furthermore, the oxidation peak potential and the anodic peak current values were found to be invariable over the successive cycles. This could be attributed to the excellent electrochemical properties

of Co_3O_4 nanosheets, such as good electrocatalytic activity and improved surface area.[57] Also, the presence of Au on the Co_3O_4 nanosheets promoted towards the efficient electrooxidation of NO_2^-.

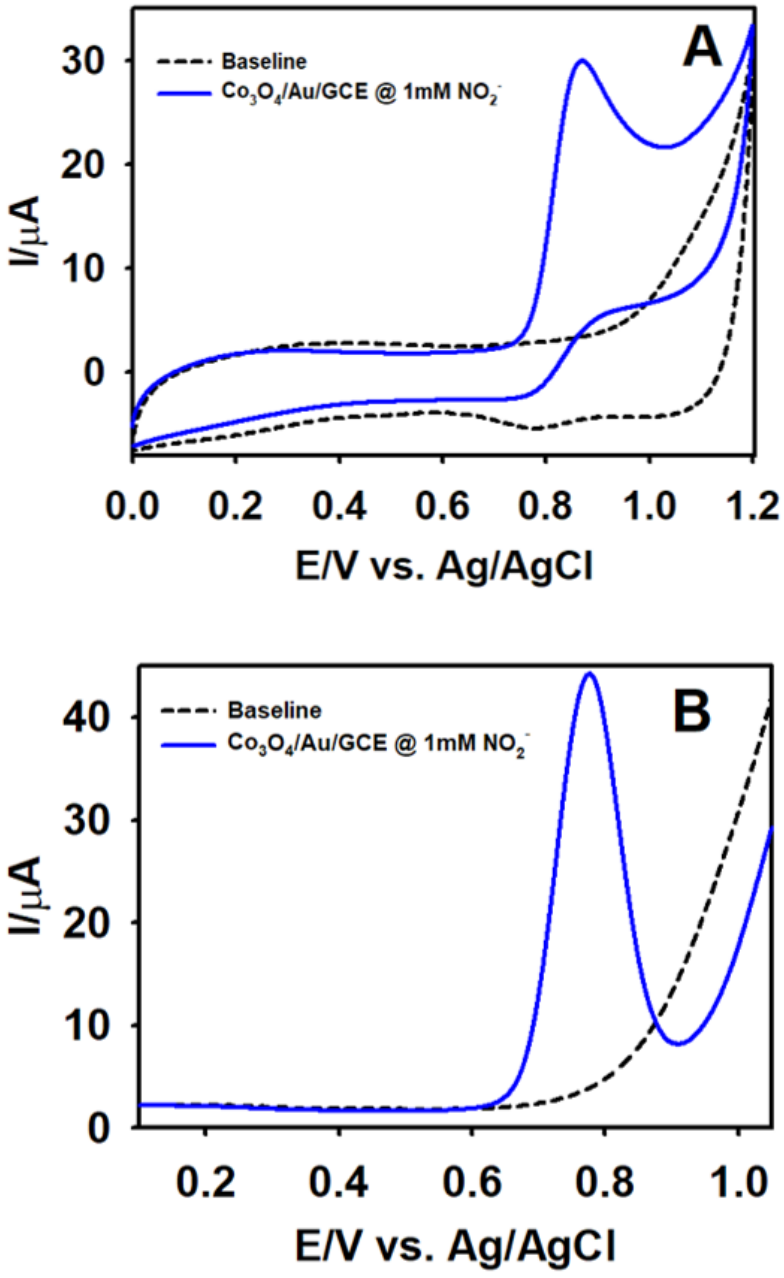

Figure. 4.4. CV (A) and DPV (B) curves of the Co_3O_4/Au/GCE recorded in the absence (dotted lines) and in the presence (solid lines) of 1.0 mM of NO_2^- where the supporting electrolyte is 0.1 M PB pH 4.5.

4.3.3 Electrochemical behaviour of NO_2^- using CV and DPV

The electrooxidation behaviour of NO_2^- molecule (using 1.0 mM $NaNO_2$) at the Co_3O_4/Au/GCE was inspected using CV. The CV scan was cycled between 0.0 and 1.2 V at the scan rate of 0.1 M PB pH 4.5. Figure 4.4A represents the response curves recorded for the oxidation of NO_2^- at the Co_3O_4/Au/GCE in 0.1 M PBS without (dashed line) and with (solid line) 1.0 mM of the analyte. This could be attributed to the following anodic reaction:

$$NO_2^- + H_2O \rightarrow NO_3^- + 2H^+ + 2e^- \quad (1)$$

Also, it is observed from Figure 4.4A, the addition of NO_2^- into the solution shows an irreversible peak in the chosen potential range. The corresponding peak current for the NO_2^- oxidation obtained with CV was calculated to be 28.72 μA. Differential pulse voltammetry (DPV) has better sensitivity in comparison with CV, hence, the techniques of DPV was used to study the oxidation behaviour of NO_2^- on the as-prepared Co_3O_4/Au/GCE (Figure 4.4B). The associated peak current was measured to be 39.43 μA and a prominent peak appeared at ~0.78 V for the electrochemical oxidation of 1.0 mM NO_2^-. The above-mentioned results from the CV and DPV results indicated that the Co_3O_4/Au/GCE greatly facilitated the oxidation of NO_2^-.

4.3.4 Effect of scan rate, concentration and electrolyte pH

The effect of scan rate was studied using LSV in 0.1 M PBS (pH 4.5). Figure 4.5A illustrates the influence of scan rate (υ) on the electro-oxidation of 500.0 μM NO_2^- at Co_3O_4/Au/GCE from 10 to 100 mV s^{-1}. For an anodic oxidation process the Randles–Sevcik equation is as follow:

$$Ip = 3.01 \times 10^5 n[(1-\alpha) n_\alpha]^{1/2} A C_b D^{1/2} v^{1/2} \quad (2)$$

where n denotes the number of electrons transferred, α signifies the electron transfer coefficient, n_α is the number of electrons, A refers to the area of the electrode, C_b is bulk concentration of the analyte (NO_2^-, 1 mM) and D stands for the diffusion coefficient of the analyte.

The values of the anodic peak current increased steadily with increasing scan rate, however, the curves observed in the voltammogram exhibited a shift in the peak potentials of nitrite oxidation (Figure 4.5A). The oxidation peak current demonstrated an increasing linear trend with the square root of the scan rate ranging from 10 - 100 mV s^{-1}, which is expressed by the following regression equation: $Ip = 4.833 + 2.605\ v^{1/2}\ (R^2 = 0.9988)$.

The results from the calibration plot (Figure 4.5B) suggest that the oxidation process of NO_2^- at the Co_3O_4/Au/GCE is diffusion controlled. Additionally, it is perceived from Figure 4.5B inset that the peak potential of nitrite oxidation shifted towards the more positive direction of the potential window with the increasing of scan rate. The calibration plot between Epa and $v^{1/2}$ displayed a linear relationship with the regression equation as follow: $Epa = 0.823 + 0.072\ log\ v\ (R^2 = 0.9976)$. Moreover, the results obtained from the calibration plot indicated that the oxidation of nitrite at the Co_3O_4/Au/GCE is irreversible.

The electrooxidation behavior of NO_2^- was further investigated using LSV in 0.1 M PBS pH 4.5 (scan rate = 50 mV s^{-1}) at various concentrations. It is evident from Figure 4.6A that there is no appearance of the peak for the absence of the analyte while a sharp response is spotted for the addition of 250.0 µM NO_2^-. The peak current value for the oxidation of NO_2^- grew linearly with each successive addition in the concentration range from 0.0 to 3000.0 µM. Figure 4.6B displays the calibration plot obtained for the peak current value for the oxidation against the different concentrations of NO_2^-.

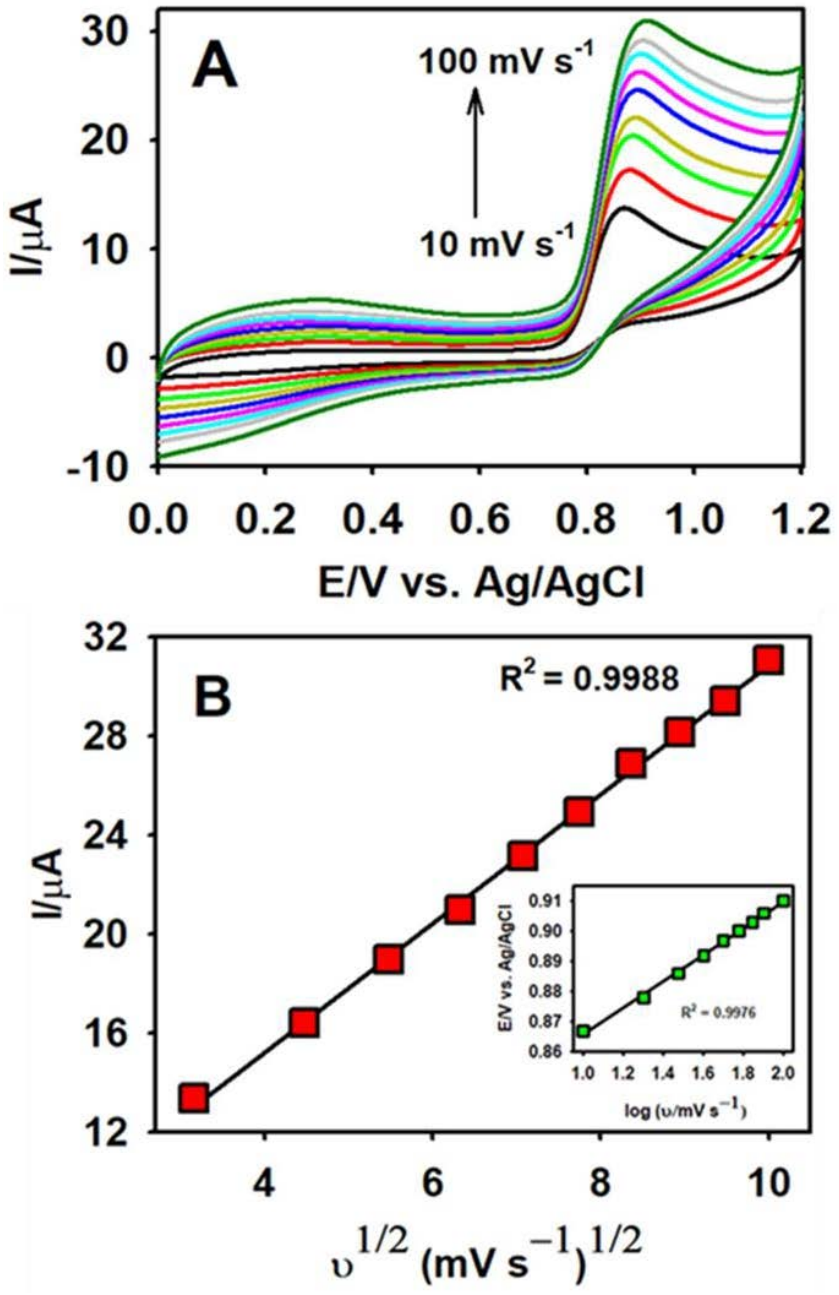

Figure. 4.5. CV curves of the Co_3O_4/Au/GCE measured in (A) 1.0 mM NO_2^- at various scan rates (10, 20, 40, 50, 60, 70, 80, 90, 100 mV s^{-1}); (B) represents the corresponding linear relationship between the oxidation peak current I_p and the square root of the scan rate $\upsilon^{1/2}$ (inset shows the relation between log of scan rate vs. peak potential, in the electrolyte medium of 0.1 M PB (pH 4.5)

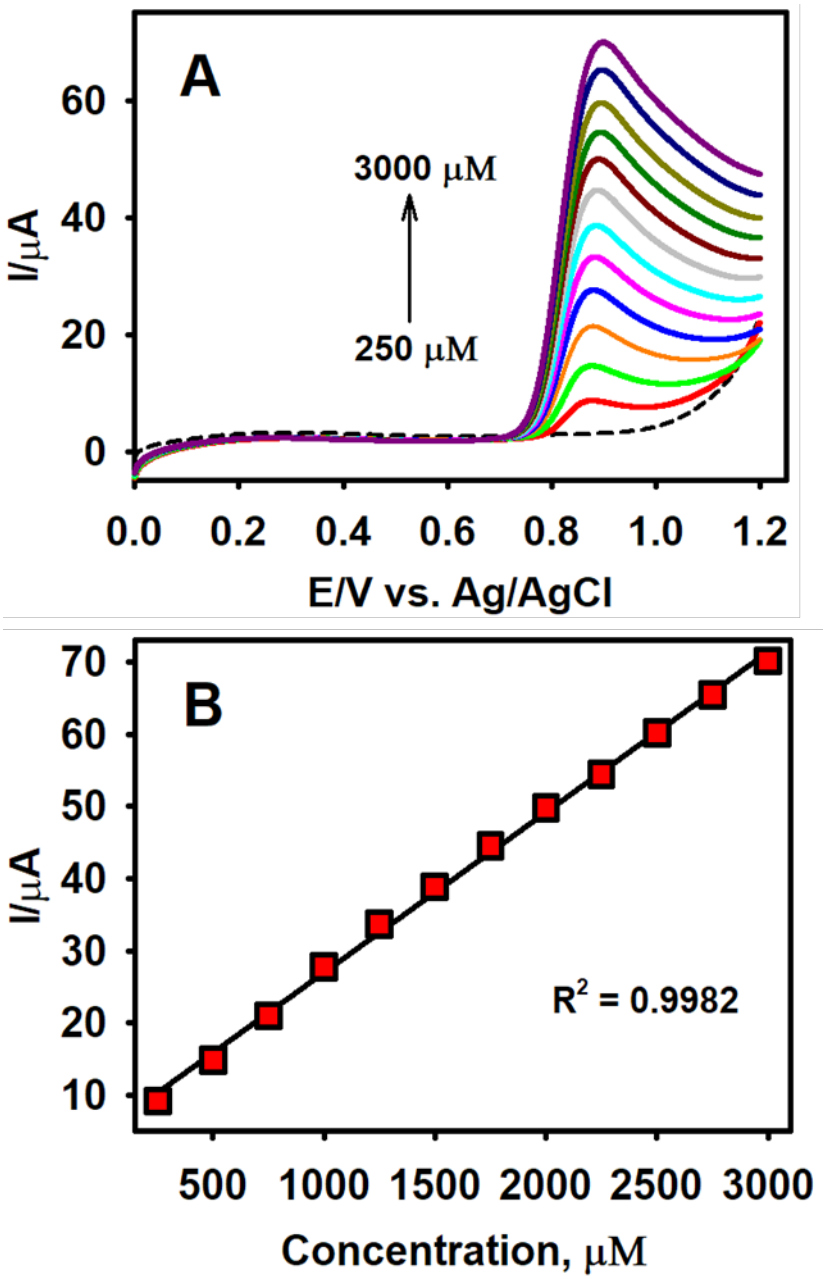

Figure 4.6. CV response recorded with the Co_3O_4/Au/GCE toward the oxidation of NO_2^- at different concentrations ranging from 250.0 to 3000.0 μM (A); and the corresponding plot of anodic peak current vs. increasing concentration of NO_2^- (B) in 0.1 M PB pH 4.5, at the scan rate of 50 mV s^{-1}.

It is visible from the calibration plot that there is excellent linearity within the selected concentration range with the following linear regression equation of *Ipa (μA)* = 4.726 *μA/μM* + 0.082 *μA* an R^2 value of 0.9982.

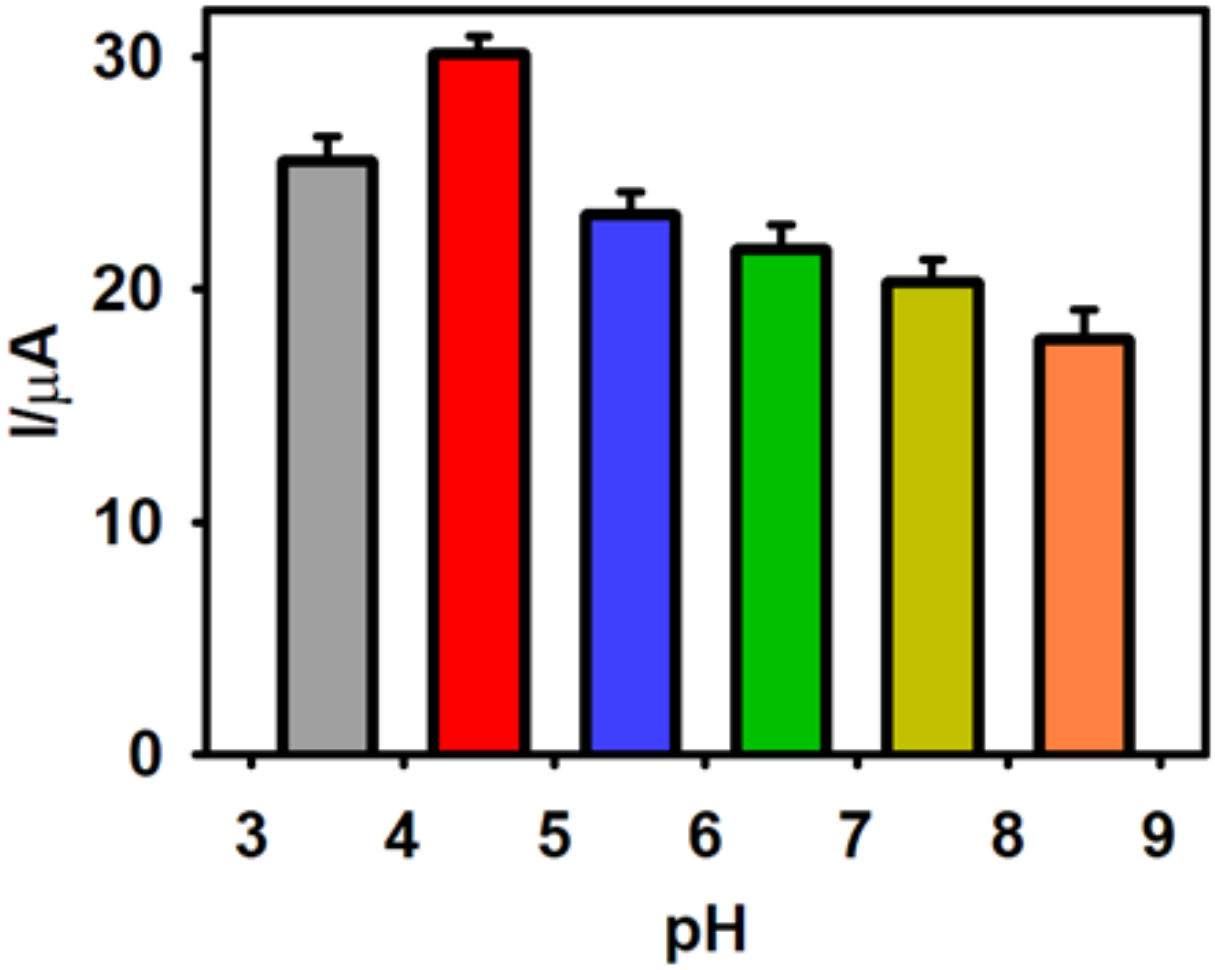

Figure 4.7. CV response of the Co_3O_4/Au/GCE toward the oxidation of 1.0 mM NO_2^- at different pHs (3.5 - 8.5), at the scan rate of 50 mV s^{-1}.

The pH of the electrolyte medium contributes significantly to enhancing the electrocatalytic performance of the sensor and determining the electrooxidation ability of the analyte. The electrochemical behaviour of NO_2^- was investigated utilizing CV in 0.1 M PBS in different pH conditions consisting of 1.0 mM of the analyte (at the scan rate of 50 mV s^{-1}). Fig.

4.7 exhibits the peak current response for the oxidation of the NO_2^- in the electrolytes with distinct pH values ranging from 3.5 to 8.5. The peak current value increased with changing pH on the scale of 3.5 to 8.5, however, the peak current value for anodic oxidation NO_2^- declined when the pH of the electrolyte was higher than 4.5 and upwards. It is known from the literature that nitrite anions are not stable in strongly acidic media (< pH 4.0) and the reaction (Eq. 2) can be written as follow:

$$2H^+ + 3NO_2^- \rightarrow 2NO + NO_3^- + H_2O \qquad (3)$$

On the other hand, because the pK_a of HNO_3 is 3.3, protonation of most nitrite anions takes place in acidic condition. When the electrolyte pH is higher than 4.5, the lesser availability of protons in the basic medium makes the electro-oxidation of nitrite more challenging.[39] Hence, 0.1 M PBS at pH 4.0 was selected as the supporting electrolyte for further experiments.

4.3.5 Analytical determination of NO_2^-

Square wave voltammetry (SWV) was employed to scrutinize the analytical capability of the developed Co_3O_4/Au sensor for the determination of NO_2^- (0.1 M PB, pH 4.5) with a range of concentrations of the analyte from 1.0 - 4000.0 μM. The Co_3O_4/Au/GCE did not show any noticeable response in the absence of NO_2^- signifying the sensor's inactivity without the molecule in the selected potential range.

As seen in Figure 4.8A, the curves recorded with SWV exhibited a linear increase in the current value for NO_2^- oxidation with respect to the increasing analyte concentration. Figure 4.8B shows the linear relationship between the concentration (c, μM) and the current (Ipa, μA) for the electrochemical oxidation of NO_2^- in the concentration ranges of 1.0 – 1000.0 μM and 1250.0 – 4000.0 μM. The linear regression equation are as follows: $Ipa = 9.165 + 0.107c\ (\mu M)$; [$R^2$ = 0.9994] and $Ipa = 78.953 + 0.097c\ (\mu M)$; [$R^2$ = 0.9994].

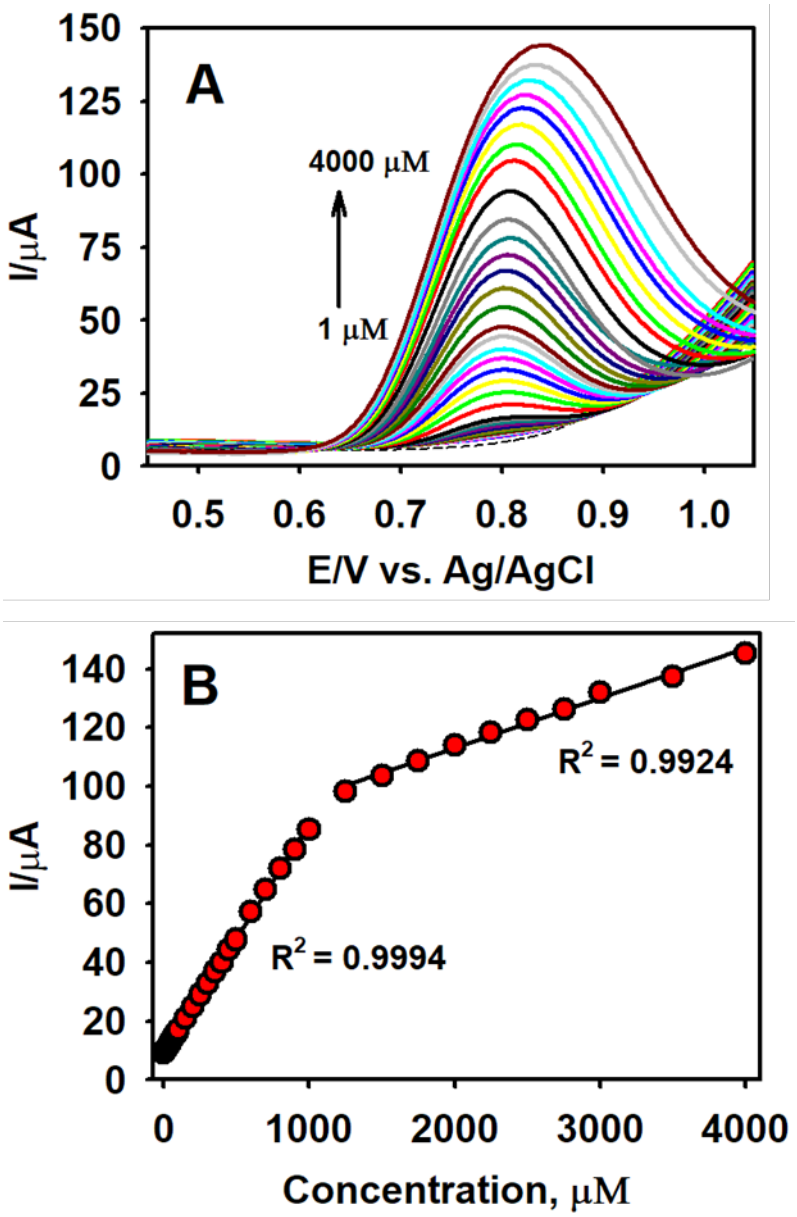

Figure 4.8. SWV responses obtained with Co_3O_4/Au/GCE toward the oxidation of NO_2^- in a concentration range from 1.0 µM to 4000.0 µM (A); the corresponding calibration plot for anodic peak current vs concentration (B) in 0.1 M PB electrolyte solution (pH 4.5).

The limit of detection (LOD) for the electrochemical sensor was calculated to be 0.112 µM using the formula:

$$\text{LOD} = \frac{3\sigma}{b}, \qquad (4)$$

where σ stands for the standard deviation of blank measurement and *s* signifies the slope estimated from the calibration plot. The two calibration plots attained from the analytical determination NO_2^- were comparable to the previously reported literature that contained the measurement of analytes such as acetaminophen and valacyclovir, ascorbic acid, dopamine, uric acid and NADH.[34,58-60]

Table 4.1. Comparison of the electrochemical performance of Co_3O_4/Au/GCE sensor other reported sensors toward NO_2^- detection

Electrode materials	Linear range (µM)	Detection limit (µM)	Ref.
PEDOT/AuNPs	3.0–300.0	0.1	[61]
RGO/MWCNT/Pt/Mb	1.0–12000.0	0.93	[62]
Au/ZnO/MWCNT	0.78 - 400.0	0.4	[63]
Heteroatom enriched porous carbon	3.0 - 90.0	0.13	[64]
Au/SG	10.0 - 3960.0	0.2	[65]
Cu-NDs/RGO	1.25–13000.0	0.4	[66]
Co_3O_4/Au/GCE	1.0 - 4000.0	0.1	**This work**

*PEDOT - poly(3,4-ethylenedioxythiophene); Au - gold; AuNPs - gold nanoparticles; RGO - reduced graphene oxide; MWCNT - multiwalled carbon nanotubes; Pt - platinum; Mb - molybdenum; ZnO - Zinc oxide; Cu-NDs - copper nanodendrites; Co_3O_4 - cobalt oxide; GCE - glassy carbon electrode

The sensitivity of the modified electrode was calculated to be 1.57 µA μM^{-1} cm^{-2}. The linear range and detection limit of other reported works on nitrite sensing was compared with the performance of Co_3O_4/Au/GCE (listed in Table 4.1).

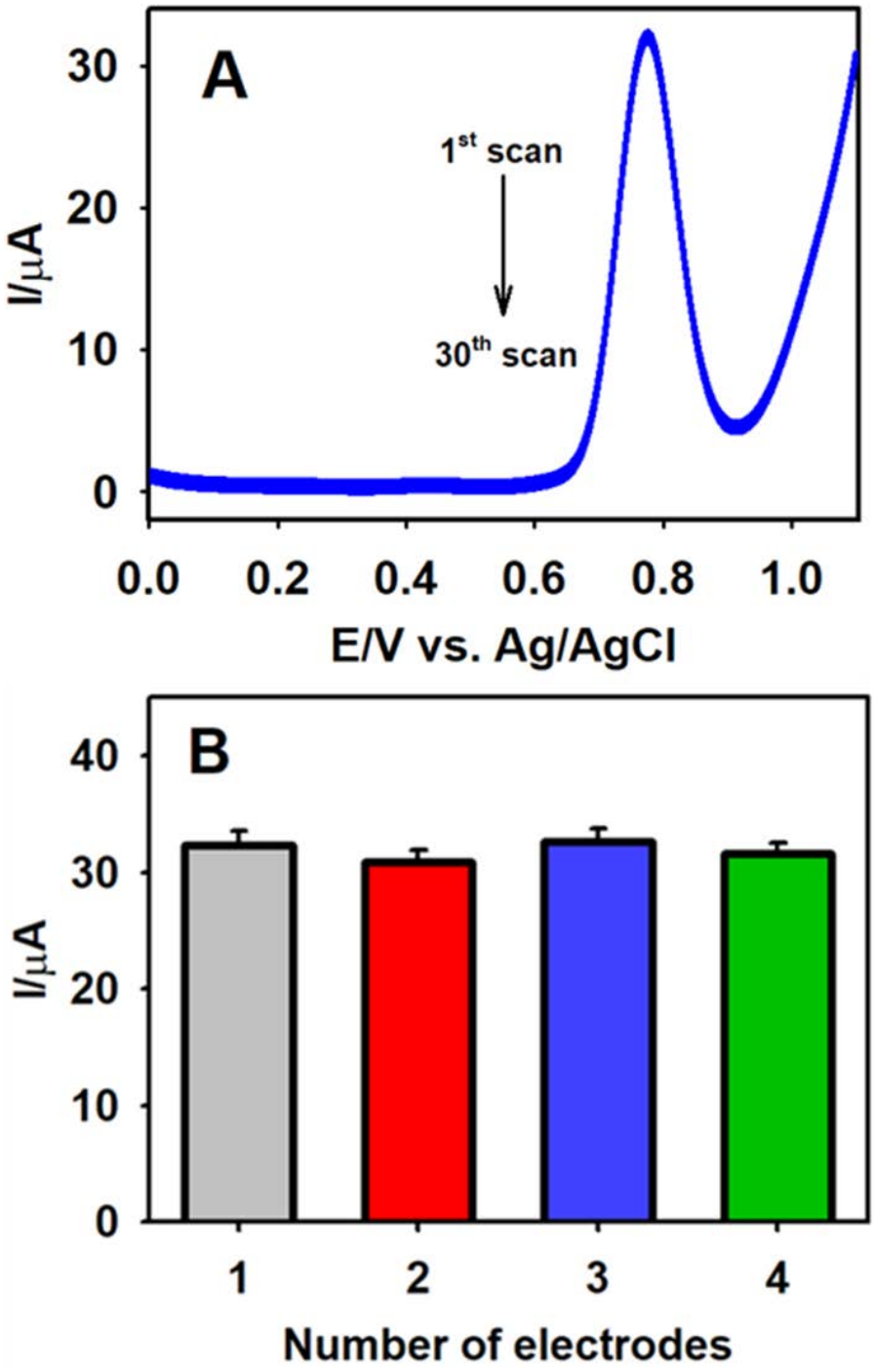

Figure 4.9. Stability measurement of the Co_3O_4/Au/GCE toward 1.0 mM NO_2^- oxidation for consecutive 30 DPV measurements (A); DPV response recorded in presence of 1.0 mM NO_2^- with 4 different Co_3O_4/Au/GCEs representing the reproducibility of the sensor (B) in 0.1 M PB buffer solution (pH 4.5).

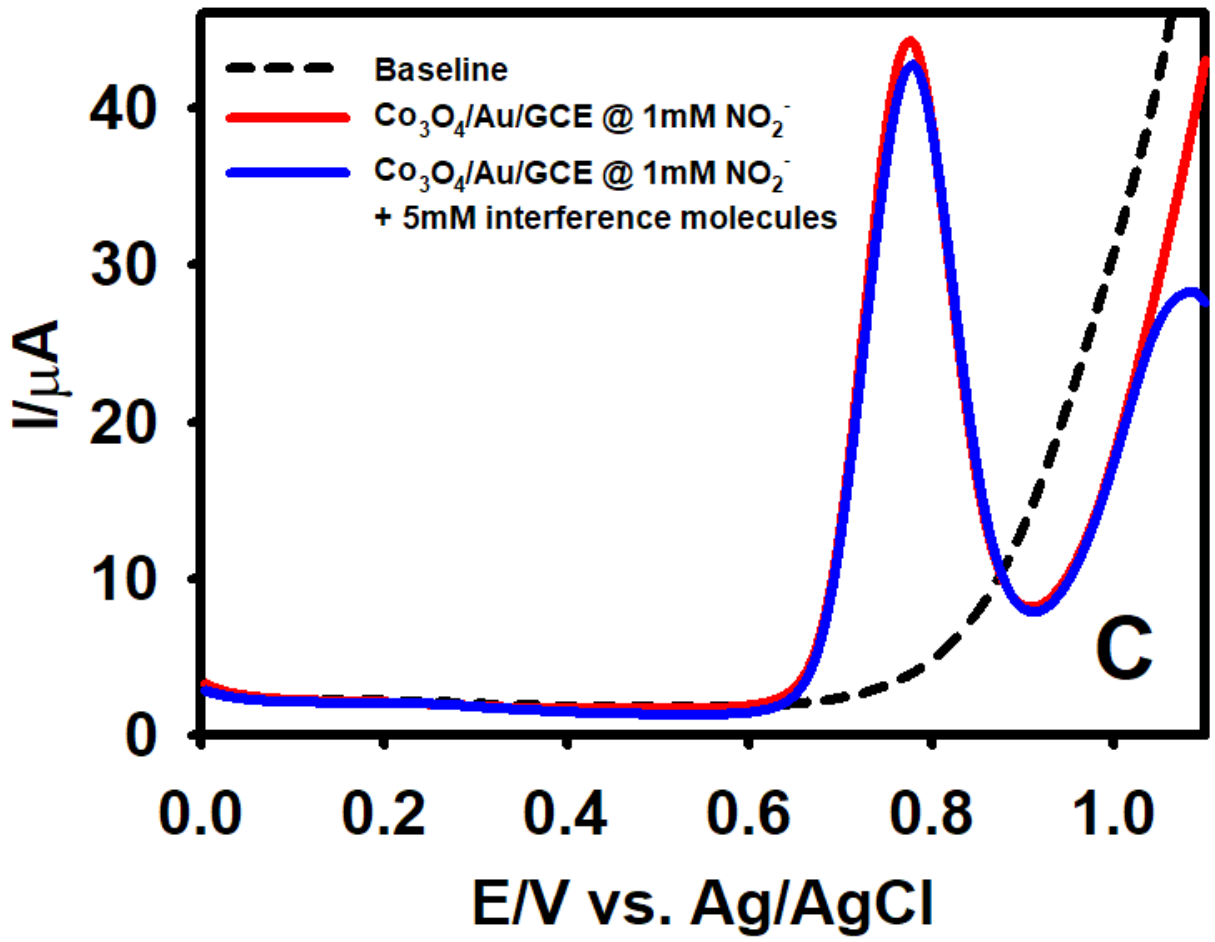

Figure 4.10. Interference response of the Co_3O_4/AuNPs/GCE for the oxidation of 1.0 mM NO_2^- in the presence of 5-fold (5.0 mM) concentration of interfering molecules (glucose, CH_3COONa, $CaCl_2$, $CuSO_4$, $MgCl_2$, KCl and NH_4NO_3), in 0.1 M PB electrolyte medium (pH 4.5).

4.3.6. Stability, reproducibility and interference measurements

The stability of the sensor was tested by utilizing DPV for 30 successive scans (Figure 4.9A). The sensor retained ~95% of its initial peak current response toward 1.0 mM NO_2^- oxidation in 0.1 M PB buffer (pH 4.5), thereby demonstrating the sensor's good stability and could be applicable in evaluating the real sample. Additionally, the reproducibility of the Co_3O_4/Au/GCE was evaluated by preparing 4 different GCEs and the experiments were performed in 0.1 M PB with 1.0 mM of NO_2^- under the same experimental conditions (Figure 4.9B). The RSD value for

the anodic peak current measured at 4 different electrodes was estimated to be 1.92%, thus signifying the Co_3O_4/Au/GCE sensor's good reproducibility.

The selectivity of the Co_3O_4/Au/GCE electrochemical sensor was verified for its anti-interference ability in the presence of interfering species using DPV. Figure 4.10 shows the DPV response obtained for the oxidation of 1.0 mM NO_2^- in the presence of 5-fold (5.0 mM) concentration of interfering molecules such as glucose, CH_3COONa, $CaCl_2$, $CuSO_4$, $MgCl_2$, KCl and NH_4NO_3. Further, the interference study revealed that the Co_3O_4/Au/GCE sensor retained 96.31% of its activity for the oxidation of 1.0 mM NO_2^- the presence of interference molecules. These aforementioned observations indicated that the developed sensor could be applicable to the real-time detection of NO_2^-.

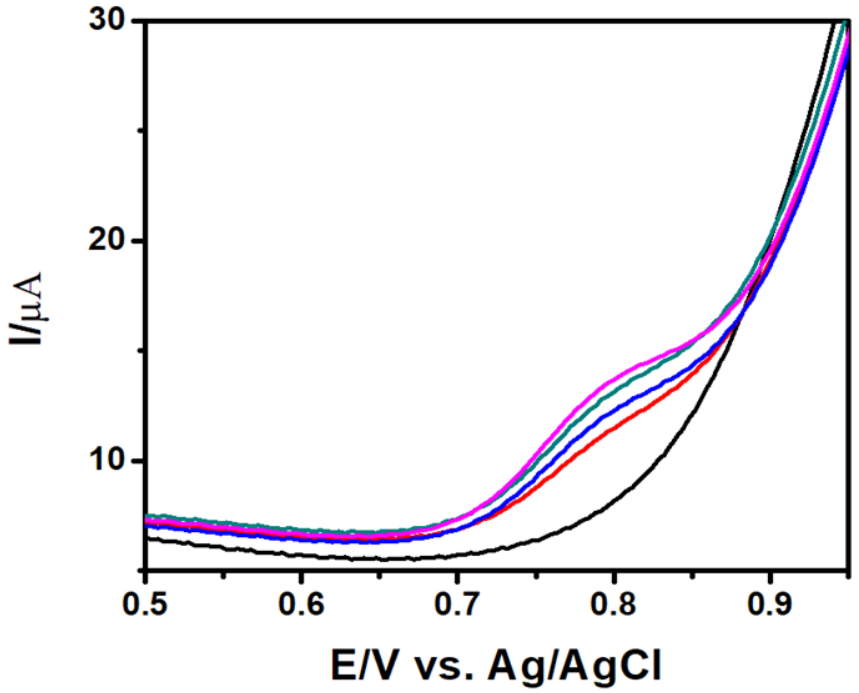

Figure 4.11. SWV of the Co_3O_4/Au/GCE recorded in 0.1 M PB (pH 4.5) showing the presence of nitrite in the Canadian minced beef sample.

Table 4.2. Performance of the Co_3O_4/Au/GCE electrode for the determination of NO_2^- in bottled water and beef sample.

Real sample	Actual (µM)	Spiked (µM)	Observed (µM)	RSD% (n = 3)	Recovery (%)
Bottled water	--	30.00	29.20	1.89	97.33
	--	40.00	39.91	2.57	99.75
	--	50.00	48.46	2.13	96.92
	--	60.00	58.72	2.26	97.84
Beef sample	1.36	2.00	3.33	2.18	98.70
	1.34	4.00	5.32	2.34	98.51

4.3.7. Real sample analysis

The practicability of the developed sensor was verified by the determination of nitrite in commercially bottled water. The water samples were spiked with known concentrations of nitrite and evaluated using Co_3O_4/Au/GCE. Table 4.2 summaries the quantities of NO_2^- found in the bottled water and the beef samples. The calculated values from the spiked samples showed good recovery rates from 96.92 to 99.75 % revealing the considerable applicability of the proposed sensor for real sample testing. Furthermore, a commercially purchased beef sample was tested for the presence of nitrite to exhibit the performance of fabricated the sensor. The DPV measured for NO_2^- in the beef sample is presented in Figure 4.11. The initial amount of nitrite in the beef sample (diluted with buffer solution) was found to be 1.36 µM. The final amount of nitrite determined in

the beef Sample was ~170.13 μM (after accounting for dilution), which was calculated by extrapolating against the constructed calibration plot and multiplying with the dilution factor. The relative standard deviation (RSD) for each sample was less than 3%, calculated based on three experimental trials. Also, the determined amount of nitrite in the beef product was within the permissible limit (~200 ppm) set by the Public Health Agency of Canada. All these results showed the effectiveness of the developed sensor for the detection of NO_2^- in real samples.

4.4. Conclusions

An electrochemical sensor based on Co_3O_4 nanosheets and Au was successfully developed and employed for the first time towards the electrochemical detection of NO_2^-. The results from the CV studies demonstrated that electro-oxidation of NO_2^- is efficient at the Co_3O_4/Au/GCE in terms of enhanced current response and a decrease in overpotential compared to bare GCE and Co_3O_4/GCE. The fabricated electrochemical sensor showed agreeable analytical capabilities with good linearity over the wide calibration range, high sensitivity and a low LOD of 0.11 μM. The sensor also displayed superior selectivity towards the NO_2^- determination in the presence of co-existing ions and other interference molecules. The developed Co_3O_4/Au/GCE sensor exhibited appreciable repeatability, good reproducibility and possessed good chemical stability. Moreover, the sensor yielded satisfactory recovery rates with the real sample studies and proved its practical applicability representing it a promising candidate for food quality control.

References

1. J. Liu, Y. Chen, L. Wang, M. Na, H. Chen and X. Chen, Modification-free fabricating ratiometric nanoprobe based on dual emissive carbon dots for nitrite determination in food samples, *J. Agric. Food Chem.* (2019) 10.1021/acs.jafc.1029b00024.

2. N. P. Sen and P. A. Baddoo, Trends in the levels of residual nitrite in Canadian cured meat products over the past 25 years, *J. Agric. Food Chem.* 45 (1997) 4714-4718.

3. W. J. R. Santos, P. R. Lima, A. A. Tanaka, S. M. C. N. Tanaka and L. T. Kubota, Determination of nitrite in food samples by anodic voltammetry using a modified electrode, *Food Chem.* 113 (2009) 1206-1211.

4. X. Ge, L. Wang, Z. Liu and Y. Ding, Nanoporous gold leaf for amperometric determination of nitrite, *Electroanal.* 23 (2010) 381-386.

5. P. Miao, M. Shen, L. Ning, G. Chen and Y. Yin, Functionalization of platinum nanoparticles for electrochemical detection of nitrite, *Anal. bioanal. chem.* 399 (2011) 2407-2411.

6. O. Ozdestan and A. Uren, Development of a cost-effective method for nitrate and nitrite determination in leafy plants and nitrate and nitrite contents of some green leafy vegetables grown in the Aegean region of Turkey, *J. Agric. Food Chem.* 58 (2010) 5235-5240.

7. H.-H. Ren, Y. Fan, B. Wang and L.-P. Yu, Polyethylenimine-capped CdS quantum dots for densitive and selective detection of nitrite in vegetables and water, *J. Agric. Food Chem.* 66 (2018) 8851-8858.

8. L. Cui, J. Zhu, X. Meng, H. Yin, X. Pan and S. Ai, Controlled chitosan coated prussian blue nanoparticles with the mixture of graphene nanosheets and carbon nanospheres as a redox mediator for the electrochemical oxidation of nitrite, *Sens. Actuators B: Chem* 161 (2012) 641-647.

9. V. S. Manikandan, B. Adhikari and A. Chen, Nanomaterial based electrochemical sensors for the safety and quality control of food and beverages, *Analyst* 143 (2018) 4537-4554.

10. A. Shpaizer, A. Nussinovich, J. Kanner and O. Tirosh, S-nitroso-N-acetylcysteine generates less carcinogenic N-nitrosamines in meat products than nitrite, *J. Agric. Food Chem.* 66 (2018) 11459-11467.

11. S. Radhakrishnan, K. Krishnamoorthy, C. Sekar, J. Wilson and S. J. Kim, A highly sensitive electrochemical sensor for nitrite detection based on Fe_2O_3 nanoparticles decorated reduced graphene oxide nanosheets, *Appl. Catal. B* 148-149 (2014) 22-28.

12. X.-R. Li, F.-Y. Kong, J. Liu, T.-M. Liang, J.-J. Xu and H.-Y. Chen, Synthesis of potassium-modified graphene and its application in nitrite-selective sensing, *Adv. Funct. Mater.* 22 (2012) 1981-1988.

13. F. Bedioui and N. Villeneuve, Electrochemical nitric oxide sensors for biological samples–principle, selected examples and applications, *Electroanal.* 15 (2003) 5-18.

14. A. Afkhami, T. Madrakian, S. J. Sabounchei, M. Rezaei, S. Samiee and M. Pourshahbaz, Construction of a modified carbon paste electrode for the highly selective simultaneous electrochemical determination of trace amounts of mercury (II) and cadmium (II), *Sens. Actuators B: Chem.* 161 (2012) 542-548.

15. H. Bagheri, A. Afkhami, H. Khoshsafar, M. Rezaei and A. Shirzadmehr, Simultaneous electrochemical determination of heavy metals using a triphenylphosphine/MWCNTs composite carbon ionic liquid electrode, *Sens. Actuators B: Chem.* 186 (2013) 451-460.

16. H. Bagheri, A. Afkhami, H. Khoshsafar, M. Rezaei, S. J. Sabounchei and M. Sarlakifar, Simultaneous electrochemical sensing of thallium, lead and mercury using a novel ionic liquid/graphene modified electrode, *Anal. Chim. Acta* 870 (2015) 56-66.

17. R. Xi, S.-H. Zhang, L. Zhang, C. Wang, L.-J. Wang, J.-H. Yan and G.-B. Pan, Electrodeposition of Pd-Pt nanocomposites on porous GaN for electrochemical nitrite sensing, *Sensors* 19 (2019) 606.

18. J. Zhang, Y. Zhang, J. Zhou and L. Wang, Construction of a highly sensitive non-enzymatic nitrite sensor using electrochemically reduced holey graphene, *Anal. Chimi. acta* 1043 (2018) 28-34.

19. H. Bagheri, S. M. Arab, H. Khoshsafar and A. Afkhami, A novel sensor for sensitive determination of atropine based on a Co_3O_4-reduced graphene oxide modified carbon paste electrode, *New J. Chem.* 39 (2015) 3875-3881.

20. Y. Sun, Q. Ren, B. Liu, Y. Qin and S. Zhao, Enzyme-free and sensitive electrochemical determination of the FLT3 gene based on a dual signal amplified strategy: controlled nanomaterial multilayers and a target-catalyzed hairpin assembly, *Biosens. Bioelectron.* 78 (2016) 7-13.

21. T. Hou, W. Li, X. Liu and F. Li, Label-free and enzyme-free homogeneous electrochemical biosensing strategy based on hybridization chain reaction: A facile, sensitive, and highly specific microRNA assay, *Anal. Chem.* 87 (2015) 11368-11374.

22. T. Madasamy, M. Pandiaraj, M. Balamurugan, K. Bhargava, N. K. Sethy and C. Karunakaran, Copper, zinc superoxide dismutase and nitrate reductase coimmobilized bi-enzymatic biosensor for the simultaneous determination of nitrite and nitrate, *Biosens. Bioelectron.* 52 (2014) 209-215.

23. H. Bagheri, A. Hajian, M. Rezaei and A. Shirzadmehr, Composite of Cu metal nanoparticles-multiwall carbon nanotubes-reduced graphene oxide as a novel and high

performance platform of the electrochemical sensor for simultaneous determination of nitrite and nitrate, *J. Hazard. Mater.* 324 (2017) 762-772.

24. L. Li, D. Liu, K. Wang, H. Mao and T. You, Quantitative detection of nitrite with N-doped graphene quantum dots decorated N-doped carbon nanofibers composite-based electrochemical sensor, *Sens. Actuators B: Chem.* 252 (2017) 17-23.
25. J. Vinoth Kumar, R. Karthik, S. M. Chen, P. Balasubramanian, V. Muthuraj and V. Selvam, A novel cerium tungstate nanosheets modified electrode for the effective electrochemical detection of carcinogenic nitrite ions, *Electroanal.* 29 (2017) 2385-2394.
26. F. Zhang, Y. Yuan, Y. Zheng, H. Wang, T. Liu and S. Hou, A glassy carbon electrode modified with gold nanoparticle-encapsulated graphene oxide hollow microspheres for voltammetric sensing of nitrite, *Microchim. Acta* 184 (2017) 1565-1572.
27. M. Ghanei-Motlagh and M. A. Taher, A novel electrochemical sensor based on silver/halloysite nanotube/molybdenum disulfide nanocomposite for efficient nitrite sensing, *Biosens. Bioelectron.* 109 (2018) 279-285.
28. X. Li, J. Ping and Y. Ying, Recent developments in carbon nanomaterial-enabled electrochemical sensors for nitrite detection, *Trends Analyt. Chem.* (2019).
29. K. Rajalakshmi and S. A. John, Highly sensitive determination of nitrite using FMWCNTs-conducting polymer composite modified electrode, *Sens. Actuators B: Chem.* 215 (2015) 119-124.
30. V. Mani, T.-Y. Wu and S.-M. Chen, Iron nanoparticles decorated graphene-multiwalled carbon nanotubes nanocomposite-modified glassy carbon electrode for the sensitive determination of nitrite, *J. Solid State Electrochem.* 18 (2014) 1015-1023.

31. B. R. Kozub, N. V. Rees and R. G. Compton, Electrochemical determination of nitrite at a bare glassy carbon electrode; why chemically modify electrodes?, *Sens. Actuators B: Chem.* 143 (2010) 539-546.

32. C. M. Welch and R. G. Compton, The use of nanoparticles in electroanalysis: a review, *Anal. Bioanal. Chem.* 384 (2006) 601-619.

33. A. Chen and S. Chatterjee, Nanomaterials based electrochemical sensors for biomedical applications, *Chem. Soc. Rev.* 42 (2013) 5425-5438.

34. M. Govindhan, M. Amiri and A. Chen, Au nanoparticle/graphene nanocomposite as a platform for the sensitive detection of NADH in human urine, *Biosens. Bioelectron.* 66 (2015) 474-480.

35. M. Govindhan, B.-R. Adhikari and A. Chen, Nanomaterials-based electrochemical detection of chemical contaminants, *RSC Adv.* 4 (2014) 63741-63760.

36. Z. Liu, A. Nemec-Bakk, N. Khaper and A. Chen, Sensitive electrochemical detection of nitric oxide release from cardiac and cancer cells via a hierarchical nanoporous gold microelectrode, *Anal. Chem.* 89 (2017) 8036-8043.

37. S.-S. Li, Y.-Y. Hu, A.-J. Wang, X. Weng, J.-R. Chen and J.-J. Feng, Simple synthesis of worm-like Au–Pd nanostructures supported on reduced graphene oxide for highly sensitive detection of nitrite, *Sens. Actuators B: Chem.* 208 (2015) 468-474.

38. G. Maduraiveeran and R. Ramaraj, A facile electrochemical sensor designed from gold nanoparticles embedded in three-dimensional sol–gel network for concurrent detection of toxic chemicals, *Electrochem. Commun.* 9 (2007) 2051-2055.

39. V. S. Manikandan, Z. Liu and A. Chen, Simultaneous detection of hydrazine, sulfite, and nitrite based on a nanoporous gold microelectrode, *J. Electroanal. Chem.* 819 (2018) 524-532.

40. X. Ge, L. Wang, Z. Liu and Y. Ding, Nanoporous gold leaf for amperometric determination of nitrite, *Electroanal.* 23 (2011) 381-386.

41. C. Kaçar, B. Dalkiran, P. E. Erden and E. Kiliç, An amperometric hydrogen peroxide biosensor based on Co_3O_4 nanoparticles and multiwalled carbon nanotube modified glassy carbon electrode, *Appl. Surf. Sci.* 311 (2014) 139-146.

42. K. T. Nam, D.-W. Kim, P. J. Yoo, C.-Y. Chiang, N. Meethong, P. T. Hammond, Y.-M. Chiang and A. M. Belcher, Virus-enabled synthesis and assembly of nanowires for lithium ion battery electrodes, *Science* 312 (2006) 885-888.

43. M. Mahmoudian, W. Basirun, P. M. Woi, M. Sookhakian, R. Yousefi, H. Ghadimi and Y. Alias, Synthesis and characterization of Co_3O_4 ultra-nanosheets and Co_3O_4 ultra-nanosheet-$Ni(OH)_2$ as non-enzymatic electrochemical sensors for glucose detection, *Mater. Sci. Eng: C* 59 (2016) 500-508.

44. Y. Gao, S. Chen, D. Cao, G. Wang and J. Yin, Electrochemical capacitance of Co_3O_4 nanowire arrays supported on nickel foam, *J. Power Sources* 195 (2010) 1757-1760.

45. L. Li, Y. Li, S. Gao and N. Koshizaki, Ordered Co_3O_4 hierarchical nanorod arrays: tunable superhydrophilicity without UV irradiation and transition to superhydrophobicity, *J. Mater. Chem.* 19 (2009) 8366-8371.

46. Y. Lu, Y. Wang, Y. Zou, Z. Jiao, B. Zhao, Y. He and M. Wu, Macroporous Co_3O_4 platelets with excellent rate capability as anodes for lithium ion batteries, *Electrochem. Commun.* 12(1) (2010) 101-105.

47. A. Numan, M. M. Shahid, F. S. Omar, K. Ramesh and S. Ramesh, Facile fabrication of cobalt oxide nanograin-decorated reduced graphene oxide composite as ultrasensitive platform for dopamine detection, *Sens. Actuators B: Chem.* 238 (2017) 1043-1051.

48. F. Xie, X. Cao, F. Qu, A. M. Asiri and X. Sun, Cobalt nitride nanowire array as an efficient electrochemical sensor for glucose and H_2O_2 detection, *Sens. Actuators B: Chem.* 255 (2018) 1254-1261.

49. M. M. Shahid, P. Rameshkumar, A. Pandikumar, H. N. Lim, Y. H. Ng and N. M. Huang, An electrochemical sensing platform based on a reduced graphene oxide–cobalt oxide nanocube@ platinum nanocomposite for nitric oxide detection, *J. Mater. Chem. A* 3 (2015) 14458-14468.

50. C.-H. Chen, Y.-C. Chen and M.-S. Lin, Amperometric determination of NADH with Co_3O_4 nanosheet modified electrode, *Biosens. Bioelectron.* 42 (2013) 379-384.

51. J. Mu, L. Zhang, M. Zhao and Y. Wang, Co_3O_4 nanoparticles as an efficient catalase mimic: Properties, mechanism and its electrocatalytic sensing application for hydrogen peroxide, *J. Mol. Catal. A: Chem.* 378 (2013) 30-37.

52. S. Farhadi, K. Pourzare and S. Bazgir, Co_3O_4 nanoplates: Synthesis, characterization and study of optical and magnetic properties, *J. Alloys Compd.* 587 (2014) 632-637.

53. S. Farhadi, J. Safabakhsh and P. Zaringhadam, Synthesis, characterization, and investigation of optical and magnetic properties of cobalt oxide (Co_3O_4) nanoparticles, *J. Nanostruct. Chem.* 3 (2013) 69.

54. B. Dinesh, V. Veeramani, S.-M. Chen and R. Saraswathi, In situ electrochemical synthesis of reduced graphene oxide-cobalt oxide nanocomposite modified electrode for selective

sensing of depression biomarker in the presence of ascorbic acid and dopamine, *J. Electroanal. Chem.* 786 (2017) 169-176.

55. L. Liu, L. Tian, G. Zhao, Y. Huang, Q. Wei and W. Cao, Ultrasensitive electrochemical immunosensor for alpha fetoprotein detection based on platinum nanoparticles anchored on cobalt oxide/graphene nanosheets for signal amplification, *Anal. Chim. Acta* 986 (2017) 138-144.

56. S. Kogularasu, M. Govindasamy, S.-M. Chen, M. Akilarasan and V. Mani, 3D graphene oxide-cobalt oxide polyhedrons for highly sensitive non-enzymatic electrochemical determination of hydrogen peroxide, *Sens. Actuators B: Chem.* 253 (2017) 773-783.

57. B. Sidhureddy, J. S. Dondapati and A. Chen, Shape-controlled synthesis of Co_3O_4 for enhanced electrocatalysis of the oxygen evolution reaction, *Chem. Commun.*, DOI: 10.1039/c8cc10194a (2019) 10.1039/C1038CC10194A.

58. B.-R. Adhikari, M. Govindhan, H. Schraft and A. Chen, Simultaneous and sensitive detection of acetaminophen and valacyclovir based on two dimensional graphene nanosheets, *J. Electroanal. Chem.* 780 (2016) 241-248.

59. L. Li, H. Lu and L. Deng, A sensitive NADH and ethanol biosensor based on graphene–Au nanorods nanocomposites, *Talanta* 113 (2013) 1-6.

60. H. Teymourian, A. Salimi and S. Khezrian, Fe3O4 magnetic nanoparticles/reduced graphene oxide nanosheets as a novel electrochemical and bioeletrochemical sensing platform, *Biosens. Bioelectron.* 49 (2013) 1-8.

61. O. Zhang, Y. Wen, J. Xu, L. Lu, X. Duan and H. Yu, One-step synthesis of poly (3, 4-ethylenedioxythiophene)–Au composites and their application for the detection of nitrite, *Synth. Met.* 164 (2013) 47-51.

62. Y. Haldorai, J. Y. Kim, A. T. E. Vilian, N. S. Heo, Y. S. Huh and Y.-K. Han, An enzyme-free electrochemical sensor based on reduced graphene oxide/Co_3O_4 nanospindle composite for sensitive detection of nitrite, *Sens. Actuators B: Chem.* 227 (2016) 92-99.

63. A.-J. Lin, Y. Wen, L.-J. Zhang, B. Lu, Y. Li, Y.-Z. Jiao and H.-F. Yang, Layer-by-layer construction of multi-walled carbon nanotubes, zinc oxide, and gold nanoparticles integrated composite electrode for nitrite detection, *Electrochim. Acta* 56(3) (2011) 1030-1036.

64. R. Madhu, V. Veeramani and S.-M. Chen, Heteroatom-enriched and renewable banana-stem-derived porous carbon for the electrochemical determination of nitrite in various water samples, *Sci. Rep.* 4 (2014) 4679.

65. S.-J. Li, G.-Y. Zhao, R.-X. Zhang, Y.-L. Hou, L. Liu and H. Pang, A sensitive and selective nitrite sensor based on a glassy carbon electrode modified with gold nanoparticles and sulfonated graphene, *Microchim. Acta* 180 (2013) 821-827.

66. D. Zhang, Y. Fang, Z. Miao, M. Ma, X. Du, S. Takahashi, J.-i. Anzai and Q. Chen, Direct electrodeposion of reduced graphene oxide and dendritic copper nanoclusters on glassy carbon electrode for electrochemical detection of nitrite, *Electrochim. Acta* 107 (2013) 656-663.

Chapter 5: Simultaneous Detection of Hydrazine, Sulfite, and Nitrite Based on a Nanoporous Gold Microelectrode*

5.1. Introduction

Despite the rapid upsurge in the domestic and international standards for food quality and safety, there continues to be a growing demand for processed foods and beverages. This translates to the food industry having to ensure the utmost quality and safety of their products for consumers. Hydrazine (N_2H_4) and its by-products are commonly used as pesticides, chemical blowing agents, intermediates in pharmaceutical industries, photography chemicals, and for corrosion control in hot water heating systems in boiler water treatments.[1] Primarily, N_2H_4 and its derivatives enter the environment due to its usage and applications in aerospace fuels, the production of explosives, and industrial chemicals.[2] Since N_2H_4 is lethal and volatile in nature, it may readily ingress into the human body either by oral means through the skin or via inhalation, and may subsequently cause detrimental effects to organs such as the kidneys, liver, and brain.[3] The Environmental Protection Agency (EPA) has categorized N_2H_4 and its derivatives as group B2 (human carcinogens). Due to the carcinogenic nature and its potential risks, N_2H_4 is a major concern of the International Agency for Research on Cancer (IARC).[4] A minimal N_2H_4 inhalation risk level is estimated to be 0.004 μg mL^{-1} according to the EPA and Agency for Toxic Substance and Disease Registry.[5] The permitted level of N_2H_4 in the workplace atmosphere should not be in excess of 0.03 μg mL^{-1} continuously over two hours, as recommended by the National Institute for Occupational Safety and Health.[6]

---

* Most of the results presented in this chapter have been published in the *Journal of Electroanalytical Chemistry,* **2018**, 819, 524-532.

Due to the environmental and toxicological implications associated with N_2H_4, sensitive and reliable analytical methods are mandatory for its determination. Electrochemical sensors based on graphene-bismuth nanoparticles, or Au/CNTs-rGO have been reported for the selective determination of N_2H_4.[7-9] Carbon-based materials such as multi-walled carbon nanotubes play a significant role in the development of sensors.[10,11]

Sulfite (SO_3^{2-}) is known for its excellent reducing properties and has been widely used as an additive in the food industry.[12] It plays a significant role in preventing oxidative deterioration and bacterial growth in foods and beverages during their production as well as in increasing the shelf life of these products.[13] The common SO_3^{2-} containing beverages include wine, alcoholic and non-alcoholic beer and cider, as well as bottled juices and concentrates.[14] According to the Food and Drug Administration (FDA), it is mandatory that caution labels should be included on any food or beverage that contains more than 10 ppm of SO_3^{2-} with a maximum concentration of up to 50 mg L^{-1} in beer and 350 mg L^{-1} in wine.[15,16] However, many people have an allergic reaction to SO_3^{2-} due to the probable toxic and harmful effects that are associated with it. Therefore, accurate monitoring of the SO_3^{2-} level is crucial as excessive ingestion might lead to headaches, nausea, dizziness, and asthma.[17] Because of its important role, Davis et al has reviewed the latest development in the determination of sulfite in food and beverages with the electroanalytical methods.[18] Besides, nanosensor comprised of K-doped graphene and graphene-gold nanocomposite have been reported for the simultaneous determination of SO_3^{2-} and NO_2^-.[19,20] Similarly, multiple studies have described the detection of SO_3^{2-} and NO_2^- using gold nanoparticles, graphene oxide, and graphene nanoribbons.[21,22] On the other hand, NO_2^- has been serving as an antimicrobial agent to preserve perishable food items such as ham, salami, and other processed meats. It is also responsible for retaining the pink color in meat products by forming

nitroso-myoglobin.[23] However, NO_2^- has a noxious impact on the human body if it is added to food products in excess of the prescribed safety standard.[24] It readily binds with hemoglobin to form methemoglobin, thereby reducing the capacity of blood to transport oxygen.[25] Moreover, NO_2^- is converted to potent *N*-nitrosamines in the stomach, which is extremely carcinogenic.[26] There are numerous conventional methods for the determination of N_2H_4, SO_3^{2-} and NO_2^-, such as titration, spectrofluorometry, chemiluminescence, phosphorimetry, spectrophotometry, and flow injection analysis (FIA). However, they require large sample volumes, essential pretreatment, and the preparation of reagents. Although there are several instrument-based methods in use, electroanalytical techniques comprise an efficacious strategy for the direct and rapid detection of N_2H_4, SO_3^{2-}, and NO_2^- [27-29], providing opportunities for the development of robust and portable devices and systems. Due to the limitations of multiple assay steps, time-consuming, irreversible loss in activity of the enzymatic electrochemical sensors, much effort has been made to develop non-enzymatic electrochemical sensors without the usage of a redox mediator.[30,31] In recent years, advancements in electrode fabrication, encompassing microfabrication and surface modifications have invigorated an ever-growing interest in the utilization of noble metals such as gold, platinum, palladium and silver towards the development of sensors for a wide array of applications.[32-36] Gold (Au), as an electrode material, is one of the most recurrently used and sought-after materials for the fabrication of microelectrodes, and also serves as a reinforcement material in the fabrication of biosensors.[37] Nanoparticles composed of Au, when incorporated in electrochemical sensors, are highly redox active with exceptional potential for applications in biological and chemical detection. Furthermore, Au-based nanomaterials possess the merits of the chemical robustness, higher rates of electron transfer, distinct catalytic activities, which leads to a larger potential profile in contrast to platinum (Pt).[38, 39] Au has been combined with palladium (Pd) to produce Au-Pd

alloys for the determination of uric acid and levodopa.[40] Yao and co-workers have recently reported a biosensor based on gold nanocluster coupled with horseradish peroxidase enzyme.[41] Sensors based on bimetallic Au-Pt/rGO nanocomposites and Au/rGO have been developed for the detection of nitric oxide in rat cardiac cells and NADH in human urine, respectively.[42,43] As acknowledged, due to the unique physicochemical properties and surface chemistry, nanoporous materials, especially gold, have received increasing attention in a wide range of energy, environmental and medical applications.[44,45] Extensive studies of Au nanoporous and Au nanocomposite electrodes have been reported on the development of sensors for the detection of glucose in the blood, Hg (II) ions in water, and various other electrochemical sensing applications.[46-48] Maduraiveeran et. al. embedded gold nanoparticles into silicate sol-gel to form a three-dimensional network and showed the possible detection of N_2H_4, SO_3^{2-}, and NO_2^-.[49] The nanoporous gold was fabricated via chemical etching of the Au-Ag alloys, and tested for the detection of N_2H_4.[5,50] However, their fabrication process was complicated; and no real sample analysis was reported.

In the present work, a facile electrochemical alloying/dealloying method was developed for the direct formation of a three dimensional (3D) nanoporous structure for the simultaneous detection of N_2H_4, SO_3^{2-}, and NO_2^-. The surface morphology of the electrode was investigated using SEM and EDX, followed by additional techniques such as cyclic voltammetry (CV) and differential pulse voltammetry (DPV), to study its electrochemical behaviours. The prepared nanoporous gold microelectrode was further employed to detect sulfite in beverages (e.g., wine and beer) and nitrite in beef.

5.2. Experimental Section

5.2.1. Reagents

Hydrazine hydrate, sodium sulfite, and sodium nitrite were purchased from Sigma-Aldrich. All reagents used for the experiments were of analytical grade. Deionized water (18.2 MΩ cm) was utilized for all experiments, and all glassware was thoroughly cleaned prior to each analysis. Phosphate buffer saline (PBS) was used as the electrolyte, which was prepared by combining Na_2HPO_4 (0.079 M), NaH_2PO_4 (0.023 M) and NaCl (0.091 M) to make up a final volume of 100 mL. The pH of the electrolyte solution was adjusted to 6.5 with 0.1 M H_3PO_4 and 0.5 M NaOH solutions.

5.2.2. Electrode preparation and modification

A nanoporous gold microelectrode was fabricated by sealing a Ø127 μm Au wire within a pipette tip. And a 10-cm length copper wire was inserted into a 10-cm glass tube and its end was plunged into a conductive gold paste, which acted as a conductive adhesive. Subsequently, a 10-mm long gold microwire (Ø127 μm, 99.9%, Sigma-Aldrich) was fed halfway through the pipet tip until the microwire gently contacted with the copper wire. An epoxy resin was used to wrap the top and bottom ends of the pipette tips to seal them firmly. The microelectrode was kept in the oven at 60ºC for 90 min, followed by cooling in ambient air; and finally, the microwire was cut to 1.0 mm. The nanoporous structure of the gold microelectrode was attained through the application of an electrochemical alloying/dealloying method [51], which was based on a three-electrode electrochemical cell, where a Zn plate and Zn wire were used as the auxiliary electrode and the reference electrode, respectively. The geometrical surface area of the gold microwire before the alloying/dealloying treatment was 0.85 mm^2. The nanoporous Au microelectrode was fabricated under an optimized condition in a mixture of benzyl alcohol and 1.5 M $ZnCl_2$ at a scan rate of 10 $mV\ s^{-1}$ (50 cycles) and 120ºC.[52] The multicyclic potential sweep was performed between -0.70 and

1.80 V (vs. Zn). The fabricated nanoporous gold microelectrode was held vertically in a micropipette tip.

5.2.3. Sample preparation

For the analysis of sulfites in beverages, three different red wine samples and one beer sample were analyzed: (i) Yellow Tail Shiraz (Australian - wine 1); (ii) Cabernet Sauvignon (chile - wine 2); (iii) Boshendal – The Pavilion (South African – wine 3); and (iv) Apple Cider beer (Canadian beer). The wine and beer samples were diluted 50 folds and adjusted to a pH of 6.5, and their respective bottles were opened only prior to the analysis. A grocery store purchased beef samples: Canadian Beef I (Tenderloin Beef) and Canadian Beef II (Minced Beef) were used for nitrite analysis. The beef samples were homogenized in a blender first; then 5.0 g of the sample was treated with 50 ml boiling water for 10 min. Finally, the mixture was filtered using Whatman filter paper, and its pH was adjusted to 6.5 for analysis.

5.2.4. Characterization techniques

The nanoporous Au microelectrode was characterized using a Hitachi SU-70 Schottky Field Emission SEM with an energy dispersive X-ray spectrometer. Voltammetric techniques such as CV and DPV were performed using a CHI-D660 potentiostat (CHI-660, CHI, USA). CV was utilized for the elucidation of the redox behaviour and kinetics of the electrodes, while DPV was suitable for the trace determination of electroactive analytes in actual systems.[38,53] The electrochemical experiments were carried out in an electrochemical cell that comprised a three-electrode system. The gold microelectrode served as the working electrode; a coiled platinum wire, which was flame treated and rinsed with double distilled water, as the counter electrode, and a standard silver-silver chloride (Ag/AgCl) electrode as the reference electrode. All measurements were performed in a PBS (0.1 M, pH 6.5) at room temperature. Prior to analysis, all of the solutions

were deaerated via purging with argon gas for 15 min. All the potentials reported in this paper are with respect to the Ag/AgCl electrode.

5.3. Results and Discussion

5.3.1. Surface morphology and electrochemical characterization

The surface morphology of the gold microwire was characterized using the SEM. Figure. 5.1A depicts a typical SEM image observed for the gold microwire following the alloying/dealloying treatment, which revealed a uniformly formed nanoporous structure on the surface of the gold microwire. Further, the nanoporous structure was consistently present throughout the surface, showing a well-defined 3D structure with pore dimensions that ranged from ~200 - 400 nm. In contrast, before the treatment, the gold microwire showed a smooth surface (Figure 5.1B). The nanoporous structure of the electrode surface exhibited high roughness and an increased surface area. Through the course of the electrochemical alloying, Zn (a highly reactive component) was deposited onto the Au film and blended to form an Au/Zn alloy. The Au/Zn alloy layer eventually lost the highly reactive Zn to form a nanoporous Au layer during the electrochemical dealloying.[54] The chemical composition of the gold microelectrode was confirmed using EDX, showing a primary Au peak.

CV was employed to electrochemically characterize the nanoporous gold microelectrode after alloying/dealloying treatment. Figure 5.2 displays the CV curves of the gold microelectrode and the nanoporous gold microelectrode recorded in 0.1 M H_2SO_4 at the scan rate of 20 mV s^{-1}. A broad anodic peak centred at 1.34 V appeared when the potential was scanned from 0.0 to 1.50 V, which can be attributed to the formation of gold oxide[55]; while a cathodic peak was observed at 0.89 V in the reverse scan, resulting from the electrochemical reduction of the gold oxide that was formed during the forward scan. The reduction peak current for the nanoporous gold

microelectrode was approximately 19.1 times higher than that of the unmodified Au microelectrode. The electrochemically active surface area (EASA) was calculated based on the integrated charge of the reduction peak, assuming that the charge for the reduction of monolayer of gold oxide is 390 μC cm^{-2}.[56]

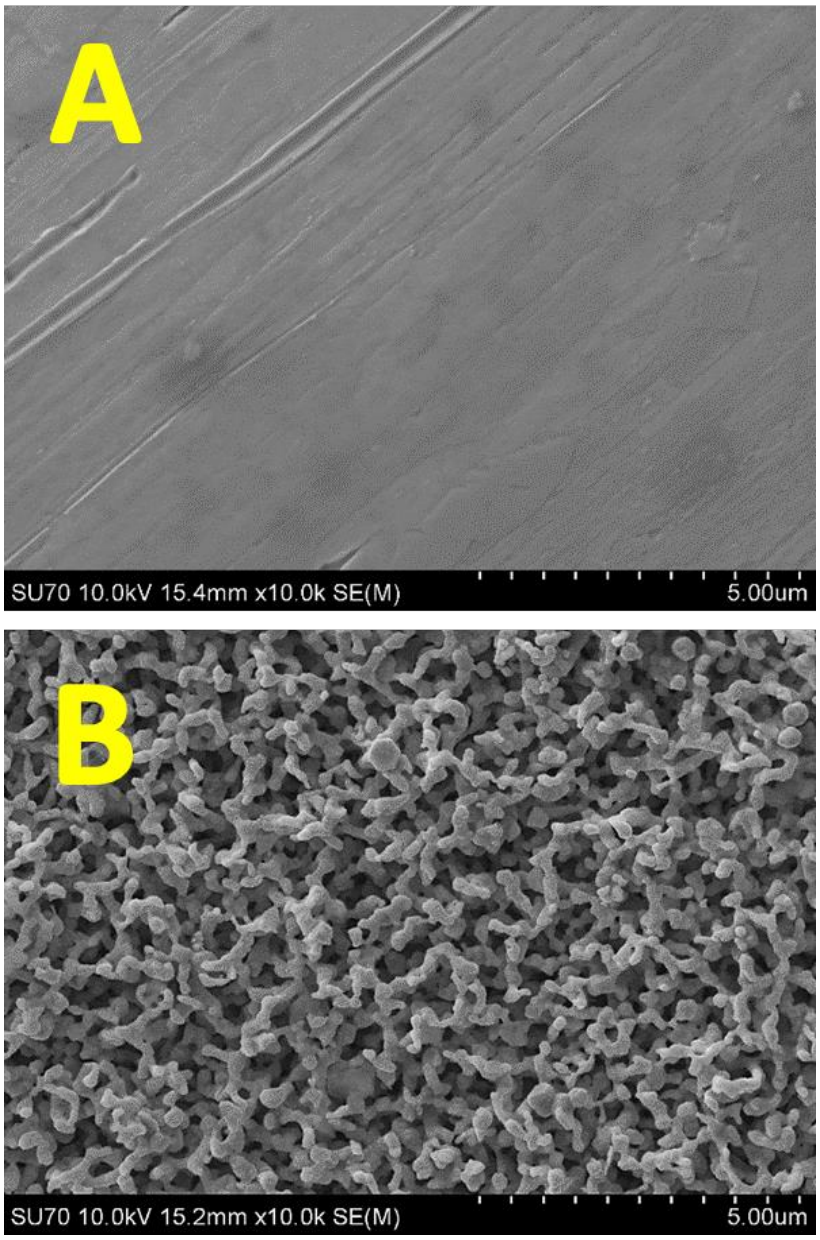

Figure 5.1. The SEM image of the gold microwire before alloying/dealloying treatment (A); SEM image of the gold microelectrode after the alloying/dealloying process.

The integrated charge of the reduction peak of the nanoporous gold microelectrode was 91.5 μC, which was 25.5 times larger than that of the unmodified gold microelectrode (4.25 μC). The roughness factor of the electrode may be estimated by dividing the EASA by its geometrical surface area. The calculated roughness factor of the nanoporous gold microelectrode was 27.7, showing that the actual surface area of the electrode was significantly enhanced following the alloying/dealloying treatment.

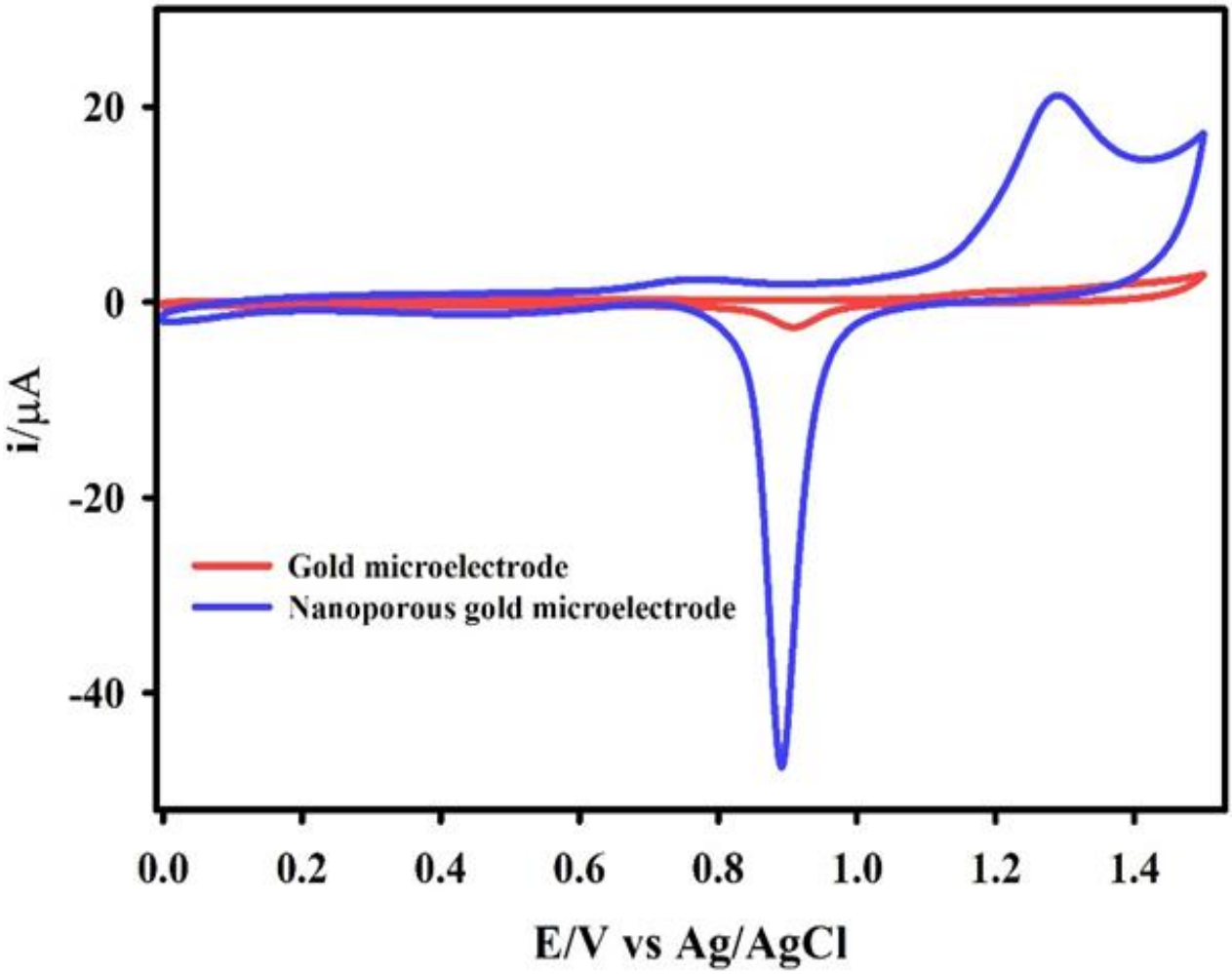

Figure 5.2. Cyclic voltammograms of the unmodified gold microelectrode (red line) and the fabricated nanoporous gold microelectrode (blue curve) recorded in 0.1 M H_2SO_4 at the scan rate of 20 mV s^{-1}.

5.3.2. Electrochemical oxidation of individual N_2H_4, SO_3^{2-} and NO_2^- analytes

The electrooxidation behaviour of N_2H_4, SO_3^{2-} and NO_2^- molecules at the nanoporous gold microelectrode was examined using CV and DPV. Figure. 5.3A and 5.3B depict the response curves for the oxidation of N_2H_4 at the nanoporous gold microelectrode recorded in 0.1 M PBS in the absence (dashed line) and in the presence (solid line) of 250.0 μM of the analyte. The electrochemical oxidation peak appeared at ~0.03 V in the CV curve and at ~ -0.01 V in the DPV curve. The anodic oxidation of N_2H_4 could be expressed as follows[57]:

$$N_2H_4 \rightarrow N_2 + 4H^+ + 4e^- \quad (1)$$

The associated peak currents were measured to be 3.48 and 3.22 μA with the CV and DPV techniques, respectively. Figure 5.3C and 5.3D reveal a strong peak centred at ~0.33 and ~0.30 V for the electrochemical oxidation of 250.0 μM oxidation of SO_3^{2-} using CV and DPV, respectively, which could be attributed to the following anodic reaction[49]:

$$SO_3^{2-} + H_2O \rightarrow SO_4^{2-} + 2H^+ + 2e^- \quad (2)$$

The associated peak current was measured to be 5.98 and 8.82 μA. Correspondingly, the anodic peaks of the CV (Figure 5.3E) and DPV (Figure 5.3F) curves for the oxidation of 250.0 μM NO_2^- were observed at ~0.75 and ~0.72 V, which was more positive than the peak potentials of the electrochemical oxidation of N_2H_4 and SO_3^{2-}. The anodic oxidation of NO_2^- could be expressed as follows[58]:

$$NO_2^- + H_2O \rightarrow NO_3^- + 2H^+ + 2e^- \quad (3)$$

The corresponding peak current for the NO_2^- oxidation obtained with CV and DPV was 1.47 and 2.33 μA, respectively. The aforementioned CV and DPV results indicated that the nanoporous

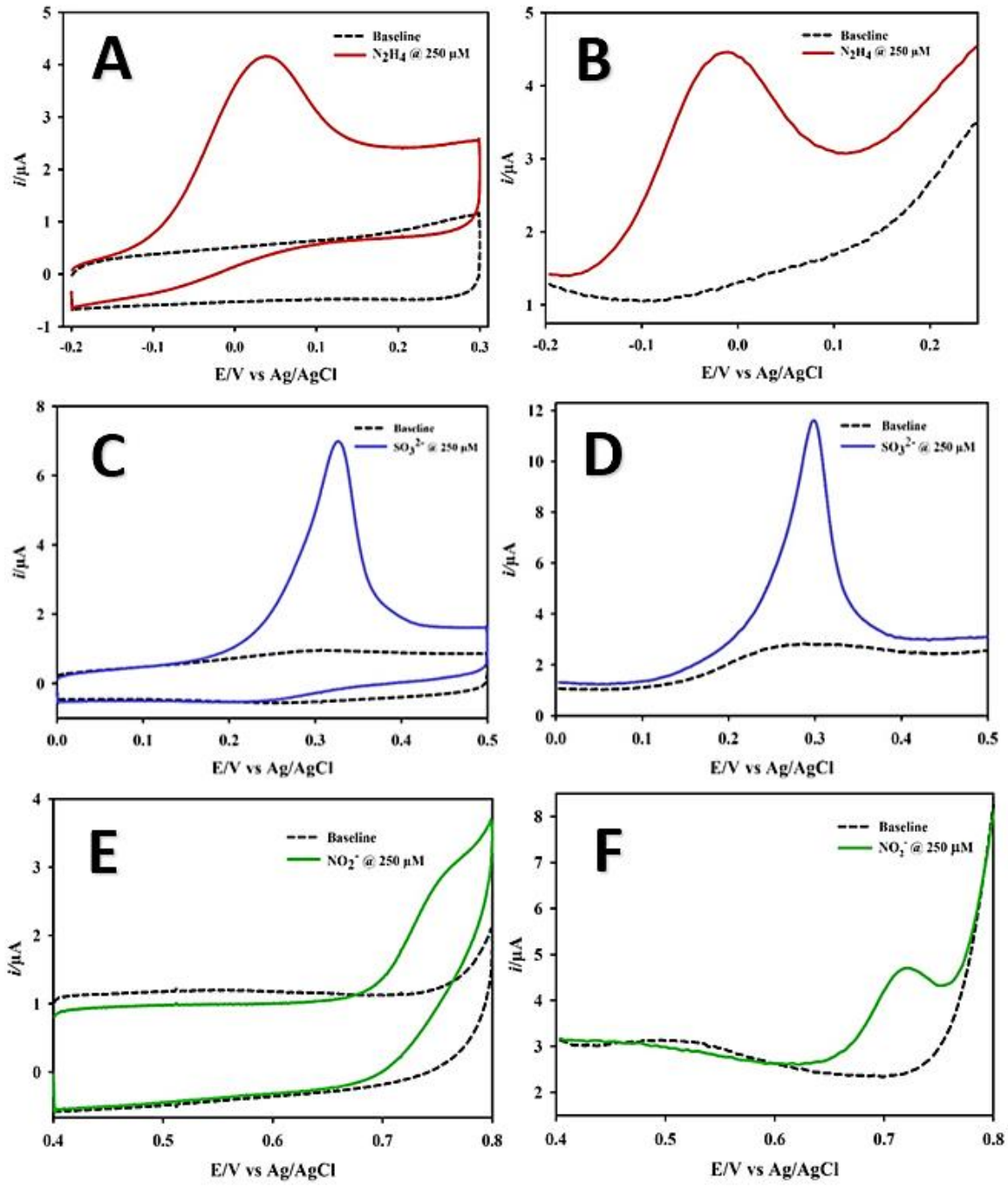

Figure 5.3. CV curves of the nanoporous gold microelectrode recorded in the absence (dotted lines) and in the presence (solid lines) of 250.0 µM of: (A) N_2H_4, (C) SO_3^{2-} and (E) NO_2^- at the scan rate of 20 mV s^{-1}, where the supporting electrolyte was 0.1 M PBS (pH 6.5). (B), (D) and (E) represents the corresponding DPV curves obtained for the oxidation of N_2H_4, SO_3^{2-} and NO_2^-.

gold microelectrode exhibited strong current responses to the individual N_2H_4, SO_3^{2-} and NO_2^- species at different electrode potentials.

Figure. 5.4A presents the CV curves of the nanoporous gold microelectrode recorded in 0.1 M PBS in the absence (dashed line) and in the presence of a mixture of N_2H_4, SO_3^{2-} and NO_2^- (solid line), with each analyte having a concentration of 500.0 μM. The peaks for the anodic oxidation of N_2H_4, SO_3^{2-} and NO_2^- appeared at ~0.05, ~0.34, and ~0.76 V, which were similar to the peak potentials observed in Figure 5.3A, C and E, respectively. The electrochemical oxidation of the mixture of the analytes was also evaluated using DPV under the same condition as shown in Figure 5.4B. The DPV response exhibited sharp and well-defined peaks for the simultaneous oxidation of N_2H_4, SO_3^{2-} and NO_2^- at ~0.00, ~0.30 and ~0.72 V (3.85, 11.10 and 4.30 μA), respectively. Additionally, the electrochemical activity of the nanoporous gold microelectrode was compared with the unmodified gold microelectrode using CV and DPV for the oxidation of N_2H_4, SO_3^{2-} and NO_2^-. In contrast to the gold nanoporous microelectrode, the behaviour of the unmodified gold microelectrode was sluggish and the analytes were oxidized at more positive potentials centred at 0.04, 0.34 and 0.76 V (Figure 5.4B) for N_2H_4, SO_3^{2-} and NO_2^-, respectively. In comparison to the electrochemical performance of the unmodified gold microelectrode, the nanoporous gold microelectrode exhibited much higher current responses to N_2H_4, SO_3^{2-} and NO_2^- with a negative shift on the oxidation potential. The enhanced activity of the nanoporous gold microelectrode might be attributed to the uniform 3D nanoporous structure, resulting in a similar effect of to the usual semi-infinite linear diffusion to the thin layer diffusion.[59-61] Further, the oxidation of N_2H_4, SO_3^{2-}, and NO_2^- at the nanoporous gold microelectrode remained stable for recurring experiments. The nanoporous structure promoted the peak-to-peak separation of the electrochemical oxidation of N_2H_4-SO_3^{2-} and SO_3^{2-}-NO_2^- for 0.27 and 0.41 V, respectively.

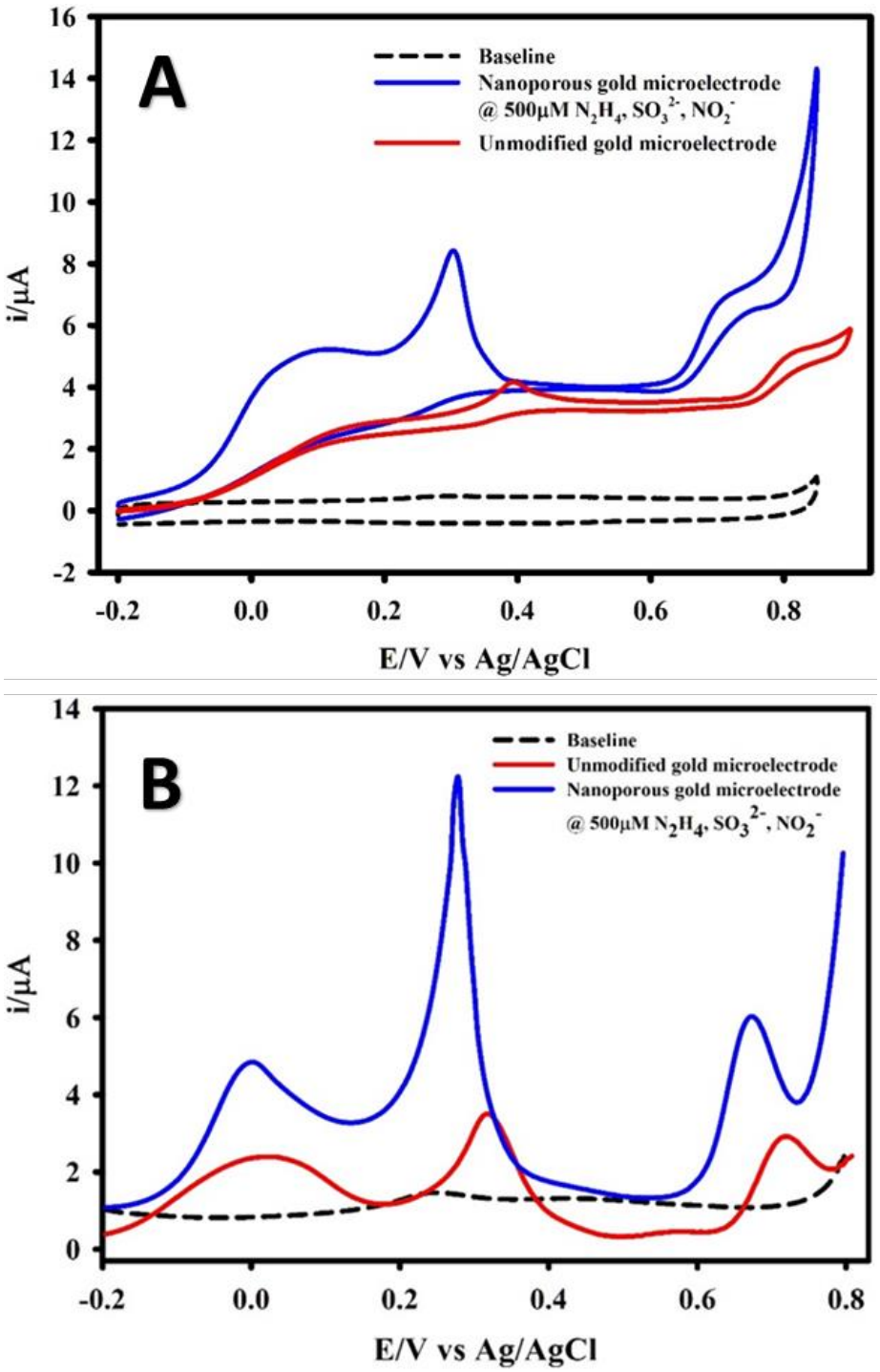

Figure 5.4. (A) CV and (B) DPV responses of the unmodified gold microelectrode (red line) and the nanoporous gold microelectrode (blue line) towards N_2H_4, SO_3^{2-} and NO_2^- in 0.1 M PBS (pH 6.5).

The concentration of each analyte is 500 μM. The black dash line was baseline derived from the nanoporous gold microelectrode. The appearance of the well-separated peaks indicated a potential application of the gold nanoporous microelectrode for the simultaneous determination of N_2H_4, SO_3^{2-} and NO_2^- species.

5.3.3. Effects of the pH of the electrolyte and the scan rate

As seen in Reactions (1) to (3), protons are involved in the electrochemical oxidation of N_2H_4, SO_3^{2-}, and NO_2^-. The pH of the supporting electrolytes may influence the electrochemical behaviour of N_2H_4, SO_3^{2-}, and NO_2^- and the electrochemical performance of the nanoporous gold microelectrode. The electrochemical oxidation of N_2H_4, SO_3^{2-}, and NO_2^- at the nanoporous gold microelectrode was investigated in a 0.1 M PBS under different pH conditions (5.0, 5.5, 6.0, 6.5 and 7.0) using DPV.

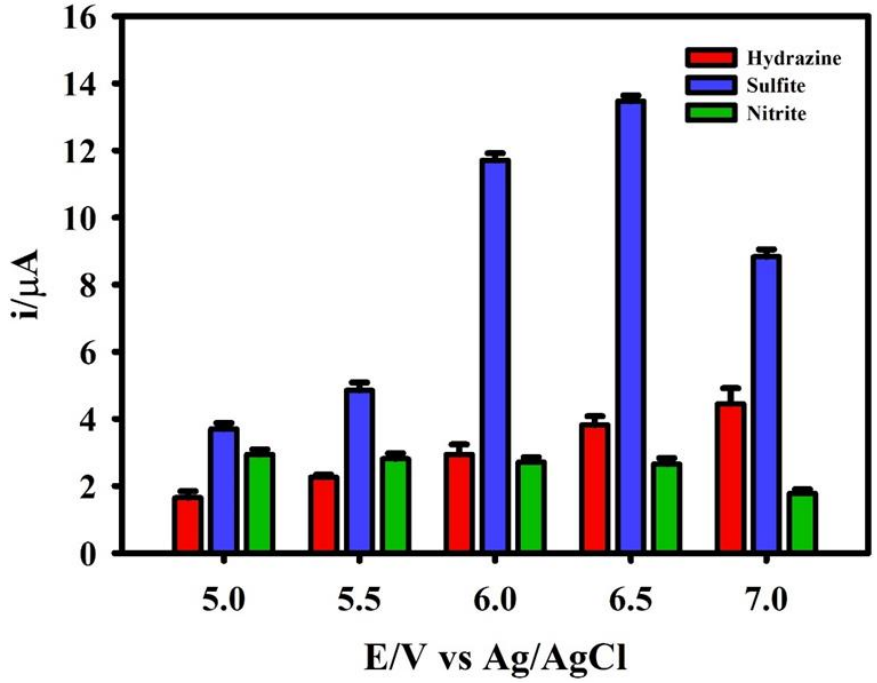

Figure 5.5. Peak current response for the oxidation of 500 μM N_2H_4, SO_3^{2-} and 250 μM NO_2^- in 0.1 M PBS solution at different pH values: 5.0, 5.5, 6.0, 6.5 and 7.0.

Figure 5.5 presents the anodic peak current response of the nanoporous gold microelectrode towards the electrochemical oxidation of N_2H_4 (red), SO_3^{2-} (blue) and NO_2^- (green). With the increase in the pH value from 5.0 to 7.0, the peak current of the N_2H_4 oxidation was gradually increased. Similarly, the peak current of the oxidation of SO_3^{2-} was increased with the increase of the pH from 5.0 to 6.5, but it was decreased with the further increase of the pH to 7.0. On the other hand, the peak current response for the oxidation of NO_2^- was slightly decreased when the pH was increased from 5.0 to 6.5; but it was notably decreased with the further increase of the pH to 7.0, which is consistent with the previous observation.[62] The decrease of the current response might be attributed to the decrease of the protonation degree of nitrite ions with the increase of the pH. The aforementioned results revealed that 6.5 was the optimal pH for the simultaneous detection of N_2H_4, SO_3^{2-}, and NO_2^- to obtain optimal anodic currents and peak separation.

By employing CV, the effect of the scan rate on the electrochemical oxidation of 250.0 μM N_2H_4 (Figure 5.6A), 250.0 μM SO_3^{2-} (Figure 5.6B) and 500.0 μM NO_2^- (Figure 5.6C) in 0.1 M PBS (pH 6.5) at the nanoporous gold microelectrode was also investigated. As seen in Figure 5.6, with the increase of the scan rate from 20 to 175 mV s^{-1}, the oxidation peak potential was shifted towards the more positive side. The corresponding plots of the oxidation peak current I_{pa} vs the square root of the scan rate ($v^{1/2}$) are presented in Figures 5.6D-F, respectively. The linear relationship, with correlation coefficients of 0.998, 0.993 and 0.994 for the electrochemical oxidation of N_2H_4, SO_3^2, and NO_2^-, indicated that the oxidation of these species occurring at the nanoporous gold microelectrode was a diffusion-controlled process. Similarly, the scan rate effect of the electrochemical oxidation of 250.0 μM N_2H_4, 250.0 μM SO_3^{2-} and 250.0 μM NO_2^- (Figure 5.7A) in a mixture in 0.1 M PBS (pH 6.5) at the nanoporous gold microelectrode was also investigated.

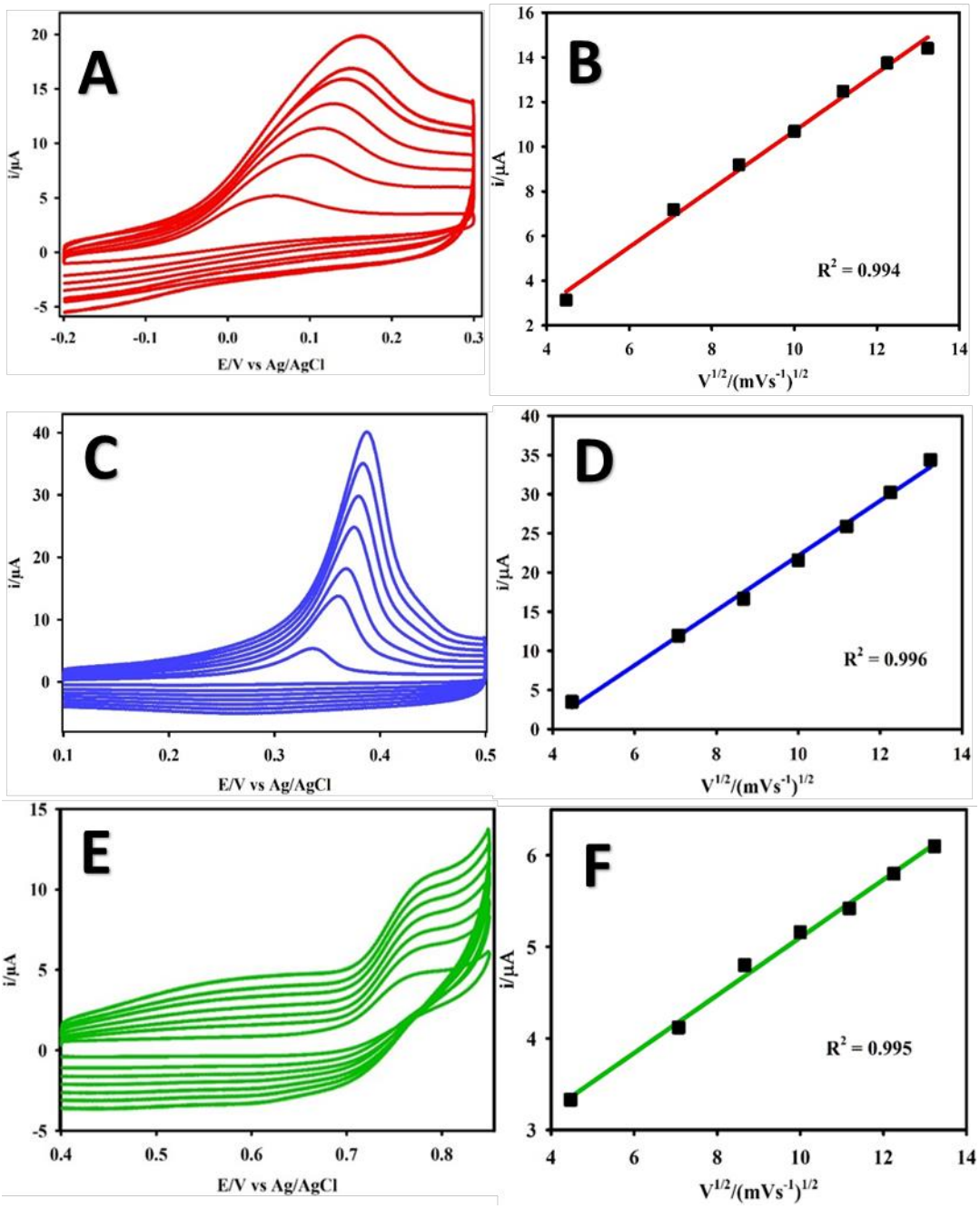

Figure 5.6. CV curves of the nanoporous gold microelectrode measured in (A) 250.0 μM H_2H_4, (B) 250 μM SO_3^{2-}, (C) 250 μM NO_2^- at various scan rates (20, 50, 75, 100, 125, 150, 175 mV s^{-1}); (D), (E) and (F) represents the corresponding linear relationship between the oxidation peak current I_p and the square root of the scan rate $v^{1/2}$ of the respective analytes in the electrolyte medium of 0.1 M PBS (pH 6.5).

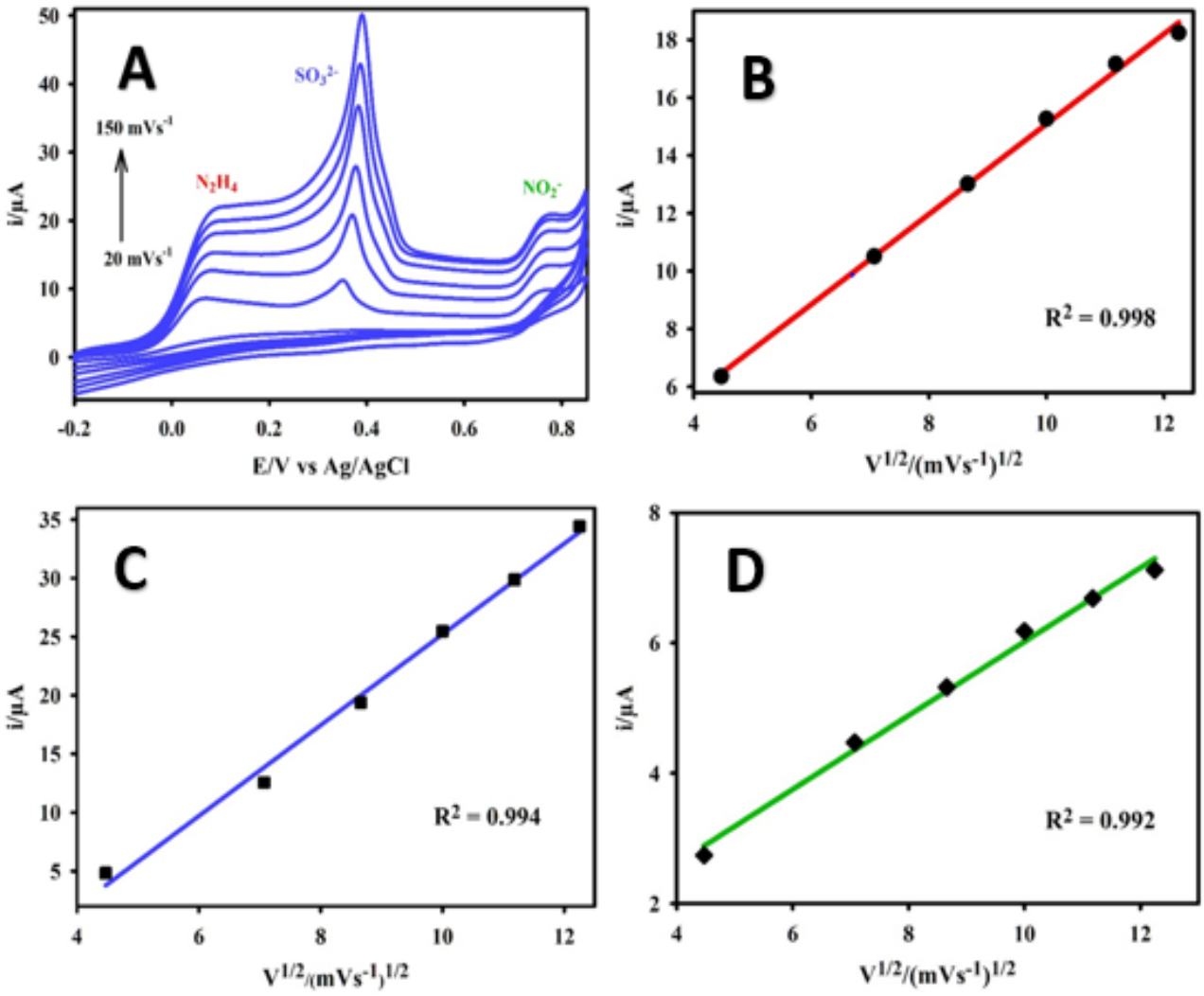

Figure 5.7. (A) CVs of the nanoporous gold microelectrode recorded in in 0.1 M PBS (pH 6.5) containing 250 µM N_2H_4, 250 µM SO_3^{2-} and 250 µM NO_2^- at different scan rates (20, 50, 75, 100, 125, 150 mV s^{-1}); (B), (C) and (D) The linear relationship between the oxidation peak current I_p and the square root of the scan rate $v^{1/2}$, respectively.

From Figure. 5.7A, it is evident that the oxidation peak potential moved towards the more positive side with the increasing scan rate (20 to 175 mV s^{-1}). The corresponding plots of the oxidation peak current I_{pa} vs the square root of the scan rate ($v^{1/2}$) are presented in Figures 5.7B-

D, respectively. The linear relationship, with correlation coefficients of 0.998, 0.993 and 0.994 for the electrochemical oxidation of N_2H_4, SO_3^2, and NO_2^-.

5.3.4. Detection limit and calibration plots

The effect of the concentrations of N_2H_4, SO_3^{2-}, and NO_2^- on the current responses of the nanoporous gold microelectrode was investigated using the DPV technique as presented in Figure 5.8. All the peak current responses to the electrochemical oxidation of N_2H_4 (Figure 5.8A), SO_3^{2-} (Figure 5.8C) and NO_2^- (Figure 5.8E) exhibited a proportional increase with respect to their concentrations increasing from 5.0 x 10^{-6} to 4.0 x 10^{-3} mol L^{-1}. The linear regression equations between the concentration (c, μM) and the current (i_{pa}, μA) for the electrochemical oxidation of N_2H_4, SO_3^{2-}, and NO_2^- individually were: $i_{Hydrazine}$ (μA) = 1.15 + 0.005[N_2H_4] (Figure 5.8B); $i_{Sulfite}$ (μA) = 1.07 + 0.011[SO_3^{2-}] (Figure 5.8D); and $i_{Nitrite}$ (μA) = 0.118 + 0.012[NO_2^-] (Figure 5.8F) with the coefficient R^2 values of 0.993, 0.991, and 0.998, respectively. The limit of detection (LOD) was calculated according to the formula $3\sigma/s$, where σ is the standard deviation of the blank measurements; and s is the slope obtained from the calibration plot.

The LODs for the oxidation of N_2H_4, SO_3^{2-}, and NO_2^- were found to be 9.11 x 10^{-7}, 3.37 x 10^{-7}, and 1.44 x 10^{-6} mol L^{-1} for N_2H_4, SO_3^{2-}, and NO_2^-, respectively. In addition, the selectivity of the nanoporous gold microelectrode was evaluated on the simultaneous determination of N_2H_4, SO_3^{2-}, and NO_2^-. As displayed in Figure 5.9, the peak currents were increased with the increase of their concentrations from 5.0 x 10^{-6} to 4.0 x 10^{-3} mol L^{-1} and the well-defined peak-to-peak separation was achieved for all the three analytes. The corresponding linear regression plots are presented in Figure 5.9B, C and D, revealing that the R^2 values obtained for the simultaneous determination were 0.994, 0.993, 0.996 for N_2H_4, SO_3^{2-}, and NO_2^-, respectively.

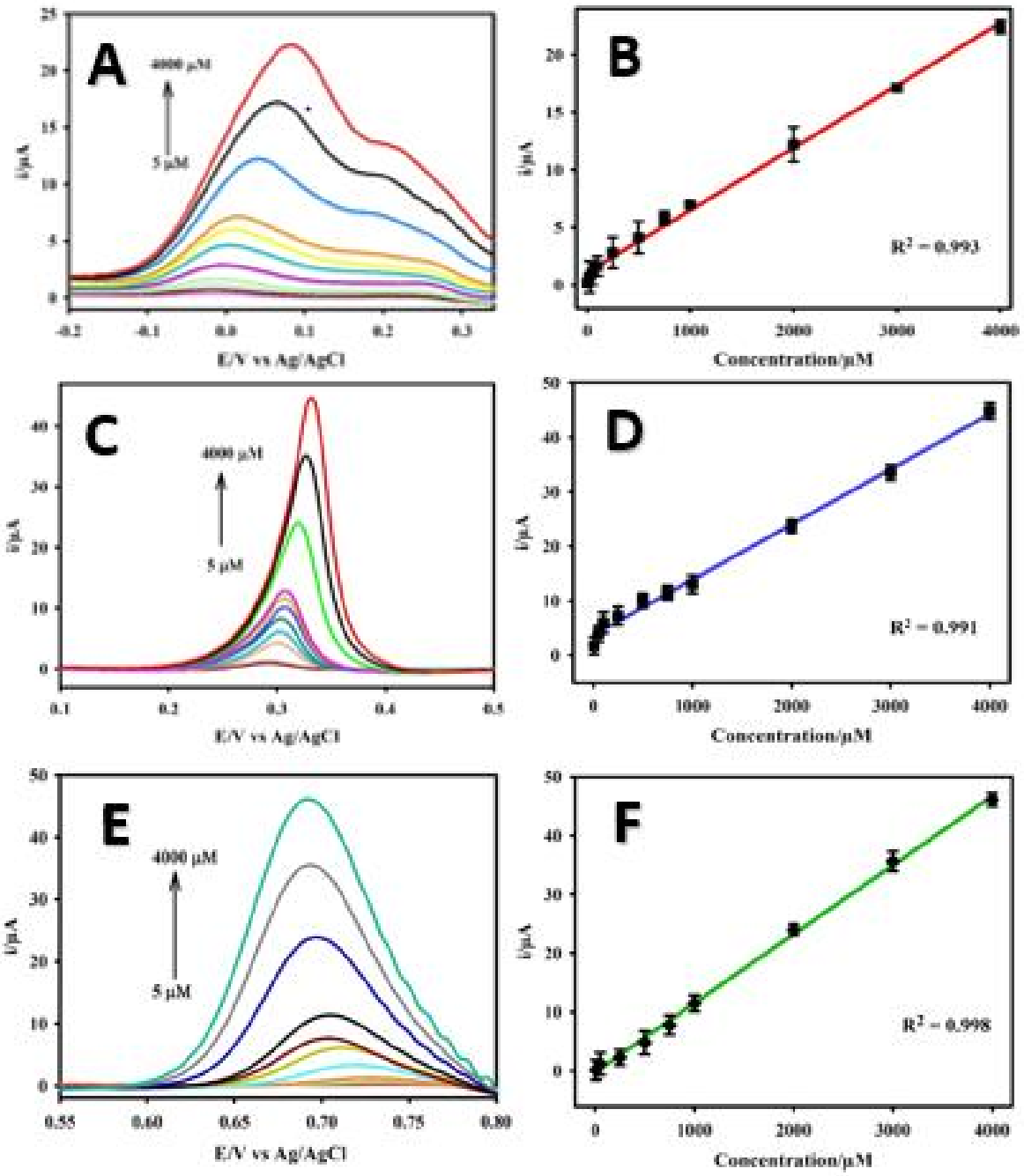

Figure 5.8. DPV responses of gold microelectrode towards the oxidation of (A) N_2H_4, (C) SO_3^{2-}, (E) NO_2^- in a concentration range from 5 μM to 4 mM in 0.1 M PBS (pH 6.5). (B), (D) and (F) The corresponding calibration plots. Each point was expressed as the mean ± standard deviation (n= 3).

Moreover, the slope values found from the calibration curves of the respective analytes were virtually the same as to the electrochemical detection of the species separately as observed from Figure 5.9, confirming that the nanoporous gold microelectrode was capable of detecting N_2H_4, SO_3^{2-} and NO_2^- independently as well as simultaneously.

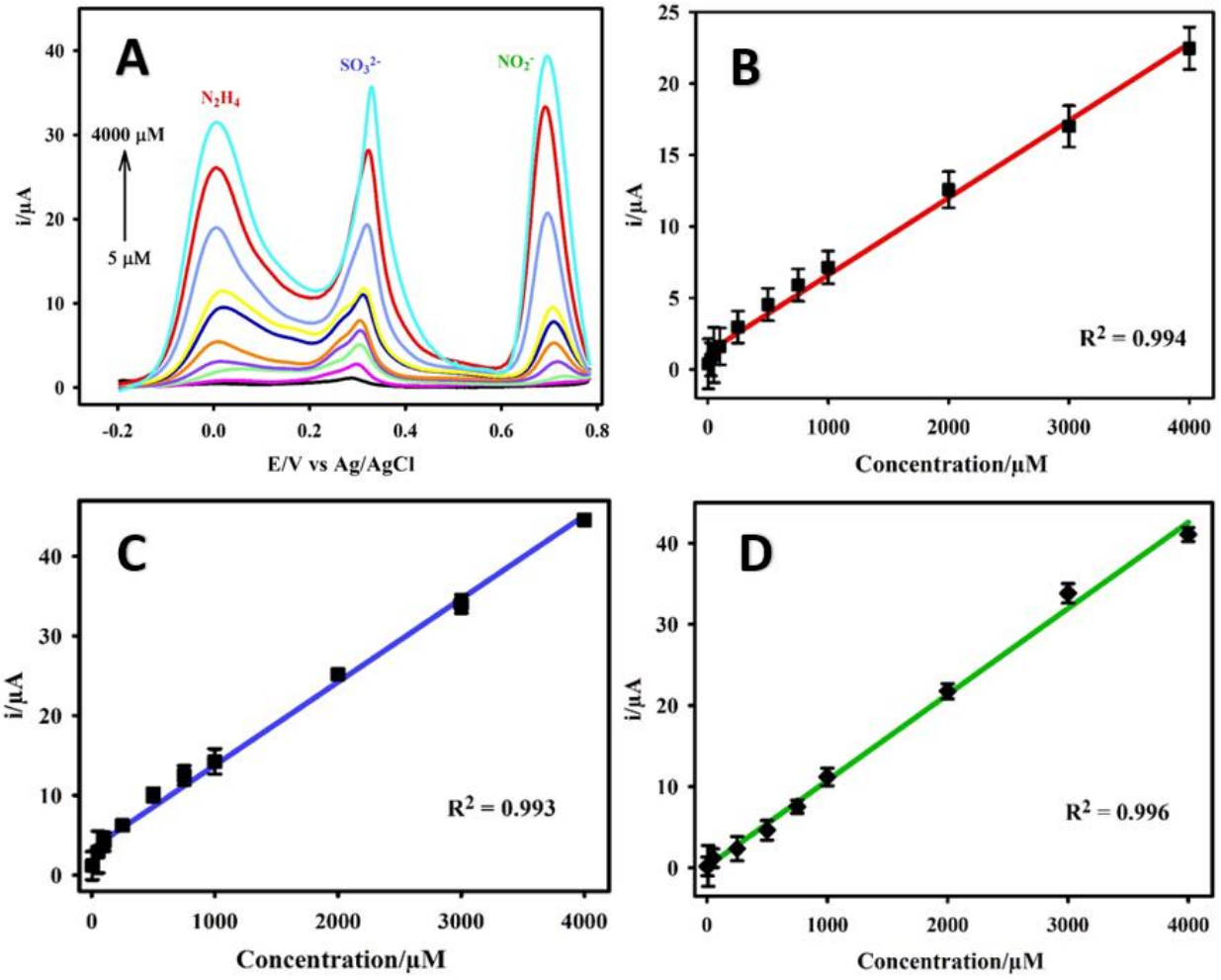

Figure 5.9. DPV responses of gold microelectrode for simultaneous oxidation of (A) N_2H_4, SO_3^{2-} and NO_2^- in a concentration range from 5 µM to 4 mM in 0.1 M PBS (pH 6.5). (B), (C) and (D) represent their corresponding calibration plots. Each point was expressed as the mean ± standard deviation (n= 3).

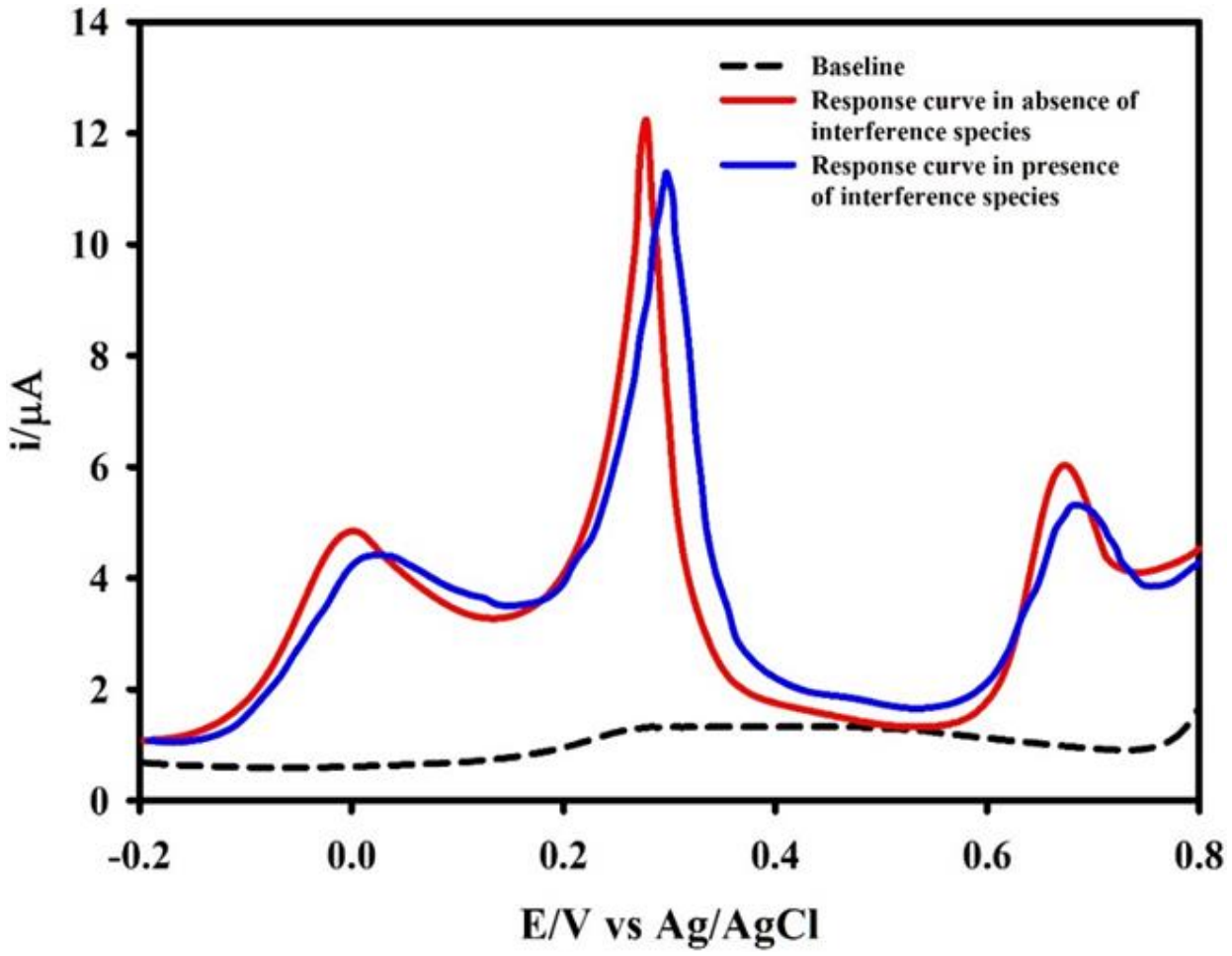

Figure 5.10. Interference response of the nanoporous gold microelectrode for the oxidation of 500.0 μM of N_2H_4, SO_3^{2-} and NO_2^- in the presence of 10-fold concentrations of $H_2PO_4^-$, HPO_4^{2-}, CO_3^{2-}, F^-, Cl^-, NO_3^-, SO_4^{2-}, Na^+, K^+, Ca^{2+}, Mg^{2+} and Zn^{2+}.

5.3.5. Interference and stability measurements

Probable interference species prevailing in actual samples were used to scrutinize the anti-interference ability of the nanoporous gold microelectrode. The DPV curves (Fig. 5.10) were recorded in 0.1 M PBS (pH 6.5) containing 500 μM N_2H_4, 500 μM SO_3^{2-} and 500 μM NO_2^- in the absence (red curve) and in the presence (blue curve) of anions (including $H_2PO_4^-$, HPO_4^{2-},

CO_3^{2-}, F^-, Cl^-, NO_3^-, and SO_4^{2-}) and cations (e.g., Na^+, K^+, Ca^{2+}, Mg^{2+} and Zn^{2+}) each (except

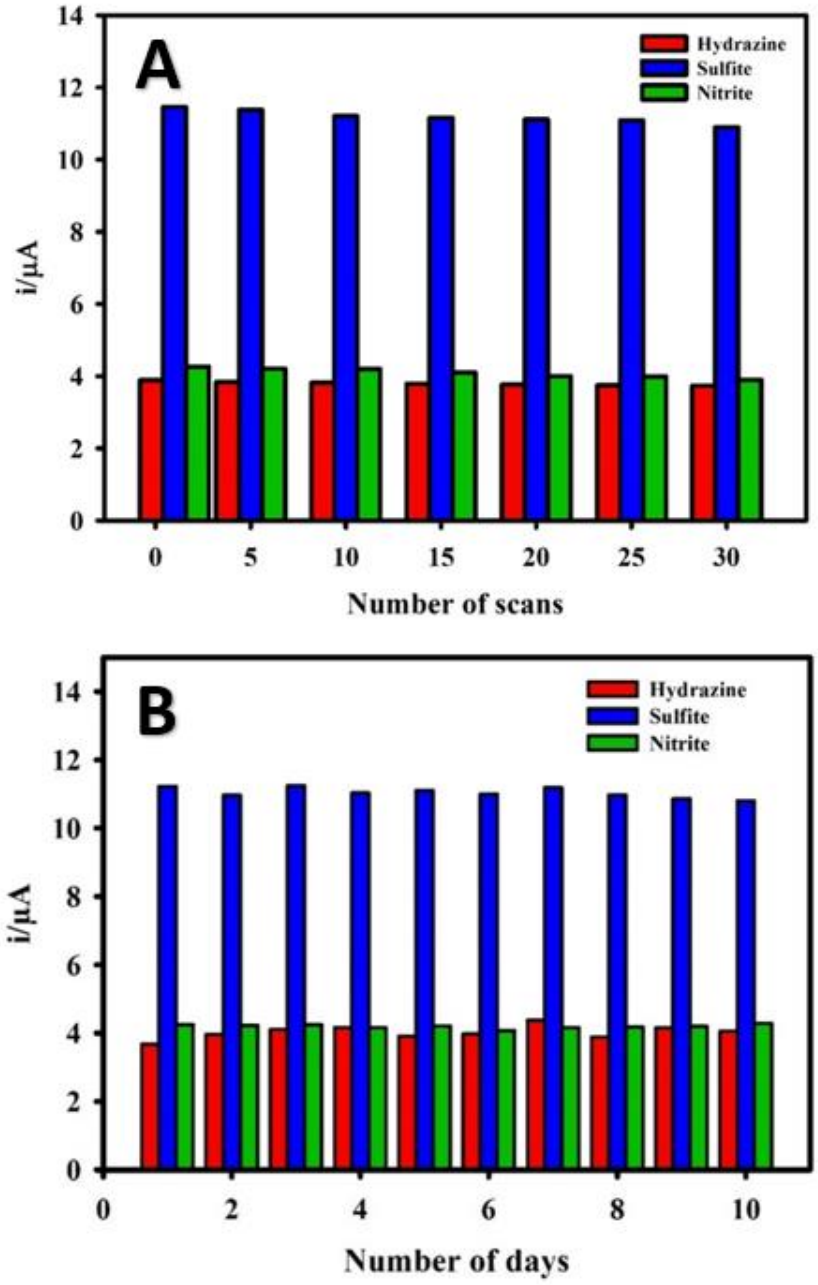

Figure 5.11. (A) Stability measurement of the nanoporous gold microelectrode on the simultaneous oxidation of N_2H_4, SO_3^{2-} and NO_2^- for 30 consecutive scans. The concentration of each was 500 μM; (B) Long-term stability of the nanoporous gold microelectrode over a period of ten days.

Na^+, Cl^-, $H_2PO_4^-$ and HPO_4^{2-}) at 5.0 mM, which was 10 times higher than the three analytes. No notable changes were observed in the current response as well as the peak potential. The small decrease of the current response and the slight shift of the peak potential might be attributed to the specific adsorption of the interfering anions and cations. The aforementioned results confirmed the high specific selectivity and anti-interference capability of the nanoporous gold microelectrode towards the simultaneous determination of N_2H_4, SO_3^{2-}, and NO_2^-.

Table 5.1. The performance of the nanoporous gold microelectrode for the simultaneous detection of the three analytes (N_2H_4, SO_3^{2-} and NO_2^-) for 30 consecutive scans.

Analytes	Number of scans	Mean	Std. Dev	Std. Error	%RSD
Hydrazine	30	3.80	0.05	0.02	1.44
Sulfite	30	11.18	0.18	0.07	1.68
Nitrite	30	4.09	0.14	0.05	3.29

Table 5.2. The long-term stability of the nanoporous gold microelectrode for the simultaneous determination of N_2H_4, SO_3^{2-} and NO_2^- over a period of ten days.

Analytes	Size	Mean	Std. Dev	Std. Error	%RSD
Hydrazine	10	4.03	0.14	0.06	3.60
Sulfite	10	11.04	0.15	0.05	1.32
Nitrite	10	4.20	0.07	0.02	1.62

The stability of the nanoporous gold microelectrode was evaluated by measuring the current response from the simultaneous oxidation of 500.0 μM N_2H_4, 500.0 μM SO_3^{2-}, and 500.0 μM NO_2^- in 0.1 M PBS (pH 6.5) under the same conditions (Figure 5.11A). The DPV scans

obtained for 30 consecutive measurements showed the peak current responses for the oxidation of the analytes with a small relative standard deviation of 1.44% for N_2H_4, 1.68% for SO_3^{2-} and 3.29% for NO_2^- (Table 5.1). The repeatability of the nanoporous gold microelectrode was also validated using DPV measurements recorded over a period of 10 days under the same conditions (Figure 5.11B), where there were 500.0 μM each of N_2H_4, SO_3^{2-}, and NO_2^- containing in 0.1 M PBS (pH 6.5). The fabricated nanoporous gold microelectrode was stored in a micropipette tip during the repeatability measurement. The results in Table 5.2 showed that the peak current response remained within an acceptable relative standard deviation of 3.60%, 1.32% and 1.62% for the electrochemical oxidation of N_2H_4, SO_3^{2-}, and NO_2^-, respectively, demonstrating the high stability of the fabricated nanoporous gold microelectrode.

5.3.6. Real sample analysis

The developed nanoporous gold microelectrode was further tested for the determination of SO_3^{2-} in wine and beer, NO_2^- in beef, and N_2H_4 in water. The wine, beer and beef samples were adjusted to pH 6.5 before the analysis. The DPV peaks obtained for SO_3^{2-} and NO_2^- from the real sample analysis of Chile wine and Canadian beef II (minced beef) are presented in Figure 5.12. Canadian Beef I (Tenderloin Beef) and Canadian Beef II (Minced Beef) samples were pretreated as described in the experimental section and adjusted to pH 6.5.

The unknown concentration of SO_3^{2-} and NO_2^- in each sample was assessed. Tap water was used to synthetically prepare the N_2H_4 sample. Table 5.3 summaries the quantities of SO_3^{2-}, NO_2^- and N_2H_4 in the assorted brands of wine, apple cider beer, beef and the synthetic water samples. The amounts of SO_3^{2-} found in Chile wine, Australian wine and South Africa wine were close, and they were well below the permissible limit of ~3000.0 μM.

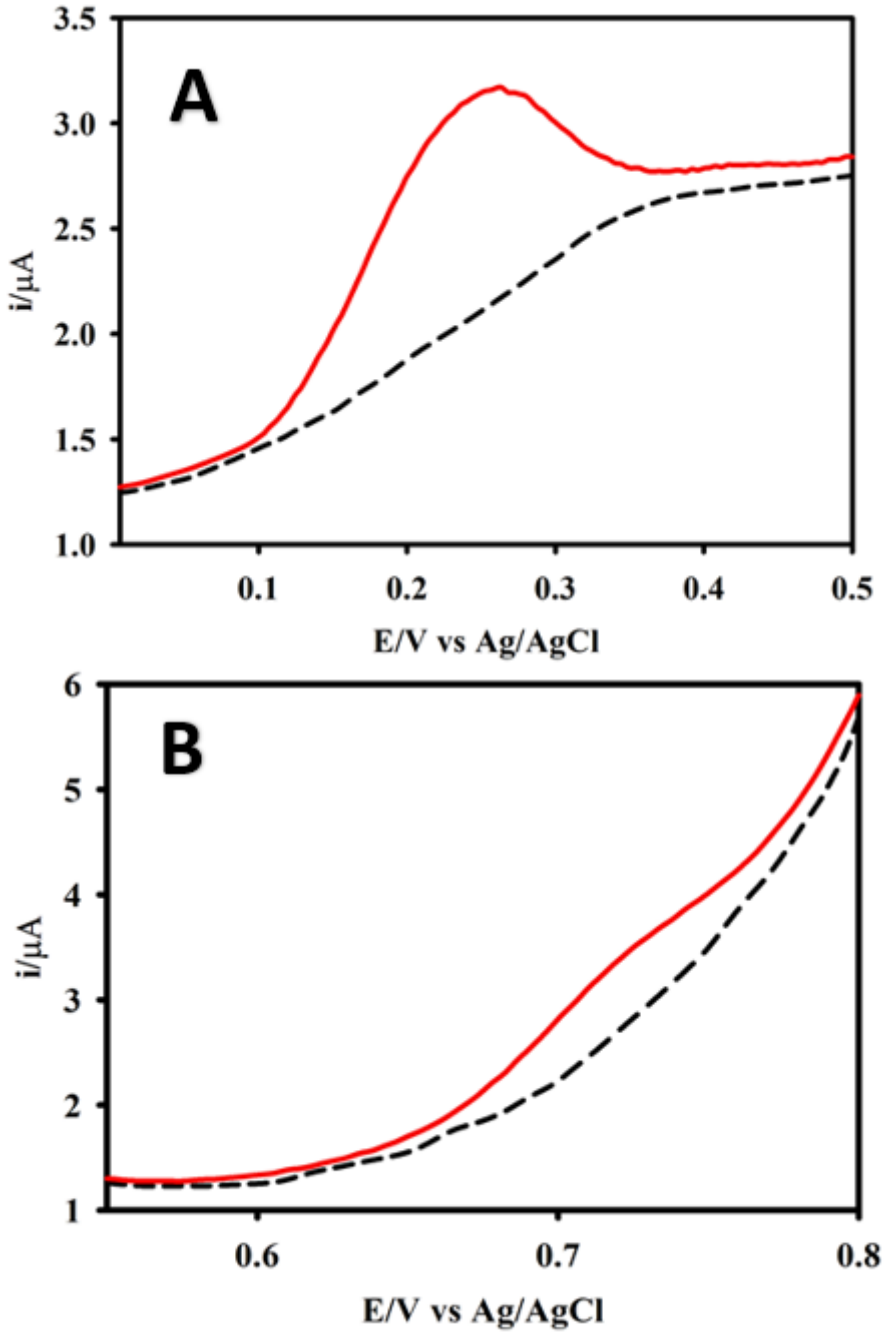

Figure 5.12. DPVs of the nanoporous gold microelectrode recorded in 0.1 M PBS (pH 6.5) showing the (A) presence of sulfite in the Chile wine and (B) the presence of nitrite in the Canadian minced beef sample. The black dashed line in the DPVs represents the baseline derived (in the absence of the analyte) from the nanoporous gold microelectrode.

Table 5.3. Performance of the nanoporous gold microelectrode for the determination of N_2H_4, $SO_3^{2-}$and NO_2^- in wine, beer, beef, and water.

Sample	Analyte	Original Amount (μM)	Spiked (μM)	Found (μM)	Recovery%	%RSD (n = 3)
Chile wine	SO_3^{2-}	204.65	10.00	212.57	99.03	1.16
Australian wine		227.43	10.00	231.62	97.55	0.76
South Africa wine		228.74	10.00	234.21	98.10	1.45
Apple Cider Beer		80.64	10.00	90.38	99.71	1.09
Canadian Beef I	NO_2^-	103.25	10.00	113.08	99.84	1.06
Canadian Beef II		130.53	10.00	140.87	100.24	1.19
Water	N_2H_4	-	10.00	9.82	98.20	0.91
		-	25.00	24.91	99.64	0.76
		-	50.00	50.07	100.14	1.18

As expected, the amount of SO_3^{2-} found in Apple Cider Beer made in Canada was 80.64 μM, which was much less than that added to the wine. The permitted level of SO_3^{2-} added in beer is 624.0 μM. The amount of nitrite determined in Beef Sample I and II was 103.25 and 130.53 μM, respectively. In turn, they were converted to be 47.43 and 60.26 ppm, which were well within the total acceptable concentration of 200 ppm in a finished meat product (recommended by the Public Health Agency of Canada). The data obtained by the standard addition method showed satisfied recovery percentages from 97.55% - 100.24% for all the three analytes. The relative standard deviation (RSD) for each sample calculated based on three experimental trials was less than 2%,

showing that the analysis was highly reproducible. All those results confirmed the effectiveness of the developed nanoporous gold microelectrode for the detection of N_2H_4, SO_3^{2-}, and NO_2^- in real samples.

5.4. Conclusions

A highly stable and selective nanoporous gold microelectrode sensor without the requirement of enzyme or redox mediators was devised for the sensitive detection of N_2H_4, SO_3^{2-}, and NO_2^- in real samples. The obtained results from the CV and DPV studies exhibited the strong ability of the sensor on the electrochemical oxidation of N_2H_4, $SO_3^{2-}$and NO_2^- individually as well as simultaneously in 0.1 M PBS (pH 6.5). The nanoporous gold microelectrode possessed a large EASA with a roughness factor of 27.7. The oxidation peaks were well-defined with the large peak-to-peak separations of 0.27 V and 0.41 V for N_2H_4-SO_3^{2-}, and SO_3^{2-}-NO_2^-, respectively. The nanoporous gold microelectrode displayed enhanced selectivity for the simultaneous measurement of N_2H_4, SO_3^{2-}, and NO_2^-. The devised microelectrode possessed superior performance for the determination of SO^{2-} and NO_2^- in commercial beverages and food samples. Further, the electrochemical sensor demonstrated good sensing ability coupled with other desirable properties such as sensitivity, robustness, and low detection limit. These combined factors confirmed that the nanoporous gold microelectrode could be applicable as a high-performance electrochemical sensor for myriad applications in food and beverage safety and quality control.

References

1. H. Schessl and K. Othmer, Othmer, Encyclopedia of chemical technology, VCH, New York,, (1995) 560.

2. U. S. E. P. Agency, Integrated risk information system (IRIS) on hydrazine/hydrazine sulfate, Natl. Cent. Environ. Assess., Washington, DC,, (1999).
3. G. Choudhary and H. Hansen, Human health perspective on environmental exposure to hydrazines: A review, *Chemosphere* 37 (1998) 801-843.
4. World Health Organization, Environmental health criteria 68: hydrazine, Geneva, Switzerland, (1987) 1-89.
5. Y. Y. Tang, C. L. Kao and P. Y. Chen, Electrochemical detection of hydrazine using a highly sensitive nanoporous gold electrode, *Anal. Chim. Acta* 711 (2012) 32-39.
6. National Institute for Occupational Safety and Health (NIOSH), Pocket Guide to Chemical Hazards, Cincinnati, OH,, (1997).
7. R. Devasenathipathy, V. Mani and S. M. Chen, Highly selective amperometric sensor for the trace level detection of hydrazine at bismuth nanoparticles decorated graphene nanosheets modified electrode, *Talanta* 124 (2014) 43-51.
8. H. Karimi-Maleh, M. Moazampour, A. A. Ensafi, S. Mallakpour and M. Hatami, An electrochemical nanocomposite modified carbon paste electrode as a sensor for simultaneous determination of hydrazine and phenol in water and wastewater samples, *Environ. Sci. Pollut. R.* 21 (2014) 5879-5888.
9. Z. T. Zhao, Y. J. Sun, P. W. Li, W. D. Zhang, K. Lian, J. Hu and Y. Chen, Preparation and characterization of AuNPs/CNTs-ErGO electrochemical sensors for highly sensitive detection of hydrazine, *Talanta* 158 (2016) 283-291.
10. Y. J. Yang, C. Yao and W. Li, Immobilization of phosphotungstic acid on multiwalled carbon nanotubes with cetyltrimethyl ammonium bromide as the molecular linker for enhanced oxidation of hydroxylamine, *J. Electroanal. Chem.* 799 (2017) 386-392.

11. Y. Zeng, Z. H. Zhu, D. Du and Y. H. Lin, Nanomaterial-based electrochemical biosensors for food safety, *J. Electroanal. Chem.* 781 (2016) 147-154.

12. R. Rawal and C. S. Pundir, Development of electrochemical sulfite biosensor based on SO_X/PBNPs/PPY modified Au electrode, *Biochem. Eng. J.* 71 (2013) 30-37.

13. R. Rawal, S. Chawla and C. S. Pundir, An electrochemical sulfite biosensor based on gold coated magnetic nanoparticles modified gold electrode, *Biosen. Bioelectron.* 31 (2012) 144-150.

14. S. L. Taylor, N. A. Higley and R. K. Bush, Sulfites in foods: Uses, analytical methods, residues, fate, exposure assessment, metabolism, toxicity, and hypersensitivity, *Adv. Food Res.* 30 (1986) 1-76.

15. Food and Drug Administration, Sulfiting agents; revocation of GRAS status for use on fruits and vegetables intended to be served or sold raw to consumers, *Fed. Reg.* 51 (1986) 25021.

16. US Food and Drug Administration, Electronic Code of Federal Regulations Title 21: Food and Drugs, Part 130 - Food Standards: General, Government Publishing Office [US], Silver Sping, MD,, (2014).

17. A. Safavi, N. Maleki, S. Momeni and F. Tajabadi, Highly improved electrocatalytic behavior of sulfite at carbon ionic liquid electrode: Application to the analysis of some real samples, *Anal. Chim. Acta* 625 (2008) 8-12.

18. A. Isaac, C. Livingstone, A. J. Wain, R. G. Compton and J. Davis, Electroanalytical methods for the determination of sulfite in food and beverages, *Trac-Trends Anal. Chem.* 25 (2006) 589-598.

19. X. Wang, H. Li, M. Wu, S. L. Ge, Y. Zhu, Q. J. Wang, P. G. He and Y. Z. Fang, Simultaneous electrochemical determination of sulphite and nitrite by a gold nanoparticle/graphene-chitosan modified electrode, *Chin. J. Anal. Chem.* 41 (2013) 1232-1237.

20. X. R. Li, J. Liu, F. Y. Kong, X. C. Liu, J. J. Xu and H. Y. Chen, Potassium-doped graphene for simultaneous determination of nitrite and sulfite in polluted water, *Electrochem. Commun.* 20 (2012) 109-112.

21. N. Rastakhiz, A. Kariminik, V. Soltani-Nejad and S. Roodsaz, Simultaneous determination of phenylhydrazine, hydrazine and sulfite using a modified carbon nanotube paste electrode, *Int. J. Electrochem. Sci.* 5 (2010) 1203-1212.

22. M. Amatatongchai, W. Sroysee, S. Chairam and D. Nacapricha, Simple flow injection for determination of sulfite by amperometric detection using glassy carbon electrode modified with carbon nanotubes-PDDA-gold nanoparticles, *Talanta* 133 (2015) 134-141.

23. W. J. R. Santos, P. R. Lima, A. A. Tanaka, S. M. C. N. Tanaka and L. T. Kubota, Determination of nitrite in food samples by anodic voltammetry using a modified electrode, *Food Chem.* 113 (2009) 1206-1211.

24. X. B. Ge, L. Q. Wang, Z. N. Liu and Y. Ding, Nanoporous Gold Leaf for Amperometric Determination of Nitrite, *Electroanalysis* 23 (2011) 381-386.

25. P. Miao, M. Shen, L. M. Ning, G. F. Chen and Y. M. Yin, Functionalization of platinum nanoparticles for electrochemical detection of nitrite, *Anal. Bioanal. Chem.* 399 (2011) 2407-2411.

26. L. Cui, J. Y. Zhu, X. M. Meng, H. S. Yin, X. P. Pan and S. Y. Ai, Controlled chitosan coated Prussian blue nanoparticles with the mixture of graphene nanosheets and carbon

nanoshperes as a redox mediator for the electrochemical oxidation of nitrite, *Sens. Actuators B-Chem.* 161 (2012) 641-647.

27. H. Hosseini, H. Ahmar, A. Dehghani, A. Bagheri, A. R. Fakhari and M. M. Amini, Au-SH-SiO_2 nanoparticles supported on metal-organic framework (Au-SH-SiO_2@Cu-MOF) as a sensor for electrocatalytic oxidation and determination of hydrazine, *Electrochim. Acta* 88 (2013) 301-309.

28. X. R. Li, F. Y. Kong, J. Liu, T. M. Liang, J. J. Xu and H. Y. Chen, Synthesis of Potassium-Modified Graphene and Its Application in Nitrite-Selective Sensing, *Adv. Funct. Mater.* 22 (2012) 1981-1988.

29. B. Molinero-Abad, M. A. Alonso-Lomillo, O. Dominguez-Renedo and M. J. Arcos-Martinez, Sulfite oxidase biosensors based on tetrathiafulvalene modified screen-printed carbon electrodes for sulfite determination in wine, *Anal. Chim. Acta* 812 (2014) 41-44.

30. Y. Y. Sun, Q. X. Ren, B. Liu, Y. Qin and S. Zhao, Enzyme-free and sensitive electrochemical determination of the FLT3 gene based on a dual signal amplified strategy: Controlled nanomaterial multilayers and a target-catalyzed hairpin assembly, *Biosen. Bioelectron.* 78 (2016) 7-13.

31. T. Hou, W. Li, X. J. Liu and F. Li, Label-Free and Enzyme-Free Homogeneous Electrochemical Biosensing Strategy Based on Hybridization Chain Reaction: A Facile, Sensitive, and Highly Specific MicroRNA Assay, *Anal. Chem.* 87 (2015) 11368-11374.

32. S. S. Chen, Y. C. Shi, A. J. Wang, X. X. Lin and J. J. Feng, Free-standing Pt nanowire networks with clean surfaces: Highly sensitive electrochemical detection of nitrite, *J. Electroanal. Chem.* 791 (2017) 131-137.

33. P. Wang, F. Y. Zhou, Z. W. Wang, C. Lai and X. G. Han, Substrate-induced assembly of PtAu alloy nanostructures at choline functionalized monolayer interface for nitrite sensing, *J. Electroanal. Chem.* 750 (2015) 36-42.

34. X. L. Luo, J. B. Pan, K. M. Pan, Y. Y. Yu, A. N. Zhong, S. S. Wei, J. Li, J. Y. Shi and X. C. Li, An electrochemical sensor for hydrazine and nitrite based on graphene-cobalt hexacyanoferrate nanocomposite: Toward environment and food detection, *J. Electroanal. Chem.* 745 (2015) 80-87.

35. T. M. H. Lee and I. M. Hsing, DNA-based bioanalytical microsystems for handheld device applications, *Anal. Chim. Acta* 556 (2006) 26-37.

36. M. Govindhan, B. R. Adhikari and A. C. Chen, Nanomaterials-based electrochemical detection of chemical contaminants, *RSC Adv.* 4 (2014) 63741-63760.

37. C. M. Welch and R. G. Compton, The use of nanoparticles in electroanalysis: A review, *Anal. Bioanal. Chem.* 384 (2006) 601-619.

38. A. C. Chen and S. Chatterjee, Nanomaterials based electrochemical sensors for biomedical applications, *Chem. Soc. Rev.* 42 (2013) 5425-5438.

39. N. Y. Stozhko, N. A. Malakhova, M. V. Fyodorov and K. Z. Brainina, Modified carbon-containing electrodes in stripping voltammetry of metals. Part II. Composite and microelectrodes, *J. Solid State Electrochem.* 12 (2008) 1219-1230.

40. B. Rezaei, L. Shams-Ghahfarokhi, E. Havakeshian and A. A. Ensafi, An electrochemical biosensor based on nanoporous stainless steel modified by gold and palladium nanoparticles for simultaneous determination of levodopa and uric acid, *Talanta* 158 (2016) 42-50.

41. F. He, X. L. Qin, L. J. Bu, Y. C. Fu, Y. M. Tan, C. Chen, Y. L. Li, Q. J. Xie and S. Z. Yao, Study on the bioelectrochemistry of a horseradish peroxidase-gold nanoclusters bionanocomposite, *J. Electroanal. Chem.* 792 (2017) 39-45.

42. M. Govindhan, M. Amiri and A. C. Chen, Au nanoparticle/graphene nanocomposite as a platform for the sensitive detection of NADH in human urine, *Biosen. Bioelectron.* 66 (2015) 474-480.

43. Z. G. Liu, H. Forsyth, N. Khaper and A. C. Chen, Sensitive electrochemical detection of nitric oxide based on AuPt and reduced graphene oxide nanocomposites, *Analyst* 141 (2016) 4074-4083.

44. H. J. Qiu, H. T. Xu, L. Liu and Y. Wang, Correlation of the structure and applications of dealloyed nanoporous metals in catalysis and energy conversion/storage, *Nanoscale* 7 (2015) 386-400.

45. R. Y. Zhang and H. Olin, Porous gold films-A short review on recent progress, *Materials* 7 (2014) 3834-3854.

46. L. Chao, W. Wang, M. Z. Dai, Y. X. Ma, L. G. Sun, X. L. Qin and Q. J. Xie, Step-by-step electrodeposition of a high-performance Prussian blue-gold nanocomposite for H_2O_2 sensing and glucose biosensing, *J. Electroanal. Chem.* 778 (2016) 66-73.

47. Y. Y. Lin, Y. Peng and J. W. Di, Electrochemical detection of Hg(II) ions based on nanoporous gold nanoparticles modified indium tin oxide electrode, *Sens. Actuators B-Chem.* 220 (2015) 1086-1090.

48. X. X. Xiao, M. E. Wang, H. Li and P. C. Si, One-step fabrication of bio-functionalized nanoporous gold/poly(3,4-ethylenedioxythiophene) hybrid electrodes for amperometric glucose sensing, *Talanta* 116 (2013) 1054-1059.

49. G. Maduraiveeran and R. Ramaraj, A facile electrochemical sensor designed from gold nanoparticles embedded in three-dimensional sol-gel network for concurrent detection of toxic chemicals, *Electrochem. Commun.* 9 (2007) 2051-2055.

50. X. L. Yan, F. H. Meng, S. Z. Cui, J. G. Liu, J. Gu and Z. G. Zou, Effective and rapid electrochemical detection of hydrazine by nanoporous gold, *J. Electroanal. Chem.* 661 (2011) 44-48.

51. F. L. Jia, C. F. Yu, Z. H. Ai and L. Z. Zhang, Fabrication of nanoporous gold film electrodes with ultrahigh surface area and electrochemical activity, *Chem. Mater.* 19 (2007) 3648-3653.

52. Z. G. Liu, A. Nemec-Bakk, N. Khaper and A. C. Chen, Sensitive electrochemical detection of nitric oxide release from cardiac and cancer cells via a hierarchical nanoporous gold microelectrode, *Anal. Chem.* 89 (2017) 8036-8043.

53. A. C. Chen and B. Shah, Electrochemical sensing and biosensing based on square wave voltammetry, *Anal. Methods* 5 (2013) 2158-2173.

54. J. H. Jiang and X. Y. Wang, Fabrication of high-surface nanoporous gold microelectrode, *Electrochem. Commun.* 20 (2012) 157-159.

55. G. M. S. Alves, J. M. C. S. Magalhaes, P. Salaun, C. M. G. van den Berg and H. M. V. M. Soares, Simultaneous electrochemical determination of arsenic, copper, lead and mercury in unpolluted fresh waters using a vibrating gold microwire electrode, *Anal. Chim. Acta* 703 (2011) 1-7.

56. A. Sukeri, L. P. H. Saravia and M. Bertotti, A facile electrochemical approach to fabricate a nanoporous gold film electrode and its electrocatalytic activity towards dissolved oxygen reduction, *Phys. Chem. Chem. Phys.* 17 (2015) 28510-28514.

57. H. R. Zare, M. R. Shishehbore, D. Nematollahi and M. S. Tehrani, Electrochemical behavior of nano-composite containing 4-hydroxy-2-(triphenylphosphonio)phenolate and multi-wall carbon nanotubes spiked in carbon paste and its application for electrocatalytic oxidation of hydrazine, *Sens. Actuators B-Chem.* 151 (2010) 153-161.

58. Y. Zhang, Y. H. Zhao, S. S. Yuan, H. G. Wang and C. D. He, Electrocatalysis and detection of nitrite on a reduced graphene/Pd nanocomposite modified glassy carbon electrode, *Sens. Actuators B-Chem.* 185 (2013) 602-607.

59. K. R. Ward, M. Gara, N. S. Lawrence, R. S. Hartshorne and R. G. Compton, Nanoparticle modified electrodes can show an apparent increase in electrode kinetics due solely to altered surface geometry: The effective electrochemical rate constant for non-flat and non-uniform electrode surfaces, *J. Electroanal. Chem.* 695 (2013) 1-9.

60. E. O. Barnes, X. J. Chen, P. L. Li and R. G. Compton, Voltammetry at porous electrodes: A theoretical study, *J. Electroanal. Chem.* 720 (2014) 92-100.

61. M. C. Henstridge, E. J. F. Dickinson and R. G. Compton, Mass transport to and within porous electrodes. Linear sweep voltammetry and the effects of pore size: The prediction of double peaks for a single electrode process, *Russ. J. Electrochem.* 48 (2012) 629-635.

62. X. Huang, Y. X. Li, Y. L. Chen and L. Wang, Electrochemical determination of nitrite and iodate by use of gold nanoparticles/poly(3-methylthiophene) composites coated glassy carbon electrode, *Sens. Actuators B-Chem.* 134 (2008) 780-786.

Chapter 6: Sensitive Electrochemical Detection of Caffeic Acid in Wine Based on Fluorine-doped Graphene Oxide*

6.1. Introduction

Caffeic acid (3, 4-dihydroxycinnamic acid) is an important compound in the classification of phenolic acids, which exists in certain vegetables (e.g., cabbage, cauliflower, and kale) and fruits (e.g., strawberries, grapes, and apples). It serves as an antioxidant, anti-inflammatory, antibacterial, and immune-modulating agent.[1-4] The molecular structure of CA is comprised of two hydroxyl groups adjacent to an aromatic ring, which provocatively contributes to its distinctive antioxidative nature.[5,6] Copious amounts of CA derivatives present in wine, and are accountable for maintaining colour, thus protecting the alcoholic beverage from oxidative deterioration.[7,8] Fascinatingly, scientific studies have reported that CA functions as an anti-tumour agent and may have the ability to lower the impacts of diabetes and cancer.[9-12]

Numerous methods, such as liquid and gas chromatography, capillary electrophoresis and spectrophotometry, have the capacity to determine phenolic acids and CA derivatives in foods and beverages.[13,14] Although these analytical instruments are advanced, their operation requires skilled personnel and involves multistep sample treatment and testing procedures. Consequently, a cost-effective and efficacious method for the detection of CA is imperative to analyze and assure the quality of the wine.

---

* Most of the results presented in this chapter have been published in the special issue of the journal *Sensors* (State-of-the-Art Sensors Technology in Canada), **2019**, 19, 1604.

One of the major challenges with CA detection is the interference from other polyphenolic compounds (*p*-coumaric acid, hydroquinone, trans-ferulic acid, gallic acid) present in wine. Therefore, the development of sensitive and selective electrochemical sensors for the quantitative detection of CA is essential.

Several previously reported works have focused on the quantitative determination of CA utilizing different types of nanostructured materials in various electrolyte media.[15-18] Fernandes et al. developed a multi-component electrochemical biosensor for the detection and quantification of CA in white wine. This biosensor was developed through the immobilization of green beans in a chitin matrix, which was subsequently incorporated into a carbon paste electrode. The CA content of white wine was determined using square wave voltammetry, and the biosensor demonstrated good selectivity.[19] Although redox mediator-based biosensors may have good selectivity, they have disadvantages including reproducibility and long-term stability.[20] Santos and co-workers fabricated an electrochemical sensor by modifying a glassy carbon electrode (GCE) with a poly(glutamic acid) (PG) film for the electrochemical detection and quantification of CA in red wine.[21] Recently, Thangavelu and co-workers reported on the electrochemical determination of CA using gold and palladium decorated with graphene (Au/Pd/Gr) for the sensitive detection of CA.[22] Yue and co-workers developed an electrochemical sensor using Pd-Au/PEDOT/graphene nanoparticles and investigated its performance for the determination of CA.[23]

As noble metals are expensive, carbon-based electrochemical sensors offer an inexpensive route toward the quantification of CA. Graphene and its derivatives are widely used in biological applications, electrochemical sensing and energy storage, due to their remarkable physicochemical properties.[24-36] Array-based sensing approaches (nose/tongue strategies) using

graphene oxide have been reported for the detection of biomatrices and organic molecules.[37-39] Chemically/electrochemically reduced graphene oxide (GO) and nitrogen doped carbon electrochemical sensors were explored for CA detection.[40-42] The doping of graphene and GO with heteroatoms (e.g., F, Cl, N, B, and S) at the molecular and atomic level, favourably enhances their electrochemical behaviour and electrocatalytic properties, while altering their electronic and physicochemical properties.[43-45] Based on the nature of dopants and their bonding conformations, the characteristics of graphene may improve and be advantageous for desired applications. As a result, the heteroatom-doped graphene derivatives have been explored for their capability as an efficient electrocatalyst for oxygen reduction, energy storage and supercapacitor applications.[46-48] F-GO and its derivatives have invigorated intense research activity due to their exceptional properties (e.g., resistance to high temperature, improved electrocatalytic activity, and outstanding chemical inertness).[49-52] In contrast to carbon, fluorine possesses a higher electronegativity, which may bring about attributes such as ionic, semi-ionic, and covalent bonding.[53,54] Further, the electronic structure of F-GO is dissimilar to that of graphene oxide. The doping of graphene with F alters its electronic structure due to the incorporation of sp3 carbon into graphene's sp2 honeycomb structure.[55] This alteration in its electronic structure might be explained by the electron withdrawing and electron donating nature of fluorine atoms due to their strong electronegativity and the presence of lone-pair electrons.[56] Consequently, fluorine-based graphene derivatives are useful across a range of applications, such as supercapacitors, batteries, metal-free electrocatalyst, and biomedical devices.[57-63]

The aims of the present study were two-fold: (i) to compare the electrochemical properties of GO and F-GO as an advanced electrochemical sensing material; and (ii) to develop

a high-performance electrochemical sensor for the sensitive detection of CA. To the best of our knowledge, this is the first report on a highly sensitive and selective F-GO based electrochemical sensor for the direct measurement of CA in different brands of wine.

6.2. Experimental section

6.2.1. Reagents

Caffeic acid, potassium ferrocyanide, potassium chloride, chloroauric acid, and other reagents were purchased from Sigma Aldrich. All reagents used for the experiments were of analytical grade. All solutions used for the experiments were prepared using deionized water (18.2 MΩ cm, Nanopure® diamond™ UV water purification system), and all glassware was thoroughly washed and dried prior to each analysis. Four different brands of red wine were purchased from a liquor store (i) Alamos (Chilean wine - Sample I); (ii) Bodacious (Canadian wine - Sample II); (iii) Radio Boka – The Pavilion (Spaniard wine - Sample III); and (iv) Santa Carolina (Argentinian wine - Sample IV). All experiments were conducted using a Britton-Robinson (B-R) electrolyte medium.[64] The B-R buffer solution was prepared from a mixture of phosphoric acid, glacial acetic acid and boric acid at a concentration of 0.1 M, and the pH values of the electrolyte solutions were adjusted with a sodium hydroxide solution (0.5 M).

6.2.2. Electrode preparation and modification

The F-GO was synthesized via an improved Hummers' method with some modifications.[65] Initially, a mixture was prepared by blending 1.0 g graphite, 90.0 mL sulfuric acid (H_2SO_4), 10.0 ml orthophosphoric acid (H_3PO_4), and 20 ml hydrogen fluoride (HF). Secondly, the prepared mixture was stirred vigorously for 2 h, and the temperature was maintained at 50 °C. Approximately 4.5 g of $KMnO_4$ was slowly added to this blend, and stirred

constantly for another 15 h. Thirdly, the reaction mixture was supplemented with 100 ml of ice, and after a short while, 5.0 ml of 30% H_2O_2 was also added. Subsequently, the obtained final product (F-GO) was separated and thoroughly rinsed with 30% hydrochloric acid (HCl), pure water, ethanol, and diethyl ether. Lastly, the resulting F-GO solid was transferred to an oven at 50°C for drying.

The prepared F-GO was mixed with water (4.0 mg/ml) and ultrasonicated for 1 h to ensure thorough mixing. A GCE was polished with 1.0 and 0.3 μm alumina slurry, then rinsed with ethanol and water ultrasonicated for 10 min. The F-GO ink was drop cast onto the surface of GCE and air dried for 4 h to obtain the F-GO/GCE. The as-prepared F-GO/GCE was then subjected to partial electrochemical reduction in 0.1 M phosphate buffer solution at pH 7.4. Similarly, another GCE was prepared by drop-casting GO onto its surface. For comparison, a bare GCE and the GO/GCE were tested alongside with F-GO/GCE for CA oxidation.[56]

6.2.3. Characterization techniques

The F-GO was characterized using a Hitachi SU-70 Schottky Field Emission SEM with an energy dispersive X-ray spectrometer and XPS (Thermo Scientific). XPS was carried out using a Thermo Scientific K-α XPS spectrometer. A monochromatic Al Kα X-ray source was employed, with a spot size of 400 μm. Voltammetry techniques such as CV and DPV were implemented using a CHI potentiostat (CHI-660D, CHI, USA). The redox behaviour of the molecule and the kinetics of the electrodes were examined using CV, whereas the analytical determination of the electroactive analyte was conducted by means of DPV.

All electrochemical experiments were conducted in an electrochemical cell consisting of a conventional three-electrode system. The F-GO/GCE functioned as the working electrode, a coiled platinum wire acted as the counter electrode, and a standard silver-silver chloride (Ag/AgCl)

electrode served as the reference electrode. All analytical quantitation was performed in a 0.1 M B-R buffer (pH 2.65) at room temperature. Preceding the analysis, all of the solutions were purged with argon gas for a duration of 15 min. The potentials specified in this paper were against an Ag/AgCl reference electrode.

6.3. Results and Discussion

6.3.1 Morphology and electrochemical characterization

The surface morphologies of the F-GO and GO were investigated using SEM. Figure 6.1A presents a typical SEM image observed for the GO and Figure 6.1B illustrates the SEM image for the F-GO, which revealed a crumpled layered structure. In addition, XPS was utilized to distinguish the composition and functional group species that were present in the F-GO and GO. All data analysis was carried out using XPS peak software. A mixture of Gaussian and Lorentzian function was used to deconvolute the peaks in HR XPS spectra and the sp^2 carbon is fitted at 284.5 eV.

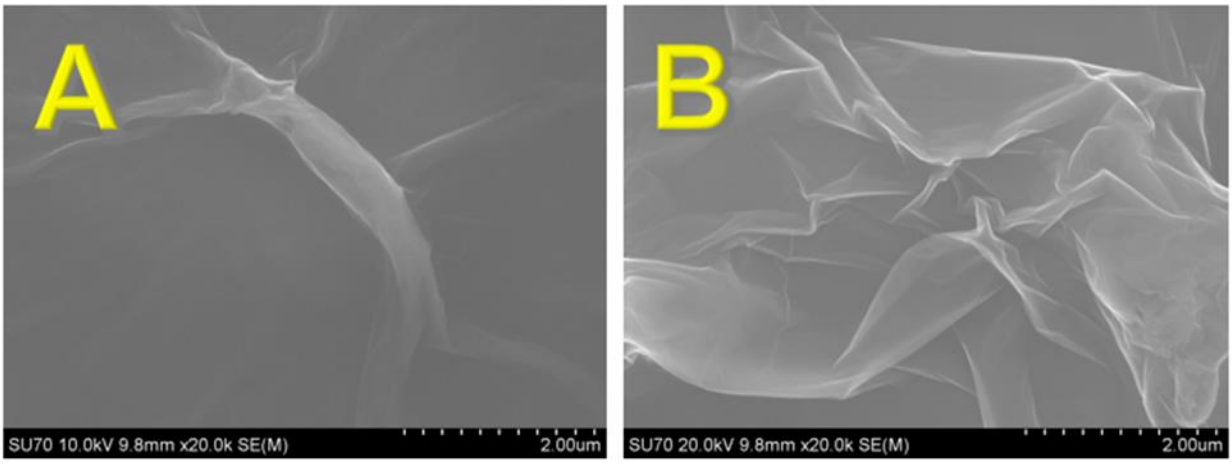

Figure 6.1. SEM images of the synthesized (A) graphene oxide (GO) and (B) fluorinated graphene oxide (F-GO).

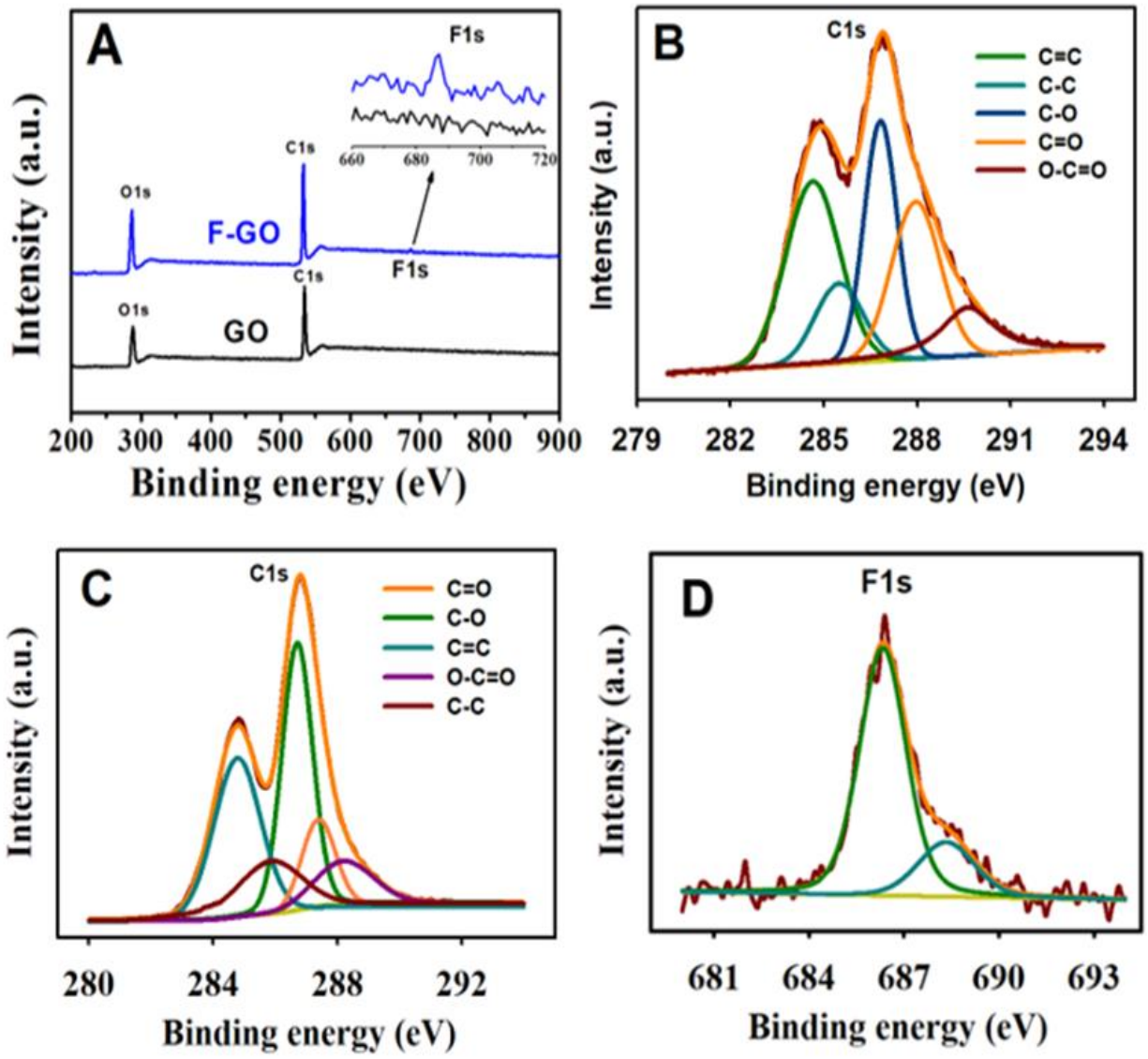

Figure 6.2. (A) XPS spectra (survey scan) of GO and FGO; (B) high-resolution XPS spectrum of C1s of GO and the fitting curves; (C) high-resolution XPS spectrum of C1s of F-GO and the fitting curves; and (D) high-resolution XPS spectrum of F1s of F-GO.

As perceived from the expanded inset of the XPS survey scans (Figure 6.2A), the presence of fluorine was verified by the occurrence of the F peak at ~ 686.75 eV. The percentages of C, O, and F analyzed from the data of F-GO were 65.20%, 33.64%, and 1.16%, respectively. In contrast, the calculation from the GO composition data revealed the percentages of C and O to be 65.17%

and 34.83%, respectively. The high-resolution C1s spectra of GO and F-GO were de-convoluted into five distinct peaks (Figures 6.2B and 6.2C). The five distinct peaks from the C1s spectrum of GO were as follows: C=C (284.7 eV), C-C (285.4 eV), C-O (286.8 eV), C=O (287.9 eV), and O-C=O (289.2 eV).

Prominent differences were observed in terms of peak intensities when the C1s spectrum F-GO was equated with that of GO. The peak heights of C=O and O-C=O displayed decreased F-GO intensity, whereas a higher intensity of C-O peak was observed, which was attributed to the attack of F on the C=O group, and the formation of C-O and C-F bonds. Further validation was supplemented by the use of the high-resolution F1s spectrum of F-GO (Figure 6.2D). It may be observed from the spectrum that the main peak appeared at 686.38 eV, which was ascribed to the semi-ionic nature of the C-F bond, and the shoulder peak appearing at 689.15 eV, paralleled to the C-F bond, which was covalent in nature.

The electrochemical characteristics of the bare GCE, GO/GCE, and F-GO/GCE were examined in a KCl-Ferricyanide medium (5.0 mM $[Fe(CN)_6]^{3-/4-}$ in 0.1 M KCl). Figure 6.3A exhibits the well-defined cyclic voltammetric curves obtained for the oxidation and reduction of 5.0 mM $[Fe(CN)_6]^{3-/4-}$ at the bare GCE, GO/GCE, and F-GO/GCE. In contrast to the bare GCE and GO/GCE, the F-GO/GCE demonstrated a higher anodic-cathodic peak current and a smaller peak-to-peak potential separation. The potential separation for the bare GCE, GO/GCE, and F-GO/GCE was calculated to be 294, 158, and 113 mV, respectively. The smaller peak-to-peak separation demonstrated the better electrochemical reversibility and improved electron transfer efficiency.[61] Furthermore, the value obtained from the ratio of the anodic to cathodic peak current (Ipa/Ipc = 0.96) confirmed that the oxidation-reduction of $[Fe(CN)_6]^{3-/4-}$ redox probe at the F-GO/GCE was reversible.

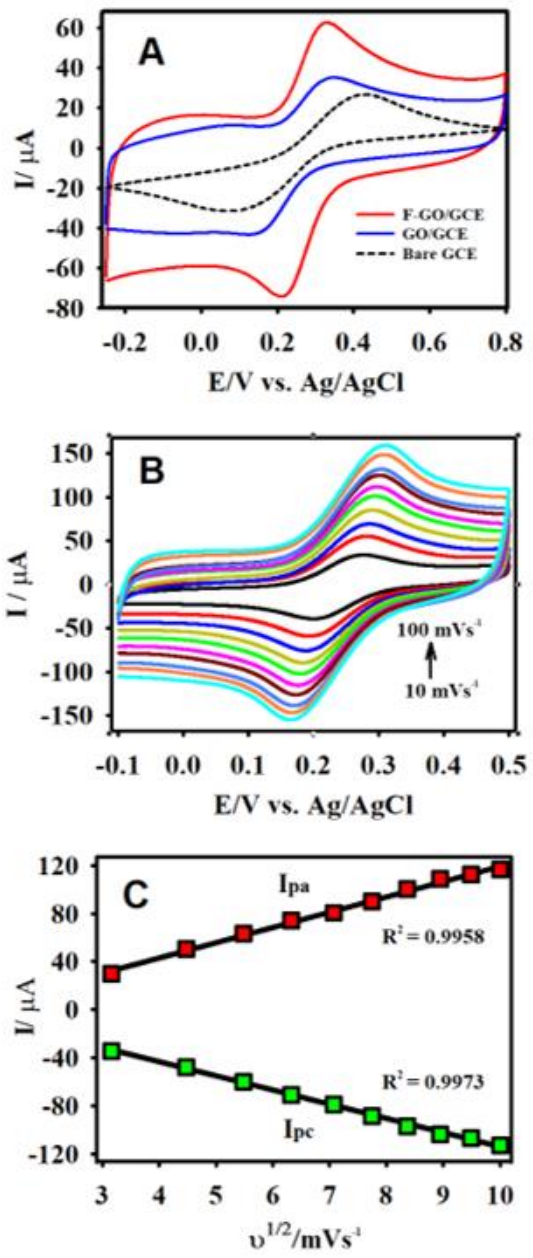

Figure 6.3. (A) CV curves of the bare GCE (black dashed line), GO/GCE (blue line), and F-GO/GCE (red line) in the presence of 0.1 M KCl containing 5.0 mM $[Fe(CN)_6]^{3-/4-}$ at the scan rate of 50 mV s^{-1}; (B) CV curves of the F-GO/GCE recorded in the presence of 5 mM $[Fe(CN)_6]^{3-/4-}$ in 0.1 M KCl at various scan rates, ranging from 10 - 100 mV s^{-1}; (C) the corresponding plots of vs the anodic/cathodic peak current vs the square root of the scan rates

Subsequently, Figure 6.3B shows a series of CV curves obtained at different scan rates (10 – 100 mV/s) in the KCl-ferricyanide medium to study the redox behaviour of the modified electrode, and to calculate the electrochemically active surface area (EASA) of the F-GO/GCE using the Randles-Sevcik equation:[66]

$$ip = 2.69 * 10^5 n^{3/2} AD^{1/2} C \upsilon^{1/2} \quad (1)$$

where *ip* represents the peak current, *D* stands for the diffusion coefficient ($cm^2 s^{-1}$), *C* denotes the concentration of the $[Fe(CN)_6]^{3-/4-}$ molecules in mol L^{-1}, *A* is the EASA (cm^2), *n* signifies the electron transfer number, and *v* is the scan rate ($V s^{-1}$). Figure 6.3C displays the slopes obtained for the Ipa versus $\upsilon^{1/2}$ plots; the EASA was calculated to be 0.045, 0.075, and 0.745 cm^2 for the bare GCE, GO/GCE, and F-GO/GCE, respectively. These observed results verified that the fabricated F-GO/GCE had a higher EASA compared to GO and bare GCE.

6.3.2 Electrooxidation behaviour of CA

Cyclic voltammetry was primarily employed to investigate the electrooxidation behavior of CA at the F-GO modified GCE. Figure 6.4A illustrates the response curves for the bare GCE, GO/GCE, and F-GO recorded in a 0.1 M B-R buffer solution at a scan rate of 50 mV/s in the absence of CA. There were no anodic/cathodic peaks that appeared for the prepared GCEs without CA in the B-R buffer solution. It was evident from the CV that the F-GO/GCE had a larger background current when equated to the bare GCE and GO/GCE which further confirmed that F-GO had a much larger EASA. From Figure 6.4B, it can be seen that the CV displayed well-defined peaks for the oxidation and reduction of 50.0 µM CA. As shown in Figure 6.4C, the modified GCEs exhibited a sharp quasi-reversible peak for the oxidation and reduction of 50.0 µM CA at different peak potentials.

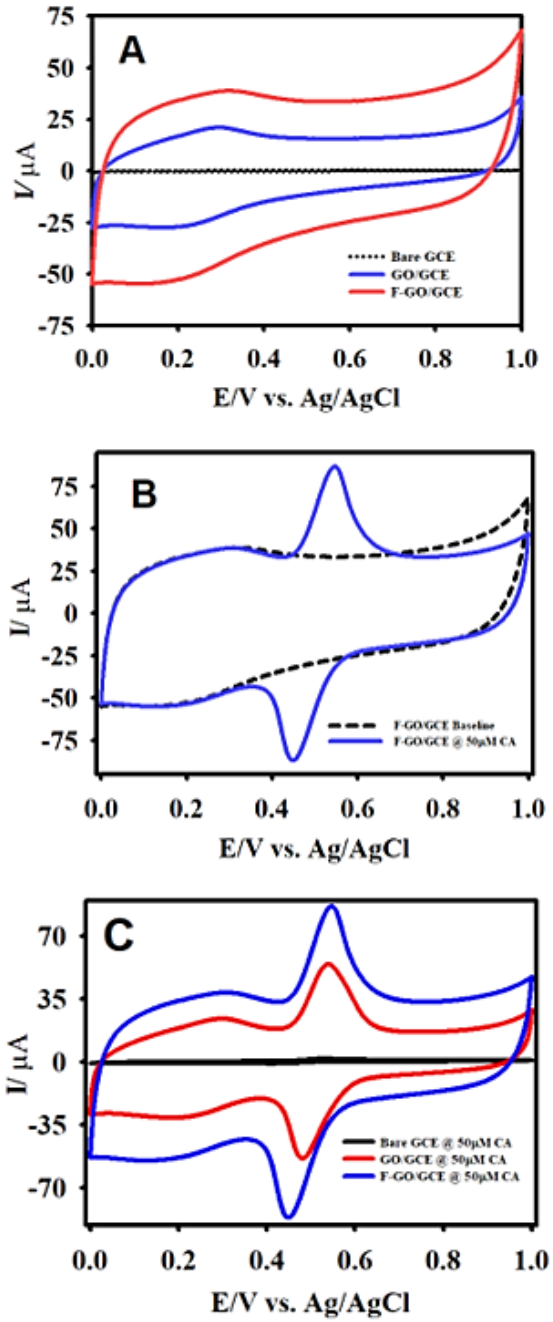

Figure 6.4. CV curves of bare GCE (dashed black line), GO/GCE (blue line), and F-GO/GCE (red line) recorded in the absence of CA (A); F-GO/GCE response in the presence of 50.0 µM CA (B); comparison of the modified GCEs in the presence of 50.0 µM CA (C) in a 0.1 M B-R buffer solution pH 2.65, at a scan rate of 50 mV s^{-1}.

The emergence of the redox peaks was due to the formation of o-quinone following CA oxidation. The chemical reaction for the oxidation of CA followed a 2-electron transfer process [41]:

$$C_9H_8O_4\ (CA) \leftrightharpoons C_9H_6O_4 + 2\ H^+ + 2\ e^-$$

The F-GO/GCE amplified the rate of the electron transfer and enhanced the overall response toward the electrochemical oxidation of CA. The current response recorded with the F-GO/GCE showed a higher anodic and cathodic peak intensity for the oxidation/reduction of CA, as opposed to the bare GCE and GO/GCE. The presence of the C-F semi-ionic bond and higher conductivity facilitated the higher electrocatalytic of F-GO toward the oxidation of CA. Further, the ΔEp values calculated from the oxidation/reduction peak potentials for the CA oxidation with F-GO/GCE (90 mV) was lower than that of the bare GCE (117 mV). These findings suggested that F-GO/GCE possessed good electrocatalytic activity toward the oxidation of CA. Furthermore, as caffeic acid is an electroactive species, the F doped GO yielded higher signal sensitivity towards the oxidation of the chosen analyte. Also, the fluorination of GO has significantly enhanced electrocatalytic activity and improved its overall oxidation toward CA.[61]

6.3.3 Effect of scan rate, electrolyte pH, and concentration

Based on the effect of the scan rate, the electrocatalytic oxidation of CA was investigated further by employing CV. Figure 6.5A illustrates the effect of the scan rate on the electrochemical oxidation of 50.0 µM CA at the F-GO/GCE recorded in a 0.1 M B-R buffer, from 10 to 200 mV s^{-1}. The values of the anodic/cathodic peak current were incremental with an increasing scan rate; however, the observations from the CV exhibited a shift in the oxidation/reduction peak potentials. indicating that the electrochemical oxidation/reduction process was quasi-reversible. At higher scan rates, the electrochemical reaction became less

reversible due to the slow electron-transfer rate.[40,67] The displaced peak potential could also be attributed to the change of the thickness of the diffusion layer, which varied with the scan rate.[68] On the contrary, the growth of the diffusion layer was substantially lower at higher scan rates. Therefore, the reason for the shift in the oxidation/reduction peak potential could be attrib-

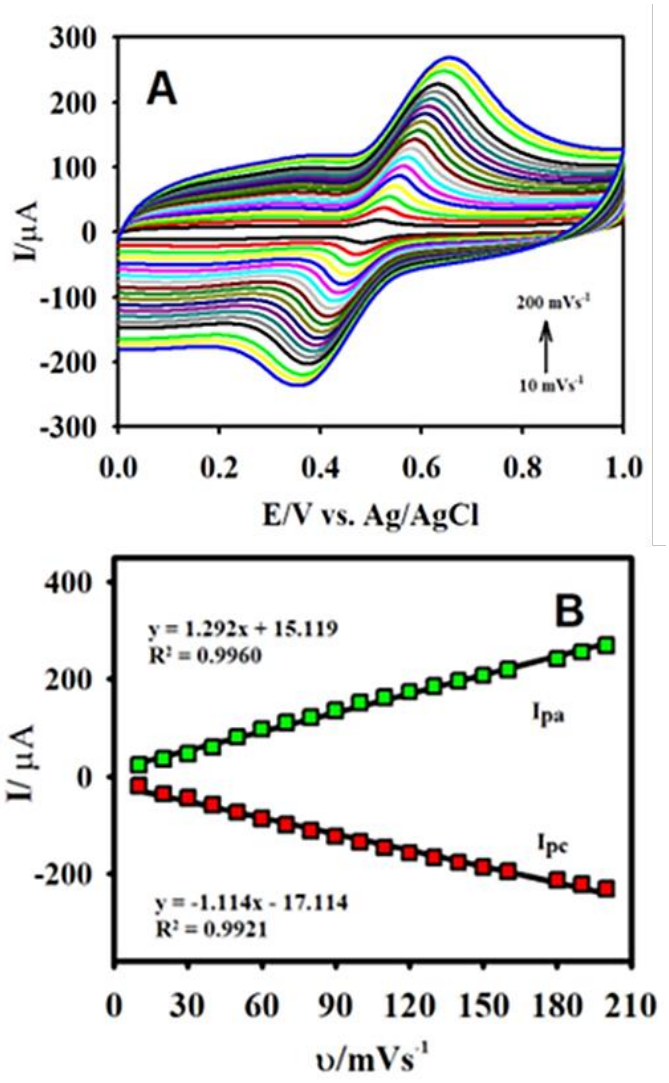

Figure 6.5. CV response of F-GO/GCE recorded in the presence of 50.0 μM CA at different scan rates varying between 10 to 200 mV s-1 (A) and the subsequent plot of anodic/cathodic peak current vs. the scan rate (mV s-1) (B), in 0.1 M B-R buffer medium.

uted to the minor variation in the flux at the surface of the electrode when cycled at lower scan rates.[42] Moreover, with higher scan rates, the electrochemical reaction became less reversible due to the slow electron-transfer rate.[40,67] The corresponding plot of the oxidation/reduction peak current Ipa/pc vs the scan rate (υ, mV s^{-1}) is presented in Figure 6.5B. The observation from the plot indicated that the CA oxidation exhibited good linearity over the incrementing scan rate.

The estimated R^2 values and the linear regression equation from the calibration plot, were: $R^2 = 0.9960$, Ipa = 1.292×10^{-6} A/mV s^{-1} + 15.119 μA; and $R^2 = 0.9921$, Ipc = -1.114×10^{-6} A/mV s^{-1} - 17.114 μA (Fig. 4B). The results from the linear relationship between Ipa/pc and the scan rate indicated that the oxidation and reduction of CA at the F-GO/GCE was a surface-controlled process.

The effect of the electrolyte pH played a vital role in enhancing the electrocatalytic performance of the sensor and determined the electrochemical oxidation behaviour of the CA molecule. The electrochemical behaviour of CA was investigated by running CV in B-R buffer solution under a diverse pH range (acidic to basic), which contained 30.0 μM of the analyte at the scan rate of 50 mV s^{-1}. Figure 6.6A displays the anodic peak current response of the F-GO/GCE toward the electrochemical oxidation of CA at different pH levels, ranging from 2.6 to 7.0. The peak potential was linearly shifted towards more negative potential with the increase of the pH as seen in the insert of Fig. 5D, which was consistent with the report in the literature.[67,69] On the other hand, the peak current was decreased with the increase of the pH as shown in Fig. 5D. As a result, the B-R buffer solution with pH 2.65 was selected for carrying out further electrochemical experiments and for the analytical determination of CA.

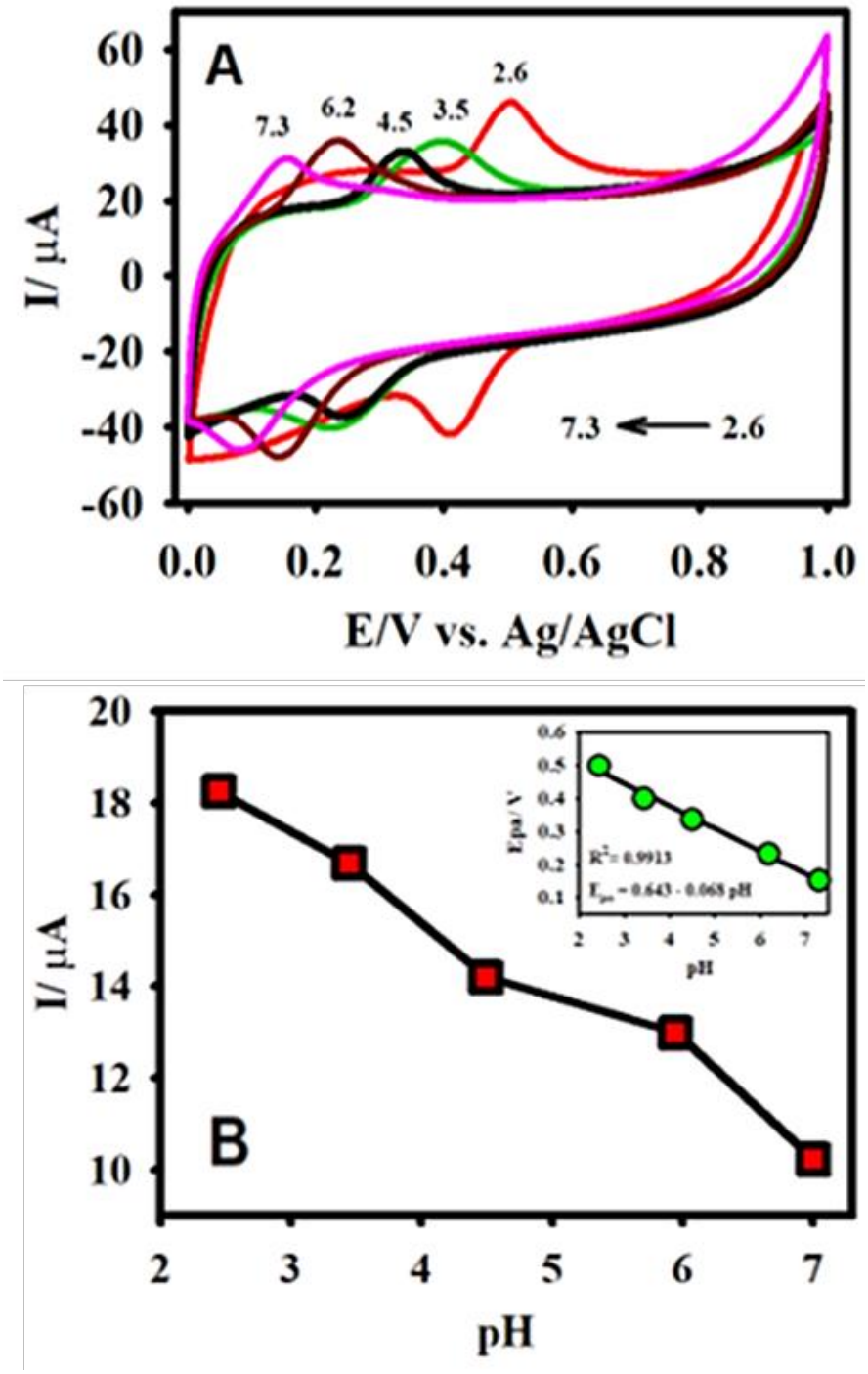

Figure. 6.6. CV curves for the oxidation of 30.0 µM CA at different pHs (2.6 - 7.3) (A); the resulting plot of anodic peak current vs pH (B) and the corresponding plot of the anodic peak potential vs pH (insert of D). Electrolyte medium: 0.1 M B-R buffer solution (pH 2.65); Scan rate : 50 mV s^{-1}.

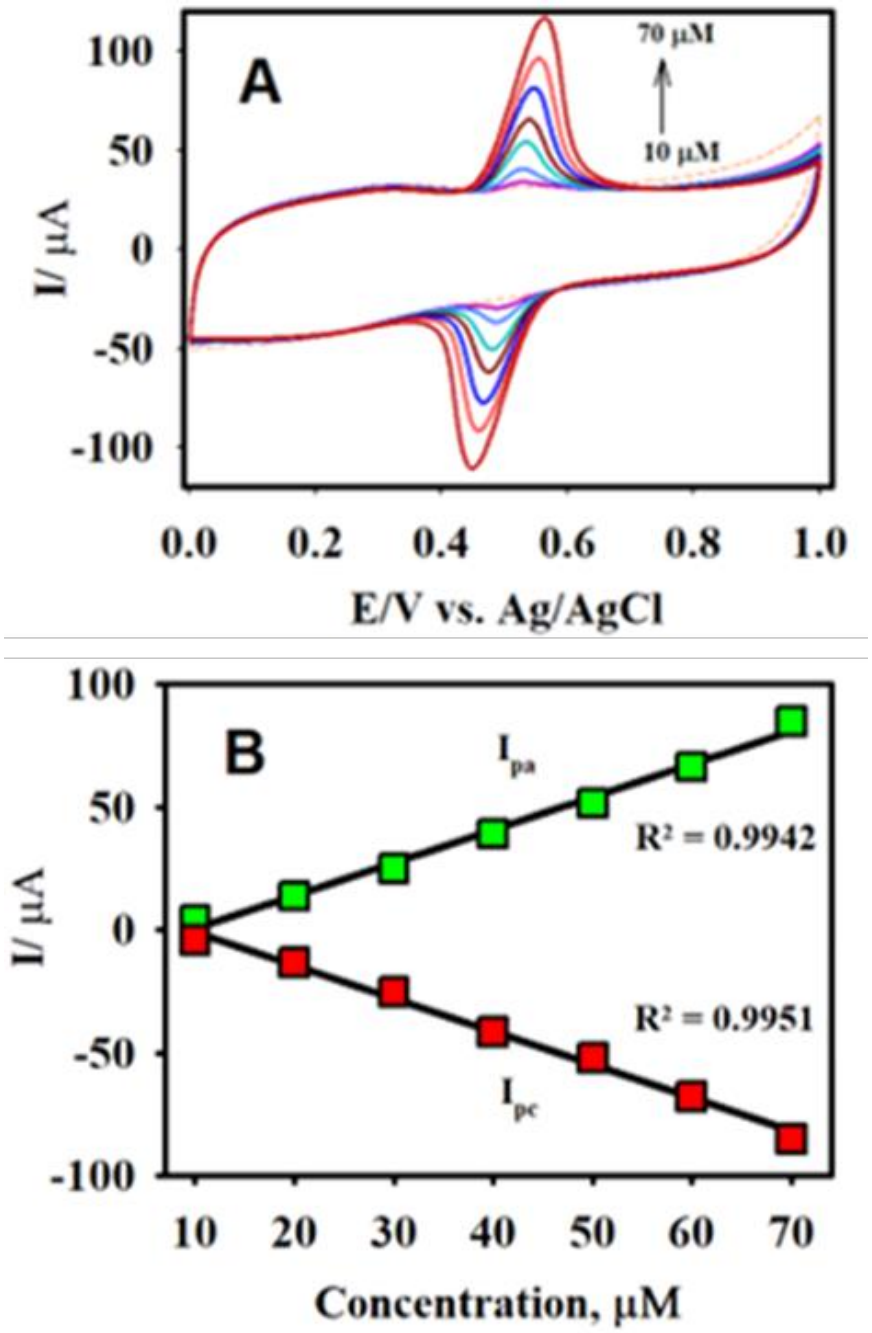

Figure 6.7. CV responses of F-GO/GCE for the oxidation/reduction of CA at different concentrations, ranging from 10.0 to 70.0 µM (A); and the corresponding plots of anodic/cathodic peak current vs. the concentration of CA (B) in a 0.1 M B-R buffer solution pH 2.65, at a scan rate of 50 mV s^{-1}.

The oxidation behavior of CA was further investigated in a 0.1 M B-R buffer solution (pH = 2.65) at a scan rate of 50 mV s^{-1} under different concentrations. It is evident from Figure 6.7A that there was no apparent peak for the absence of the CA molecule, whereas a clear response was observed for the addition of 10.0 μM CA. The peak current for the oxidation and reduction of CA increased linearly, with each subsequent addition in a selected concentration range from 0.0 to 70.0 μM. The anodic and cathodic peak current values obtained from the CVs were plotted against the various concentrations of CA (Figure 6.7B).

It may be perceived from the calibration plot that there was good linearity within the selected calibration range, with the linear regression equations of Ipa (μA) = 1.354 μA/μM - 13.61 μA and Ipc = −1.362 μA/μM − 3.06 μA with the R^2 value of 0.9942 for Ipa and 0.9951 for Ipc.

6.3.4 Analytical determination of CA

The analytical capacity of the F-GO/GCE was investigated by employing DPV. In contrast to CV, DPV is more sensitive and has the ability to lower the background current.[70] Figure 6.8A illustrates the characteristic DPV responses for different concentrations of CA using the F-GO/GCE electrochemical sensor. The working parameters for the DPV technique were: amplitude = 0.08 V, pulse width = 0.08 s, sampling width = 0.0167 s, and pulse period = 0.2 s. The F-GO/GCE did not exhibit any response in the absence of CA, which suggested that the sensor was inactive in the absence of the CA molecule within the selected potential window. However, the DPV responses obtained from the electrochemical oxidation of CA demonstrated a linear increase with respect to its increasing concentration, ranging from 0.5 - 100.0 μM. The linear regression equation between the concentration (c, μM) and the current (Ipa, μA) for the electrochemical

oxidation of CA in the concentration ranges from 0.5 – 10.0 µM and 15.0 – 100.0 µM (Figure 6.8B) were Ipa = 3.935 c (µM) + 1.919 and Ipa = 0.261 c (µM) + 38.658.

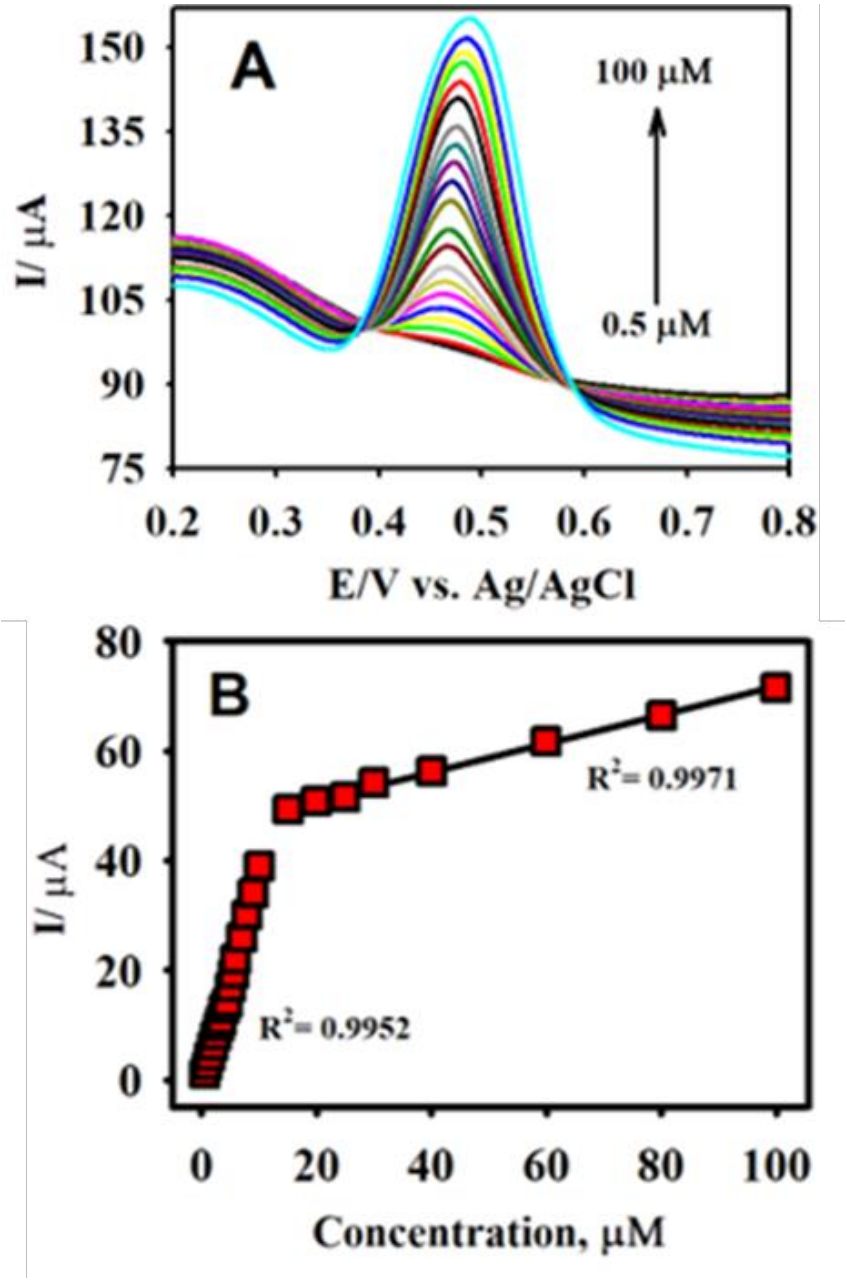

Figure 6.8. DPV responses of F-GO/GCE for the detection of CA in the concentration ranging from 0.5 to 100.0 µM (A); the corresponding calibration plot for the anodic peak current vs concentration (B) in a 0.1 M B-R buffer solution (pH 2.65).

The associated R^2 coefficient values from the calibration plot were calculated to be 0.9960 and 0.9971, respectively. The sensitivities from the calibration plots were calculated to be 5.27 and 0.35 $\mu A \mu M^{-1}$ cm^{-2}. The limit of detection (LOD) was further calculated to be 0.018 µM using the formula $3\sigma/s$, where σ denotes the standard deviation of three blank measurements, and s represents the slope calculated from the calibration plot.

Table 6.1. Comparison of the electrochemical performance of the F-GO/GCE sensor with other reported sensors for the detection of CA

Modified electrode	Voltammetric technique	Linear range (µM)	Limit of detection (µM)	Ref
Molecularly imprinted siloxanes	DPV	0.5 - 60.0	0.15	[76]
Electrochemically reduced graphene oxide-Nafion	SWAdSV	0.1 - 10.0	0.09	[40]
Laccase-MWCNT-chitosan/Au	Amperometric	0.7-10.0	0.15	[77]
Nafion/Tyre/Sonogel-Carbon	Amperometric	0.08 - 2.0	0.06	[78]
Glassy polymeric carbon	DPV	0.1 - 96.5	0.29	[79]
Glassy carbon electrode	DPV	10.0 - 120.0	0.10	[80]
Poly(Glutamic Acid)/GCE	CV	4.0 - 30.0	3.91	[21]
Fluorine doped graphene oxide/GCE	DPV	0.5 - 100.0	0.018	This work

*DPV - Differential pulse voltammetry, SWAdSV - Square wave anodic stripping voltammetry, CV - Cyclic voltammetry, MWCNT - Multi-walled carbon nanotubes, GCE - Glassy carbon electrode.

The two calibration plots acquired in this study were similar to studies that involved the measurement of molecules, such as acetaminophen and valacyclovir, ascorbic acid, dopamine, uric acid, and NADH.[25,59,71,72] This observation might be explained based on the mechanism of the inner-sphere electrode reaction.[25,73] Important attributes such as the novelty analytical advantages and capabilities (e.g., linear range and LOD) of the developed F-GO/GCE electrochemical sensor were confirmed by comparing the performance of the CA sensors formerly reported in the literature as shown in Table 6.1.

6.3.5. Stability, reproducibility, and interference measurements

The stability of the sensor was scrutinized by employing DPV for 30 consecutive scans (Figure 6.9A). The sensor retained 94.7% of its initial peak current response for 50.0 μM CA oxidation in a 0.1 M B-R buffer medium (pH 2.65). In addition, the long-term stability of the fabricated sensor was tested over ten days, where the sensor preserved 95% of its primary response with a relative standard deviation (RSD) value of 2.41%. This demonstrated the good stability of the sensor and could be applied to the evaluation of actual samples (Figure 6.9B).

Further, the reproducibility of the F-GO/GCE was inspected via the preparation of four different electrodes. The reproducibility tests were carried out in 0.1 M PBS containing 50.0 μM CA under identical experimental conditions (Figure 6.10A). The RSD value for the anodic peak current measured at the four different electrodes was calculated to be 2.1%, thereby indicating the excellent reproducibility of the F-GO/GCE sensor.

The selectivity of the developed electrochemical sensor was an essential factor for the detection of CA to enable the testing of actual samples. Henceforth, the prepared F-GO/GCE sensor was tested for its anti-interference capabilities in the presence of potentially interfering species using DPV. Figure 6.10B illustrates the DPV response recorded for the oxidation of 100.0

μM in the presence of a 10-fold (1.0 mM) concentration of interfering ions, such as *p*-coumaric acid, hydroquinone, trans-ferulic acid, glucose, gallic acid, and ascorbic acid. The results obtained from the interference study revealed that the F-GO/GCE sensor retained 92% of its activity for 100.0 μM CA oxidation in the presence of interference molecules. Therefore, the developed F-GO/GCE electrochemical sensor could be applied to the real-time analysis of CA.

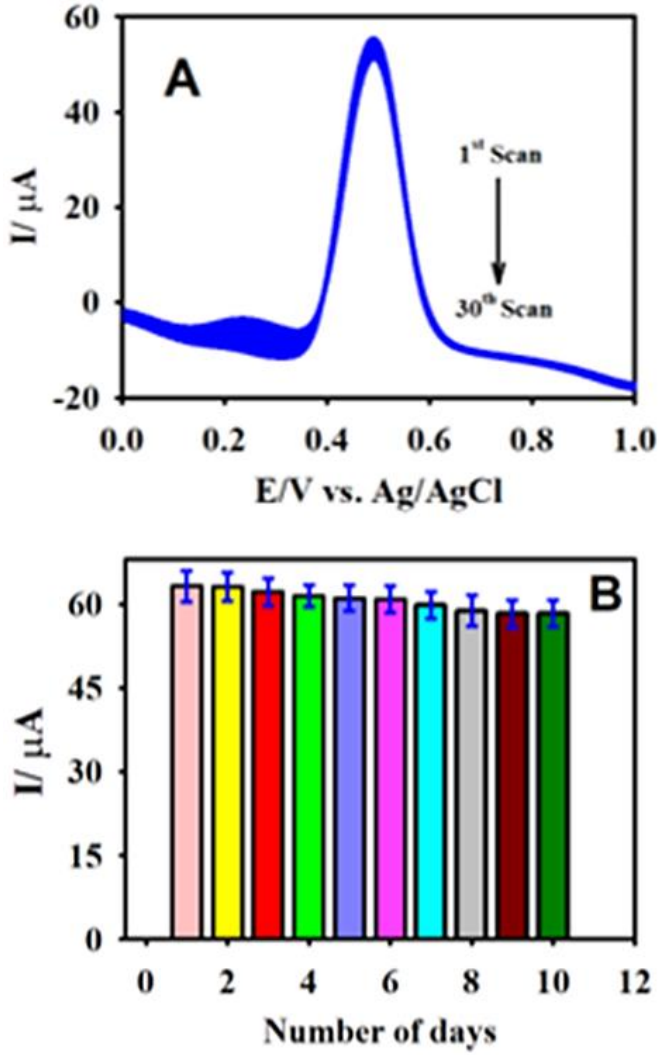

Figure 6.9. DPV curves of the F-GO/GCE recorded in 50.0 μM CA over 30 consecutive measurements (A); DPV response of F-GO/GCE measured in 50.0 μM CA for 10 days (B). Electrolyte: a 0.1 M B-R buffer solution (pH 2.65).

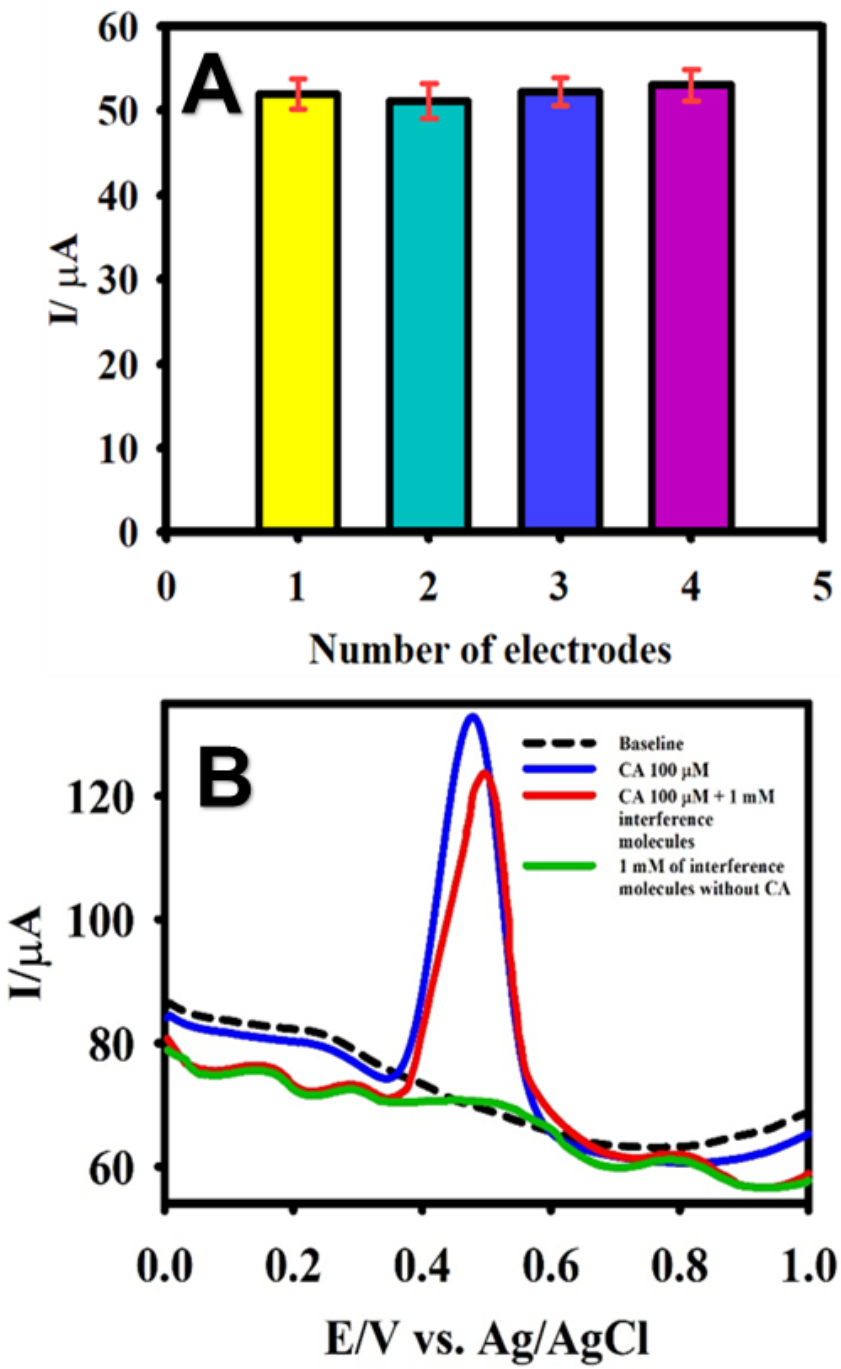

Figure 6.10. DPV response recorded in the presence of 50.0 μM CA with four different F-GO/GCEs (C); and interference response of the F-GO/GCE for the detection of 100.0 μM CA in the presence of 1.0 mM *p*-coumaric acid, hydroquinone, trans-ferulic acid, gallic acid, glucose and ascorbic acid (D). Electrolyte: a 0.1 M B-R buffer solution (pH 2.65).

6.3.6 Real sample analysis

The electrochemical performance of the designed F-GO/GCE sensor was further validated for its real-time determination of CA in wine. Four different samples of red wine were used for the determination of CA. The wine was tested by injecting raw samples directly into the 0.1 M B-R buffer solution, and the concentrations of CA were determined from their respective DPV peaks. The DPV peaks obtained for the determination of CA in wine samples (50.0 µL to 300.0 µL) are included in the supplementary information (Figures 6.11A-D). The peak current values from DPV toward CA oxidation for the injected volume of the wine sample was compared against the calibration plot, thereby estimating the unknown concentration of CA. The concentration of CA found in four different wine samples was quantified in the range from 72.4 - 94.5 µM, with an average RSD value of 2.3%. The exact procedure was followed for analyzing the concentrations of CA in other wine samples, and the results of the quantification of CA in the assorted brands of wine are presented in Table 6.2.

Table 6.2. Performance of the F-GO/GCE electrode for the determination of CA in different brands of wine.

Red wine sample	Found (µM)	% RSD
Alamos (Chile)	74.4	2.3
Bodacious (Canada)	84.3	2.0
Radio Boka (Spain)	85.1	2.2
Santa Carolina (Argentina)	94.5	2.1

Further high-performance liquid chromatography (HPLC, Agilent) analysis showed that the CA concentration in Wine Sample II was 77.5 µM, which is consistent with the value measured by the F-GO electrochemical sensor. The wine samples were diluted with the B-R electrolyte medium. Based on the constructed calibration plot using DPV, the amount of CA in the commercial red wine was calculated, which were comparable with the results reported in the literature.[42,74,75] Furthermore, the fabricated electrochemical sensor was able to detect CA directly in wine (wine as the electrolyte) without the use of a buffer solution (Figure 6.12). These results suggest that the developed F-GO/GCE sensor could be effectively used for the determination of CA in wine and has real-time applicability.

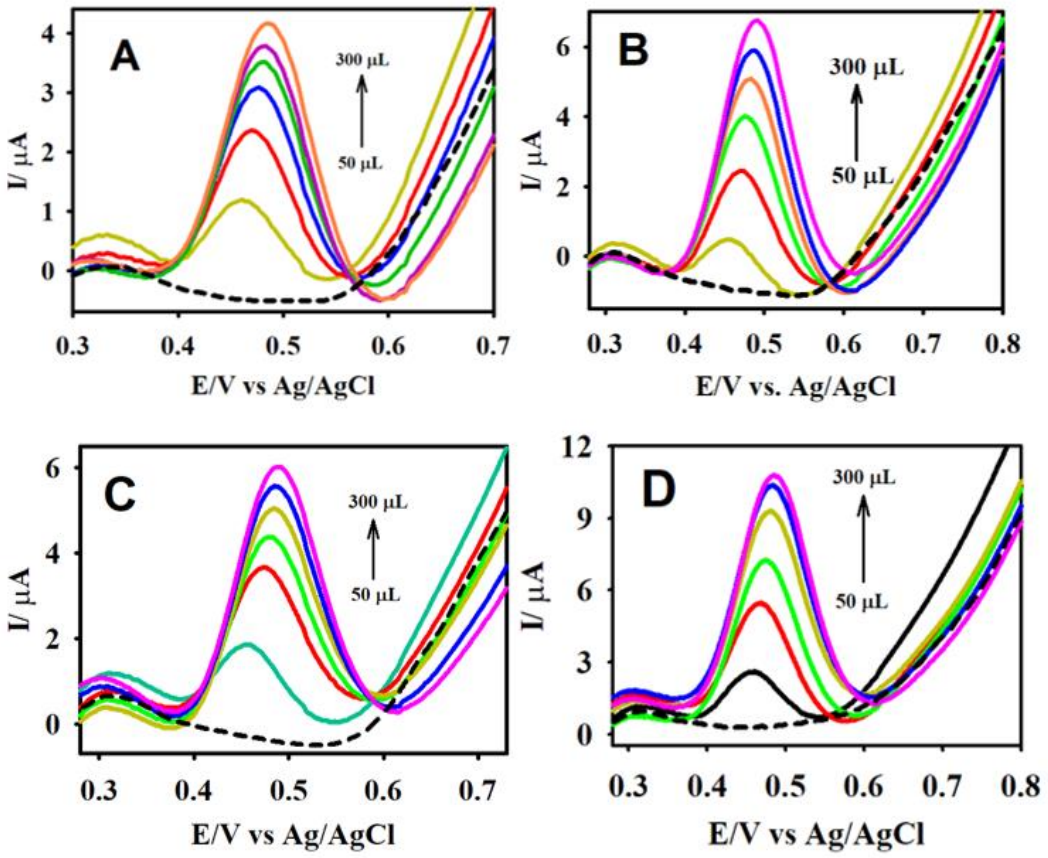

Figure 6.11. DPV response of F-GO/GCE for the detection of CA in different brands (wine samples I - IV) of red wine. Electrolyte: 0.1 M B-R buffer solution (pH 2.65).

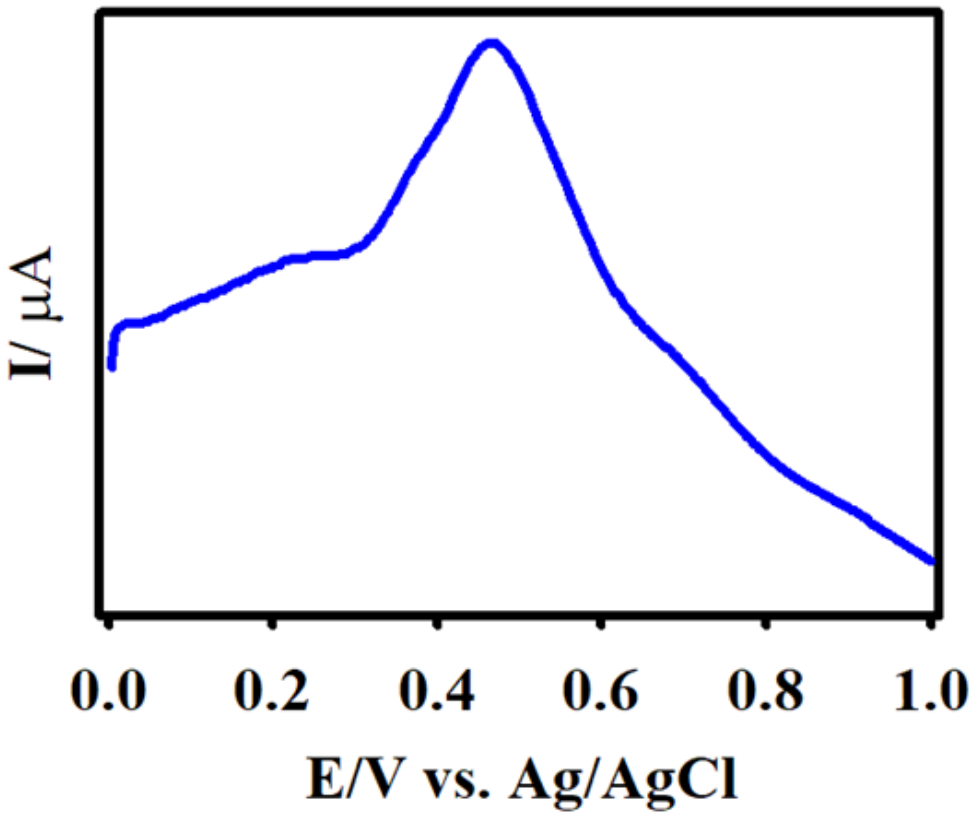

Figure 6.12. DPV response of F-GO sensor obtained for the detection of CA directly in wine sample.

6.4. Conclusion

A highly selective F-GO based sensor was developed for the sensitive detection of CA in assorted brands of wine. The results obtained from the CV investigations indicated that the F-GO's enhanced the electrocatalytic behaviour in contrast to bare GCE and GO modified GCE. The F-GO/GCE exhibited higher EASA and improved the electrochemical performance as opposed to the GO/GCE. The analytical quantitation performed using DPV revealed the strong capability of the electrochemical sensor for the determination of CA within a wide linear concentration range in a 0.1 M B-R buffer (pH 2.65). The F-GO/GCE sensor demonstrated superior selectivity for the oxidation of CA in the presence of additional polyphenolic compounds. The developed

electrochemical sensor exhibited good long-term stability, sensitivity, a low detection limit, and satisfactory reproducibility. Further, it was effectively employed for the detection and quantification of CA in various brands of red wine. The sensor also displayed a superior sensing capacity to detect CA directly in wine without the requirement of an external electrolyte medium. These collective factors confirmed that the developed F-GO/GCE sensor could be incorporated for the quality control of wine.

References

1. J. Li, J. Jiang, M. Liu, Z. Xu, P. Deng, D. Qian, C. Tong, H. Xie and C. Yang, Facile synthesis of MnO_2-embedded flower-like hierarchical porous carbon microspheres as an enhanced electrocatalyst for sensitive detection of caffeic acid, *Anal. Chim. Acta* 985 (2017) 155-165.
2. X. Xu, G. Xu, F. Wei, Y. Cen, M. Shi, X. Cheng, Y. Chai, M. Sohail and Q. Hu, Carbon dots coated with molecularly imprinted polymers: A facile bioprobe for fluorescent determination of caffeic acid, *J. Colloid Interface Sci.* 529 (2018) 568-574.
3. G. C. Moreira and F. de Souza Dias, Mixture design and doehlert matrix for optimization of the ultrasonic assisted extraction of caffeic acid, rutin, catechin and trans-cinnamic acid in Physalis angulata L. and determination by HPLC DAD, *Microchem. J.* 141 (2018) 247-252.
4. J. J. García-Guzmán, D. López-Iglesias, L. Cubillana-Aguilera, C. Lete, S. Lupu, J. M. Palacios-Santander and D. Bellido-Milla, Assessment of the polyphenol indices and antioxidant capacity for beers and wines using a tyrosinase-based biosensor prepared by sinusoidal current method, *Sensors* 19 (2018) 66.

5. Z. Bo, X. Shuai, S. Mao, H. Yang, J. Qian, J. Chen, J. Yan and K. Cen, Green preparation of reduced graphene oxide for sensing and energy storage applications, *Sci. Reports* 4 (2014) 4684.

6. S. Ramki, P. Balasubramanian, S.-M. Chen, T.-W. Chen, T.-W. Tseng and B.-S. Lou, Voltammetric determination of caffeic acid using Co_3O_4 microballs modified screen printed carbon electrode, *Int. J. Electrochem. Sci* 13 (2018) 1241-1249.

7. R. J. Robbins, Phenolic acids in foods: An overview of analytical methodology, *J. Agric. Food Chem.* 51 (2003) 2866-2887.

8. J. Alanko, A. Riutta, P. Holm, I. Mucha, H. Vapaatalo and T. Metsä-Ketelä, Modulation of arachidonic acid metabolism by phenols: relation to their structure and antioxidant/prooxidant properties, *Free Radic. Biol. Med.* 26 (1999) 193-201.

9. N. J. Kang, K. W. Lee, B. J. Shin, S. K. Jung, M. K. Hwang, A. M. Bode, Y.-S. Heo, H. J. Lee and Z. Dong, Caffeic acid, a phenolic phytochemical in coffee, directly inhibits Fyn kinase activity and UVB-induced CO_X-2 expression, *Carcinogenesis* 30 (2009) 321-330.

10. M. Nardini, C. Scaccini, L. Packer and F. Virgili, In vitro inhibition of the activity of phosphorylase kinase, protein kinase C and protein kinase A by caffeic acid and a procyanidin-rich pine bark (Pinus marittima) extract, *Biochim. Biophys. Acta (BBA) - General Subjects* 1474 (2000) 219-225.

11. K. Robards and M. Antolovich, Analytical chemistry of fruit bioflavonoids: A review, *Analyst* 122 (1997) 11R-34R.

12. F.-L. Hsu, Y.-C. Chen and J.-T. Cheng, Caffeic acid as active principle from the fruit of xanthiumstrumarium to lower plasma glucose in diabetic rats, *Planta Med.* 66 (2000) 228-230.

13. P. Youyuan, L. Fanghua and Y. Jiannong, Determination of phenolic acids and flavones in lonicera japonica thumb. by capillary electrophoresis with electrochemical detection, *Electroanal.* 17 (2005) 356-362.

14. V. S. Manikandan, B. Adhikari and A. Chen, Nanomaterial based electrochemical sensors for the safety and quality control of food and beverages, *Analyst* 143 (2018) 4537-4554.

15. C.-C. Zeng, C.-F. Liu, J. Zeng and R.-G. Zhong, Electrochemical synthesis of 6-arylsulfonyl caffeic acid derivatives in aqueous medium, *J. Electroanal. Chem.* 608 (2007) 85-90.

16. O. Makhotkina and P. A. Kilmartin, Uncovering the influence of antioxidants on polyphenol oxidation in wines using an electrochemical method: Cyclic voltammetry, *J. Electroanal. Chem.* 633 (2009) 165-174.

17. K. Sivasankar, R. Devasenathipathy, S.-F. Wang, K. Kohila rani, D. S. Raja and C.-H. Lin, Synthesis of hierarchical mesoporous graphite oxide/Al_2O_3 from MIL-100(Al) for the electrochemical determination of caffeic acid in red wine samples, *J. Taiwan Inst. Chem. E.* 84 (2018) 188-195.

18. L. Gao, R. Yue, J. Xu, Z. Liu and J. Chai, Pt-PEDOT/rGO nanocomposites: One-pot preparation and superior electrochemical sensing performance for caffeic acid in tea, *J. Electroanal. Chem.* 816 (2018) 14-20.

19. S. C. Fernandes, I. R. W. Z. de Oliveira and I. C. Vieira, A green bean homogenate immobilized on chemically crosslinked chitin for determination of caffeic acid in white wine, *Enzyme Microb. Technol.* 40 (2007) 661-668.

20. Y. Yao, Y. Wen, L. Zhang, Z. Wang, H. Zhang and J. Xu, Electrochemical recognition and trace-level detection of bactericide carbendazim using carboxylic group functionalized poly(3,4-ethylenedioxythiophene) mimic electrode, *Anal. Chim. Acta* 831 (2014) 38-49.

21. D. P. Santos, M. F. Bergamini, A. G. Fogg and M. V. B. Zanoni, Application of a glassy carbon electrode modified with poly(glutamic acid) in caffeic acid determination, *Microchim. Acta* 151 (2005) 127-134.

22. K. Thangavelu, N. Raja, S.-M. Chen and W.-C. Liao, Nanomolar electrochemical detection of caffeic acid in fortified wine samples based on gold/palladium nanoparticles decorated graphene flakes, *J. Colloid Interface Sci.* 501 (2017) 77-85.

23. Z. Liu, B. Lu, Y. Gao, T. Yang, R. Yue, J. Xu and L. Gao, Facile one-pot preparation of Pd-Au/PEDOT/graphene nanocomposites and their high electrochemical sensing performance for caffeic acid detection, *RSC Adv.* 6 (2016) 89157-89166.

24. M. Taghioskoui, Trends in graphene research, *Mater. Today* 12(10) (2009) 34-37.

25. B.-R. Adhikari, M. Govindhan, H. Schraft and A. Chen, Simultaneous and sensitive detection of acetaminophen and valacyclovir based on two dimensional graphene nanosheets, *J. Electroanal. Chem.* 780 (2016) 241-248.

26. B.-R. Adhikari, M. Govindhan and A. Chen, Carbon nanomaterials based electrochemical sensors/biosensors for the sensitive detection of pharmaceutical and biological compounds, *Sensors* 15 (2015) 22490-22508.

27. B.-R. Adhikari, M. Govindhan and A. Chen, Sensitive detection of acetaminophen with graphene-based electrochemical sensor, *Electrochim. Acta* 162 (2015) 198-204.

28. B. Shah, T. Lafleur and A. Chen, Carbon nanotube based electrochemical sensor for the sensitive detection of valacyclovir, *Faraday Discuss.* 164 (2013) 135-146.

29. M. Govindhan, T. Lafleur, B. R. Adhikari and A. Chen, Electrochemical sensor based on carbon nanotubes for the simultaneous detection of phenolic pollutants, *Electroanal.* 27 (2015) 902-909.

30. C. Cheng, S. Li, A. Thomas, N. A. Kotov and R. Haag, Functional graphene nanomaterials based architectures: Biointeractions, fabrications, and emerging biological applications, *Chem. Rev.* 117 (2017) 1826-1914.

31. R. E. Mapasha, E. Igumbor, N. F. Andriambelaza and N. Chetty, Electronic properties of B and Al doped graphane: A hybrid density functional study, *Physica B: Condens. Matter.* 535 (2018) 287-292.

32. M. Baghayeri, Pt nanoparticles/reduced graphene oxide nanosheets as a sensing platform: Application to determination of droxidopa in presence of phenobarbital, *Sens. Actuators B: Chem.* 240 (2017) 255-263.

33. M. Hernaez, C. R. Zamarreño, S. Melendi-Espina, L. R. Bird, A. G. Mayes and F. J. Arregui, Optical fibre sensors using graphene-based materials: A review, *Sensors* 17 (2017) 155.

34. J. Huang, X. Yang, S.-C. Her and Y.-M. Liang, Carbon nanotube/graphene nanoplatelet hybrid film as a flexible multifunctional sensor, *Sensors* 19 (2019) 317.

35. P. Suvarnaphaet and S. Pechprasarn, Graphene-based materials for biosensors: A review, *Sensors* 17 (2017) 2161.

36. K. Chen, Z.-L. Zhang, Y.-M. Liang and W. Liu, A graphene-based electrochemical sensor for rapid determination of phenols in water, *Sensors* 13 (2013) 6204.

37. L. Wu, H. Ji, Y. Guan, X. Ran, J. Ren and X. Qu, A graphene-based chemical nose/tongue approach for the identification of normal, cancerous and circulating tumor cells, *NPG Asia Mater.* 9 (2017) e356.

38. S. S. Chou, M. De, J. Luo, V. M. Rotello, J. Huang and V. P. Dravid, Nanoscale graphene oxide (nGO) as artificial receptors: implications for biomolecular interactions and sensing, *J. Am. Chem. Soc.* 134 (2012) 16725-16733.

39. M. R. Cavallari, G. S. Braga, M. F. da Silva, J. E. Izquierdo, L. G. Paterno, E. A. Dirani, I. Kymissis and F. J. Fonseca, A hybrid electronic nose and tongue for the detection of ketones: Improved sensor orthogonality using graphene oxide-based detectors, *IEEE Sens. J.* 17 (2017) 1971-1980.

40. H. Filik, G. Çetintaş, A. A. Avan, S. Aydar, S. N. Koç and İ. Boz, Square-wave stripping voltammetric determination of caffeic acid on electrochemically reduced graphene oxide–Nafion composite film, *Talanta* 116 (2013) 245-250.

41. A. T. Ezhil Vilian, S.-M. Chen, Y.-H. Chen, M. Ajmal Ali and F. M. A. Al-Hemaid, An electrocatalytic oxidation and voltammetric method using a chemically reduced graphene oxide film for the determination of caffeic acid, *J. Colloid Interface Sci.* 423 (2014) 33-40.

42. N. Karikalan, R. Karthik, S.-M. Chen and H.-A. Chen, A voltammetric determination of caffeic acid in red wines based on the nitrogen doped carbon modified glassy carbon electrode, *Sci. Reports* 7 (2017) 45924.

43. V. Georgakilas, M. Otyepka, A. B. Bourlinos, V. Chandra, N. Kim, K. C. Kemp, P. Hobza, R. Zboril and K. S. Kim, Functionalization of graphene: Covalent and non-covalent approaches, derivatives and applications, *Chem. Rev.* 112 (2012) 6156-6214.

44. D. D. Chronopoulos, A. Bakandritsos, M. Pykal, R. Zbořil and M. Otyepka, Chemistry, properties, and applications of fluorographene, *Appl. Mater. Today* 9 (2017) 60-70.

45. H. Ji, F. Zhou, J. Gu, C. Shu, K. Xi and X. Jia, Nitrogen-doped carbon dots as a new substrate for sensitive glucose determination, *Sensors* 16 (2016) 630.

46. B. Zheng, J. Wang, F.-B. Wang and X.-H. Xia, Synthesis of nitrogen doped graphene with high electrocatalytic activity toward oxygen reduction reaction, *Electrochem. Commun.* 28 (2013) 24-26.

47. A. Vizintin, M. Lozinšek, R. K. Chellappan, D. Foix, A. Krajnc, G. Mali, G. Drazic, B. Genorio, R. Dedryvère and R. Dominko, Fluorinated reduced graphene oxide as an Interlayer in Li–S batteries, *Chem. Mater.* 27 (2015) 7070-7081.

48. J. Han, L. L. Zhang, S. Lee, J. Oh, K.-S. Lee, J. R. Potts, J. Ji, X. Zhao, R. S. Ruoff and S. Park, Generation of B-doped graphene nanoplatelets using a solution process and their supercapacitor applications, *ACS Nano* 7 (2013) 19-26.

49. K.-J. Jeon, Z. Lee, E. Pollak, L. Moreschini, A. Bostwick, C.-M. Park, R. Mendelsberg, V. Radmilovic, R. Kostecki, T. J. Richardson and E. Rotenberg, Fluorographene: A Wide Bandgap Semiconductor with Ultraviolet Luminescence, *ACS Nano* 5 (2011) 1042-1046.

50. L. Cheng, S. Jandhyala, G. Mordi, A. T. Lucero, J. Huang, A. Azcatl, R. Addou, R. M. Wallace, L. Colombo and J. Kim, Partially fluorinated graphene: Structural and electrical characterization, *ACS Appl. Mater. Interfaces* 8 (2016) 5002-5008.

51. X. Wang, G. Sun, P. Routh, D.-H. Kim, W. Huang and P. Chen, Heteroatom-doped graphene materials: syntheses, properties and applications, *Chem. Soc. Rev.* 43 (2014) 7067-7098.

52. F. Withers, M. Dubois and A. K. Savchenko, Electron properties of fluorinated single-layer graphene transistors, *Phys. Rev. B* 82 (2010) 073403.

53. F. Wei, L. Peng, F. Yiyu and L. Yu, Two-dimensional fluorinated graphene: synthesis, structures, properties and applications, *Adv. Sci.* 3 (2016) 1500413.

54. J. T. Robinson, J. S. Burgess, C. E. Junkermeier, S. C. Badescu, T. L. Reinecke, F. K. Perkins, M. K. Zalalutdniov, J. W. Baldwin, J. C. Culbertson and P. E. Sheehan, Properties of fluorinated graphene films, *Nano lett.* 10(8) (2010) 3001-3005.

55. P. Chantharasupawong, R. Philip, N. T. Narayanan, P. M. Sudeep, A. Mathkar, P. M. Ajayan and J. Thomas, Optical power limiting in fluorinated graphene oxide: an insight into the nonlinear optical properties, *J. Phys. Chem. C* 116 (2012) 25955-25961.

56. A. R. Thiruppathi, B. Sidhureddy, W. Keeler and A. Chen, Facile one-pot synthesis of fluorinated graphene oxide for electrochemical sensing of heavy metal ions, *Electrochem. Commun.* 76 (2017) 42-46.

57. G. Rui, S. Zdeněk, Š. Filip, J. Zbyněk and P. Martin, Electrochemical fluorographene: Hybrid electrocatalysis of biomarkers, hydrogen evolution, and oxygen reduction, *Chemistry – A Eur. J.* 21 (2015) 16474-16478.

58. D. Damien, P. M. Sudeep, T. N. Narayanan, M. R. Anantharaman, P. M. Ajayan and M. M. Shaijumon, Fluorinated graphene based electrodes for high performance primary lithium batteries, *RSC Adv.* 3 (2013) 25702-25706.

59. R. A. Rebeca, N. T. N., N. Yutaka, H. Takashi, M. T. M., F. Takahiro, C. P. J., B. R. R., M. Toru, K. D. Sakthi, T. S. V., M. S. A. and A. P. M., Fluorinated graphene oxide; a new multimodal material for biological applications, *Adv. Mater.* 25 (2013) 5632-5637.

60. F.-G. Zhao, G. Zhao, X.-H. Liu, C.-W. Ge, J.-T. Wang, B.-L. Li, Q.-G. Wang, W.-S. Li and Q.-Y. Chen, Fluorinated graphene: facile solution preparation and tailorable properties by fluorine-content tuning, *J. Mater. Chem. A* 2 (2014) 8782-8789.

61. S. Boopathi, T. N. Narayanan and S. Senthil Kumar, Improved heterogeneous electron transfer kinetics of fluorinated graphene derivatives, *Nanoscale* 6 (2014) 10140-10146.

62. R. Romero-Aburto, T. N. Narayanan, Y. Nagaoka, T. Hasumura, T. M. Mitcham, T. Fukuda, P. J. Cox, R. R. Bouchard, T. Maekawa and D. S. Kumar, Fluorinated graphene oxide; a new multimodal material for biological applications, *Adv. Mater.* 25 (2013) 5632-5637.

63. K. Jayaramulu, K. K. R. Datta, C. Rösler, M. Petr, M. Otyepka, R. Zboril and R. A. Fischer, Biomimetic superhydrophobic/superoleophilic highly fluorinated graphene oxide and zif-8 composites for oil–water separation, *Angew. Chem. Int. Ed.* 55 (2016) 1178-1182.

64. C. Mongay and V. Cerda, Britton–Robinson buffer of known ionic strength, *Anal. Chim. Acta* 64 (1974) 409-412.

65. D. C. Marcano, D. V. Kosynkin, J. M. Berlin, A. Sinitskii, Z. Sun, A. Slesarev, L. B. Alemany, W. Lu and J. M. Tour, Improved synthesis of graphene oxide, *ACS Nano* 4 (2010) 4806-4814.

66. N. Karikalan, R. Karthik, S.-M. Chen, M. Velmurugan and C. Karuppiah, Electrochemical properties of the acetaminophen on the screen printed carbon electrode towards the high performance practical sensor applications, *J. Colloid Interface Sci.* 483 (2016) 109-117.

67. Z. Liu, J. Xu, R. Yue, T. Yang and L. Gao, Facile one-pot synthesis of Au–PEDOT/rGO nanocomposite for highly sensitive detection of caffeic acid in red wine sample, *Electrochim. Acta* 196 (2016) 1-12.

68. C. Giacomelli, K. Ckless, D. Galato, F. S. Miranda and A. Spinelli, Electrochemistry of caffeic acid aqueous solutions with pH 2.0 to 8.5, *J. Brazil. Chem. Soc.* 13 (2002) 332-338.

69. D. Nematollahi, H. Shayani-Jam, M. Alimoradi and S. Niroomand, Electrochemical oxidation of acetaminophen in aqueous solutions: kinetic evaluation of hydrolysis, hydroxylation and dimerization processes, *Electrochim. Acta* 54 (2009) 7407-7415.

70. S. Palanisamy, K. Thangavelu, S.-M. Chen, B. Thirumalraj and X.-H. Liu, Preparation and characterization of gold nanoparticles decorated on graphene oxide@polydopamine composite: Application for sensitive and low potential detection of catechol, *Sens. Actuators B: Chem.* 233 (2016) 298-306.

71. H. Teymourian, A. Salimi and S. Khezrian, Fe_3O_4 magnetic nanoparticles/reduced graphene oxide nanosheets as a novel electrochemical and bioeletrochemical sensing platform, *Biosens. Bioelectron.* 49 (2013) 1-8.

72. M. Govindhan, M. Amiri and A. Chen, Au nanoparticle/graphene nanocomposite as a platform for the sensitive detection of NADH in human urine, *Biosens. Bioelectron.* 66 (2015) 474-480.

73. Allen J. Bard and L. R. Faulkner, Electrochemical methods: Fundamentals and applications, 2nd edition, ed., WILEY, 2000.

74. M. del Alamo Sanza, I. N. Domınguez, L. C. Cárcel and L. N. Gracia, Analysis for low molecular weight phenolic compounds in a red wine aged in oak chips, *Anal. Chim. Acta* 513 (2004) 229-237.

75. M.-Á. Rodríguez-Delgado, G. González-Hernández, J.-E. a. Conde-González and J.-P. Pérez-Trujillo, Principal component analysis of the polyphenol content in young red wines, *Food Chem.* 78 (2002) 523-532.

76. F. R. F. Leite, W. d. J. R. Santos and L. T. Kubota, Selective determination of caffeic acid in wines with electrochemical sensor based on molecularly imprinted siloxanes, *Sens. Actuators B: Chem.* 193 (2014) 238-246.

77. M. Diaconu, S. C. Litescu and G. L. Radu, Laccase–MWCNT–chitosan biosensor—A new tool for total polyphenolic content evaluation from in vitro cultivated plants, *Sens. Actuators B: Chem.* 145 (2010) 800-806.

78. M. ElKaoutit, I. Naranjo-Rodriguez, K. R. Temsamani, M. P. Hernández-Artiga, D. Bellido-Milla and J. L. H.-H. d. Cisneros, A comparison of three amperometric phenoloxidase–Sonogel–Carbon based biosensors for determination of polyphenols in beers, *Food Chem.* 110 (2008) 1019-1024.

79. d. S. L. Fernando, R. S. Nelson and O. H. Paulino, Determination of caffeic acid in red wine by voltammetric method, *Electroanal.* 20 (2008) 1252-1258.

80. A. J. Blasco, M. C. González and A. Escarpa, Electrochemical approach for discriminating and measuring predominant flavonoids and phenolic acids using differential pulse voltammetry: towards an electrochemical index of natural antioxidants, *Anal. Chim. Acta* 511 (2004) 71-81.

Chapter 7: Electrochemical Sensor Based on Gold and Fluorine-doped Graphene Oxide for the Detection of Vanillin

7.1 Introduction

Vanillin, also known as 4-hydroxy-3-methoxybenzaldehyde, is the integral chemical constituent which is integral to of vanilla. Generally, vanillin is used as a flavouring agent in food and beverages, confectionaries, and pharmaceutical products because ofdue to its desirable attributes such as aroma and flavour attributes.[1-3] It possesses beneficial antioxidative and antimicrobial properties. In addition, it has been reported that vanillin has the ability to lower the risk of cardiac disease in humans by preventing the oxidation of low-density lipoproteins (LDL) and it has the ability to reverse the effects of sickle cell anemia.[4,5] On the contrary, when synthetic vanillin is consumed in excess, it can lead to headaches, nausea, and have detrimental effects on liver and kidney function.[6,7] Therefore, it is of significant importance to develop a selective, sensitive, and efficient sensor for the electrochemical determination of vanillin. Currently, many conventional analytical methods are cused for the quantification of vanillin in food and beverages, such as high-performance liquid chromatography (HPLC), UV-Vis spectrophotometry, gas chromatography, and chemiluminescence.[8-11] These techniques and their corresponding analysis methods are accurate; however, their operational costs are very high, involve multiple sample pretreatment steps, and necessitates skilled personnel. Electrochemical nanosensors might serve as ideal replacements for the determination of vanillin, as this molecule can be detected via electrochemical methods. However, the electrochemical detection of vanillin at a bare glassy carbon electrode (GCE) is a challenge, as the oxidation of vanillin molecules occur at higher positive potentials; thus, reproducibility is affected due to the electrode fouling effect.[12] Therefore,

the modification of the GCE surface with good electrocatalysts is imperative to increase the electrochemical response toward the oxidation of vanillin.

Several reported works have focused on the quantitative determination of vanillin utilizing different types of nanostructured materials in various buffer media.[13-15] Using an adsorptive stripping voltammetry technique, Şentürk and co-workers reported on a vanillin detection method based on a boron-doped diamond electrode.[16] Hu et. al biosynthesized a gold-silver (Au-Ag) alloy based nanoparticle on GCE substrate for the detection of vanillin. The sensor exhibited good electrochemical performance compared to an unmodified GCE.[17] In other work, Cruz Vieira and co-workers reported on the fabrication of a nanosensor based on Au nanoparticles (AuNPs) stabilized with poly(allylamine hydrochloride), which were synthesized for the determination of vanillin.[18] Although the abovementioned works showed good selectivity and sensitivity, they were expensive to produce and not commercially feasible.

The coupling of noble metals with carbon-based electrochemical sensors offer an inexpensive route toward the detection and quantification of vanillin.[19-21] Commonly, graphene and its derivatives are widely used in a variety of applications owing to their remarkable physicochemical properties.[22-34] Graphene (GN) possesses attributes such as exalted electron mobility (~200,000 $cm^2 V^{-1} s^{-1}$)[35] and high specific surface area (2600 $m^2 g^{-1}$)[36] which directly offers a platform for developing electrochemical sensors as it can enable electron transfer between the electrode and the target analytes/species.[37] The oxygen-containing groups of graphene oxide (GO) can facilitate the loading of metal ions. Gold nanoparticles (AuNPs) are recurrently found in graphene-based nanocomposites owing to their high electrical conductivity, high surface area, and excellent electrocatalytic properties.[38-41] The doping of graphene with heteroatoms (e.g., F, Cl, N, B, and S) at the molecular and atomic level favourably enhances the electrochemical behaviour,

electrocatalytic properties, while altering the electronic and physicochemical properties of graphene and graphene oxide (GO).[42-44] Moreover, as the structure of vanillin contains electroactive groups, the development of electrochemical nanosensors based on Au and fluorine doped graphene oxide (F-GO) nanocomposites can be employed for the efficient detection of this analyte.

To the best of our knowledge, this is the first report that describes the development of a vanillin nanosensor based on Au/F-rGO/GCE. This electrochemical nanosensor was prepared by drop casting F-GO ink on a GCE, followed by the electrodeposition of Au, which was utilized for the sensitive detection of vanillin. The electrochemical performance and analytical capabilities of this novel vanillin sensor were investigated using electrochemical techniques such as linear sweep voltammetry (LSV), cyclic voltammetry (CV), and differential pulse voltammetry (DPV). The fabricated nanosensor demonstrated good sensitivity, stability and suitable reproducibility.

7.2. Experimental section

7.2.1. Reagents

Vanillin, potassium ferrocyanide, potassium chloride, potassium nitrate, chloroauric acid, and other reagents were purchased from Sigma Aldrich. All reagents used for the experiments were of analytical grade. All solutions used for the experiments were prepared using deionized water (18.2 MΩ cm), and all glassware was thoroughly washed and dried prior to each analysis. All experiments were conducted in a 0.1 M PBS electrolyte medium, the pH of which was adjusted with a sulfuric acid (0.1 M, H_2SO_4) and sodium hydroxide solution (NaOH, 0.5 M).

7.2.2. Electrode preparation and modification

FGO was synthesized by the improved Hummers' method with some modifications. The initial step involved the preparation of a mixture by blending 1.0 g graphite, 90.0 mL of sulfuric acid (H_2SO_4), 10.0 ml of orthophosphoric acid (H_3PO_4), and 20.0 ml of hydrogen fluoride (HF). Followed by that, the blended mixture was under vigorous stirring for 2 h at 50 °C. Furthermore, 4.5 g of $KMnO_4$ was gradually added to this blend and constantly kept under stirring for 15 h. After that, 100.0 ml of ice was added to the prepared mixture, along with 5.0 ml of 30% H_2O_2. Additionally, the final product (i.e. F-GO) was separated using 30% hydrochloric acid (HCl) and washed with ultrapure water, ethanol, and diethyl ether. Finally, the purified F-GO solid was dried in the oven at 50°C.

The F-GO ink prepared by mixing 2.0 mg/ml with water was ultrasonicated for 1 h. Glassy carbon electrode (GCE) was polished with 1.0 and 0.05 μm alumina slurry, then the polished electrodes were ultrasonicated in water for 5 min. The prepared F-GO ink was drop cast on the surface of the GCE and left to air-dry for 4 h (F-GO/GCE). The as-prepared F-GO/GCE was subjected to electrochemical reduction in 0.1 M Phosphate buffer solution at pH 7.4 (F-rGO/GCE).[45]

Additionally, the Au was electrochemically deposited onto the Au/F-rGO/GCE electrode by immersing the F-rGO/GCE in a 0.1 M KNO_3 solution that contained 2.0 mM $HAuCl_4$. Similarly, an additional GCE was prepared by electrodepositing Au onto its surface using the same procedure (Au/GCE). To compare their electrochemical performance, the Au/GCE and bare unmodified GCE were tested together with Au/rF-GO/GCE for vanillin oxidation.

7.2.4. Characterization techniques

Using a CHI potentiostat (CHI-660D, CHI, USA), voltammetry techniques such as cyclic voltammetry (CV) and linear sweep voltammetry (LSV) were employed to electrochemically characterize the fabricated nanosensor and the target analyte. In addition, differential pulse voltammetry (DPV) was utilized to study the analytical capabilities, sensitivity, and selectivity of the developed electrochemical sensor. All electrochemical experiments were performed in an electrochemical cell with a conventional three-electrode system. The Au/F-rGO/GCE functioned as the working electrode; a coiled platinum wire served as the counter electrode, while a standard silver-silver chloride (Ag/AgCl) electrode operated as the reference electrode. All electrochemical measurements and analytical determinations were handled in a 0.1 M PBS buffer (pH 7.0) at room temperature. Prior to the experiments, all of the solutions were purged with argon gas for 15 min. The potentials indicated in this paper were against a standard Ag/AgCl reference electrode.

7.3. Results and discussion

7.3.1 Electrochemical characteristic of Au/F-rGO/GCE

The electrochemical behaviour of Au/F-rGO/GCE, F-rGO/GCE and bare GCE was studied by employing the CV technique with potassium ferricyanide ($K_3[Fe(CN)_6]^{3-/4-}$) as an electrochemical probe. This study was conducted in 0.1 M KCl containing 5.0 mM $K_3[Fe(CN)_6]^{3-/4-}$ at a scan rate of 50 mVs^{-1}. The CV of the modified electrodes revealed a pair of well-defined redox peaks corresponding to the oxidation and reduction of $[Fe(CN)6]^{3-/4-}$. In relation to bare GCE, the Au/F-rGO/GCE and F-rGO/GCE electrodes exhibited higher redox peak current values and hinted a lower peak-to-peak separation value (ΔEp). Further, the calculated difference between anodic and cathodic peak potential (ΔEp) at the Au/F-rGO/GCE and F-rGO/GCE electrodes was less in comparison with bare GCE indicated that the amalgamation of Au and F-rGO increased the surface area to volume ratio and improved the electrochemical

behaviour. The ΔEp value is 89 mV for Au/F-rGO/GCE, indicative of a reversible redox process and 88 mV for F-rGO/GCE modified electrodes for a single electron transfer of Fe^{3+}/Fe^{2+} redox reaction which is 208 mV lower than the *ΔEp* value (396 mV) obtained for the bare GCE. The decreased *ΔEp* value during the redox reaction could be attributed to the faster electron-transfer kinetics. Additionally, the value attained from the calculation of the ratio of anodic to cathodic peak current (I_{pa}/I_{pc} = 0.96) established that the oxidation/reduction of $[Fe(CN)_6]^{3-/4-}$ redox probe at the Au/F-rGO/GCE and F-rGO/GCE is reversible. From Figure 2, both the cathodic and anodic peak current maximas for the redox probe oxidation/reduction at Au/F-rGO/GCE is noticeably higher.

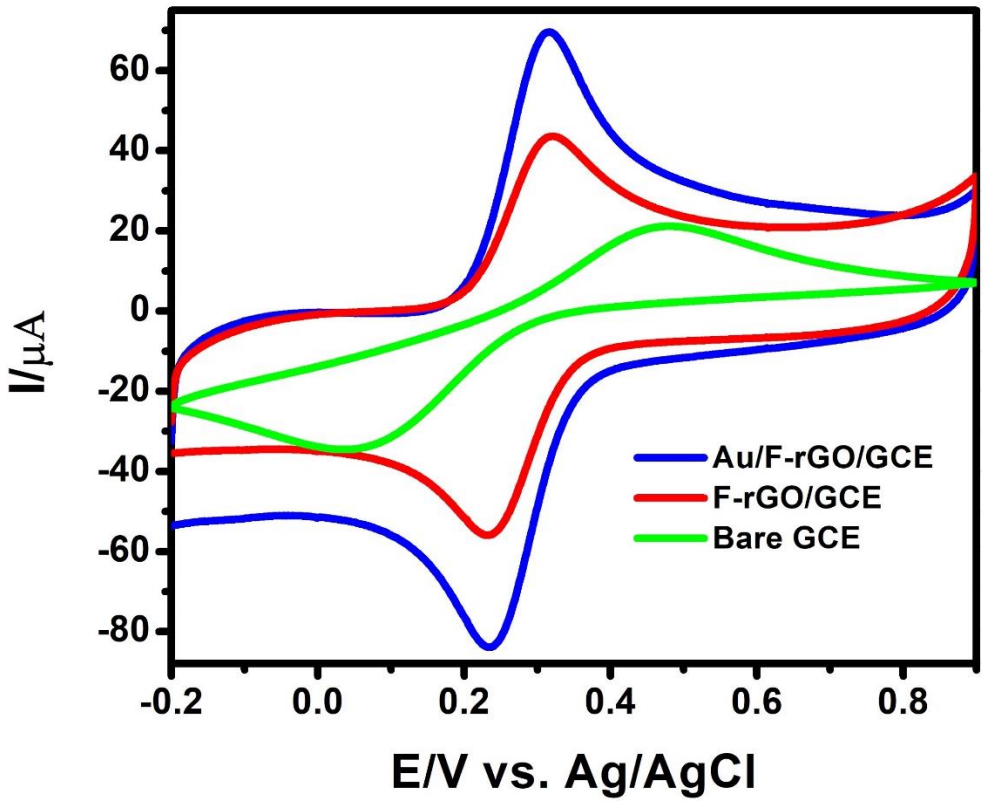

Figure 7.1 CV curves of the bare GCE (green line), GO/GCE (red line) and Au/F-rGO/GCE (red line) in the presence of 0.1 M KCl containing 5.0 mM $[Fe(CN)_6]^{3-/4-}$ at the scan rate of 50 mV s^{-1}

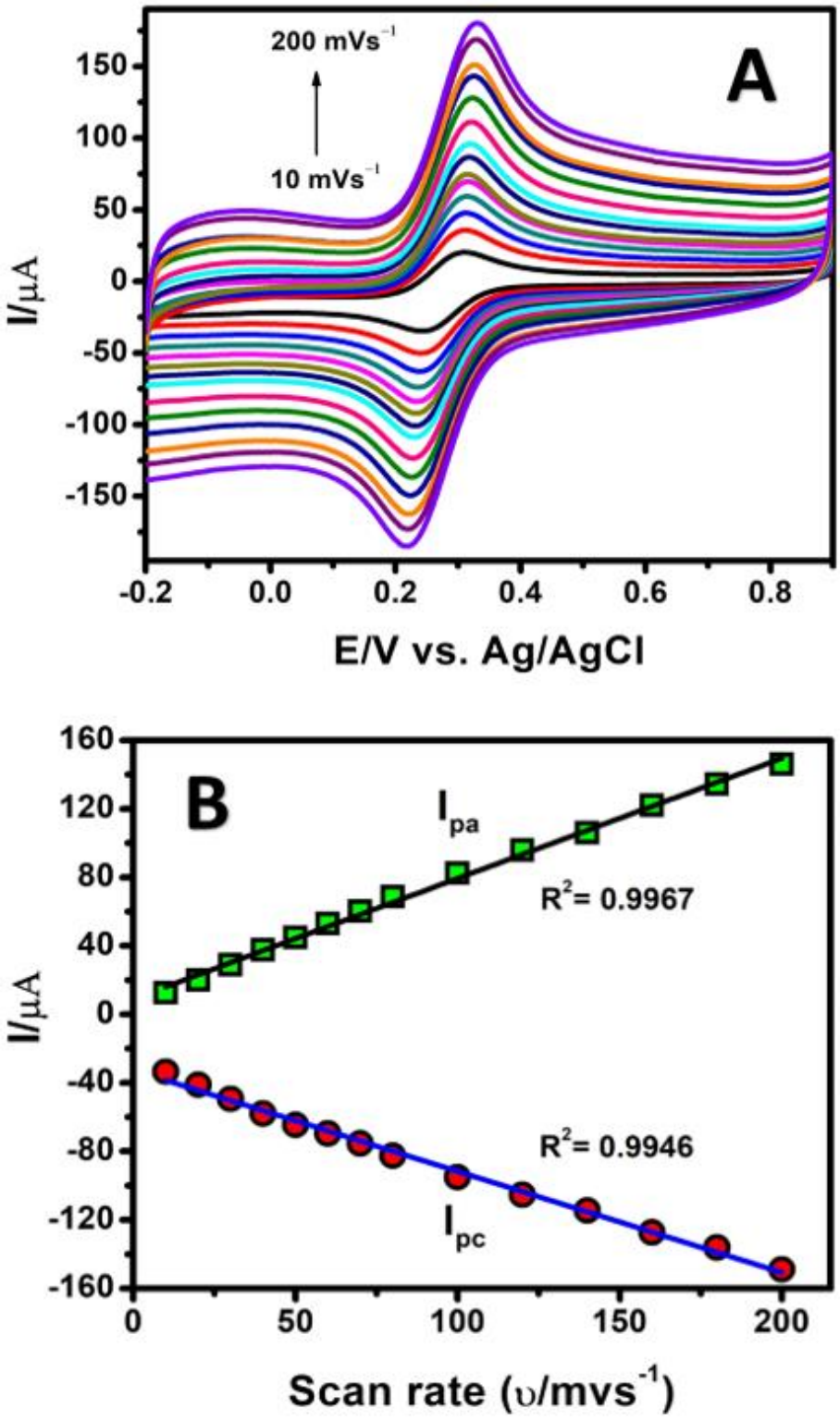

Figure 7.2. CV curves at various scan rates (10 - 200 mV s^{-1}) (A); the corresponding plot of scan rate vs anodic/cathodic peak current values.

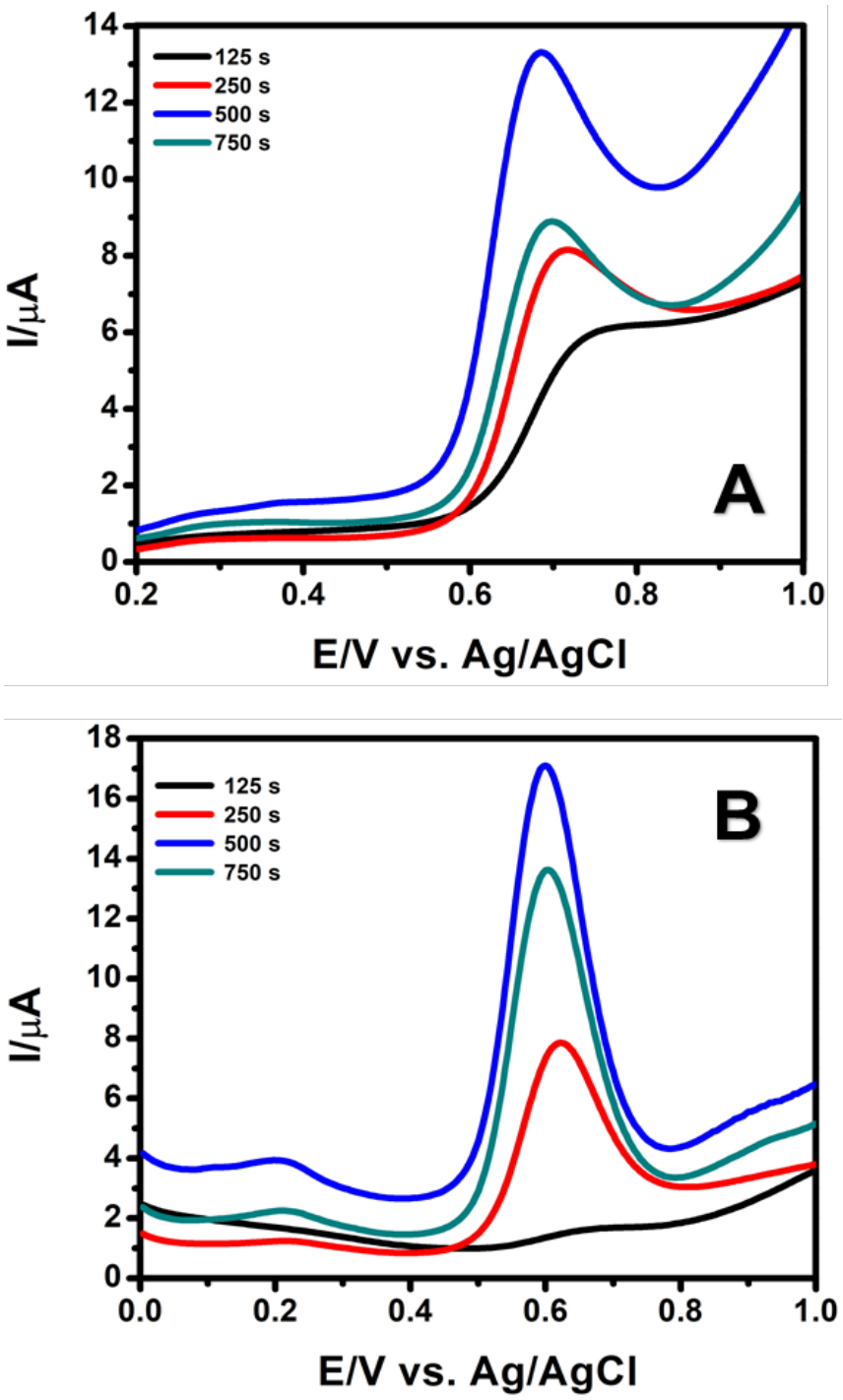

Figure 7.3. LSV (A) and DPV (B) displaying the curves recorded with Au modified Au/F-rGO/GCE towards the oxidation of 500.0 μM vanillin (with Au deposition at different times: 125, 250, 500 and 750 s.

This enhanced electrocatalytic behaviour could be attributed to the combined effect of the presence of electronegative F atom on the F-GO structure by means of semi-ionic (C-F) and the highly conductive Au. Subsequently, CV scans were performed at different scan rates, ranging from 10 – 200 mV/s in KCl-ferricyanide medium (Figure 7.2A and 7.2B).

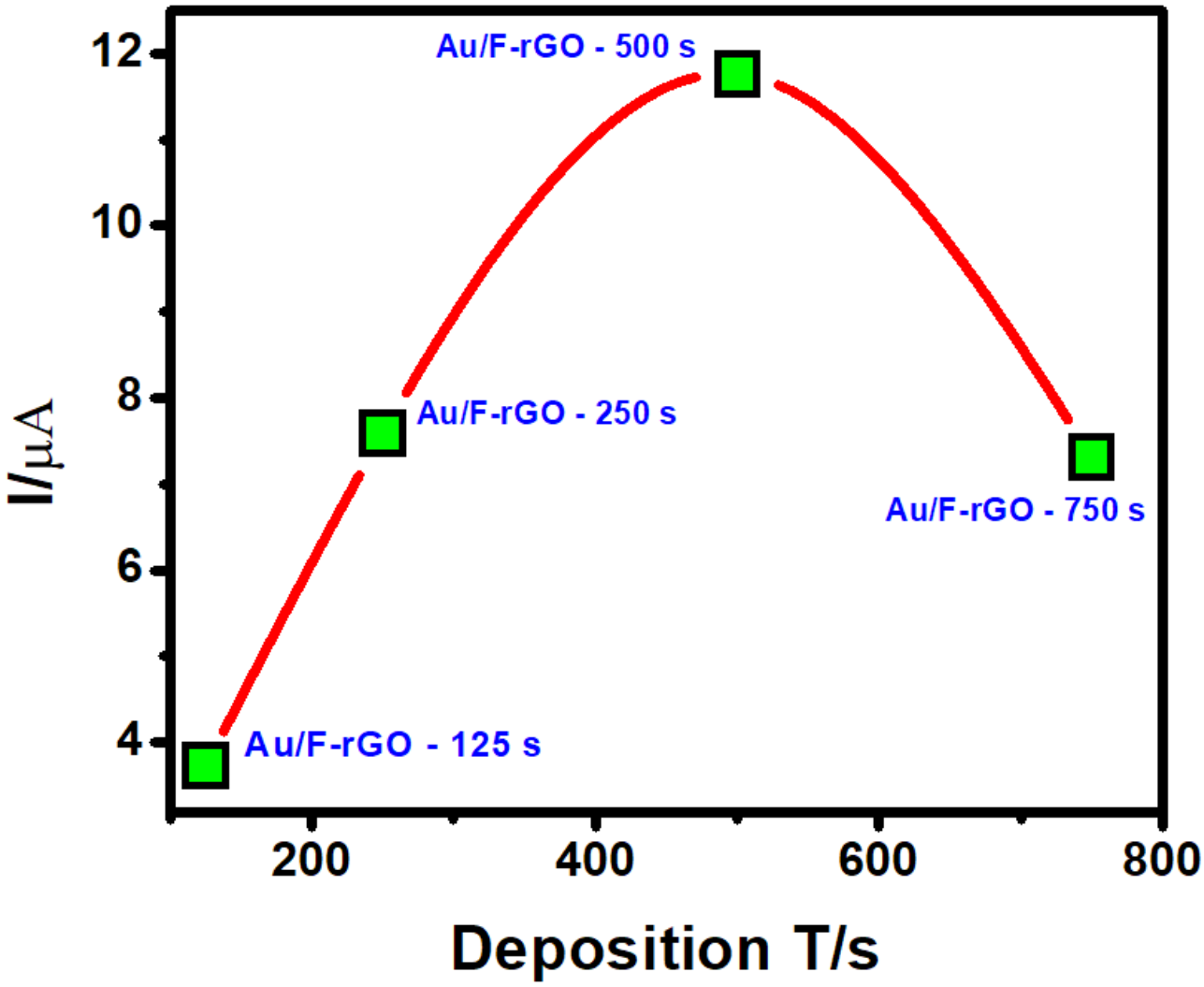

Figure 7.4. Plot displaying the trend in increasing Au deposition time and changing anodic peak current (values calculated from the LSV curves)

7.3.3 Optimization of the Au deposition time

The outcome of the Au deposition on the Au/rF-GO/GCE was studied using LSV and DPV (Figure 7.3A and 7.3B). The Au was deposited on the rF-GO/GCE using the amperometric i-t curve technique in 0.1 M KNO_3 electrolyte medium at a potential of −0.4 V (vs. Ag/AgCl) at 4 different times, i.e. 125, 300, 500 and 750 s. The obtained electrodes were denoted as Au/F-rGO/GCE - 125 s, Au/F-rGO/GCE - 250 s , Au/F-rGO/GCE - 500 s, Au/F-rGO/GCE - 750 s. The current response toward the vanillin oxidation was recorded in 0.1 M PBS buffer medium. The anodic peak current increased with growing Au deposition time and a peak current value for the oxidation of vanillin was attained at 500 s. On the contrary, when the duration of Au deposition was increased from 500 to 750 s (Figure 7.4), it exhibited a decrease in current value recorded for the oxidation of vanillin. Therefore, 500 s was adopted as the desired Au deposition time and was used in the electrode preparation.

7.3.2 Electrochemical behaviour of vanillin using CV and DPV

The electrooxidation behaviour of vanillin at the Au/rF-GO/GCE was inspected using CV in 0.1 M PBS, pH 7.0 without (black curve) and with (blue curve) 500.0 µM of the analyte (Figure 7.5A). The corresponding peak current for the vanillin oxidation obtained with CV was 13.01 µA. Additionally, differential pulse voltammetry (DPV) was used to study the oxidation behaviour of vanillin on the as-prepared Au/F-rGO/GCE (Figure. 4C), as this technique has improved sensitivity as opposed to CV. The associated peak current was found to be 15.63 µA and a strong peak appeared at ~0.6 V for the electrochemical oxidation of 500.0 µM. The anodic peak current values recorded with CV and DPV indicated that the Au/F-rGO/GCE revealed strong oxidation response toward vanillin.

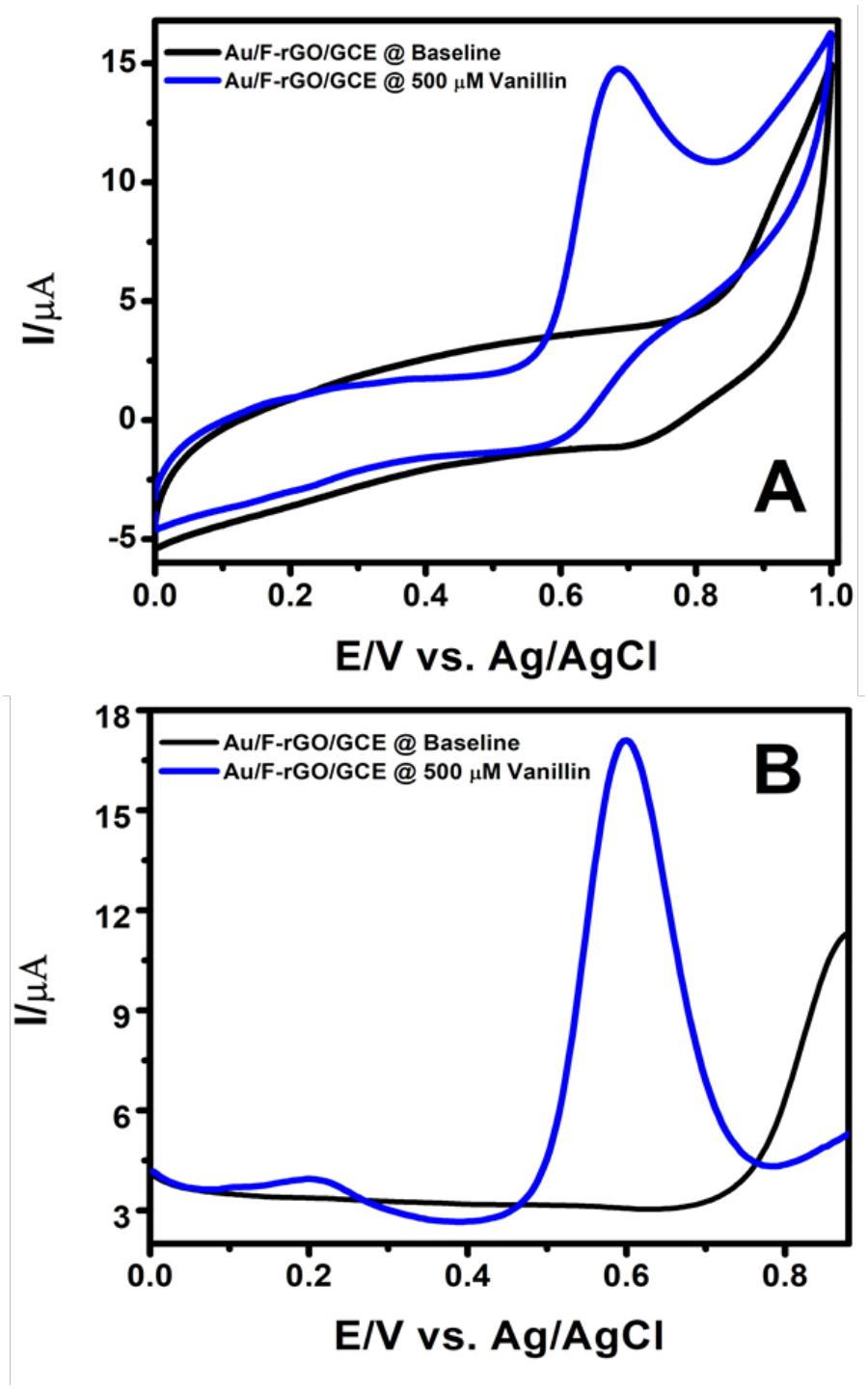

Figure 7.5. CV displaying the curves obtained with Au/rF-GO/GCE towards the oxidation of 500.0 µM vanillin, at the scan rate of 50 mVs^{-1} (A); DPV response recorded with Au/F-rGO/GCE toward the oxidation of 500.0 µM, in 0.1 M PBS electrolyte medium, pH 7.0.

The cyclic voltammograms recorded for the electro-oxidation of 500.0 µM vanillin at different modified electrodes (bare GCE, Au/GCE and Au/F-rGO/GCE) are displayed in Figure 7.6. The electro-oxidation of vanillin produced a larger anodic peak at the Au/F-rGO/GCE than at GCE, indicating that graphene and Au nanoparticles promoted the reaction between the electro-active species and the modified electrode. The associated anodic peak currents estimated from the CVs were found to be 3.74, 8.15 and 13.33 µA for bare GCE, Au/GCE and Au/F-rGO/GCE.

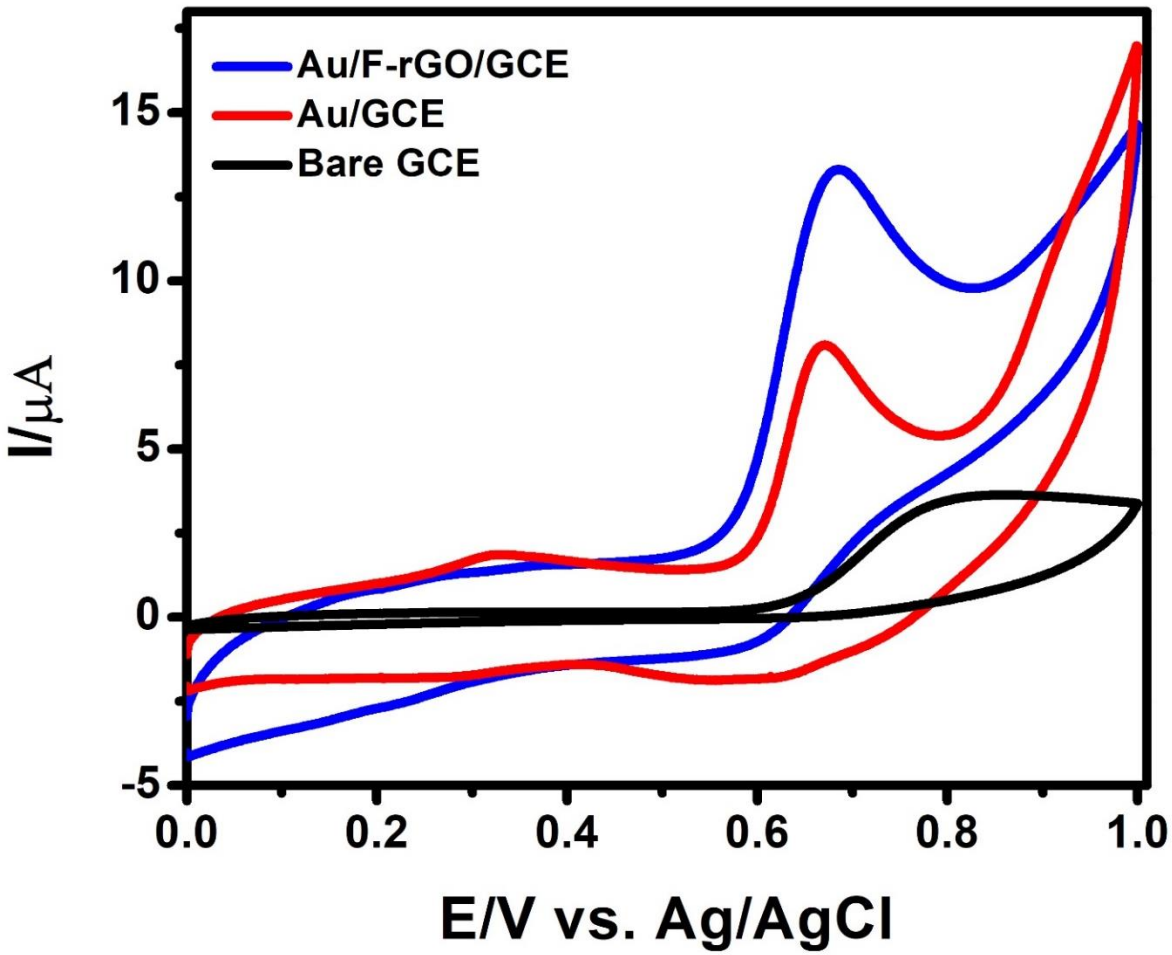

Figure 7.6. CV curves recorded with bare GCE (black line), Au/GCE (red line) and Au/F-rGO/GCE (blue line) toward the oxidation of 500.0 µM, at the scan rate of 50 mVs^{-1}, electrolyte medium: 0.1 M PBS (pH 7.0)

Besides, the higher electrocatalytic activity of Au/F-rGO/GCE could be attributed to the synergistic effect between Au and F-rGO. At the surface of the Au/F-rGO electrode, the peak current obtained from vanillin oxidation is 4 times larger than that recorded with unmodified GCE. Therefore, the Au/F-rGO is considered a worthier catalyst toward the electrooxidation of vanillin.

7.3.4 Effect of concentration and scan rate

The electrooxidation behavior of vanillin was further investigated using linear sweep voltammetry (LSV) in 0.1 M PBS pH 7.0 (scan rate = 50 mV s^{-1}) at different concentrations. It is obvious from Figure 7.7A that there is no appearance of the peak for the absence of the analyte while a sharp response is seen for the addition of 300.0 μM of the analyte. The peak current value for the oxidation of vanillin increased linearly with each sequential addition in the concentration range from 300.0 to 1500.0 μM.

Figure 7.7B displays the calibration plot obtained for the peak current value for the oxidation against the different concentrations of vanillin. It is visible from the calibration plot that there is good linearity within the picked concentration range with the following linear regression equation of Ipa (μA) = 4.671 μA/μM + 0.152 μA an R^2 value of 0.9968.

The effect of scan rate was studied using linear sweep voltammetry (LSV) in 0.1 M PBS (pH 4.5). Figure 7.8A illustrates the influence of scan rate (υ) on the electro-oxidation of 100.0 μM vanillin at Au/F-rGO/GCE from 10 to 100 mV s^{-1}. For an anodic oxidation process the Randles–Sevcik equation is as follow:

$$Ip = 3.01 \times 10^5 n[(1-\alpha) n_\alpha]^{1/2} A C_b D^{1/2} v^{1/2} \quad (1)$$

Where n implies the number of electrons transferred, α indicates the electron transfer coefficient, n_α is the number of electrons, A denotes to the area of the electrode, C_b is the bulk

concentration of the analyte (Vanillin, 100.0 µM) and *D* signifies the diffusion coefficient of the analyte.

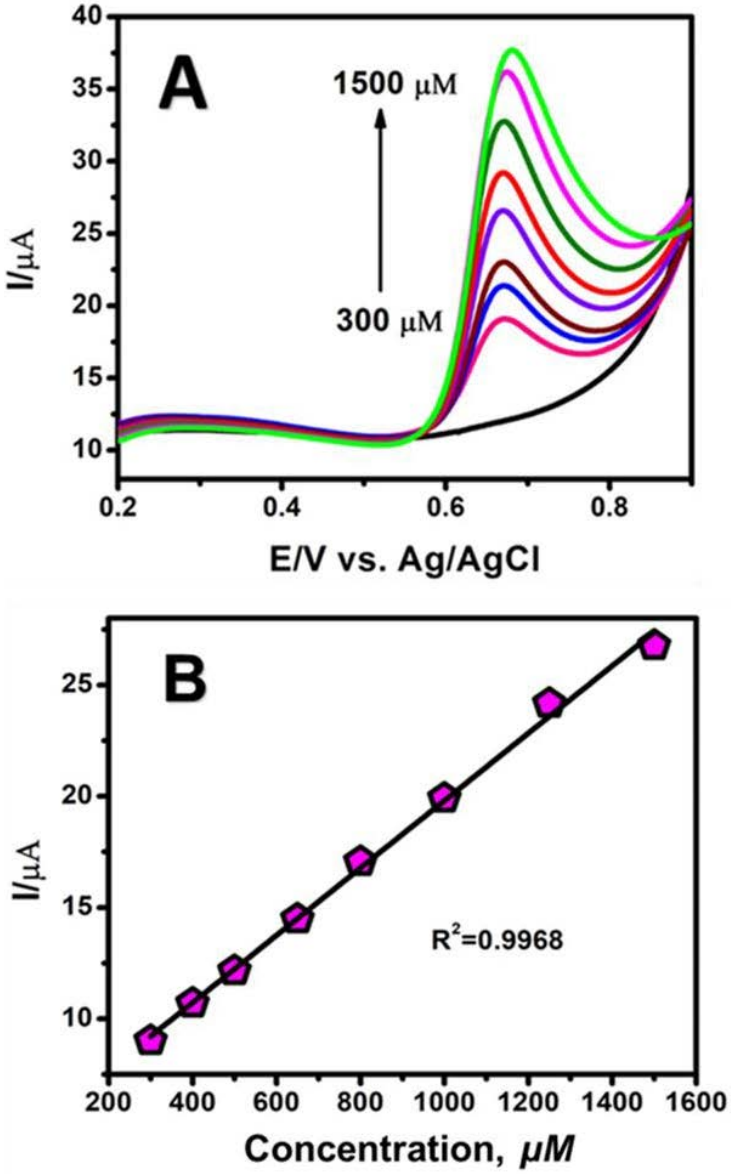

Figure 7.7. LSV responses of Au/F-rGO/GCE toward the oxidation/reduction of vanillin at different concentrations ranging from 300.0 to 1500.0 µM (A); and the corresponding plot of anodic peak current vs. concentration of vanillin (B), in 0.1 M PBS buffer solution pH 7.0, at the scan rate of 50 mV s^{-1}.

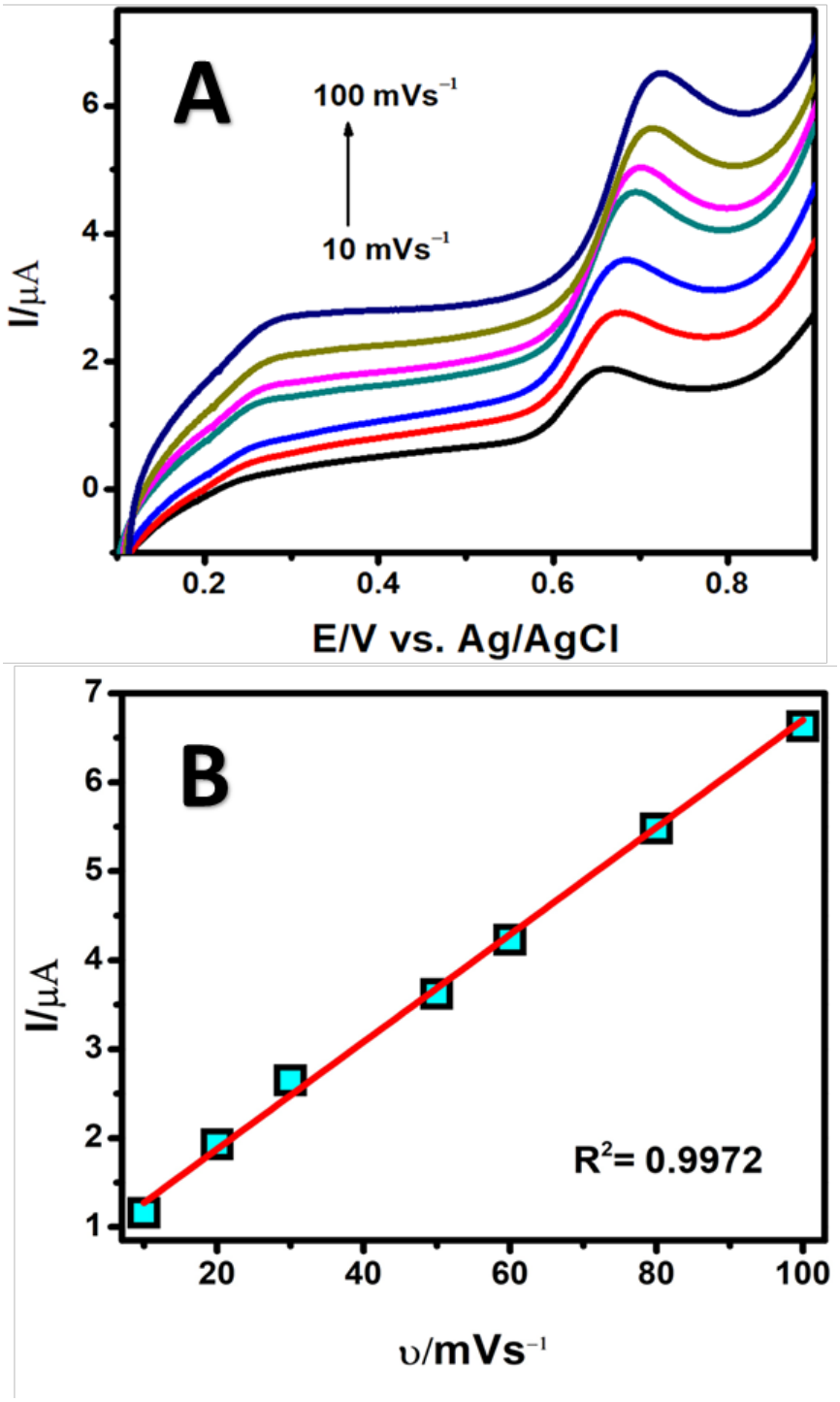

Figure 7.8. CV response of F-rGO/GCE recorded in the presence of 50.0 μM CA at numerous scan rates varying between 10 to 200 mV/s (A); and the subsequent plot of anodic peak current vs. scan rate (mV s^{-1}) (B), in 0.1 M PBS pH 7.0.

The values of the anodic peak current observed in the voltammogram progressively increasing with ascending scan rate, however, the LSV curves exhibited a shift in the peak potentials of vanillin oxidation. The oxidation peak current demonstrated an increasing linear trend with the square root of the scan rate ranging from 10 - 100 mV s^{-1}, which is expressed by the following regression equation: $Ip = 0.681 + 0.086v$ ($R^2 = 0.9972$). The results from the calibration plot (Figure 7.8B) suggest that the oxidation process of vanillin at the Au/F-rGO/GCE is adsorption controlled. Additionally, it is perceived from the Figure 7.8B inset that the peak potential of vanillin oxidation moved towards the positive potential window with the increasing scan rate. The calibration plot between *Epa* and log *v* exhibited a good linearity with their regression equation expressed as follow: $Epa = 0.578 + 0.073 \log v$ ($R^2 = 0.9976$). The results obtained from the calibration plot showed that the oxidation of vanillin at the Au/F-rGO/GCE is irreversible.

7.3.5 Analytical determination of vanillin

Under the optimized conditions, the calibration curves for vanillin were constructed by DPV using the proposed sensor (Au/F-rGO/GCE), as shown in Figure 7.9. The differential pulse voltammograms attained with different concentrations of vanillin using the developed electrochemical sensor are depicted in Figure 7.9A The anodic peak current values obtained from the electrochemical oxidation of vanillin on the electrode surface are proportional to the vanillin concentrations in solution. Figure 7.9B illustrates the linear relationship between the concentration (*c*, μM) and the current (Ipa, μA) for the electrochemical oxidation of vanillin in the concentration ranges of 1.0 – 150.0 μM. the following regression equation is presented as Ipa (μA) = 0.8772 μA/μM + 0.114 μA (R^2=0.9952). The limit of detection (LOD), which was calculated as 0.15 μM, is based on 3 times the standard deviation of the blank divided by the slope,

$$\text{LOD} = \frac{3\sigma}{b}, \qquad (2)$$

where σ denotes the standard deviation of five blank measurements and s represents the slope obtained from the calibration plot.

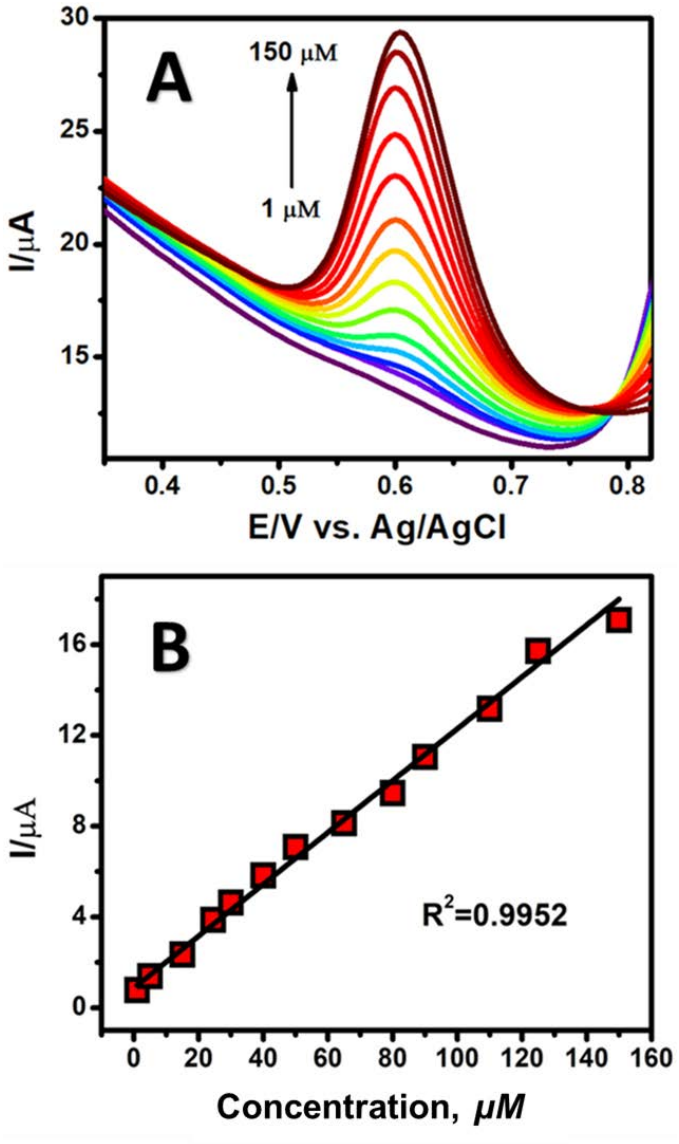

Figure 7.9. DPV responses of Au/F-rGO/GCE the oxidation of CA in a concentration range from 0.5 μM to 100.0 μM (A); the corresponding calibration plot for anodic peak current vs concentration (B) in 0.1 M B-R buffer solution (pH 2.65).

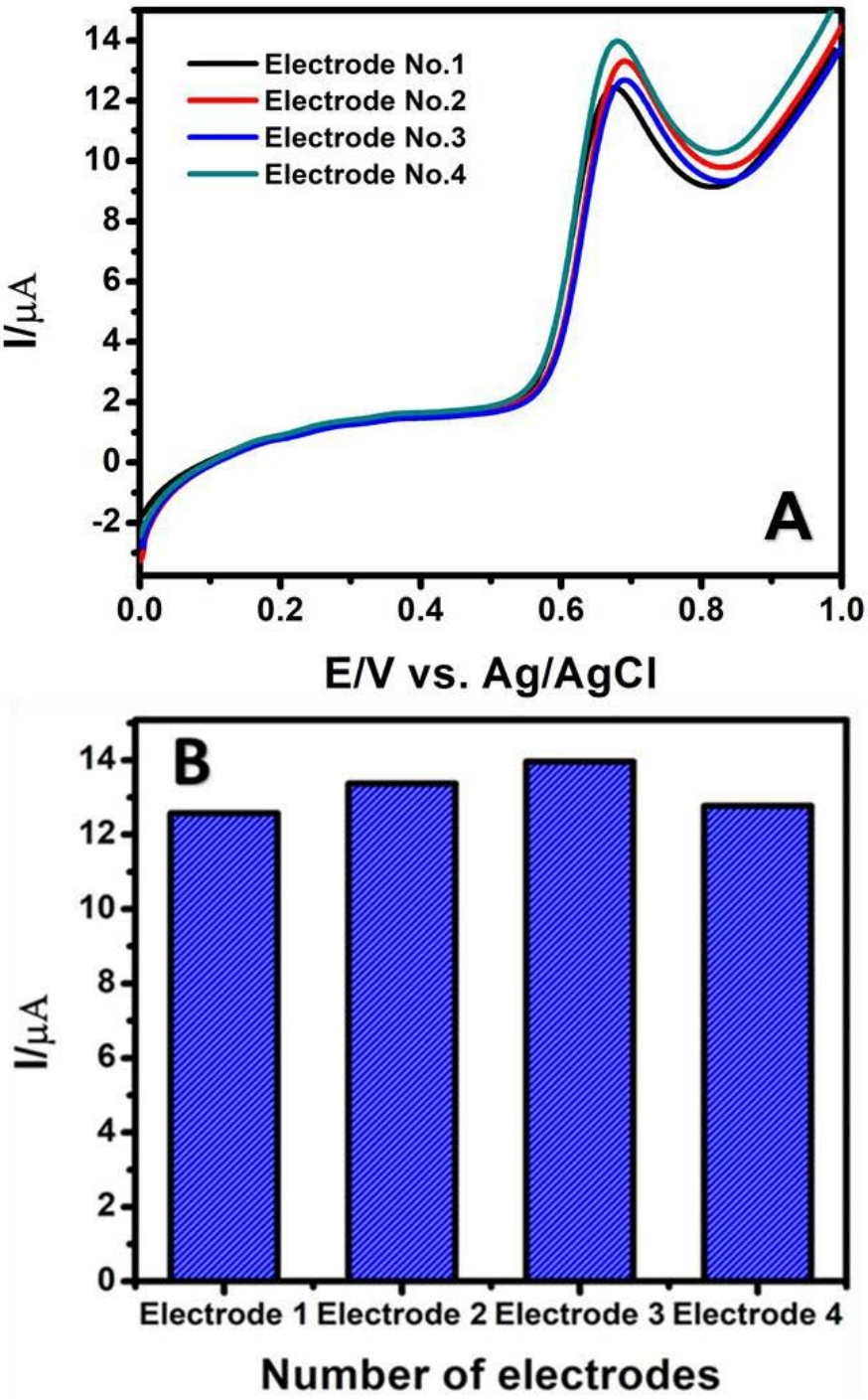

Figure 7.10. LSV response recorded in the presence of 500.0 μM vanillin with 4 different Au/F-rGO/GCEs (A); and their corresponding plot representing the estimated anodic peak current value from the individual electrodes (B), in 0.1 M PBS electrolyte solution (pH 7.0)

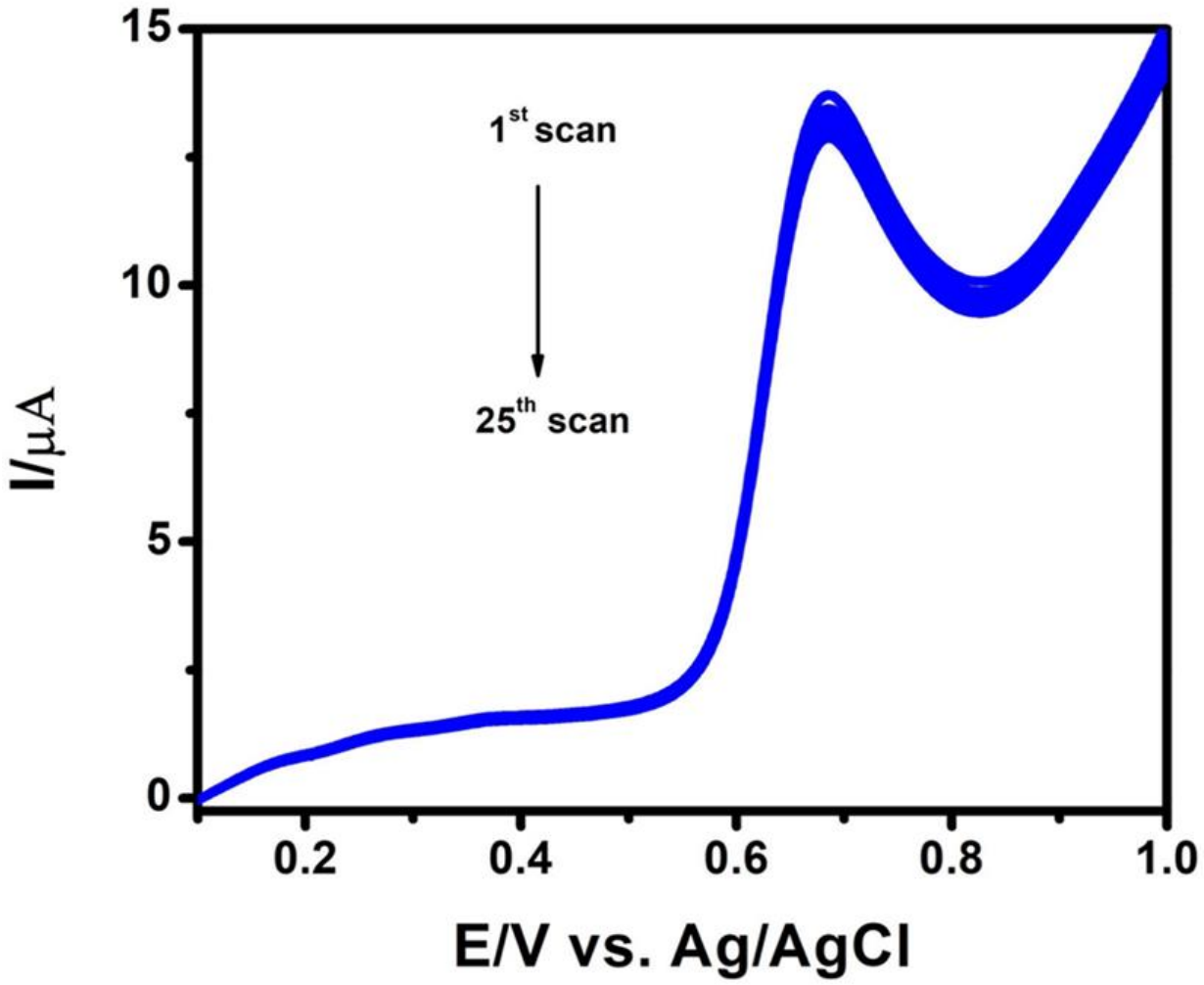

Figure 7.11. Stability measurement of the Au/F-rGO/GCE toward 500.0 μM vanillin oxidation over 25 consecutive LSV scans, in 0.1 M PBS electrolyte solution (pH 7.0)

7.3.6 Stability, reproducibility and interference measurements

The reproducibility of the Au/F-rGO/GCE was evaluated by preparing 4 separate GCEs and the experiments were performed in 0.1 M PBS with 500.0 μM of vanillin under the same experimental conditions (Figure 7.10A and 7.10B). The RSD value for the anodic peak current measured at 4 different electrodes was estimated to be 2.82%, thus signifying the Au/F-rGO/GCE sensor's good electrode-to-electrode reproducibility. The stability of the sensor was tested by

utilizing DPV over 30 successive scans (Figure 7.11). The sensor preserved ~94% of its initial peak current response toward 500.0 μM vanillin oxidation in 0.1 M PBS buffer (pH 7.0), thereby demonstrating the sensor's good stability.

The selectivity of the Au/F-rGO/GCE electrochemical sensor was verified for its anti-interference ability in the presence of interfering species using DPV. The sensor also exhibited good performance for the oxidation of 500.0 μM vanillin in the presence of 5-fold (2.5 mM) concentration of interfering molecules such as glucose, gallic acid, CH_3COONa, $CuSO_4$, $MgCl_2$, KCl and NH_4NO_3. The interference study revealed that the Au/F-rGO/GCE sensor retained 95.17% of its activity for the oxidation of 500.0 μM of vanillin in the presence of interference molecules. These abovementioned results suggested that the developed Au/F-rGO/GCE sensor could be applied to real-time detection of vanillin.

7.4. Conclusion

A novel Au/F-rGO/GCE nanosensor was successfully developed and used for the first time for the electrochemical detection of vanillin. The results of the electrochemical characterization demonstrated that Au/F-rGO was efficient for oxidizing vanillin in terms of enhanced current response and a decrease in overpotential, compared to bare GCE and F-rGO/GCE. The fabricated electrochemical nanosensor displayed satisfactory analytical capabilities with good linearity over the selected calibration range, coupled with excellent sensitivity and a low LOD value. The nanosensor also exhibited superior selectivity for the detection of vanillin in the presence of co-existing ions and other interferent molecules. Moreover, the results yielded from the nanosensor showed satisfactory recovery rates from real sample studies, which confirmed its practical

applicability. Furthermore, the Au/F-rGO/GCE nanosensor exhibited appreciable repeatability, good reproducibility, and possessed excellent chemical stability.

References

1. H. B. Heath, The AVI Publishing Company Inc., Westport, Connecticut 1980, vol. 24, pp. 199 - 207.
2. Y. H. Hui, John Wiley & Sons, New York, 1992, vol. 4, pp. 2641 - 2657.
3. N. J. Walton, M. J. Mayer and A. Narbad, Vanillin, *Phytochemistry* 63 (2003) 505-515.
4. P. Teissedre and A. Waterhouse, Inhibition of oxidation of human low-density lipoproteins by phenolic substances in different essential oils varieties, *J. Agric. Food Chem.* 48 (2000) 3801-3805.
5. D. Farthing, D. Sica, C. Abernathy, I. Fakhry, J. D. Roberts, D. J. Abraham and P. Swerdlow, High-performance liquid chromatographic method for determination of vanillin and vanillic acid in human plasma, red blood cells and urine, *J. Chromatogr. B: Biomed. Sci. Appl.* 726 (1999) 303-307.
6. X. Han, Developing survey of vanillin in China, *Shichuan Chemical Industry and Eroding Control* 5 (2002) 36-37.
7. P. Deng, Z. Xu, R. Zeng and C. Ding, Electrochemical behavior and voltammetric determination of vanillin based on an acetylene black paste electrode modified with graphene–polyvinylpyrrolidone composite film, *Food Chem.* 180 (2015) 156-163.
8. K. N. Waliszewski, V. T. Pardio and S. L. Ovando, A simple and rapid HPLC technique for vanillin determination in alcohol extract, *Food Chem.* 101 (2007) 1059-1062.

9. A. Longares-Patrón and M. Canizares-Macias, Focused microwaves-assisted extraction and simultaneous spectrophotometric determination of vanillin and p-hydroxybenzaldehyde from vanilla fragans, *Talanta* 69 (2006) 882-887.

10. A. Pérez-Silva, E. Odoux, P. Brat, F. Ribeyre, G. Rodriguez-Jimenes, V. Robles-Olvera, M. García-Alvarado and Z. Günata, GC–MS and GC–olfactometry analysis of aroma compounds in a representative organic aroma extract from cured vanilla (Vanilla planifolia G. Jackson) beans, *Food Chem.* 99 (2006) 728-735.

11. M. Timotheou-Potamia and A. C. Calokerinos, Chemiluminometric determination of vanillin in commercial vanillin products, *Talanta* 71 (2007) 208-212.

12. J. L. Hardcastle, C. J. Paterson and R. G. Compton, Biphasic sonoelectroanalysis: Simultaneous extraction from, and determination of vanillin in food flavoring, *Electroanal.* 13 (2001) 899-905.

13. F. Bettazzi, I. Palchetti, S. Sisalli and M. Mascini, A disposable electrochemical sensor for vanillin detection, *Anal. Chim. Acta* 555 (2006) 134-138.

14. J. Ning, Q. He, X. Luo, M. Wang, D. Liu, J. Wang, J. Liu and G. Li, Rapid and Sensitive Determination of Vanillin Based on a Glassy Carbon Electrode Modified with Cu2O-Electrochemically Reduced Graphene Oxide Nanocomposite Film, *Sensors* 18 (2018) 2762.

15. D.-J. Kong, S.-F. Shen, H. Y. Yu, J. Wang and N. Chen, Chemical modification of multi-walled carbon nanotubes by tetraaminophthalocyaninatocobalt for the electrocatalytic oxidation of vanillin, *Chinese J. Inorg. Chem.* 26 (2010) 817-821.

16. Y. Yardım, M. Gülcan and Z. Şentürk, Determination of vanillin in commercial food product by adsorptive stripping voltammetry using a boron-doped diamond electrode, *Food Chem.* 141 (2013) 1821-1827.

17. D. Zheng, C. Hu, T. Gan, X. Dang and S. Hu, Preparation and application of a novel vanillin sensor based on biosynthesis of Au–Ag alloy nanoparticles, *Sens. Actuators B: Chem.* 148 (2010) 247-252.

18. T. R. Silva, D. Brondani, E. Zapp and I. Cruz Vieira, Electrochemical sensor based on gold nanoparticles stabilized in poly(Allylamine hydrochloride) for determination of vanillin, *Electroanal.* 27 (2015) 465-472.

19. J. Li, H. Feng, J. Li, J. Jiang, Y. Feng, L. He and D. Qian, Bimetallic Ag-Pd nanoparticles-decorated graphene oxide: a fascinating three-dimensional nanohybrid as an efficient electrochemical sensing platform for vanillin determination, *Electrochim. Acta* 176 (2015) 827-835.

20. L. Huang, K. Hou, X. Jia, H. Pan and M. Du, Preparation of novel silver nanoplates/graphene composite and their application in vanillin electrochemical detection, *Mater. Sci. Eng. C.* 38 (2014) 39-45.

21. L. Shang, F. Zhao and B. Zeng, Sensitive voltammetric determination of vanillin with an AuPd nanoparticles−graphene composite modified electrode, *Food Chem.* 151 (2014) 53-57.

22. M. Taghioskoui, Trends in graphene research, *Mater. Today* 12(10) (2009) 34-37.

23. B.-R. Adhikari, M. Govindhan, H. Schraft and A. Chen, Simultaneous and sensitive detection of acetaminophen and valacyclovir based on two dimensional graphene nanosheets, *J. Electroanal. Chem.* 780 (2016) 241-248.

24. B.-R. Adhikari, M. Govindhan and A. Chen, Carbon nanomaterials based electrochemical sensors/biosensors for the sensitive detection of pharmaceutical and biological compounds, *Sensors* 15 (2015) 22490-22508.

25. B.-R. Adhikari, M. Govindhan and A. Chen, Sensitive detection of acetaminophen with graphene-based electrochemical sensor, *Electrochim. Acta* 162 (2015) 198-204.

26. B. Shah, T. Lafleur and A. Chen, Carbon nanotube based electrochemical sensor for the sensitive detection of valacyclovir, *Faraday Discuss.* 164 (2013) 135-146.

27. M. Govindhan, T. Lafleur, B. R. Adhikari and A. Chen, Electrochemical sensor based on carbon nanotubes for the simultaneous detection of phenolic pollutants, *Electroanal.* 27 (2015) 902-909.

28. C. Cheng, S. Li, A. Thomas, N. A. Kotov and R. Haag, Functional graphene nanomaterials based architectures: biointeractions, fabrications, and emerging biological applications, *Chem. Rev.* 117 (2017) 1826-1914.

29. R. E. Mapasha, E. Igumbor, N. F. Andriambelaza and N. Chetty, Electronic properties of B and Al doped graphane: A hybrid density functional study, *Physica B: Condens. Matter.* 535 (2018) 287-292.

30. M. Baghayeri, Pt nanoparticles/reduced graphene oxide nanosheets as a sensing platform: Application to determination of droxidopa in presence of phenobarbital, *Sens. Actuators B: Chem.* 240 (2017) 255-263.

31. M. Hernaez, C. R. Zamarreño, S. Melendi-Espina, L. R. Bird, A. G. Mayes and F. J. Arregui, Optical fibre sensors using graphene-based materials: A review, *Sensors* 17 (2017) 155.

32. J. Huang, X. Yang, S.-C. Her and Y.-M. Liang, Carbon nanotube/graphene nanoplatelet hybrid film as a flexible multifunctional sensor, *Sensors* 19 (2019) 317.

33. P. Suvarnaphaet and S. Pechprasarn, Graphene-based materials for biosensors: A review, *Sensors* 17 (2017) 2161.

34. K. Chen, Z.-L. Zhang, Y.-M. Liang and W. Liu, A graphene-based electrochemical sensor for rapid determination of phenols in water, *Sensors* 13 (2013) 6204.

35. K. I. Bolotin, K. J. Sikes, Z. Jiang, M. Klima, G. Fudenberg, J. Hone, P. Kim and H. L. Stormer, Ultrahigh electron mobility in suspended graphene, *Solid State Commun.* 146 (2008) 351-355.

36. J. Shen, Y. Hu, M. Shi, N. Li, H. Ma and M. Ye, One step synthesis of graphene oxide−magnetic nanoparticle composite, *J. Phys. Chem. C* 114 (2010) 1498-1503.

37. R. K. Srivastava, S. Srivastava, T. N. Narayanan, B. D. Mahlotra, R. Vajtai, P. M. Ajayan and A. Srivastava, Functionalized multilayered graphene platform for urea sensor, *ACS Nano* 6 (2012) 168-175.

38. B. Zheng, J. Wang, F.-B. Wang and X.-H. Xia, Synthesis of nitrogen doped graphene with high electrocatalytic activity toward oxygen reduction reaction, *Electrochem. Commun.* 28 (2013) 24-26.

39. A. Vizintin, M. Lozinšek, R. K. Chellappan, D. Foix, A. Krajnc, G. Mali, G. Drazic, B. Genorio, R. Dedryvère and R. Dominko, Fluorinated reduced graphene oxide as an interlayer in li–s batteries, *Chem. Mater.* 27 (2015) 7070-7081.

40. J. Han, L. L. Zhang, S. Lee, J. Oh, K.-S. Lee, J. R. Potts, J. Ji, X. Zhao, R. S. Ruoff and S. Park, Generation of B-Doped Graphene Nanoplatelets Using a Solution Process and Their Supercapacitor Applications, *ACS Nano* 7 (2013) 19-26.

41. L. Jiang, Y. Ding, F. Jiang, L. Li and F. Mo, Electrodeposited nitrogen-doped graphene/carbon nanotubes nanocomposite as enhancer for simultaneous and sensitive voltammetric determination of caffeine and vanillin, *Anal. Chim. Acta* 833 (2014) 22-28.

42. V. Georgakilas, M. Otyepka, A. B. Bourlinos, V. Chandra, N. Kim, K. C. Kemp, P. Hobza, R. Zboril and K. S. Kim, Functionalization of Graphene: Covalent and Non-Covalent Approaches, Derivatives and Applications, *Chem. Rev.* 112 (2012) 6156-6214.

43. D. D. Chronopoulos, A. Bakandritsos, M. Pykal, R. Zbořil and M. Otyepka, Chemistry, properties, and applications of fluorographene, *Appl. Mater. Today* 9 (2017) 60-70.

44. H. Ji, F. Zhou, J. Gu, C. Shu, K. Xi and X. Jia, Nitrogen-doped carbon dots as a new substrate for sensitive glucose determination, *Sensors* 16 (2016) 630.

45. A. R. Thiruppathi, B. Sidhureddy, W. Keeler and A. Chen, Facile one-pot synthesis of fluorinated graphene oxide for electrochemical sensing of heavy metal ions, *Electrochem. Commun.* 76 (2017) 42-46.

Chapter 8: Conclusion and Future Work

To summarize, an electrochemical sensor based on distinct classes of nanostructured materials was successfully fabricated for the sensitive detection of different molecular species in beverage and food matrices. As described in Chapter 4, a Co_3O_4/Au/GCE sensor was successfully developed and employed for the electrochemical detection of NO_2^-. The results of CV studies demonstrated that the electrooxidation of NO_2^- was efficient at the Co_3O_4/Au/GCE in terms of enhanced current response and a decrease in overpotential, in contrast to bare GCE and Co_3O_4/GCE. The fabricated electrochemical sensor exhibited good analytical capabilities and linearity over a wide calibration range, high sensitivity, and a low LOD of 0.11 μM. The sensor also showed excellent selectivity for the determination of NO_2^- in the presence of co-existing ions and other molecular interferents. Moreover, the sensor yielded satisfactory recovery rates with actual samples, which verified its practical applicability. Furthermore, the Co_3O_4/Au/GCE sensor showed appreciable repeatability, good reproducibility, and chemical stability.

Chapter 5 of this thesis summarized a study that was based on a highly stable and selective nanoporous gold microelectrode sensor for the individual and simultaneous electrochemical oxidation of N_2H_4, SO_3^{2-}, and NO_2^- in 0.1 M PBS (pH 6.5). The nanoporous gold microelectrode possessed a large EASA with a roughness factor of 27.7. The oxidation peaks were well-defined with large peak-to-peak separations of 0.27 V and 0.41 V for N_2H_4-SO_3^{2-}, and SO_3^{2-}-NO_2^-, respectively. The nanoporous gold microelectrode exhibited enhanced selectivity for the simultaneous measurement of N_2H_4, SO_3^{2-}, and NO_2^-. The developed microelectrode demonstrated superior performance for the determination of SO^{2-} and NO_2^- in commercial beverages and food samples. Further, the electrochemical sensor showed a good sensing ability coupled with other

desirable properties such as sensitivity, robustness, and low detection limit. These combined factors confirmed that the nanoporous gold microelectrode could be applied as a high-performance electrochemical sensor for myriad applications in food and beverage safety and quality control.

A highly selective and novel F-GO based sensor developed for the sensitive detection of CA was discussed in Chapter 6. The results obtained from the CV investigations implied the enhanced electrocatalytic behavior of the F-GO in contrast to a bare GCE and GO modified GCE. The F-GO/GCE exhibited higher EASA and improved electrochemical performance over the GO/GCE. The analytical quantitation performed using the DPV revealed the strong capacity of electrochemical sensor for the determination of CA within a wide linear concentration range in a 0.1 M B-R buffer (pH 2.65). The F-GO/GCE sensor demonstrated superior selectivity for the oxidation of CA in presence of other phenolic compounds. The developed electrochemical sensor exhibited good long-term stability, sensitivity, a low detection limit, and satisfactory reproducibility. Additionally, it was effectively employed for the detection and quantitation of CA in assorted brands of red wine. The sensor also exhibited superior sensing for the direct detection of CA in wine without the need of an external electrolyte medium. These collective factors confirmed that the developed F-GO/GCE sensor could be incorporated for maintaining food quality control.

Finally, an electrochemical sensor developed for the detection of vanillin with Au and F-GO was presented in Chapter 7. The electrochemical characterization results demonstrated that Au/r-FGO was efficient at oxidizing vanillin in terms of enhanced current response and a decrease in overpotential, compared to bare GCE and F-rGO/GCE. The fabricated electrochemical sensor showed substantial analytical capabilities with good linearity over the selected calibration range, coupled with excellent sensitivity and a low LOD value. This sensor also exhibited superior

selectivity for the determination of vanillin in the presence of co-existing ions and other interference molecules. Moreover, the results yielded from the sensor had satisfactory recovery rates from real sample studies and proved its practical applicability. Furthermore, the Au/F-rGO/GCE sensor demonstrated appreciable repeatability, good reproducibility, and possessed good chemical stability. As reviewed in this thesis, great progress has been made by addressing these challenges through the use of effective nanomaterials such as Co_3O_4 nanosheets, nanoporous gold, and F-GO to overcome the challenges of selective oxidation of targeted molecules. These nanomaterials demonstrated increased sensitivity and electrocatalytic activity toward the analytes of interest.

Most chemical and instrumentation analysis performed in centralized laboratories require skilled labour, and only allow for a limited number of samples to be tested in a short period of time. To address the setbacks that are linked to food-related diseases, electrochemical-based analytical methods are an excellent choice to effectively ease the investigation of additives and contaminants for large batches of product in the food industry. Besides, a variety of electrochemical sensors based on other reported bimetallic, conductive polymer infused nanomaterials and their fabrication methods have shown superior performance, which could also serve as an alternative to instrumentation-based analysis methods. Furthermore, precise and thorough proof-of-concept studies will be required to fully elucidate the behaviour of the electrochemical sensors under variable conditions. Finally, the validation and testing of statistically relevant numbers of samples, comparability, and interlaboratory studies are the next critical steps for the successful transition of these electrochemical sensors to real applications in the industrial model for food and beverage safety testing.

The development of smart sensors remains in its nascent stages and encompasses another unexplored area for future research. Improved portability may be attained through the connectivity and integration of electrochemical sensors with communications devices, such as smartphones and tablets, for food safety applications. There is also the strong possibility for this technology to gain momentum and acceptance by modern society in addressing its day-to-day needs. Such integration of two distinct areas of research would pave the way for the next generation of smart sensors in food processing industries. to increase the quality and safety of food and beverages.